Copyright Undertaking

SYNTHESIS, CHARACTERIZATION AND PHOTOPHYSICAL STUDIES OF TRIAZINE-BASED LANTHANIDE(III) β-DIKETONATE COMPLEXES

LO WAI SUM

Ph.D

The Hong Kong Polytechnic University

2017

The Hong Kong Polytechnic University

Department of Applied Biology and Chemical Technology

Synthesis, Characterization and Photophysical Studies of Triazine-based Lanthanide(III) β-Diketonate Complexes

LO Wai Sum

A thesis submitted in partial fulfilment of the requirements

for the degree of Doctor of Philosophy

May 2016

Certificate of Originality

I hereby declare that this thesis is my own work and that, to the best of my knowledge and belief, it reproduces no material previously published or written, nor material that has been accepted for the award of any other degree or diploma, except where due acknowledgement has been made in the text.

__________________________ (Signed)

______Lo Wai Sum________ (Name of student)

Abstract

A review on the general background, coordination properties and optical properties of trivalent lanthanides is presented, with particular emphasis on their characteristic photoluminescent properties. Ln(III) are excellent emitters which cover most regions of the visible spectrum and extend to the near-infra red (NIR) region, with long lifetimes and distinctive emission profiles. However, their poor ability to absorb light means an external antenna is required to channel excited energy prior to radiative deactivation and careful design of the ligand system is necessary to minimize numerous competitive non-radiative processes.

This work encompasses the photophysical studies of europium(III), samarium(III) and ytterbium(III) complexes in a bi-chromophoric system. The well-known chelate – and sensitizer – 2-thenoyltrifluoroacetate (TTA) and a 1,3,5-triazine-based tridentate ligand complements the coordination of the trivalent lanthanides. The incorporation of an *N*,*N*-diethylanilinyl moiety imparts intraligand charge transfer (ILCT) character to the tridentate ligand which will be discussed following the general syntheses of various ligands and complexes in Chapter 3.

Chapter three focuses on the visible luminescence from the Eu(III) and Sm(III) complexes and evaluates the sensitization efficiencies and quantum efficiencies between the TTA and ILCT antennae. As ILCT transitions are solvatochromic, the photophysical properties were measured in various solvents and discussed in details. It was found that in non-polar solvents such as benzene, the luminescence quantum yield of the Sm(III) complexes are quite high compared to literature.

As Sm(III) is dual-emissive – emitting in both the visible and NIR regions, the NIR photophysical properties were investigated. Originating from the same emitting state as the visible luminescence transitions, the NIR transitions were studied and compared. In addition to solvatochromic studies, this chapter discusses the validity of the energy gap law in estimating the extent of quenching by high energy oscillators and thus provide a blueprint for maximizing the intrinsically weak NIR luminescence by manipulating the coordination environment. NIR luminescence from the ytterbium(III) complex was also presented, as the energy transfer mechanism of Yb(III) has always been sort of an enigma due to the large energy difference between the Yb(III) *only* excited state and the donating state of common antennae.

Chapter five focuses on the syntheses of a multidentate water-soluble pocket for lanthanide(III) complexes. The ligand system extends the aforementioned studies by using a single multi-chelate in place of multiple tri-/bi-dentate ligands as an effort to increase the stability of the complexes in solution state and thus creates a platform for exploring the non-triplet ILCT energy transfer pathway for lanthanide(III) luminescence sensitization in water to expand the scope of potential applications.

Acknowledgements

My sincerest gratitude to the following persons in making this journey possible:

First and foremost, I would like to thank my chief supervisor Prof. Wing-tak Wong for giving me this life-changing opportunity. Since our first acquaintance which left me nervously trembling afterwards, he has been a figure of wisdom, patience, incisiveness and flexibility, worthy of my respect and appreciation all along. His perspectives in scientific discussions and advice in casual sharing sessions were as enlightening as they were impactful on both research and personal levels.

I am in debt to my co-supervisor Dr. Ga-lai Law for taking a gamble on me. She was relentless and persistent with only good intentions and I am often humbled by her patience. Her passion and commitment towards doing good research were as impressive as they were influential, and her creativity was constantly overwhelming. My wholehearted gratitude goes to her for my immense transformation and I hope her gamble has paid off decently.

The name of Dr. Ho-lun Yeung, a former group member of Prof Wong's research group, is never forgotten. I feel much privileged to be his mentee during my early days, albeit briefly. He was my captain; he was my lighthouse. His advice, particularly 'Go home disappointed, come back with hope', gave me strength throughout the hardest days.

Equally important is Dr. Chi-tung Yeung, a current member of Prof Wong's research group who leads by example with his uncompromising standards and undivided attention. With an alter ego *sans* lab coat, he treated my problems like his. His commanding presence is greatly appreciated.

My special thanks also go to past and present group members from Prof Wong's and Dr. Law's research group, particularly Dr. K.-L. Wong, Dr. Y.-J. Gu, Dr. J, Jin, Dr. Arthur H.-H. Leung, Dr. Y. O. Fung, Dr. F. Zheng, Dr. W. Jin, Mr. Y.-W. Yip, Mr. L. Dai, Mr. T.-H. Tsoi, Ms. S. Guo, Mr. K.-M. Yu, Mr. Chris 'Handsome, Strong, Godfather' H.-Y. Wong, Mr. T. Zhong and Mr. D. Liang.

I would also like to thank Dr. T. K. W. Chan (Hong Kong Polytechnic University), Dr. C.-F. Chan and Dr. H. Li (Hong Kong Baptist University), and Dr. K.-L. Ho (City University of Hong Kong) for their support and friendship that extends beyond my study.

Help from Dr. Y. S. Lee and Dr. C.-S. Tsang for cyclic voltammetry experiments, and technicians and scientific officers of the Department of Applied Biology and Chemical Technology is also greatly acknowledged.

Table of Contents

Abbreviations

ACN	acetonitrile
a.u.	arbitrary unit
PhCl	chlorobenzene
$CHCl_3$	chloroform
CH_2Cl_2	dichloromethane
DMSO	dimethyl sulfoxide
DMF	dimethylformamide
ESI	electron spray ionization
EA	ethyl acetate
PhF	fluorobenzene
K	kelvin
MS	mass spectroscopy
m/z	mass-to-charge ratio
MeOH	methanol
μs	microsecond
mmol	millimole
ms	millisecond
m	multiplet
nm	nanometer
ns	nanosecond
NMR	nuclear magnetic resonance

s	singlet
THF	tetrahydrofuran
TTA	2-thenoyltrifluoroacetonate
t	triplet
UV-vis	ultraviolet-visible

1. Introduction to Lanthanides

1.1. General Background

The lanthanides represent the elements with atomic number 57-71 sitting on the first row of the f-elements in the periodic table. Their 4f orbitals are progressively filled along the series with notable exceptions at gadolinium ([Xe] $4f^7$ $5d^1$ $6s^2$) and lutetium ([Xe] $4f^{14}$ $5d^1$ $6s^2$) due to orbital stability brought about by half-filled and full-filled 4f subshells. Lanthanides are predominantly found in their most stable trivalent oxidation state (Ln(III)), and the chemistry of lanthanides hence encompasses the electronic configuration of [Xe] $4f^n$ ($n = 0 – 14$), which gives rise to unique physical and chemical properties.[1]

1.2. Electronic Properties

The 5s and 5p orbitals of the Xe core have a larger radial expansion than the 4f orbitals and are shielded from the nucleus by the latter, so, as the atomic number increases along the lanthanide series, the increase in effective nuclear charge leads to a decrease in ionic radii of Ln(III) which is termed as ‘lanthanide contraction’ (Table 1.1). The 4f electrons, conversely, are well-shielded from outermost interaction by the 5s and 5p electrons and are considered to have no participation in bonding, leading to spectroscopic and magnetic properties independent of the proximal environment. Interactions of the highly electropositive Ln(III) ions with ligands are thus mainly ionic with preference for ‘hard’ donor ligands with minimal perturbation to the 4f orbitals.

Table 1. 1 Ionic radii of Ln(III) (pm)[1]

La	Ce	Pr	Nd	Pm	Sm	Eu	Gd	Tb	Dy	Ho	Er	Tm	Yb	Lu
103.2	101.0	99.0	98.3	97.0	95.8	94.7	93.8	92.3	91.2	90.1	89.0	88.0	86.8	86.1

In the $4f^n$ configurations of Ln(III) ions, each electron can be associated with one of the seven 4f orbitals. Such association is characterized by a set of 'total' quantum numbers used in a polyelectronic system[2]: L (total orbital angular), M_L (total magnetic orbital angular momentum), S (total spin angular momentum) and M_S (total magnetic spin) and is summarized in the form of a spectroscopic term, i.e. ^{2S+1}L. The multiplicity of a spectroscopic term, ($2S$+1) x ($2L$+1), denotes the number of micro states of similar energies the term regroups, and the sum of the total micro states every spectroscopic term contains in an electronic configuration is the degeneracy of the configuration, which for the $4f^5$ configuration of Sm(III) can be calculated as:

$$\frac{(4l\ +2)!}{n!\,(4l+2-n)!}=\frac{14!}{5!\,(14-5)!}=2002$$

The calculation of all 2002 micro states is feasible but tedious; the calculation of the ground state term symbol, however, is made easier by obeying the Hund's rule, which states the ground state has 1) the largest spin multiplicity and 2) the largest orbital multiplicity. For Sm(III), the largest spin multiplicity S is 5 x 1/2 = 5/2 and the largest orbital multiplicity L is 5 (as the f electrons are associated with orbitals with magnetic quantum numbers +3, +2, +1, 0 and -1). The ground state term symbol of Sm(III) is thus ^{6}H.

The Russell-Saunders coupling scheme is used to approximate the separate coupling of spin angular momenta (*S*) and orbital angular momenta (*L*) in light atomic systems with negligible spin-orbit coupling. However, in heavy systems like the lanthanides, spin-orbit coupling becomes significant and a new total angular momentum quantum number ($J = L + S$, $L + S - 1$, …, $|L\text{-}S|$) is put forward to account for the interaction which further splits the ground state term symbol in various spectroscopic levels with a multiplicity of ($2J$+1).

The third rule of Hund's rule states that J_{min} is lowest in energy if the outermost subshell is less than half-filled and J_{max} is lowest in energy on the contrary. If the subshell is half filled, $L = 0$ and $J = S$. Thus for Sm(III), the ground state energy level is ${}^6H_{5/2}$. Similarly, the ground state energy levels of the Ln(III) series are summarized in Table 1.2.

Table 1. 2 Selected electronic properties of Ln(III)

Ln(III) (electronic configuration)	***S***	**2*S*+1**	***L***	J_{max}, J_{min}	${}^{2S+1}L_J$
Ce(III) ($4f^1$)	1/2	2	3	7/2, 5/2	${}^2F_{5/2}$
Pr(III) ($4f^2$)	1	3	5	6, 4	${}^3H_4$
Nd(III) ($4f^3$)	3/2	4	6	15/2, 9/2	${}^4I_{9/2}$
Pm(III) ($4f^4$)	2	5	6	8, 4	${}^5I_4$
Sm(III) ($4f^5$)	5/2	6	5	15/2, 5/2	${}^6H_{5/2}$
Eu(III) ($4f^6$)	3	7	3	6, 0	${}^7F_0$
Gd(III) ($4f^7$)	7/2	8	0	7/2, 7/2	${}^8S_{7/2}$
Tb(III) ($4f^8$)	3	7	3	6, 0	${}^7F_6$
Dy(III) ($4f^9$)	5/2	6	5	15/2, 5/2	${}^6H_{15/2}$
Ho(III) ($4f^{10}$)	2	5	6	8, 4	${}^5I_8$
Er(III) ($4f^{11}$)	3/2	4	6	15/2, 9/2	${}^4I_{15/2}$
Tm(III) ($4f^{12}$)	1	3	5	6, 4	${}^3H_6$

Yb(III) (4f^{13})	½	2	3	7/2, 5/2	$^{2}F_{7/2}$
Lu(III) (4f^{14})	0	1	0	0, 0	$^{1}S_{0}$

1.3. Coordination Properties

Ln(III) ions are highly electropositive Lewis acids with a high charge density that increases across the series due to lanthanide contraction. The f electrons are localized ‘inside’ 5s and 5p orbitals and do not participate in bonding. Ln(III) interact preferentially with hard Lewis bases (in the order of O > N > S)[3] in an electrostatic fashion, hence the bonding interaction is non-directional and the coordination number varies from 6-12 (8-9 being most common) with steric factors and the ionic radius of Ln(III) taken into consideration as well; multidentate ligands are thus commonly designed to form stable Ln(III) complexes by chelate effect. Selected representative examples of Ln(III) coordination compounds are shown in Figure 1.1.

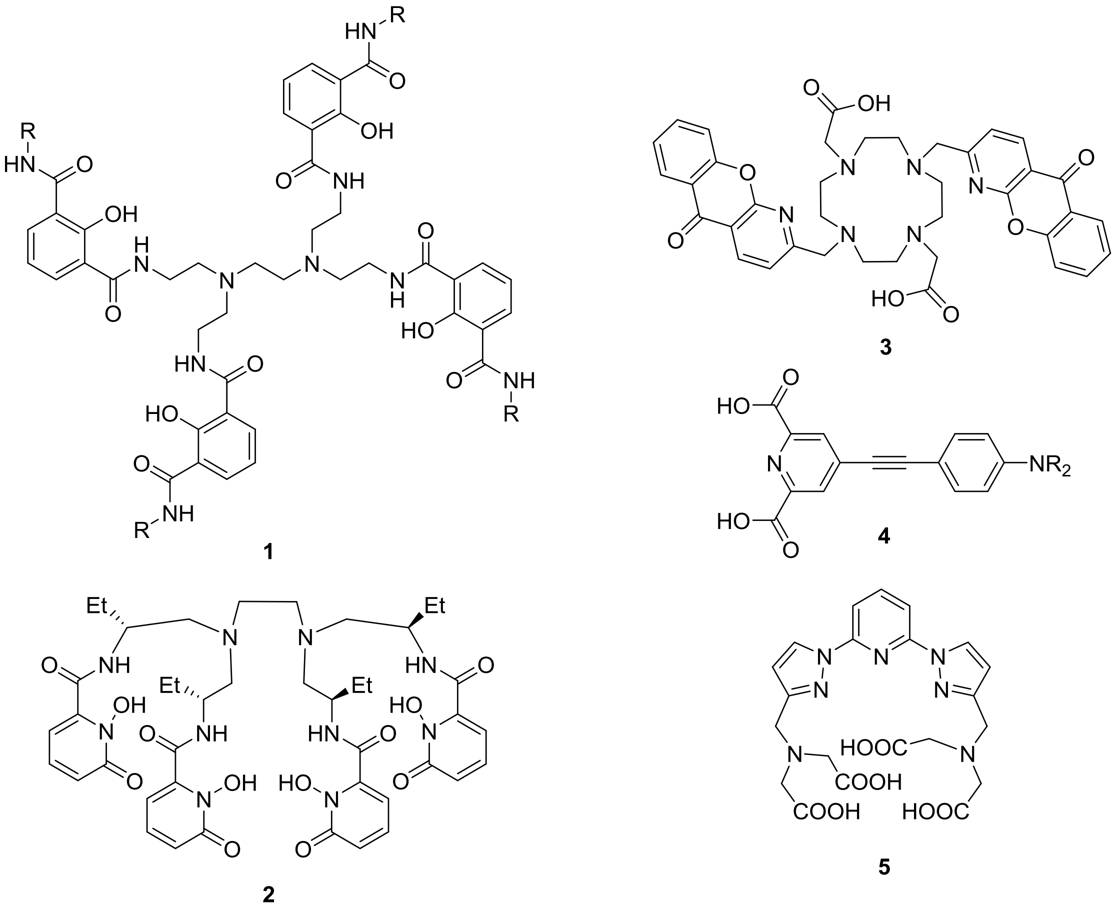

1

2

3

4

5

Figure 1. 1 Representative examples of chromophore-incorporated multidentate ligands[2]

1.4. Optical Properties

1.4.1. Absorption

In 1934, the absorption spectra of the whole Ln(III) series in solution in the range of 200 – 700 nm were obtained by Prandtl and Scheiner,[4] showing a symmetric pattern of a blue-shift in absorption from Ce(III) and Yb(III) towards Gd(III). The sharp absorption bands were attributed to transitions within the $4f^n$ configuration, so-called intraconfigurational $4f^N$-$4f^N$ transitions (simplified as f-f hereafter), and such transition is forbidden according to Laporte's rule as the initial and final states are of the same parity, hence the molar extinction coefficients of Ln(III) are quite low ($\varepsilon \approx$ 1-10 L mol^{-1} cm^{-1}).

The absorption spectra are still observable, however, due to the relaxation of Laporte's rule by spin-orbit coupling which is more pronounced in heavier elements.

1.4.2. Emission

The emission of trivalent lanthanides covers a wide spectral range from the UV (Gd(III)), visible (Pr(III), Sm(III), Eu(III), Tb(III), Dy(III) and near-infrared (Nd(III), Er(III), Yb(III)), with some being dual-emissive – i.e. capable of emitting in both the visible and NIR region. The nature of Ln(III) emission can be characterized as fluorescence ($\Delta S = 0$) or phosphorescence ($\Delta S \neq 0$) yet Ln(III) emission is commonly referred as luminescence as to avoid confusion with the photophysics of other elements or organic compounds.

A unique feature of Ln(III) emission is their sharp emission lines. It's because the 4f orbitals are well-shielded from the environment and experience great nuclear attraction, therefore the internuclear distance of the molecule at excited state is very similar to that at ground state, resulting in small or negligible (environment-dependent) Stokes shift. Like absorption, f-f emissions are also governed by parity selection rules. The f-f emissions of Ln(III) are achieved by either the even-parity magnetic dipole, odd-parity electric dipole or the electric quadrupole mechanism. Spin-orbit coupling relaxes the Laporte-forbidden electric dipole (ED) mechanism as the symmetry is broken through non-centrosymmetric interactions and the f-orbitals would mix with some d-orbitals, hence the transition then becomes partially allowed, so-called a forced electric dipole transition which could be mathematically represented as $w[4f^{N}(i)] + x[4f^{N-1}5d(i)] \rightarrow y[4f^{N}(f)] + z[4f^{N-1}5d(f)]$ (where $w \gg x$ and $y \gg z$).[5,6] The oscillator strength of a forced ED transition is approximately 10^{-4} times of a fully allowed ED transition. Magnetic dipole (MD) and electric quadrupole (EQ) transitions (considered simply as two dipoles arranged in a fashion that cancel out each other) are parity-allowed; the former is weak, yet the latter is often too weak to be observed (with oscillator strengths at around 10^{-6} and 10^{-10} times of a fully allowed ED transition). Table 1.3 describes the selection rules simplified by Judd[7] and Ofelt[8] for the forced ED transitions.

Table 1. 3 Selection rules for f-f transitions via ED, MD or QE transitions

Forced Electric Dipole (ED) Transitions	**Magnetic Dipole (MD) Transitions**	**Electric Quadrupole (EQ) Transitions**
$\lvert\Delta S\rvert = 0$	$\Delta S = 0$	$\lvert\Delta S\rvert = 0$
$\lvert\Delta L\rvert \leq 6$; $\lvert\Delta \mathrm{L}\rvert = 2, 4, 6$ if $L = 0$ or $L' = 0$	$\Delta L = 0$	$\lvert\Delta L\rvert \leq 2$
$\lvert\Delta J\rvert \leq 6$; $\lvert\Delta J\rvert = 2, 4, 6$ if $J = 0$ or $J' = 0$	$\Delta J = 0, \pm 1$	$\lvert\Delta J\rvert \leq 2$

Some f-f transitions are very sensitive to the environment such as symmetry and ligand field, and are referred to as hypersensitive transitions. Jorgensen and Judd also refer these transitions as pseudo-quadrupole transitions as they obey the selection rules for EQ transitions[9] but with intensities larger than ordinary EQ transitions by several orders of magnitude. The sensitivity is reflected in the transitions' intensities, spectral shifts and band shape. The intensity of hypersensitive transitions is zero if the Ln(III) is at a center of symmetry but could also be enhanced 200 times relative to the aqua ions. Some transitions which are not usually hypersensitive, such as those of Nd(III) and Pr(III), show marked sensitivity to minute changes in the coordination environment, and a possible explanation is the presence of ligands in the coordination sphere would mediate pseudohypersensitivity by increasing the oscillator strength of the transitions, suggesting an increased nephelauxetic effect (4f orbital covalency) that leads to intensifying the hypersensitive transitions. Eu(III) is one of the most used trivalent lanthanide emitting centers for having decent quantum yields and a hypersensitive transition in the visible region. The f-f transitions from the $^5D_0$ excited state of Eu(III) are summarized in Table 1.4.

Table 1. 4 Features of f-f transitions from $^5D_0$ level of Eu(III)[1, 10]

Transition	Character	Spectral Region (nm)	Relative Intensity	Remarks
$^5D_0 \rightarrow {}^7F_0$	ED	577-581	Very weak	Non-degenerate; absent in high symmetry
$^5D_0 \rightarrow {}^7F_1$	MD	585-600	Strong	Intensity largely independent of environment
$^5D_0 \rightarrow {}^7F_2$	ED	610-625	Very weak to very strong	Hypersensitive; absent if Eu(III) is on inversion center
$^5D_0 \rightarrow {}^7F_3$	ED	640-655	Very weak	Forbidden transition
$^5D_0 \rightarrow {}^7F_4$	ED	680-710	Medium to strong	Sensitive to environment
$^5D_0 \rightarrow {}^7F_5$	ED	740-770	Very weak	Forbidden transition
$^5D_0 \rightarrow {}^7F_6$	ED	810-840	Weak	Hypersensitive; absent if Eu(III) is on inversion center; rarely measured and observed

1.5. Antenna Effect

As mentioned above, the forbidden nature of f-f transitions gives Ln(III) characteristic line-like emission profiles and is also the reason for their long emission lifetimes. The poor light absorbing ability, however, stands between a convenient excitation source and the unique emission properties. Direct excitation of Ln(III) by laser (high power and narrow spectral width) is possible but not practical for applications. This problem could be solved by introducing a chromophore (antenna) at proximal distance to harvest light and transfer its excited energy towards the Ln(III) and decay radiatively *via* f-f transitions, a process also termed as sensitization. A Jablonski diagram depicting the processes involved in the antenna effect is shown in Figure 1.2.

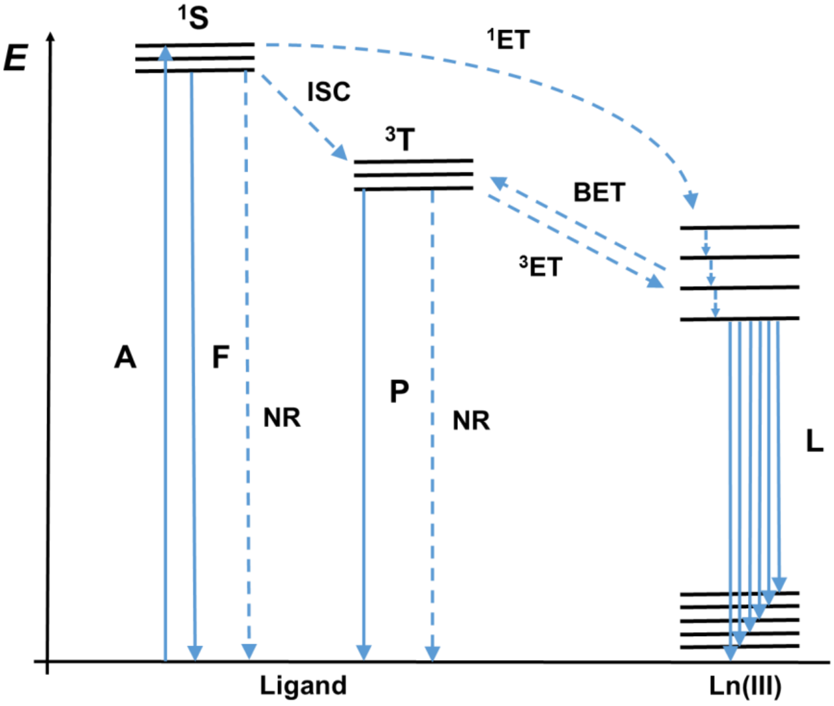

Figure 1. 2 A simplified Jablonski depicting possible processes involved in the antenna effect. A – absorption, F – fluorescence, P – phosphorescence, L – luminescence, NR – non-radiative deactivation, ^{1}S – first excited singlet state, ^{3}T – lowest excited triplet state, ISC – intersystem crossing, ET – energy transfer, BET – back energy transfer. Dotted arrows describe non-radiative processes.

1.5.1. Energy Transfer Pathways

The most common energy transfer pathway from the chromophore to Ln(III) involves the excited triplet state of the former. Excitation of the chromophore through Laporte and spin-allowed absorptions is followed by the formation of an excited triplet state *via* intersystem crossing (ISC) – a spin-forbidden process facilitated[11] by the spin-orbit coupling of the nearby heavy atom such as Ln(III). The excited energy is then transferred to the Ln(III)'s accepting states *via* several mutually non-exclusive mechanisms and subsequent radiative decay would yield characteristic f-f emissions. According to Latva's[12] empirical rule, from the library of ligands the authors screened, the gap between the chromophore's lowest triplet state and the accepting state of Ln(III) should be in the range of 2500 – 4000 cm^{-1}. If the difference is too large, energy transfer would not be favorable and if the difference is too small, thermally-promoted back energy transfer may become efficient.

Energy transfer can also take place from the excited singlet state directly to the Ln(III), as proposed by Kleinerman[13] in 1969 after studying the solutions of more than 600 chelate systems, provided that the accepting levels of Ln(III) is lower than the lowest excited singlet state and such energy transfer pathway may predominate if the rate of intersystem crossing is less than 10^{11} sec^{-1}. Direct sensitization from the singlet state was also observed by other groups.[14-17] Besides, intra-ligand charge transfer states of the Ln(III) complex and the metal to ligand charge-transfer states of transition metal complexes were also shown to be antennae for sensitizing Ln(III) luminescence.

1.5.2. Energy Transfer Mechanisms

There are two distance-dependent mechanisms (Figure 1.3) through 1which the excited energy of the chromophore is transferred to the trivalent lanthanide center. Firstly, a double-electron exchange mechanism requiring orbital overlap between the chromophore (donor) and Ln(III) (acceptor) is proposed by Dexter. Since this interaction requires physical contact between the two, the separation distance (r) has a dependence of $e^{(-2r/L)}$. The other mechanism, in comparison, is a 'through space' interaction that does not require orbital overlap, but the overlap of the emission spectrum of donor and the absorption spectrum of acceptor – Förster mechanism[18,19]. Energy transfer proceeds *via* a coulombic interaction in which the dipole moment of the excited triplet state induces a dipole in the acceptor with its rate of transfer proportional to r^{-6}. As the absorption of the f-f transitions is quite sharp and situated at scattered regions along the spectrum, it is reasonable that reaching the spectral overlap required for Förster mechanism is less easily achieved, so the Dexter mechanism, with a harsher distance-dependence, is more common, directly influencing the design strategy of incorporating the chromophore into the ligand.

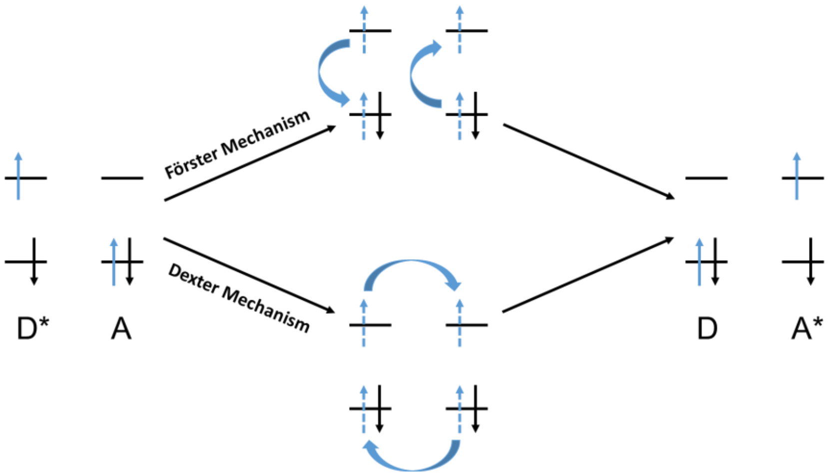

Figure 1. 3 Graphical representation of the Förster and Dexter mechanisms

All excited states involved in the sensitization process are susceptible to quenching. The excited singlet state of the antenna can be quenched by its own fluorescence if the rate of intersystem crossing is much lower than its radiative decay. It could also be quenched by colliding with halide ions, resulting in an electron transfer from the halide anion to the excited chromophore. Intramolecular electron transfer may also occur, with the donor being the excited singlet state and the acceptor another part of the molecule. The excited triplet state could also be quenched by molecular oxygen, forming singlet oxygen as a result.

1.6. Non-Radiative Quenching of Excited States

Furthermore, the emitted states of Ln(III) are also quenched by harmonics of high energy vibrational oscillators, such as O-H, N-H, C-H – which are commonly found in organic chelates – in proximity. The energy gap law[20] describes the relationship between the ΔE of the emitting state and the next lower state and the energy of oscillators that may cause multiphonon relaxation. As a rule of thumb[21], the emitting level would decay radiatively if the ΔE with the next lower energy level exceeds four vibrational quanta of the highest energy oscillator. Initially developed for aromatic hydrocarbons, it is applicable onto Ln(III) compounds as well as the energy levels are unperturbed by the molecular environment. Non-radiative multiphonon relaxation by harmonics of the high energy oscillators becomes prominent when certain harmonics resonate with the emitting states of Ln(III); and the less harmonics required to reach resonance, the more efficient the quenching. A numerical representation of applying the energy gap law onto trivalent lanthanides is presented in Table 1.5 and Figure 1.4 show a graphical example of how the third harmonic of O-H matches with the $^5D_0$ level of Eu(III), competing with radiative decay for deactivation of the excited state.

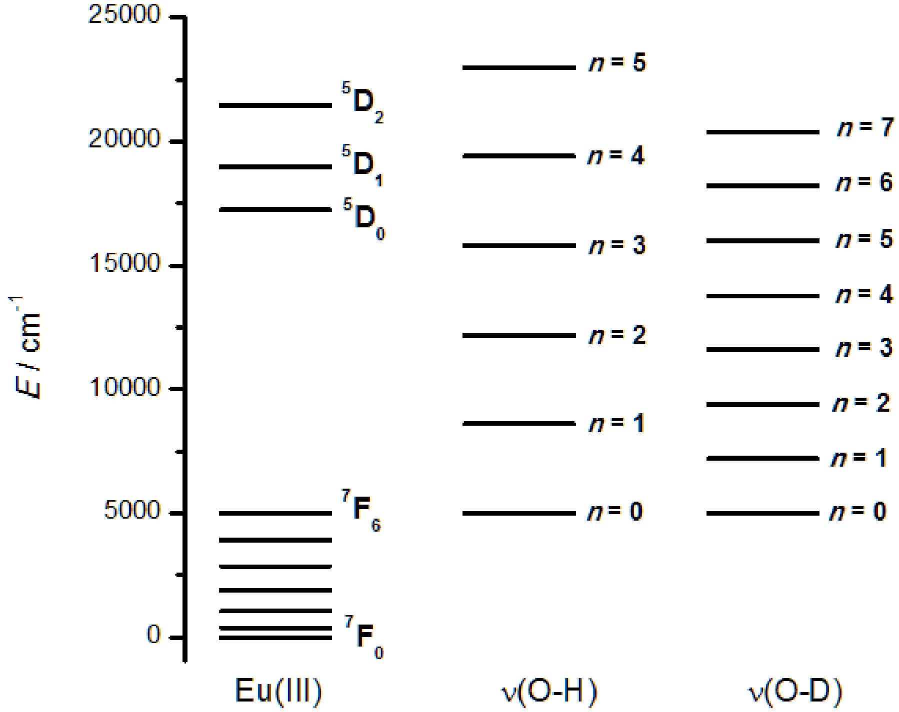

Figure 1. 4 Graphical representation of the Δ*E* between the excited states of Eu(III) and the next lower state with harmonics of O-H and O-D oscillators

Since three vibrational quanta of O-H oscillator are required only compared to five of O-D, this explains why europium(III) complexes have longer emission lifetimes and higher quantum yields in deuterated water. To avoid solvents – mainly water – entering the first coordination sphere of Ln(III) and quenching its luminescence, macrocyclic ligands are often devised to protect the trivalent center from solvent molecules by having a rigid skeleton and fulfilling the coordination capacity of the trivalent lanthanide center.

Table 1. 5 Relationship between ΔE of Ln(III) and harmonics of O-H and O-D oscillators in luminescence quenching reflected by emission lifetimes[2]

Ln(III)	**ΔE (cm^{-1})**	**No. of Phonons**		**Emission Lifetimes (μs)**	
		OH	OD	H_2O	D_2O
Gd(III)	32,100	9	15	2,300	/
Tb(III)	14,800	4	7	467	3,800
Eu(III)	12,300	3-4	5-6	108	4,100
Yb(III)	10,250	3	4.5	0.17	3.95
Dy(III)	7,850	2-3	3-4	2.6	42
Sm(III)	7,400	2	3	2.7	60
Er(III)	6,600	2	3	/	0.37
Nd(III)	5,400	1-2	2-3	0.031	0.14

While multiphonon relaxation quenches Ln(III) luminescence, it is also a useful phenomenon in determining the number of coordinated water molecules q, which could be measured with the emission lifetimes of the Ln(III) compounds in H_2O and D_2O using equations derived by various groups with a general relationship:

$$q = A[(1/\tau_{H2O}) - (1/\tau_{D2O}) - B] - C$$

where A, B and C are constants related to the inner-sphere contribution, presence of vibrational oscillators around and out-sphere contribution respectively. The number of other oscillators are also taken into consideration in several formulae. Water-insoluble compounds could also use the relationship with methanol. Selected equations for determining the number of coordinating water and methanol molecules are shown below:

$$q^{Eu(III)} = 1.2[1/\tau_{H2O})-(1/\tau_{D2O})-0.25-0.075n_{(NH)}]^{22}$$

$$q^{Eu(III)} = 1.11\ [(1/\tau_{H2O})-(1/\tau_{D2O})-0.31+0.45n_{(OH)}+0.99n_{(NH)}+0.075n_{(O=CNH)}]^{23}$$

$q^{\mathrm{Ln(III)}} = 5.0[1/\tau_{\mathrm{H2O}})-(1/\tau_{\mathrm{D2O}})-0.06]$;

$q^{\mathrm{Sm(III)}} = 0.026(1/\tau_{\mathrm{H2O}})-1.6$[24]

$q^{\mathrm{Sm(III)}} = 0.0225[1/\tau_{\mathrm{H2O}})-(1/\tau_{\mathrm{D2O}})-31.5]$[25]

$q^{\mathrm{Yb(III)}} = 1.0[1/\tau_{\mathrm{H2O}})-(1/\tau_{\mathrm{D2O}})-0.2]$[26]

$m^{\mathrm{Ln(III)}} = A[(1/\tau_{\mathrm{MeOH}})-(1/\tau_{\mathrm{MeOD}})-0.125)$; A = 8.4, 2.4, 0.05 ms for Tb(III), Eu(III), Sm(III)[27, 28]

1.7. Quantum Yield of Lanthanide Luminescence

The emission efficiency of a fluorophore is termed as fluorescence quantum yield, defined as:

$$\Phi = \frac{number\ of\ photons\ emitted}{number\ of\ photons\ absorbed}$$

For lanthanide complexes, the entities responsible for absorbing and emitting the photons are different and therefore the above definition is strictly non-applicable. The overall quantum yield of a complex (Φ_{L}^{Ln}) could also be obtained experimentally by absolute or relative measurements but information regarding the efficiency of energy transfer during antenna effect, luminescence quenching at the Ln(III) excited states and other processes involved (Figure 1.2) are not implied.

$$\Phi_L^{Ln} = \eta_{pop}^{D}\eta_{et}Q_{Ln}^{Ln} = \eta_{sens}Q_{Ln}^{Ln}$$

The overall quantum yield of a lanthanide complex relates the efficiency of sensitization with the intrinsic quantum yield of the Ln(III) center (obtained experimentally by direct excitation). The sensitization efficiency, η_{sens} , is defined as the product of 1) η_{pop}^{D} – the efficiency of populating the donor level which energy transfer to the Ln(III) takes place, e.g. the triplet state for a triplet-mediated pathway; and 2) η_{et} – the energy transfer efficiency from the donor level to the Ln(III) accepting states. The sensitization efficiency could be measured by obtaining both the overall quantum yield and intrinsic quantum experimentally, or calculated with lifetimes:

$$\eta_{sens} = \frac{Q_L^{Ln}}{Q_{Ln}^{Ln}} = Q_L^{Ln} \frac{\tau^{rad}}{\tau_{obs}}$$

The observed lifetimes are obtained experimentally *via* antenna effect. The radiative lifetime, on the other hand, relates to the spontaneous emission from an initial state to a final state, such are the excited and ground state multiplets of Ln(III), governed by Einstein's coefficient. Mathematical derivation of the relationship could be found in references 29 and 30 and a simplified relationship[31] regarding Eu(III) is shown below, due to the $^5D_0 \rightarrow {}^7F_1$ transition having a purely magnetic dipole character:

$$\frac{1}{\tau^{rad}} = A_{MD,0} \cdot n^3 \left(\frac{I_{tot}}{I_{MD}}\right)$$

where $A_{MD,0}$ is the spontaneous emission probably (Einstein coefficient) for the $^5D_0 \rightarrow {}^7F_1$ transition (14.65 s^{-1}), n is the refractive index and I_{tot} and I_{MD} are the integrated intensities of all the $^5D_0 \rightarrow {}^7F_J$ transitions and just the $^5D_0 \rightarrow {}^7F_1$ transition respectively.

As a result, with the sensitization efficiency deducible from experimental lifetime measurements and luminescence spectra, and the overall quantum yield obtained from relative or absolute measurements, the intrinsic quantum yield can be found without using direct excitation means. These parameters provide important information for evaluating the sensitization process in antenna effect, as the extent of quenching of the chromophore and lanthanide excited states can be revealed by the sensitization efficiency and the intrinsic quantum yield respectively.

1.8. Spectroscopic Techniques

1.8.1. Luminescence Quantum Yields

Many radiative and non-radiative deactivation processes are involved after photoexcitation of a chromophore *(vide supra)* and luminescence quantum yield describes the probability that the excited state of the chromophore is deactivated through energy transfer to the trivalent lanthanide center and subsequent lanthanide f-f emission. The most common and convenient way to measure quantum yields is by the relative method,[32] in which a well-characterized standard with a known quantum yield is compared.

The ideal pre-requisite is that both the excitation and emission range of the standard and the sample should be the same in order to minimize the difference in sensitivity of the spectrophotometer in different spectral range. Quantum yield standards should also be cross-calibrated to ensure of their stability and quality prior to measurements. It is vital to keep the excitation and emission slit widths the same throughout the experiment to maintain the validity of the comparison. The absorbances of the samples should be kept at 0.1 or lower to avoid the inner-filter effect, as self-absorption will occur and the ratio of photons absorbed and emitted will vary as the effect decreases with lower concentration.

$$\Phi_X = \Phi_{ST}\left(\frac{m_X}{m_{ST}}\right)\left(\frac{n_X^2}{n_{ST}^2}\right)$$

The relationship between the quantum yield of the sample (Φ_X) and the standard (Φ_{ST}) could be found above, where n is the refractive index and m is the gradient of the integrated intensities against absorbances. Table 1.6 shows some common quantum yield standards; note that the quantum yields vary with different solvent, concentration of sample and excitation wavelength.

The absolute quantum yield can be measured with an integrating sphere.[39,40] The interior of the integrating sphere is coated with a material of close to 100 % reflectance (barium sulfate or Teflon), thus the light that enters from the sphere to the detector would be proportional to the total photons emitted for both isotropic and anisotropic emissions. The absolute quantum yield can be calculated with measurements of the blank and sample in the integrating sphere[41]:

$$\Phi = \frac{(I_i I_d) - (I_d I_i)}{(I_i I_b) - (I_d I_b)}$$

where I_d, I_b are the integrated intensities of the sample and blank (solvent or specific blank with identical material as the sphere coating) respectively and I_i is the integrated intensity of the emission spectrum obtained when the excitation light is directed onto the wall of the integrating sphere whilst the sample is placed within in order to take into account the possible emission arising from re-excitation of the sample by reflected excitation light inside the sphere.

Table 1. 6 Common quantum yield standards used in relative measurements

Compound	**Solvent**	**Literature QY**	**Emission Range (nm)**	**Ref.**
Quinine sulfate	0.1 M H_2SO_4	0.546	400-600	33
$[Ru(bpy)_3]Cl_2$	Aerated water De-aerated water	0.028 0.043	550-800	34, 35
$Cs_3[Tb(dpa)_3]$	Aerated water	0.22	480-670	36, 37
$Cs_3[Eu(dpa)_3]$	Aerated water	0.24	580-690	36, 37
$[Yb(tta)_3(H_2O)_2]$	Toluene	0.0035	950-1080	38

1.9. Applications of Lanthanide Luminescence

1.9.1. Optical Imaging

Trivalent lanthanides, especially Eu(III) and Tb(III) due to their higher quantum yields, are excellent alternatives for organic fluorophores and quantum dots for optical imaging probes due to their various characteristics. First and foremost, they exhibit sufficiently high quantum yields to serve the main purpose of imaging. Second, Ln(III) as emitters do not suffer from photobleaching, a phenomenon in which the fluorophore becomes unable to fluoresce due to prolonged photo-damage. Third, careful design of ligand gives the Ln(III) compound rigidity, increased brightness, high water-solubility and low cytotoxicity. Fourth, the long emission lifetimes of Ln(III), from microseconds to seconds, allow differentiation from other background fluorescent entities such as proteins with autofluorescence in the nanosecond range by time-resolved spectroscopy – a technique utilizing pulsed excitation and time-gated technology to manipulate signal detection in controlled time windows (Figure 1.5).

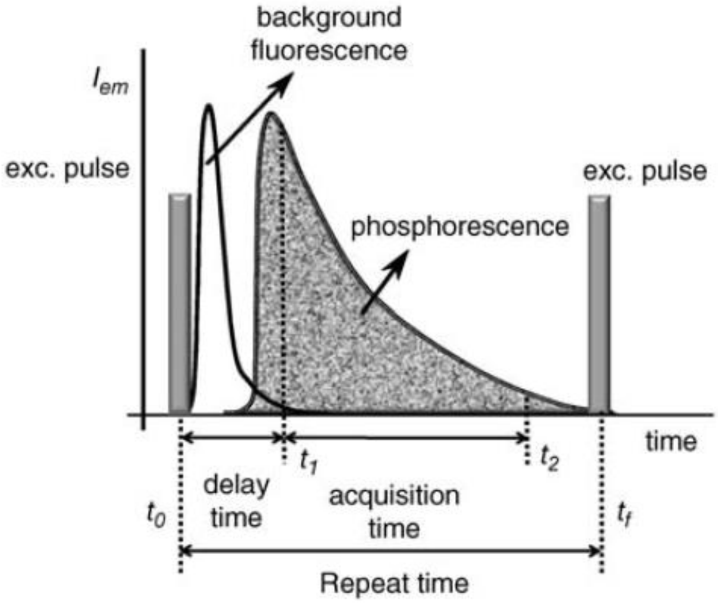

Figure 1. 5 Time-resolved emission detection[42]

Last but not least, the intrinsic property of hypersensitive emissions coupled with the above advantages put Ln(III) as the front-runner amongst other fluorophores. By designing the sensing and/or probing sites near the Ln(III) center with hypersensitive transitions, the environmental changes which corresponds to structural or geometrical modifications would be reflected in the intensities of the hypersensitive transitions and more systematically by the ratio between the hypersensitive transitions and the environmental-independent magnetic dipole transitions; Eu(III) is an excellent candidate. Tb(III), without hypersensitive transitions however, has generally higher quantum yields than Eu(III) and are used commonly as ratiometric probes. Excellent reviews on utilizing the aforementioned properties for optical sensing and imaging purposes can be found in references 43-47.

While multiphoton excitation is not considered as an intrinsic property of the lanthanides, it is however a rather ubiquitous idea that hovers around their applications, especially optical imaging. The main advantage of multiphoton excitation is the circumvention of using high energy excitation in the UV region – preventing tissue damage – and replace it with a lower energy excitation source which is also more tissue-transparent, leading to better excitation efficiency.

1.9.2. Magnetic Resonance Imaging

Magnetic resonance imaging (MRI) is a powerful *in vivo* imaging tool for visualizing anatomical structures in the medical field without subjecting the live body to ionization radiation. Protons of water molecules in the body are aligned by a strong magnetic field and the unmatched spins are pulsed with a matching radio frequency and signals will be detected by a scanner. Different protons in different environments will produce different signal intensities and result in a three-dimensional image contrast. Contrast agents are often used to enhance the image contrast by increasing the rate of relaxation of water protons.

Gadolinium(III) compounds are common contrast agents due to the large number of unpaired electrons ($4f^7$ configuration) and large magnetic moment of Gd(III), efficiently relaxing nearby nuclei and shortening T_1 relaxation times which involves through space dipole-dipole interaction. The access to inner-sphere water molecules also leads to larger relaxivity values, hence the design of Gd(III) compounds must reserve sufficient space for water molecules to penetrate to the inner coordination sphere but retain adequate stability to the Gd(III) to prevent toxic leaching of the free ion.

Recently, the development of Eu(II), isoelectronic with Gd(III), as an MRI contrast agent is gaining pace.[49-53] The Eu(II) center is susceptible to oxidation to form the diamagnetic Eu(III) which has little enhancement effect and therefore ligands should provide equally sufficient chelate and redox stability to the Eu(II) center. Selected examples of Eu(II)-based and clinically approved Gd(III)-based[54] contrast agents are shown in Figure 1.6.

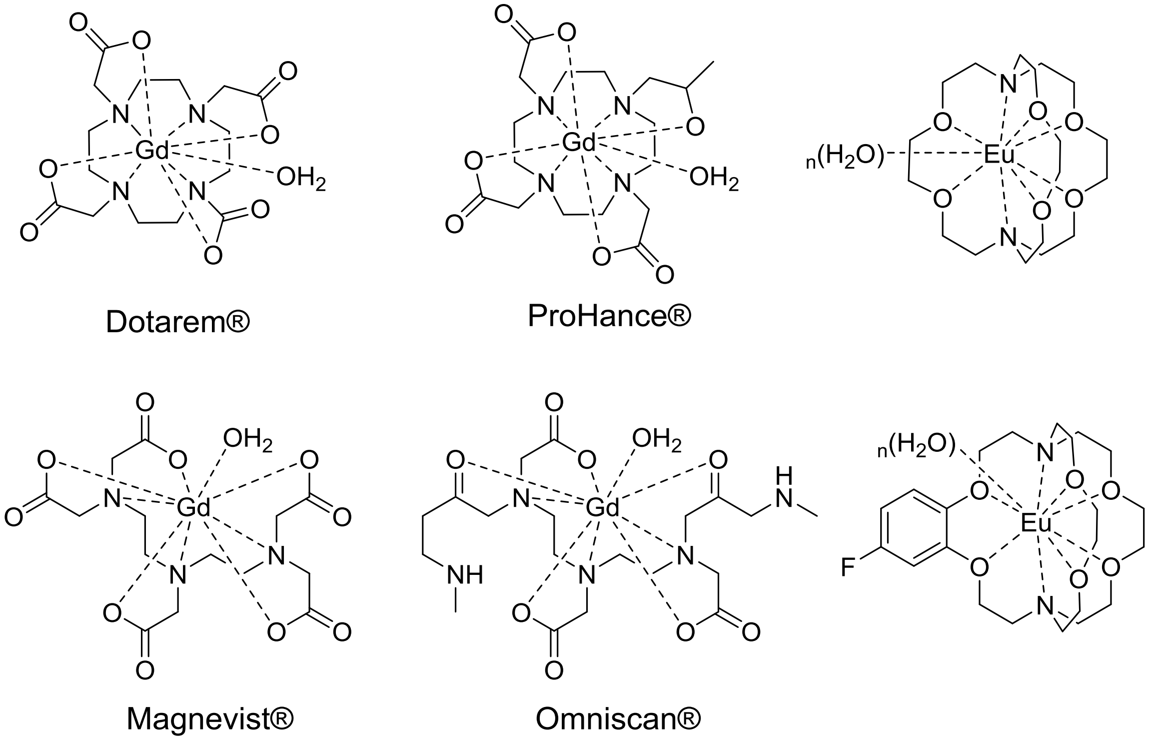

Figure 1. 6 Selected Eu(II)-based and clinically approved Gd(III)-based MRI contrast agents

1.9.3. Organic Light Emitting Diodes

An organic light emitting diode (OLED) is a light emitting diode (LED) with an organic electroluminescent emitting layer. Electrons and holes are injected from the cathode and anode respectively in the presence of a voltage bias and recombine at the emissive layer after being transported through the transport layers. Charge recombination leads to formation of excitons and they deactivate *via* light emission (Figure 1.7). The emission layer of early OLEDs are made of fluorescent materials (singlet-singlet deactivation) and theoretically only 25 % of the excitons will be deactivated as fluorescence whereas the remaining 75 % at the triplet state will decay through non-radiative deactivation.[55] Like transition metal complexes, lanthanide complexes offer to utilize the 75 % of exciton for light emission as well due to their intrinsic properties, drastically increasing the quantum efficiency and one of the first OLEDs with a Ln(III)-based emissive layer is presented by Kido[56] and coworkers in 1990, utilizing a Tb(acac)$_3$(phen) complex. Since then, many research groups have focused on developing Ln(III)-based complexes as the emissive layer due to their ability to harness the triplet excitons as well by antenna effect and high color purity (monochromaticity), such as Tb(III),[57] Eu(III),[58,59] Sm(III)[60] and Dy(III)[61] complexes. Furthermore, a combination of several of these Ln(III)-based complexes at a certain ratio to form one emissive layer would generate white light.

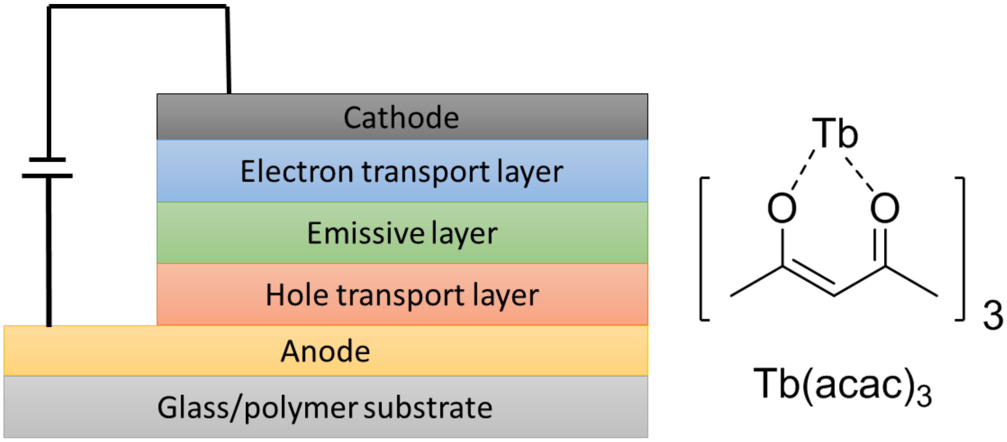

Figure 1. 7 Diagram showing an OLED device set-up and the structure of Tb(acac)$_3$(phen)

2. Triazine-based Ligands and Complexes

Triazine is a group of heterocyclic compounds with a general formula of C_3N_3 and 3 possible isomers: 1,2,3-triazine, 1,2,4-triazine and 1,3,5-triazine (*s*-triazine). The work in this thesis envelopes a ligand structure with an *s*-triazine (hereafter referred simply as triazine) core, which is used in extensive applications[62] such as materials (plastic and rubber syntheses), textile, pharmaceutical, and, more commonly, pesticides. Its use in coordination chemistry is popular as well and in this work, it is chosen as the core structure to form an auxiliary tridentate ligand which resembles the commonly used 2,2':6',2''-terpyridine ligand – a tridentate planar ligand widely used in coordination chemistry. Despite that terpyridine and its derivatives are commercially available, the variation in terpyridine-related ligands is mostly lateral and derivatives with modifications at the 4-position are either expensive or difficult to synthesize. *s*-Triazine offers much flexibility in structural modifications due to the relative ease in synthetic procedures. This chapter will discuss about the choice of triazine as the ligand skeleton and the syntheses of triazine-based ligands and complexes used for subsequent chapters.

2.1. General Properties

Cyanuric chloride (2,4,6-trichloro-1,3,5-triazine) is the starting material used for the syntheses of triazine-based compounds and is commonly made by the trimerization of cyanogen chloride (NCCl). It is readily available at commercial sources, so its synthesis will not be discussed here. It is soluble in acetonitrile, tetrahydrofuran, dioxane, acetic acid and absolute ethanol, although not stable in the latter two solvents. It also hydrolyzes in water into cyanuric acid (1,3,5-triazine-2,4,6-trione) and hydrochloric acid above 10 °C and interestingly, the hydrolysis does not stop until all three chlorine atoms have been hydrolyzed without increasing the temperature, rather than the three displacements having incremental activation energies. Reaction with alcohols yields cyanuric acid and the corresponding halide along with violent heat generation.

As the acid chloride of cyanuric acid, the chlorine atom is much more reactive than alkyl chloride but is less reactive than acyl chlorides and by no means are they similar to the inert aromatic halogens such as 1,3,5-trichlorobenzene. The reaction of cyanuric chloride with secondary amines can be summarized in a rule of thumb deduced from multiple literature reports,[63,64] the sequential substitution of the chlorine atoms could be estimated as: the first and second chlorine atoms are substituted at 0 °C and around 30-50 °C respectively, while the third and final chlorine atom may not be substituted at all even at 100 °C.[65] This relationship does not hold for all experimental conditions; in this work, nonetheless, the rule is adequately applied in tetrahydrofuran. While steric factors play a predominant role in the substitution with aliphatic amines, the basicity should also be considered for aromatic amines. If the basic character of the aromatic amine is significantly weakened in the product, then the reaction may not occur.

2.2. Synthesis of N-N-N Tridentate Triazine-Based Ligands

To mimic the tridentate structure of terpyridine, pyrazole was chosen as the heterocycle to complement the side units due to their potential in further modifications at different positions of the pyrazole ring compared to pyridine. According to the above information, substitution of the chlorine atoms is, to a certain degree, temperature-dependent, so a straightforward attempt is to deprotonate the pyrazole and use it to attack the triazine core. Pyrazole, a weak base itself, is deprotonated by potassium metal and the resulting pyrazolide was reacted with cyanuric chloride. In tetrahydrofuran, which both cyanuric chloride and pyrazole were readily soluble, a careful control over the stoichiometry would give the di-substituted product **WSL001** (2-chloro-4,6-bis(3,5-dimethyl-1H-pyrazol-1-yl)-1,3,5-triazine) as the main product even at refluxing temperature. **WSL001** could also be synthesized in a much milder condition[66] – demonstrating the peculiar reactivity of cyanuric chloride in different solvents – with *N*,*N*-diisopropylethylamine (DIPEA) as the base in toluene at room temperature. The latter method, however, requires slow addition of the 3,5-dimethylpyrazole to avoid formation of the tri-substituted product.

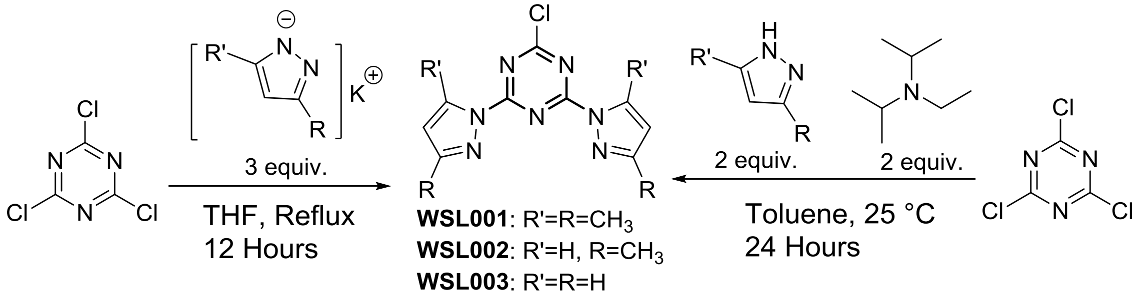

Scheme 2. 1 Synthetic routes for WSL001-003

In this thesis, the main modifications of the chlorine atom on the 2-position are replacing it with a phenyl ring or an *N*,*N*-diethylaniline. There are two possible approaches: pyrazole-substitution first or 2-position modification first; however, the reactivity of the chlorine atoms varies with different reaction conditions and hence several synthetic routes were investigated:

2.2.1. n-Butyllithium

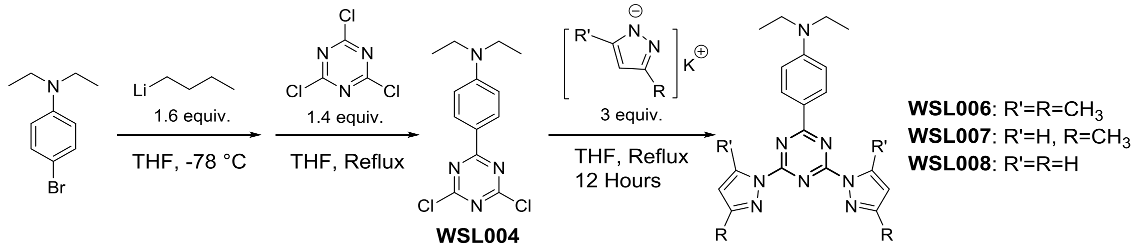

Scheme 2. 2 Syntheses of WSL004, WSL006-008 using *n*-butyllithium

In Scheme 2.2, 4-bromo-*N*,*N*-diethylaniline was deprotonated by *n*-butyllithium in THF at -78 °C and dropped slowly into cyanuric chloride at -78 °C. The reaction was very reactive as color change was rapidly observed as soon as the drop entered the cyanuric chloride solution. The extent of substitution was efficiently controlled by stoichiometry, temperature and the rate of addition, with the mono-substituted product obtained as the major product with a 40 % yield. **WSL004** was then attacked by potassium 3,5-dimethylpyrazolide to give **WSL006**. It should be noted that, reversal of these two steps will not give **WSL006** as the high basicity of the presence of organolithium reagents may cleave the C-N bond between the triazine and pyrazole, resulting in undesirable fragments and a much lower yield. By changing the pyrazole used in the above scheme, **WSL007** and **WSL008** can also be synthesized.

2.2.2. Grignard Reaction

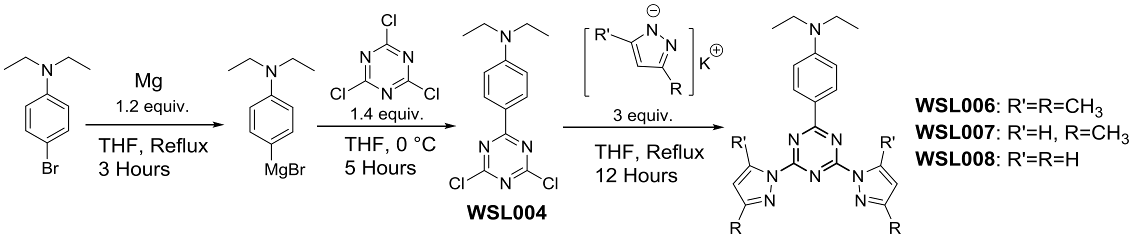

Scheme 2. 3 Syntheses of WSL004-006 using Grignard reagents

The low temperature requirement for the above reaction is critical because *n*-butyllithium will deprotonate and eventually degrade THF – our solvent of choice due to its great solubility and selectivity. Therefore, another nucleophile is being considered. With the same starting material, a Grignard reagent, 4-(diethylamino)phenylmagnesium bromide, was generated *in situ* with magnesium metal in THF, which was subsequently dropped into cyanuric chloride in THF to give **WSL004** as the major product if the reaction temperature was maintained at 0 °C. The same experimental conditions were applicable to synthesize the phenyl analog **WSL005** (2,4-dichloro-6-phenyl-1,3,5-triazine) with commercially available phenylmagnesium bromide. Similarly, subsequent nucleophilic substitution of the two chlorine atoms by appropriate potassium pyrazolides gave **WSL009** – **WSL0011**. While Grignard reagents are not as destructive as organolithium reagents due to their lower basicity, the third chlorine atom could still not be substituted, even at reflux temperature. Temperature, however, may not be such a deciding factor as the synthesis of **WSL001** could result in the tri-substituted product even at room temperature. Reports of using Grignard reagents to substitute the third chlorine atom could not be found as well.

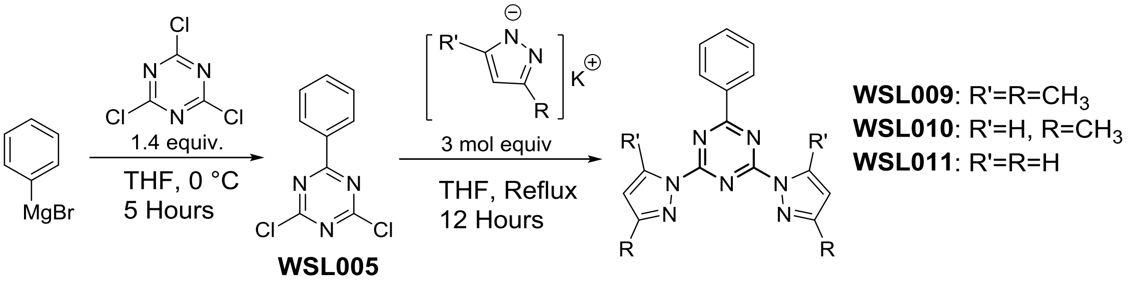

Scheme 2. 4 Syntheses of WSL009-011 using Grignard reagents

2.2.3. Suzuki Coupling

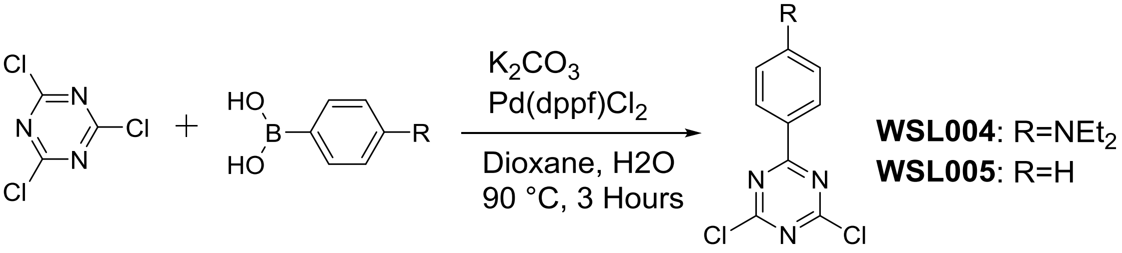

Scheme 2. 5 Synthesis of WSL004-005 by Suzuki Coupling

The reactivity of the chlorine atom does not limit modifications by nucleophilic substitution, the replacement of the C-Cl bond could be achieved by palladium-assisted cross-coupling,[67] too, treating it as an aryl chloride. A phenyl ring can be coupled onto the cyanuric chloride with good control of stoichiometry, and the temperature has little effect on the extent of substitution, so the phenyl ring could be coupled after incorporation of pyrazole on the triazine core. By changing phenylboronic acid to 4-(diethylamino)phenylboronic acid, **WSL004** was also synthesized, although in a lower yield due to the lower quality of boronic acid available commercially (15 %). The low yield could also be attributed to the chelation of the palladium catalyst by the tridentate ligand.

2.3. Synthesis of S-N-S/S-N-N Triazine-Based Ligands

The previous section discusses the synthesis of N-N-N ligands, which are relatively hard donors that trivalent lanthanide ions prefer to bind, and the first chapter also discusses the rather irrelevant role f-electrons play in the bonding of Ln(III) – the covalency of a Ln(III)-ligand bond is at most 5-7 %.[2] Sulfur, situated under oxygen in the periodic table, is a softer donor than nitrogen. Lanthanide(III)-sulfur bonds are not extremely rare, though, especially if the complexation takes place in non-polar solvents, with dithiocarbamates ($Ln(S_2CNR_2)_3$) and dithiophosphates ($Ln(S_2PR_2)_3$) among the simplest forms. Thiolates of Ln(III) were also obtained, with the help of bulky ligands, in the form of $[Yb(SPh)_3py_3]$.

To introduce sulfur atoms to the triazine core while retaining its properties as a chromophore, thiophene is chosen due to its aromaticity which extends the conjugated system of the ligand design and the presence of a sulfur atom. A new series of ligands was synthesized with thiophene taking the place of either one or both of the pyrazoles of the N-N-N ligands.

2.3.1. Grignard Reaction

The most convenient and straightforward way to incorporate the thiophene moiety is by Grignard reaction,[67,68] which is common in literature and also proven to be effective against cyanuric chloride for obtaining mono- or di-substituted products. Commercially available 2-bromothiophenpe and 2-bromo-5-methylthiophene were reacted with magnesium metal to generate the Grignard reagent which was used to attack the cyanuric chloride. The extent of substitution was controlled by the stoichiometry and more importantly the temperature, as shown in Scheme 2.6.

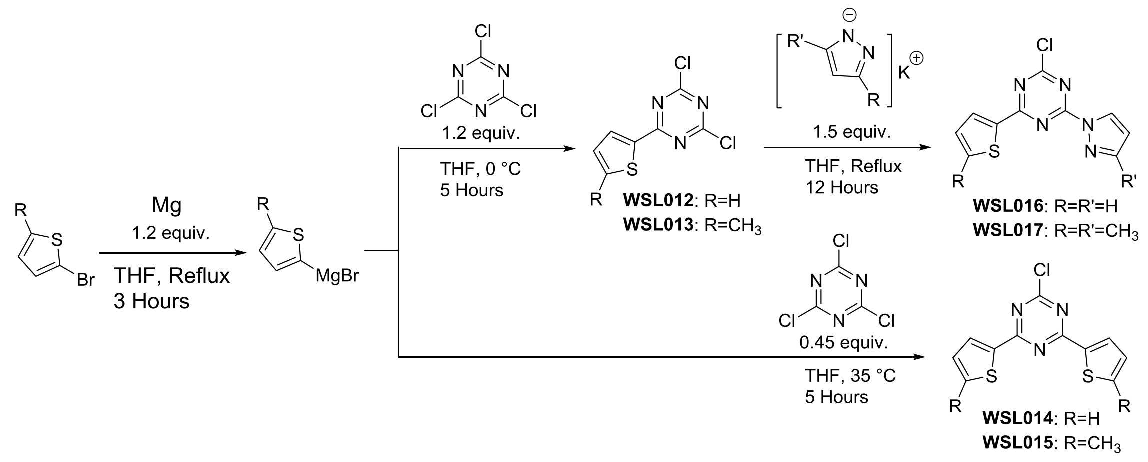

Scheme 2. 6 Syntheses of Sulfur-Containing WSL012-017

Similarly, the *N*,*N*-diethylanilinyl and phenyl moiety were incorporated by coupling reagent as it is the most suitable route amongst the three discussed above, due to the difficulty in reacting with the third and final chlorine atom. The poorer chelating ability of the sulfur atom also inhibited chelation towards the palladium catalyst, resulting in higher reaction yields. The structures **WSL018-025** are shown below.

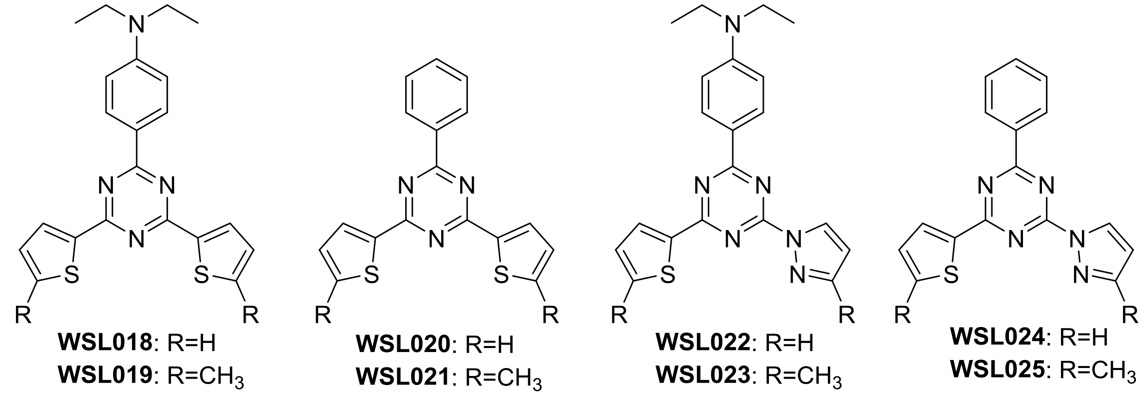

Figure 2. 1 Structures of S-N-S Tridentate Ligands WSL018-025

2.4. Design of Complex

As mentioned in Chapter 1, the nature of Ln(III) bonding is predominantly ionic and their coordination numbers are not governed by the number of bonding electrons but the non-directional electrostatic interaction and steric factors. Ln(III) luminescence is also easily quenched by oscillators of solvent molecules in the coordination sphere. To fulfill the coordination and efficiently protect the Ln(III) center from solvent coordination, macrocycles such as the cyclen-based 1,4,7,10-tetraazacyclododecane-1,4,7,10-tetraacetic acid (DOTA) (see designs of Gd(III) MRI contrast agents in Chapter 1) serves both purpose well. The added stability from chelate effect is also appreciated especially when water-soluble complexes are devised for biological applications in which leaching of free Ln(III) is highly toxic.[69,70]

However, as discussed in the section of energy transfer in antenna effect, the distance between the chromophore and the Ln(III) is extremely pivotal in determining the energy transfer efficiency. Therefore, the incorporation of a chromophore into macrocycles and modifying the chromophore to become one of the donors is a common strategy to enhance antenna effect by synthetic techniques.

The previous section detailed about triazine-based tridentate ligands. Tridentate ligands, like terpyridine, forms a $[ML_2]^{n+}$ or $[ML_3]^{n+}$ complex with transition metals. However, the ionic radii of transition metals are quite different to the Ln(III) – 94.7 pm of Eu(III) *vs.* 68 pm of Ru(III), and due to the ionic nature of Ln(III)-ligand interaction, the space vacated – insufficient for a third tridentate ligand – is likely to be filled by solvent molecules. Nonetheless, there is always more than one solution to a problem. To complement the coordination, a chromophoric bidentate β−diketone (1,3-diketone) ligand is introduced – thenoyltrifluoroacetonate (TTA).

A wide range of β−diketones are readily available from commercial sources and when deprotonated, the anionic oxygen atoms are hard donors that Ln(III) prefers. Lanthanide β−diketonates are primarily synthesized in two forms: neutral tris (Ln(β−diketonate)$_3$) and anionic tetrakis form (Ln(β−diketonate)$_4$)$^-$).[71] The tetrakis complex is eight-coordinated and depending on the structure of the β−diketone, steric factors may restrict further coordination. The tris complex is only six-coordinated and usually exists as a hydrate, and the detrimental water molecules can be displaced by the addition of neutral hard donors. One of the most well-known Ln(III) β−diketonate complexes is Eu(tta)$_3$(phen), where phen is 1,10-phenanthroline and tta is the conjugate base of 2-thenoyltrifluoroacetone. A detailed review on lanthanide(III) β−diketonate complexes on the syntheses, luminescence and applications can be found in literature.[72,73]

β−Diketones are generally good antennae for Eu(III) emission, but not particularly good for Tb(III) due to the energy level of their triplet states, which are at an appropriate distance with the accepting states of Eu(III) ($^5D_1$, $^5D_0$) with minimal back energy transfer, but are lower than the $^5D_4$ of Tb(III), resulting in very poor energy transfer; although certain aliphatic[74-76] or aromatic β−diketonates with higher energies are able to sensitize Tb(III) emission.[77] The excited singlet state, though, has no role to play[78] in the energy transfer according to studies.

Some β−diketonates, such as tris(1,1,1,-trifluoro-4-(2-thienyl)-2,4-butanediono)aquo-europium(III) (Eu(tta)$_3$), are quite common and commercially available. Fortunately, due to the similar physical properties of the lanthanide(III) series, other lanthanide β–diketonates could be synthesized according to old but not obsolete procedures.[79-81] Neutral lanthanide(III) β–diketonates, despite primarily being an ionic compound, have low water solubility and thus can be easily purified from the water-soluble precursors. Excess HTTA in small amounts could also be removed by recrystallization in petroleum ether.

The $Ln(tta)_3$ was then further reacted with a neutral auxiliary ligand to eliminate water molecules in the coordination sphere and fulfill coordination. It is also reported that a rigid planar molecular structure would lead to higher luminescence intensities, therefore a neutral, planar ligand with relatively hard donors such as the aforementioned tridentate ligands was reacted to give a thermodynamically favorable product in refluxing methanol (Scheme 2.7). The complexes were then purified by dissolving the crude in minimal amount of diethyl ether and precipitation with *n*-hexanes, repeated for three times. The complex was then characterized by electrospray ionization mass spectrometry and elemental analyses.

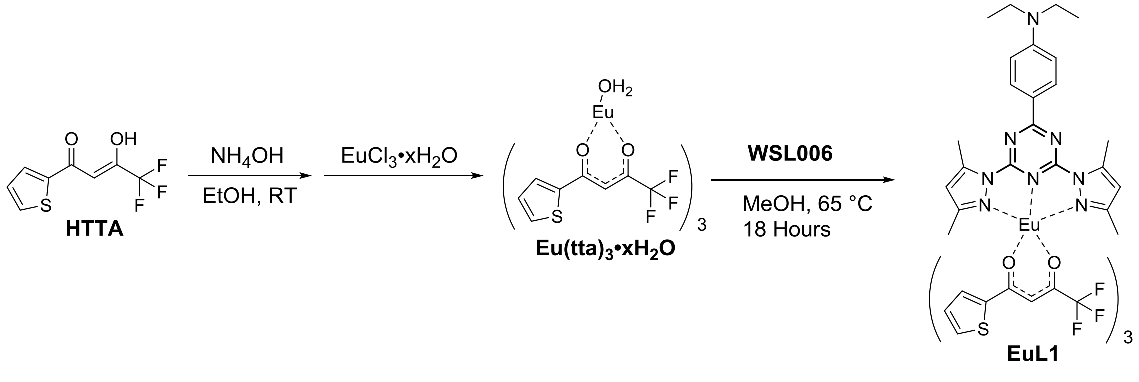

Scheme 2. 7 Synthesis of EuL1 with $Eu(tta)_3$ and WSL006

3. Non-Triplet Intraligand Charge Transfer Sensitization and Solvent Effect on Europium(III) and Samarium(III) Complexes

3.1. Background and Introduction

3.1.1. Europium(III) and Samarium(III) as Luminescent Centers

Trivalent europium has been widely studied in the previous decades due to its characteristic optical properties (see section 1.4.2) which has yielded a diverse range of applications from phosphors to bio-imaging probes. The $^5D_0 \rightarrow {}^7F_J$ transition profile, especially the transitions with electric dipole character, provides abundant structural information around the europium(III) center, especially in solid state materials. An excellent tutorial review on interpreting the electronic spectra of Eu(III) is available in the literature. [6]

Samarium(III) receives much less attention than europium(III) and terbium(III), most probably because of the weaker luminescence quantum yields of its chelates. This intrinsic disadvantage is a result of the more complex energy levels of Sm(III) than Eu(III). As shown in Figure 3.1, the energy gap between the lowest excited state and the next lower ground state between the three Ln(III) varies greatly: $\Delta E(^5D_0 \rightarrow {}^7F_6)$ of Eu(III), $\Delta E(^4G_{5/2} \rightarrow {}^6F_{11/2})$ of Sm(III) and $\Delta E(^5D_4 \rightarrow {}^7F_0)$ of Tb(III) are ca. 12500 cm^{-1}, 7500 cm^{-1} and 14700 cm^{-1} respectively. The smaller gap of Sm(III) requires less quanta of phonons for non-radiative quenching and vice versa, which explains why Eu(III) and Tb(III) are in general more luminescent amongst the lanthanides. Nevertheless, the accepting state of Sm(III), $^4G_{5/2}$, is at a similar position to the $^5D_1$ and $^5D_0$ accepting states of Eu(III), it is therefore reasonable to conjecture chromophores that transfer energy to Eu(III) would decently sensitize Sm(III) as well and this is precisely the rationale behind this work. While it is not pragmatic to imagine Sm(III) having similar luminescence quantum yields as Eu(III) in the same ligand system, to enhance Sm(III) luminescence by improving antenna effect or minimizing non-radiative deactivation would lead to possible multiplexing applications.[82,83]

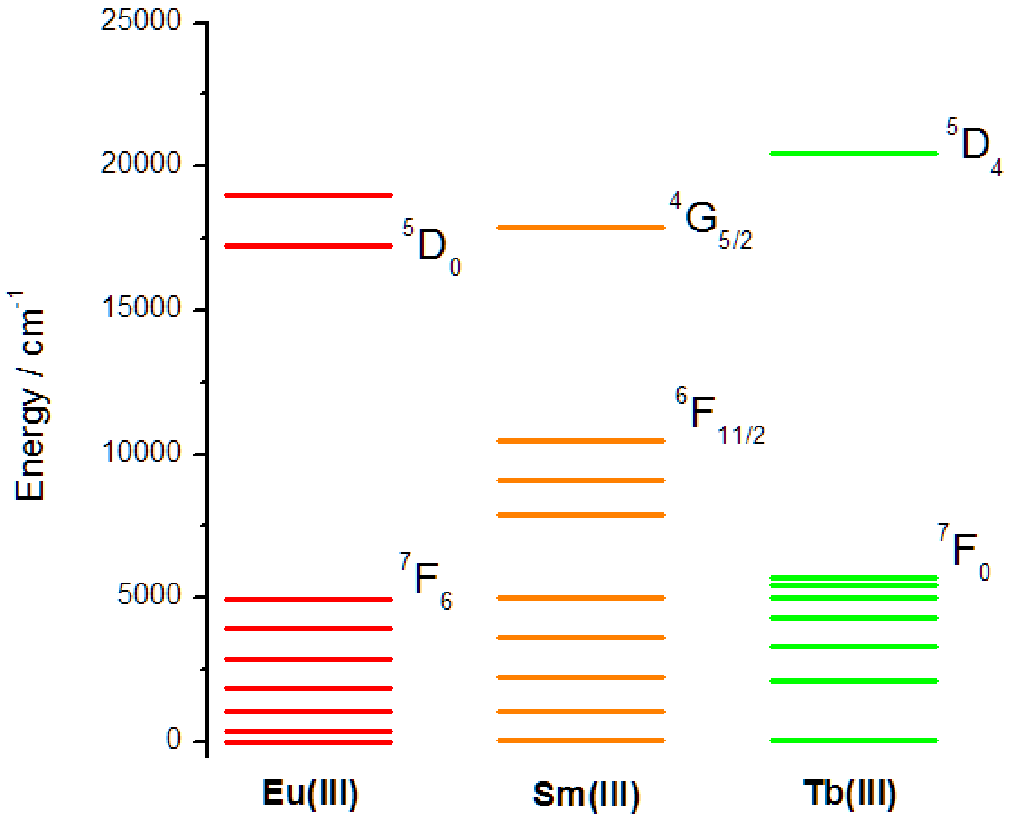

Figure 3. 1 Energy levels of Eu(III), Sm(III) and Tb(III)

3.1.2. Intraligand Charge Transfer Sensitization Pathway

Sensitization of Ln(III) luminescence is achieved by energy transfer from a light-harvesting chromophore at proximity to the accepting states of Ln(III) of appropriate energies. There are no definite and exclusive pathways for energy transfer. It must be stated that the term ‘antenna effect’ is a general description of the processes involved after the photoexcitation of the chromophore and before the deactivation of the Ln(III) accepting states. As mentioned in section 1.5, there are two distinct parts concerned: 1) energy transfer pathway and 2) nature/mechanism of energy transfer to the accepting states; and this chapter puts emphasis on the former.

The most common pathway is the triplet-mediated pathway, in which the excited singlet state of the chromophore undergoes intersystem crossing – induced by heavy effect of the Ln(III) in a close distance – to give an excited triplet state. Subsequently, the excited energy is transferred to the accepting states *via* different mechanisms. The spin-forbidden transition to yield the excited triplet state results in a longer lifetime and this offers an advantage for energy transfer to the Ln(III) by allowing more time for the transfer to occur. However, to accommodate for intersystem crossing and the ΔE between the accepting state at an optimum difference at ca. 2500 – 4000 cm^{-1}, the energy of the excited singlet state would have to be quite high; in other words, the excitation energy required would also have to be high, usually in the UV region. It is not ideal for any applications to use a high energy excitation source; it causes photo-damage to living cells in biological applications and is hazardous in material applications.

To shift the excitation to a longer wavelength, alternate energy transfer pathway has to be introduced. In late 1960s, Kleinerman's work[13] proposed that energy transfer from an excited singlet state could dominate intersystem crossing. Progress on more elucidation or experimental proof have stalled since, though, until in the 21st century when research on sensitization from the singlet delocalized intraligand charge transfer (ILCT) state picked up pace and more Ln(III) complexes with ILCT sensitization were reported.[84-89]

Charge transfer states are generally present in structures with electron-donating and accepting moieties conjugated by a π-system (D-π-A) in a push-pull fashion and differ distinctly from the ground states in both molecular geometry and electronic structure,[90-91] hence resulting in a vast difference of the electron density of the donor and acceptor before and after photoexcitation. The delocalized nature renders charge transfer states to situate around the visible light region and the emission can be further shifted by modifying the strength of the donor and/or acceptor. The emission and absorption bands of charge transfer transitions are broad and structureless and a large Stokes shift is observed due to the rearrangement of electronic density to give a marked difference in the dipole moments of the ground and excited states.

In 2004, Yang et al.[92] reported a 'direct observation' europium(III) sensitization *via* the singlet pathway using **EuL1** from results of time-resolved luminescence spectroscopic experiments. They observed that on the nanosecond timescale, the rise time of $^5D_1 \rightarrow {}^7F_3$ transition of Eu(III) matches well with the decay time of the $S_1 \rightarrow S_0$ fluorescence of the ligand (1.8 ns). Furthermore, they correlated the decay of $^5D_1 \rightarrow {}^7F_{1-3}$ transitions (387 ns) with the rise of $^5D_0 \rightarrow {}^7F_2$ transition (392 ns), postulating the transfer of excited state energy from $^5D_1$ to $^5D_0$. While these results suggested energy transfer from the excited singlet state of the ligand to first the $^5D_1$ then $^5D_0$ of Eu(III), the authors also obtained an emission spectrum of the Eu(III) complex at 77 K which consisted of a broad and asymmetric phosphorescence band with a lifetime of 3.9 s; compared to the 0.65 ms of Eu(III), they excluded the possibility of the triplet-mediated energy transfer pathway, stating it as 'inactive'.

The group then followed up with their work by studying the excited state dynamics of the same complex.[93] A ligand-to-metal charge transfer (LMCT) state was proposed which effectively quenches the excited singlet state by 98 %, dominating over intersystem crossing, hindering the triplet-mediated energy transfer pathway and concluded with a non-triplet sensitization pathway.

This chapter set out to continue along this direction and further elucidate the character of this non-triplet sensitization pathway which seemingly efficiently sensitizes Eu(III) luminescence. Sensitization of Tb(III) *via* ILCT transitions are rarely seen due to the high energy of $^5D_4$ level, yet the potential of Sm(III) sensitization but this ligand system will be explored as well.

3.1.3. Solvatochromism

The environment also has a role to play in charge transfer transitions. The polarity of solvent molecules governs the extent of stabilization of the ground and excited states, leading to a different ΔE that would be reflected in absorption and emission spectra.[94] This phenomenon describing the correlation between increasing solvent polarity and the energy of a molecule is called solvatochromism, as depicted in Figure 3.2. If the ground state is more polar than the excited state, an increase in solvent polarity will stabilize the ground state to a greater extent than the non-polar excited state, resulting in a larger energy gap and a higher energy absorption band; this is termed negative solvatochromism. If the ground state is less polar relative to the excited state, a smaller energy gap will be observed in polar environments and the absorption band will be observed in a higher wavelength region. Therefore, the nature of solvatochromism could be determined by simply measuring the absorption spectra in solvents of different polarities.[95]

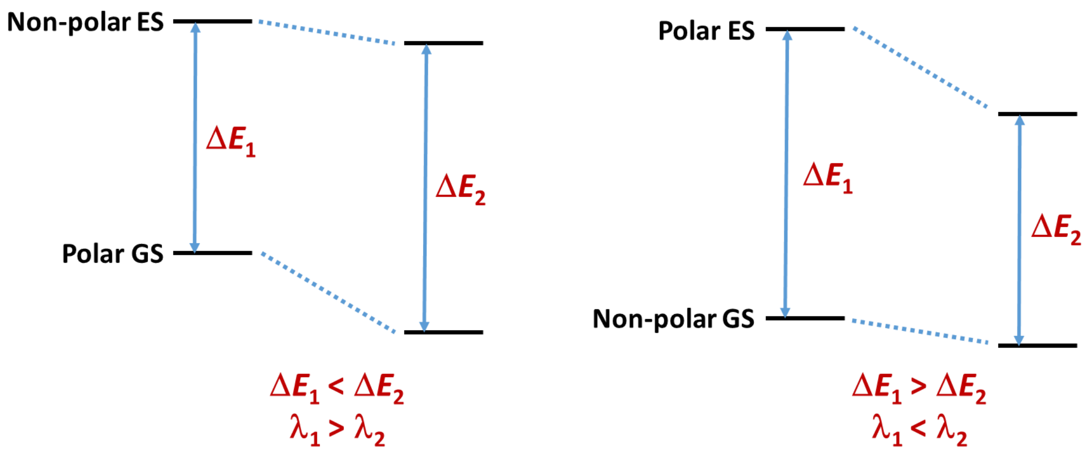

Figure 3. 2 Depiction of negative (left) and positive (right) solvatochromism in polar environment

In this work, the shift in energy level of the ILCT states would lead to different sensitization efficiencies of lanthanide luminescence. Optimum sensitization could be probed in solvatochromic experiments. Various interactions between the charge transfer chromophore and solvents molecules were investigated and the effects were revealed in detailed photophysical measurements.

3.2. Results and Discussion

3.2.1. Structural Characterization

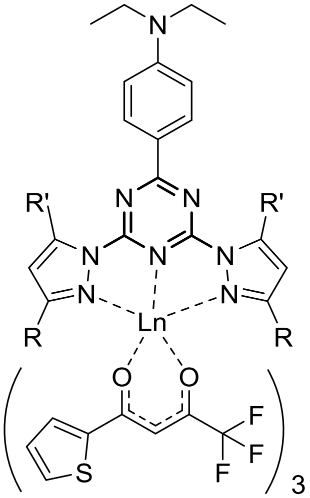

LnL1: R'=R=CH_3
LnL2: R'=H, R=H
LnL3: R'=R=H

Figure 3. 3 Structures of LnL1-3 used in this work

Europium(III) and samarium(III) complexes of the above structures were synthesized for this study. Unfortunately, crystal structures could not be obtained. Mass spectrometry was able to reveal formation of the complex, but obtaining structural information would aid in correlating the experimental results to elucidate the energy transfer pathway. A newly-developed computation software developed by a research group in Brazil was used to simulate the structure of our complexes – Lanthanide **LUM**inescence **PAC**kage Software.[96,97]

The structures of **SmL1-3** were optimized by LUMPAC using the Sparkle/RM1 model and are shown in Figure 3.4. The molecules are highly asymmetric due to the 'freely' coordinated TTA moieties (C1 space group) but the significance of finding out the geometry lies in the tridentate ligand. The differing methyl groups on the pyrazole rings of **SmL1-3** have little effect on the overall geometry of the ligand, as expected due to their relatively peripheral positions. The skeleton from the diethylanilinyl terminus to the triazine core is planar as well, which would lead us to expect that the rigidity of the molecule would result in higher energy transfer efficiency.

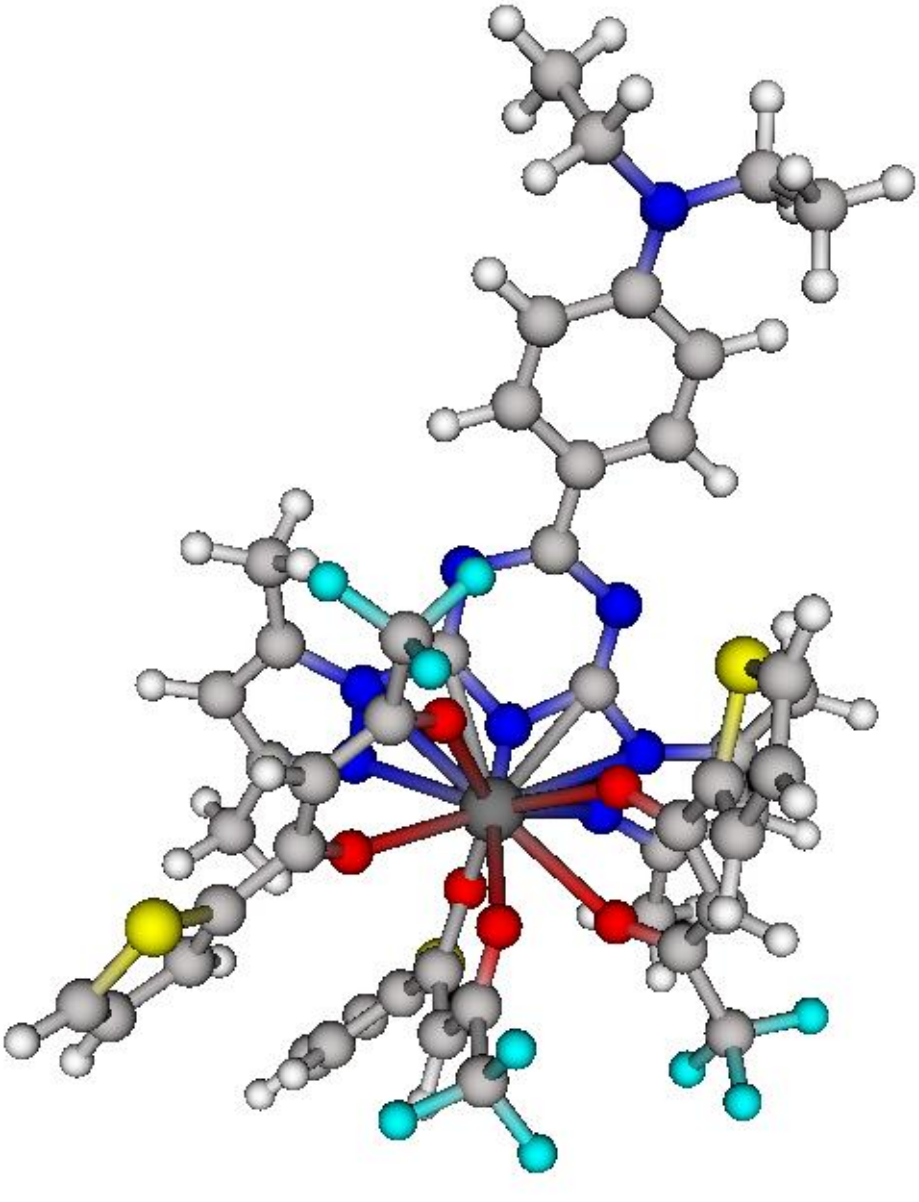

Figure 3. 4 Optimized structure of SmL1

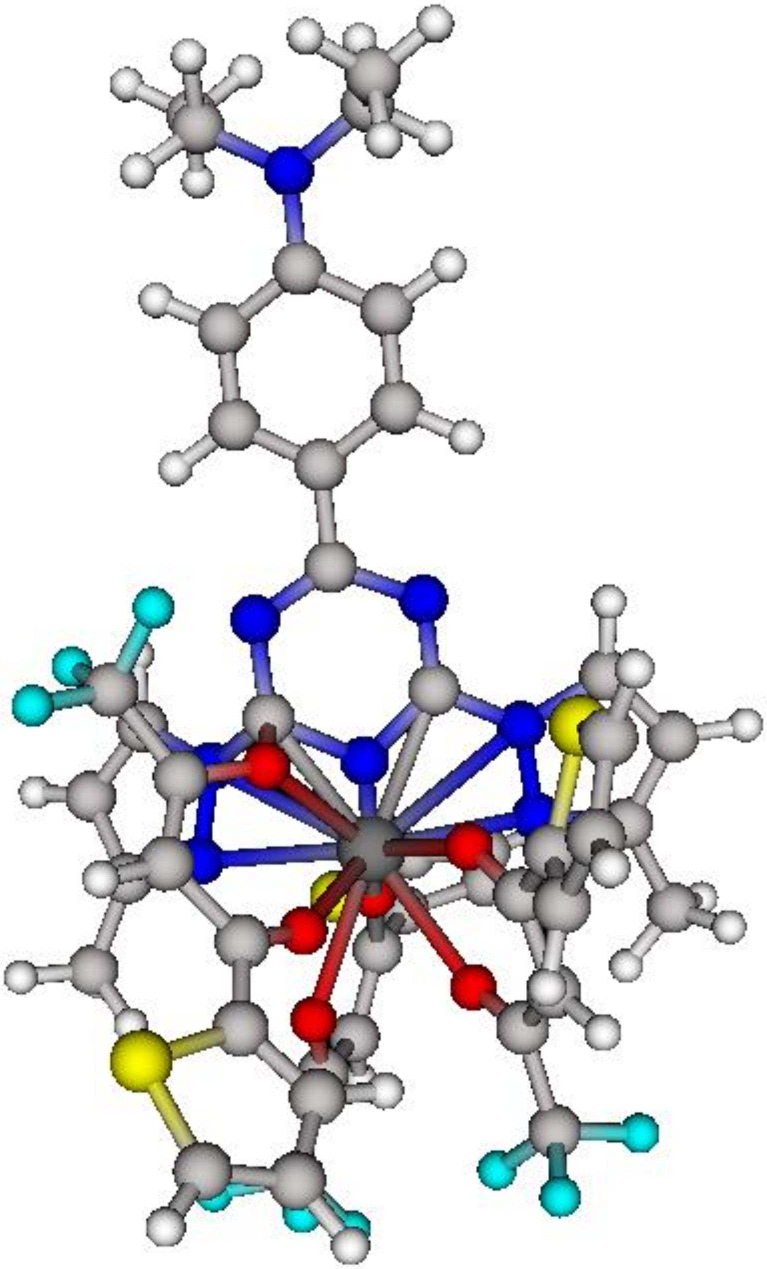

Figure 3. 5 Optimized structure of SmL2

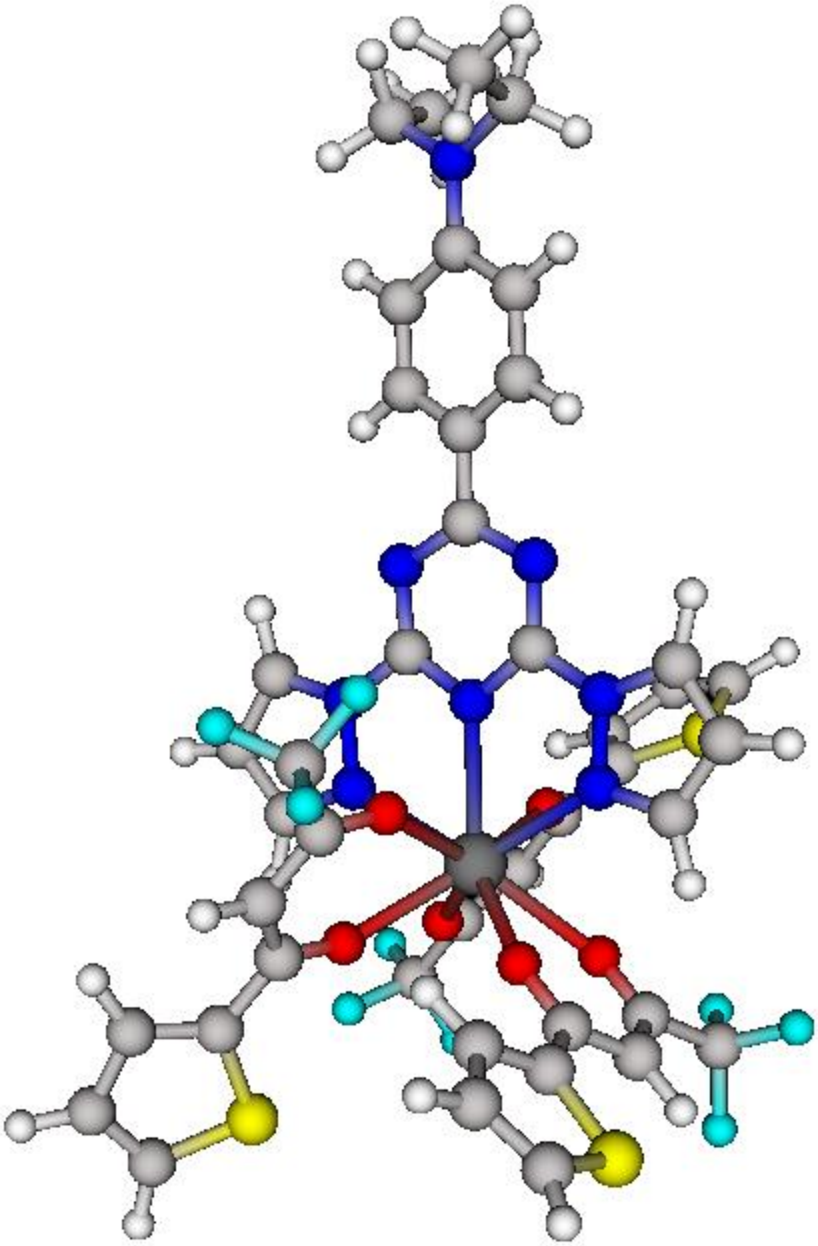

Figure 3. 6 Optimized structure of SmL3

The radii of Eu(III) and Sm(III) are very similar, 95.8 and 94.7 pm hence it is believed the two set of complexes would be isostructural.

3.2.2. Photophysical Studies

Absorption and Excitation Spectra

The absorption and excitation spectra were obtained in various solvents with different polarity – evaluated by the dipole moment. Besides dipole-dipole interactions, this study will also look into the effect of hydrogen bonding on the lone-pair electrons on the anilinyl nitrogen atom and nucleophilic solvents on the luminescent Ln(III) center.

The complexes, **EuL1-3** and **SmL1-3**, exhibit consistent absorption profiles in various solvents. The absorption band before 300 nm corresponds to the π-π* absorption of the bis(pyrazol-1-yl)-1,3,5-triazine scaffold and another band with its maximum at around 340 nm is the π-π* absorption of the TTA moiety. Excitation spectra were monitored from the most intense f-f transitions, which were $^5D_0 \rightarrow {}^7F_2$ for and $^4G_{5/2} \rightarrow {}^6H_{9/2}$ for Eu(III) and Sm(III) respectively.

The ILCT absorption band, as mentioned previously, is sensitive to the polarity of the environment and hence the absorption maximum exhibits a blue shift with increasing solvent polarity, i.e. negative solvatochromism. The shift of the band may cause it to merge with the TTA absorption such as the case in acetone, or remain as far as around 400 nm in non-polar solvents. Protic solvents such as methanol, isopropanol and highly polar solvents like DMSO would also form hydrogen bonds with the lone-pair electrons on the anilinyl nitrogen, hindering the formation the ILCT transition, as reflected in the weakened absorption intensities. As expected, the excitation spectra did not always superimpose with the absorption spectra, implying different extents of sensitization from the ILCT band.

For **EuL1**, the excitation bands of the TTA moiety are clearly visible in the spectra in all solvents, and showed minimal deviation from the absorption maxima, indicating the TTA's insensitivity towards polarity. The excitation bands of the ILCT bands display a clear blue-shift as the solvent polarity increases. In non-polar solvents such as benzene (Figure 3.9) and toluene (Figure 3.17), the ILCT absorption maxima is at around 405 nm. Increase in solvent polarity from methanol (Figure 3.15) shifts the maxima to around 380 nm. Comparison between the absorption and excitation revealed that the polarity of the environment plays an important role in governing whether the ILCT band would be able to take part in the sensitization of lanthanide luminescence.

In some solvents, notably acetonitrile (Figure 3.8) and DMSO (Figure 3.12), the ILCT absorption bands are sometimes rather distinct, even though excitation of the band does not sensitize lanthanide(III) luminescence. It is believed that their highly polarizing nature (dielectric constant (ε) = 37.5 and 46.7 respectively) enhances the rate of charge transfer from the donor to the acceptor to an extent that dipole-dipole stabilization between the solvent and compound is insignificant compared to the time required to reach electrostatic equilibrium instantaneously.

The absorption spectra for **EuL2** and **EuL3** (Figures 3.18-3.41) as well as the Sm(III) analogs (Figures 3.42-4.77) are expectedly similar as well, as the methyl substituents on the pyrazoles are irrelevant to the photophysical properties of both the TTA and ILCT moieties.

Emission Spectra (Eu(III))

The emission spectra for the complexes were measured with three different excitation wavelengths – 330, 350 and 390 nm. Irradiation at 330 nm only excites the TTA moiety and whereas 390 nm would only excite the ILCT transition. Thus, 350 nm was chosen as a median excitation wavelength which could potentially excite both the TTA and ILCT transitions. The $^5D_0 \rightarrow {}^7F_J$ transitions (ΔJ = 0–4 at 578, 590, 612, 650 and 695 nm respectively) could be observed as a result of antenna effect.

Excitation at 330 and 350 nm produced expectedly good sensitization of Eu(III) luminescence, with little residual fluorescence, indicating efficient energy transfer from TTA. Solvent polarity had minimal effect towards the sensitization process, which is consistent with the absorption spectra.

On the other hand, the ILCT band is shifted to higher energy in polar solvents and is often not at an appropriate level for energy transfer, resulting in ligand fluorescence. In non-polar solvents, the luminescence intensities of ILCT excitation in non-polar solvents were indeed quite high. Taking the molecular structure into consideration, one molecule of the ILCT-character ligand is able to sensitize Eu(III) luminescence as much as, if not higher than, three molecules of the well-known good sensitizer TTA. Even though ILCT sensitization is decent, ligand fluorescence was sometimes still observed. It is attributed by the short lifetime of the excited ILCT non-triplet state, resulting in competition between fluorescence and sensitization as deactivation pathways.

The hypersensitive $^5D_0 \rightarrow {}^7F_2$ transition of Eu(III) is extremely sensitive to the change of coordination environment. Although the determination of coordination geometry and structural symmetry is much difficult in solution state than in solid state, the splitting patterns as well as luminescence intensities in different solvents would be a useful factor to compare the environment around Eu(III). In benzene and toluene, the splitting patterns of the hypersensitive transition is consistent for all three excitation wavelengths, implying that the coordination environment is near identical. The splitting patterns are different for 390 nm excitation from 330 and 350 nm excitations in polar solvents, however, and this indicates that there are at least two solution-state structures that are excited by different energies.

The difference in methyl substituents amongst the ligands had minimal effect on the absorption and excitation spectra in various solvents; but it could be observed from the splitting patterns from the emission spectra of the same solvent of different complexes, demonstrating the hypersensitivity of the transition.

The asymmetry ratio is defined as the ratio between the integrated intensities of the $^5D_0 \rightarrow {}^7F_2$ and $^5D_0 \rightarrow {}^7F_1$ transitions of a Eu(III) molecule. The former transition is a forced electric dipole transition with the transition intensity proportional to the square of ligand dipolar polarizability;[6,98] the latter is a magnetic dipole transition which is independent of the environment around Eu(III). Theoretically, he $\Delta J = 2$ transition would be absent in a centrosymmetric structure, therefore the asymmetry ratio is strictly a measure of deviation from centrosymmetry. However, solution state structures of organolanthanide complexes are hardly centrosymmetric as the ligands' movements are not restricted, so the asymmetry ratio is commonly used to imply the extent of loss of symmetry. Table 3.1 presents the asymmetry ratio of **EuL3** in increasing solvent polarity to illustrate the different spatial arrangements of ligands around the Eu(III) center in various solvents.

A marked difference could be found between the asymmetry ratios in polar and non-polar solvents, with 12 and 10 in methanol and DMSO respectively compared to 19.5 in benzene when excited at 350 nm. The asymmetry ratio in non-polar solvents were very similar when the excitation was changed to 390 nm. Some asymmetry ratios were not measured as the interference from ligand fluorescence on the europium(III) luminescence are not negligible. The discrepancy of asymmetry ratios between polar and non-polar solvents implies, and reconfirms the earlier postulate, that two emitting species that are excited by different energies are present.

It was mentioned in the beginning that the choice of solvents includes nucleophilic solvents. It is reasonable to deduce that solvent coordination and subsequent displacement of the tridentate ligand would take place, resulting in a totally different coordination environment as indicated by the hypersensitive transitions as well as the asymmetry ratios.

The oxygen and nitrogen atoms on different solvents are also relatively hard donors which the lanthanide(III) centers prefer. In comparison, the triazine-core tridentate ligand has nitrogen donors but are not conjugated with particularly electron-donating groups to increase its donor strength, whereas the solvent molecules with a higher dipole moment – and thus higher donating property – may displace the ligand and generate new emitting species *in situ*. Coordination of solvent molecules, which are much smaller in size than the tridentate ligand, would lead to a significant change in coordination environment due to the rearrangement of spatial distribution among the electrostatically-interacted ligands. The electron-donating properties of the methyl groups give methanol and DMSO high coordination strength, therefore giving the lowest asymmetry ratios. Despite its relatively low dipole moment compared to DMSO, methanol also gives a lower asymmetry ratio; this once again demonstrates the non-direction and sterically-governed nature of bonding with Ln(III) as the small size of methanol molecules allow flexible rearrangement of bonding ligands.

In acetonitrile, the asymmetry ratio at 350 nm excitation is quite high, unlike other polar solvents. It is possibly due to the relative softness compared to the oxygen donors which may be similar to the nitrogen donor of the pyrazoles, therefore not readily displacing the tridentate ligand. However, the asymmetry ratio is drastically different under 390 nm excitation, it is attributed to the poor sensitization which led to more residual ligand fluorescence and thus interfering with the area under curve of the $^5D_0 \rightarrow {}^7F_1$ transition.

The non-polar solvents have lower dipole moment as they do not bear any electronegative atoms (e.g. O, N), therefore displacement of the tridentate ligand is not expected to happen, retaining a high asymmetry ratio.

Excitation at 390 nm does not excite the TTA at all in any solvents. However, in some more polar solvents, such as ethyl acetate and acetonitrile, the emissions were decent enough for measuring the asymmetry ratio, implying sensitization by the ILCT band. While the previous paragraphs postulate ligand displacement by solvent molecules, it is also believed that the displacement may not necessarily be quick – as it should exhibit a concentration-dependence – or complete. The remaining, unperturbed complexes, which may somewhat retain the tridentate ligand, may then still be able to be excited by the ILCT transition and as a result give lanthanide luminescence without exciting TTA. The low ratios, though, is attributed to the interference of the $^5D_0 \rightarrow {}^7F_1$ transition by residual ligand fluorescence.

Table 3. 1 Asymmetry ratio of EuL3 under two excitation wavelengths in various solvents

Solvents	**μ (D)**	**EuL3 *R* (λ_{ex}=350 nm)**	**EuL3 *R* (λ_{ex}=390 nm)**
CCl_4	0	18.4	18.5
Benzene	0	19.5	19.5
Toluene	0.37	19.0	19.2
$CHCl_3$	1.04	17.1	16.9
i-PrOH	1.56	15.3	/
CH_2Cl_2	1.6	14.3	12.4
CH_3OH	1.7	12.0	/
THF	1.75	16.6	/
EA	1.78	16.0	6.5
DCA	1.8	17.1	11.6
Acetone	2.88	16.6	/
CH_3CN	3.92	19.6	6.7
DMSO	3.96	10.0	/

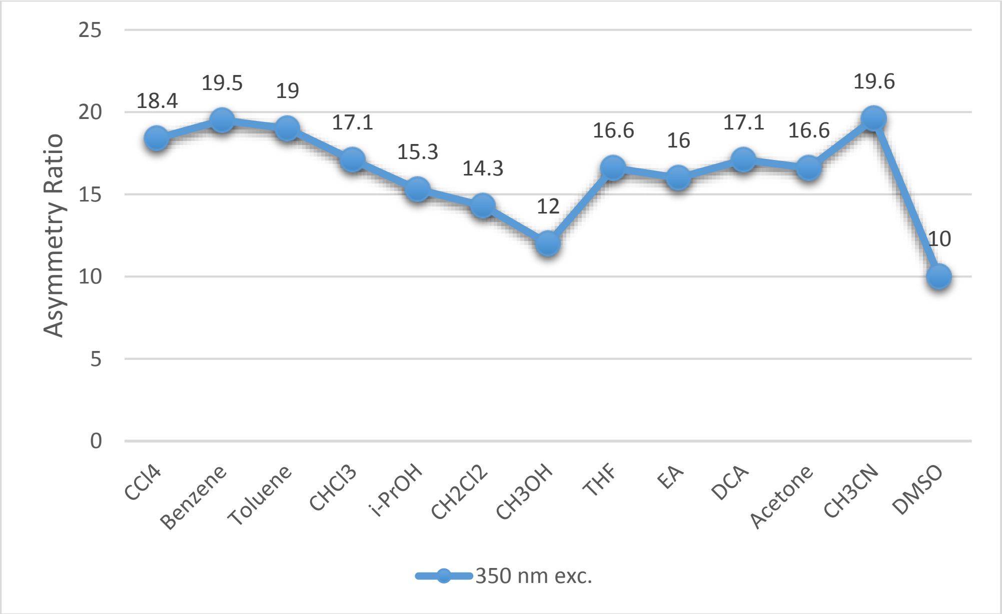

Chart 3. 1 Asymmetry ratios of EuL3 under TTA excitation in different solvents

Chart 3. 2 Asymmetry ratios of EuL3 under ILCT excitation in different solvents

Luminescence Lifetimes (Eu(III))

The excited state lifetime is defined as the average time the excited energy resides at a particular energy level before it decays. The measurement of luminescence lifetimes would indicate the number of radiatively decaying species present in the medium upon photo-excitation, which would provide more insight on the issue of multiple emitting species aforementioned.

Table 3. 2 Emission lifetimes and quantum yields of EuL1-3 in various solvents

Solvent	**μ (D)**	**EuL1 τ (ms) (λ_{ex}=350 nm)**	**EuL2 τ (ms) (λ_{ex}=350 nm)**	**EuL3 τ (ms) (λ_{ex}=350 nm)**	**EuL3 Φ (%) (λ_{ex}=350 nm)**
Benzene	0	0.541	0.472	0.432	23.8
Toluene	0.37	0.577	0.485	0.425	30.6
$CHCl_3$	1.04	0.177; 0.571	0.131; 0.49	0.116; 0.510	n/a
i-PrOH	1.56	0.353	0.353	0.353	17.2
CH_2Cl_2	1.6	0.041; 0.394	0.039; 0.328	0.013; 0.196	n/a
CH_3OH	1.7	0.26; 0.58	0.239; 0.55	0.226 0.547	2.9
CD_3OD	1.7	/	/	0.315; 1.109	/
THF	1.75	0.374	0.378	0.383	10.7
EA	1.78	0.366	0.357	0.187; 0.397	7.1
Acetone	2.88	0.624	0.607	0.290; 0.578	7.1
CH_3CN	3.92	0.652	0.626	0.618	12.6
DMSO	3.96	0.79; 1.733	0.709; 1.434	0.752	12.9

The luminescence lifetimes, monitored at the $^5D_0 \rightarrow {}^7F_2$ transition, were measured with excitation of the TTA at 350 nm, as excitation of the ILCT band did not give luminescence in all solvents. A general trend of decrease in lifetime with increasing dipole moments of solvents is observed. Bi-exponential lifetimes – denoting two radiatively decaying species – were obtained in chlorinated solvents and several polar solvents.

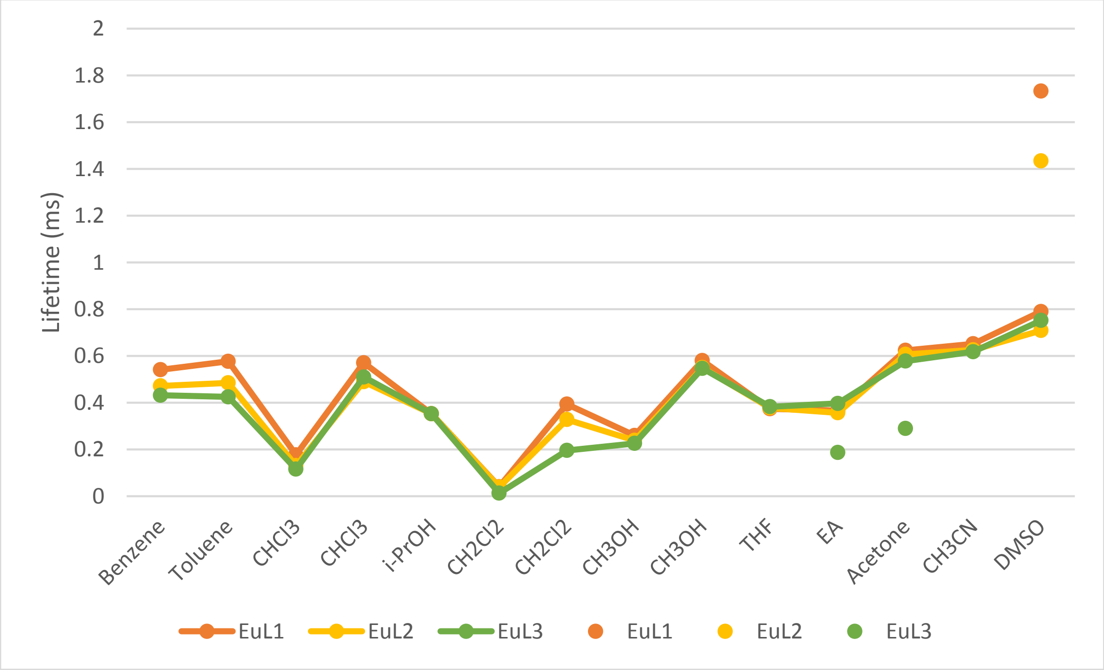

Chart 3. 3 Luminescence lifetimes of EuL1-3 in various solvents

In methanol, which is strongly coordinating, bi-exponential lifetimes were measured for all three Eu(III) complexes. This further corroborates with the previous postulate that displacement of the tridentate ligand by solvent molecule led to the formation of a new species of different coordination environment. The decaying species with a shorter lifetime would correspond to the species with solvent coordination, as high energy oscillators (e.g. O-H, N-H) would effectively quench the excited energy levels of europium(III). The longer lifetime could either be the original molecule with the tridentate ligand retained or simply lesser coordinating solvent molecules. This phenomenon is also observed in the lifetimes of ethyl acetate and acetone in **EuL3**, of which is believed to be due to solvent coordination of the oxygen atom as well.

To demonstrate the effect of non-radiative multiphonon quenching by the oscillators, the luminescence lifetimes were also measured in deuterated methanol, in which the O-H oscillator (νO-H: 3500 cm^{-1}) was replaced with a lower energy O-D oscillator (νO-D: 3900 cm^{-1}). The emission lifetimes of **EuL3** in methanol-d_4 was significantly longer than the luminescence lifetime in methanol. According to the *m* equation below (refer to chapter 1), the lifetimes of ordinary and deuterated methanol can be used to calculate the number of methanol molecules coordinated onto the europium(III) center. The *m* value was found to be 1.9, hence approximately two methanol molecules are coordinated onto Eu(III), implying ligand displacement as well.

$$m^{Ln(III)} = A[(1/\tau_{MeOH})-(1/\tau_{MeOD})-0.125);\ A = 2.4\text{ ms for Eu(III)}$$

It is also interesting to note that, bi-exponential lifetimes were obtained in DMSO for **EuL1** (Figure 3.83) and **EuL2** (Figure 3.91) but not **EuL3** (Figure 3.103). The lifetime of **EuL3** in DMSO is similar to the shorter one of the two of **EuL2** and **EuL3**. In ethyl acetate and acetone, on the contrary, the lifetimes of **EuL1** (Figure 3.84) and **EuL2** (Figure 3.92) are mono-exponential whereas two decay species were observed in **EuL3** (Figure 3.104). The inconsistency of the number of decaying species in the same solvent among different compounds implies that donor strength is not the only factor governing ligand displacement. A shorter lifetime was observed in ethyl acetate and acetone for **EuL3** only, and the longer lifetime could only be observed in **EuL1** and **EuL2** in DMSO.

These two sets of lifetimes imply to a better protection of the Eu(III) center by the surrounding ligands in which, despite the strength of donor strength of the molecules, does not lead to ligand displacement in **EuL1** and **EuL2** or incomplete displacement in **EuL3**. These results once again demonstrate that steric factors also play a deciding role in lanthanide(III) bonding interactions.

Luminescence Quantum Yields (Eu(III))

The relative luminescence quantum yields[99] of **EuL1-3** were measured against quinine sulfate ($\Phi = 0.577$, $\lambda_{ex} = 350$ nm)[100] at excitation of 350 nm. Ideally, the excitation wavelengths and the emission regions of the standard and the sample should be similar for ideal comparison; however, the pseudo-Stokes shift of lanthanide(III) complexes makes it difficult to find a suitable standard. Hence, the excitation wavelength was chosen to be constant and the emissions at different regions were corrected to instrumental response in order to compensate for the different sensitivities.

Fluorescence quantum yield is proportional to the fluorescence lifetime ($k_r = \Phi/\tau$), and the relationship is legitimately demonstrated in the luminescence quantum yields and lifetimes of the complexes. Likewise, the luminescence quantum yields were higher in non-polar solvents than in polar and/or coordinating solvents. Decent values were obtained in benzene and toluene and the quantum efficiency in methanol is expectedly low.

The luminescence quantum yield measured by relative method is fundamentally a measure of the ratio of photon input to the antenna and the photon output of the lanthanide center. The antenna effect is implied but not taken into account, it is therefore also more appropriately the overall quantum yield of the lanthanide(III) complex system. As discussed in chapter 1, it is possible to determine the sensitization efficiency by measuring the overall quantum yield and the intrinsic quantum yield of the complex – the latter denotes the luminescence quantum yield in which the Ln(III) was directly excited. The relationship could also be calculated on the basis of Judd-Ofelt parameters:

$$\eta_{sens} = \frac{Q_L^{Ln}}{Q_{Ln}^{Ln}} = Q_L^{Ln}\frac{\tau^{rad}}{\tau_{obs}}; \quad \frac{1}{\tau^{rad}} = A_{MD,0}\cdot n^3\left(\frac{I_{tot}}{I_{MD}}\right)$$

The intrinsic quantum yields (Q_{Ln}^{Ln}) were then obtained with the help of luminescence lifetimes and the emission spectra, and Table 3.3 summarizes the overall and intrinsic quantum yields as well as the calculated sensitization efficiencies in various solvents.

Table 3. 3 Overall and intrinsic quantum yields and sensitization efficiency of EuL3 (TTA Excitation at 350 nm)

Solvent	**μ (D)**	**$Q^{Ln}{}_L$ (%, TTA)**	**$Q^{Ln}{}_{Ln}$ (%, TTA)**	**η_{sens} (%,TTA)**
CCl_4	0	/	n/a	n/a
Benzene	0	23.8	40	59.5
Toluene	0.37	30.6	37	82.6
$CHCl_3$	1.04	/	n/a	n/a
i-PrOH	1.56	17.2	29	59.2
CH_2Cl_2	1.6	/	n/a	n/a
CH_3OH	1.7	2.9	13.7	21.2
THF	1.75	10.7	33	32.4
EA	1.78	7.1	13.6	52
Acetone	2.88	7.1	23	31
CH_3CN	3.92	12.6	53.8	23.4
DMSO	3.96	12.9	52.9	24.4

The computed intrinsic quantum yield concerns the competitive deactivation pathways of the excited energy of the antenna with energy transfer, compared to directly exciting the Ln(III) center without involving the energy levels of the antenna. The values are in an apparent trend of decreasing intrinsic quantum yield with increasing solvent polarity.

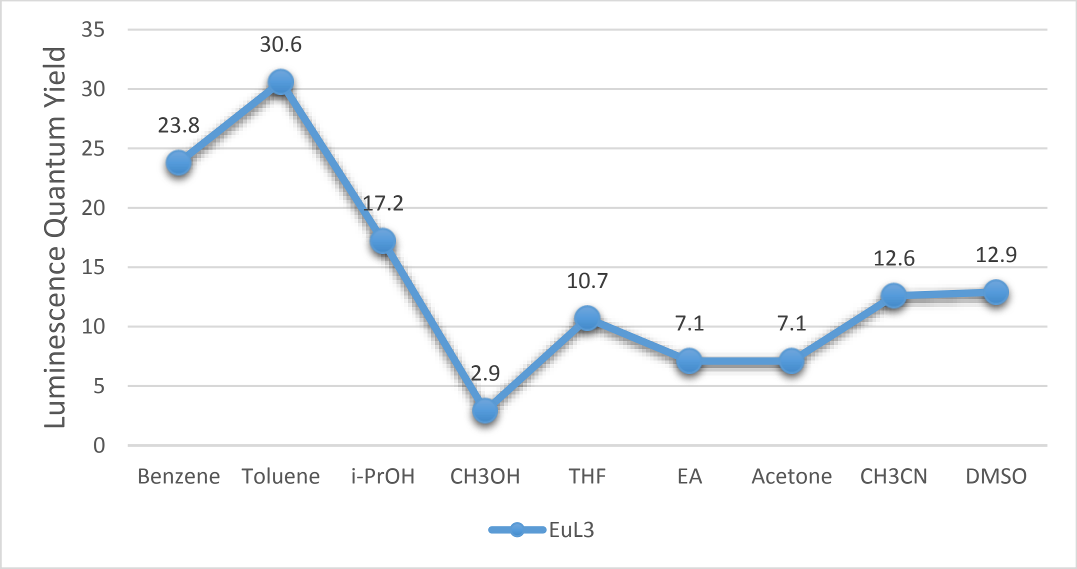

Chart 3. 4 Luminescence quantum yields of EuL3 in various solvents

The π-π interaction of benzene/toluene molecules and the planar tridentate ligand is an important factor that imparted rigidity to the complex in solution state, minimizing vibrational energy loss. The inability of the solvent molecules to coordinate also minimizes non-radiative quenching by oscillators, which is also the case for isopropanol and tetrahydrofuran, as their molecular size may be too large to coordinate. In other solvents, the quantum yield decreases noticeably as the solvent coordinating strength increases, indicating that non-radiative quenching by solvent oscillators dominates f-f transition decay. The same observation that the most polar solvents do not have the lowest value of intrinsic quantum yields is consistent with the luminescence lifetimes.

One would notice that in acetonitrile and DMSO, the intrinsic quantum yields are indeed higher than in non-polar solvents, the same exception was observed in luminescence lifetimes but not overall quantum yields. The results imply the excited energy at the excited states of the antenna has a larger probability of undergoing radiative decay. It is postulated that the strong dipole-dipole interaction between the solvent molecules and the D-π-A structure would lead to a stabilization effect similar to π-π interaction and reduces the flexibility of the molecule. Note that excitation of the TTA does not lead to a charge transfer process hence the D-π-A structure would be obtained, which justifies the postulate while the poor sensitization at 390 nm excitation is due to re-distribution of electronic density of the D-π-A structure.

The sensitization efficiency is a ratio of the intrinsic and overall quantum yield; while simple, it represents the extent of excited energy loss prior to energy transfer to the excited states of Ln(III) upon photoexcitation of the antenna. In Table 3.3, the sensitization efficiencies exhibit a different trend than the intrinsic quantum yields. The efficiency is quite high in benzene and toluene, reasonably due to the rigidity leading to more efficient energy transfer. In polar solvents, though, the sensitization efficiencies are similar and are rather independent of solvent polarity and coordination strength.

Table 3. 4 Overall and intrinsic quantum yield and sensitization efficiency of EuL3 (ILCT Excitation)

Solvent	μ (D)	Q^{Ln}_{L} (%, ILCT)	Q^{Ln}_{Ln} (%, ILCT)	η_{sens} (%, ILCT)
CCl_4	0	31	43	75
Benzene	0	32	53	61
Toluene	0.37	30	51	59
$CHCl_3$	1.04	18	46	37
CH_2Cl_2	1.6	6	27	22

The absolute overall quantum yields of **EuL3** at excitation of the ILCT band were also measured using an integrating sphere. Solvents in which the complex was able to show negligible interference from ligand fluorescence were used for measurements and the results, including the calculated intrinsic quantum yields and sensitization efficiencies are summarized above in Table 3.4. The absolute and intrinsic quantum yields of benzene and toluene are quite similar.

Compared to excitation of TTA, the overall quantum yields were similar as well, scientifically confirming the similar intensities observed in the emission spectra in these two solvents. The sensitization efficiencies are quite different, though. Aromatic in nature and with 0 and 0.37 net dipole moments respectively, the interactions between benzene, toluene and the planar tridentate ligand with ICLT character is believed to be very similar, neither having any perturbation towards the lone pair electrons on the *N*,*N*-diethylanilinyl nitrogen atom. Alternatively, when the chromophore of interest is the TTA, the interaction between the solvents and the TTA molecules should be different, according to the sensitization efficiencies in Table 3.3. The enhanced value in toluene led to a higher overall quantum yield in spite of a lower intrinsic quantum yield. It is postulated that the aromatic thiophene moiety on TTA may interact differently with the benzene and toluene, in which certain non-radiative quenching processes is facilitated by the former and not the latter, resulting in the discrepancy.

The absolute quantum yields of the chlorinated solvents demonstrated a clear relationship of stabilization of the polar ILCT ground state with solvent polarity. As the dipole moment increases, the ILCT ground state is further stabilized and the mismatch between energy levels increases; this could be reflected in the gradually drastic decrease in the overall quantum yields as well as the sensitization efficiencies in from carbon tetrachloride to dichloromethane.

Emission Spectra (Sm(III))

The emission spectra for the Sm(III) complexes were measured with the same three excitation wavelengths, as the project intended to compare the sensitization of Sm(III) luminescence with Eu(III) due to their proximal emitting states (Figure 3.1). The visible $^4G_{5/2} \rightarrow {}^6H_J$ transitions were obtained by antenna effect. The f-f transitions of J = 5/2, 7/2, 9/2, 11/2 are found near 563, 599, 645 and 704 nm, with minute shifts in various conditions.

Table 3. 5 Asymmetry ratio of SmL3 under two excitation wavelengths in different solvents

Solvents	μ (D)	SmL3 *R* (λ_{ex}=350 nm)	SmL3 *R* (λ_{ex}=390 nm)
CCl_4	0	10.8	12.8
Benzene	0	10.6	10.2
Toluene	0.37	10.7	10.5
$CHCl_3$	1.04	8.8	6.8
i-PrOH	1.56	2.8	/
CH_2Cl_2	1.6	5.4	3.8
CH_3OH	1.7	3.0	/
THF	1.75	5.3	/
EA	1.78	3.7	/
DCA	1.8	4.6	/
Acetone	2.88	2.7	/
CH_3CN	3.92	4.7	/
DMSO	3.96	2.1	/

Excitation of the TTA at 330 and 350 nm were also able to sensitize Sm(III) luminescence with little residual TTA fluorescence. Similar to Eu(III), it also showed no intensity-dependence with solvent polarity. Sensitization was also observed when the ILCT band was excited at 390 nm in non-polar solvents, whereas intense ligand fluorescence was observed in polar solvents. These trends were consistent with the europium(III) complexes, proving that similar energy transfer pathways were undertaken by the excited energy to sensitize both Eu(III) and Sm(III).

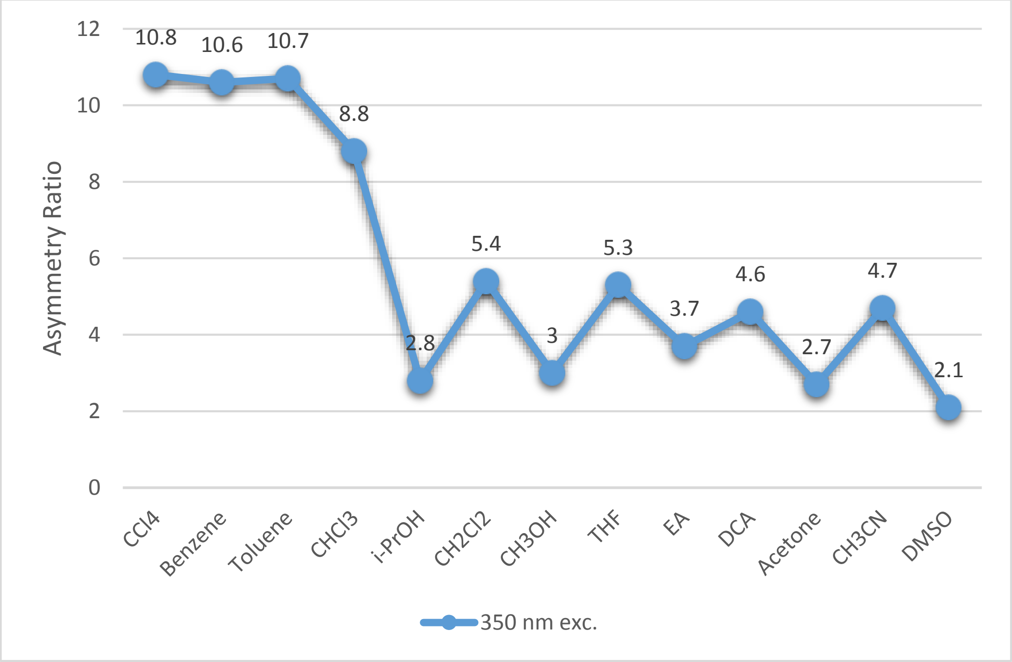

Chart 3. 5 Asymmetry ratio of SmL3 under TTA excitation in different solvents

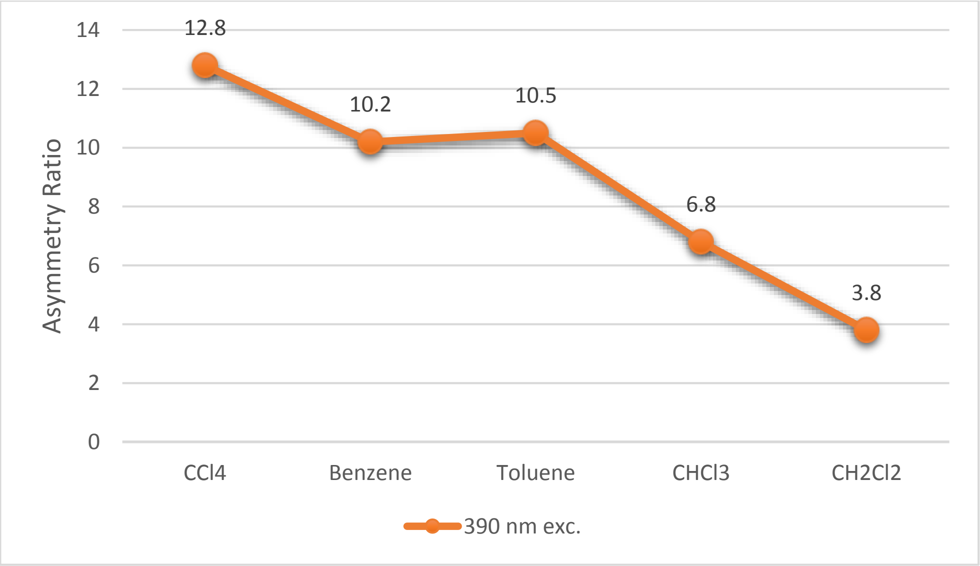

Chart 3. 6 Asymmetry ratio of SmL3 under ILCT excitation in different solvents

Sm(III) does not have a hypersensitive transition like Eu(III), but it is a common practice to compare the $^4G_{5/2} \rightarrow {}^6H_{9/2}$ and $^4G_{5/2} \rightarrow {}^6H_{5/2}$ transitions, of which the former is 'semi-hypersensitive' and the latter is predominantly a magnetic dipole transition (i.e. insensitive to environment). As seen in Table 3.5 and Chart 3.4, the asymmetry ratios decrease gradually with increasing dipole moments, with a sudden drop from isopropanol onwards, due to the ability to coordinate to Ln(III). The zig-zag trend onwards represents the difference in coordination strengths between oxygen and nitrogen atoms, as well as the steric hindrance of the solvent molecules with the same donor atom, as in the case of tetrahydrofuran.

When the ILCT transition is excited, the asymmetry ratios are gradually decreasing as the dipole moment increase, similar to that observed with Eu(III) and TTA excitation of **SmL3**.

Luminescence Lifetimes (Sm(III))

The luminescence lifetimes were measured at the most intense $^4G_{5/2} \rightarrow {}^6H_{9/2}$ transition under excitation at 350 nm. The trend of decreasing lifetime with increasing solvent polarity is observed for the samarium(III) complexes as well, with slightly higher lifetimes for ethyl acetate and acetonitrile amongst the polar solvents. Bi-exponential lifetimes were obtained in chloroform (Figures 3.114, 3.125, 3.137) dichloromethane (Figures 3.114, 3.126, 3.139) and acetonitrile (Figures 3.110, 3.134).

Table 3. 6 Emission lifetimes of SmL1-3 in various solvents

Solvent	μ (D)	SmL1 τ (μs) (λ_{ex}=350 nm)	SmL2 τ (μs) (λ_{ex}=350 nm)	SmL3 τ (μs) (λ_{ex}=350 nm)
CCl_4	0	134	133	159
Benzene	0	114	113	106
Benzene-d_6	0	103	126.9	123.9
Toluene	0.37	102	103	93.5
$CHCl_3$	1.04	66.3; 124.2	64; 206	27; 118.2
i-PrOH	1.56	22.8	21.9	22.4
CH_2Cl_2	1.6	27.8; 102.2	26.8; 89.1	22.4; 120.9
CD_2Cl_2	1.6	40.1; 93.6	47.4; 104.7	27; 163.8
CH_3OH	1.7	12.7	12.3	15.9
CD_3OD	1.7	132	131.9	130.9
THF	1.75	30.7	30.7	34.3
EA	1.78	54.7	57.7	58.7
Acetone	2.88	24.9	96.0	26.1
CH_3CN	3.92	71.2; 109.3	98.1; 261.4	55.6; 174.1
CD_3CN	3.92	84.8; 173.3	95; 191.8	73.1; 162.9
DMSO	3.96	28.8	28.9	25.9

The coordination of solvent molecules enhances the quenching of excited energy by high energy oscillators, as are the cases in hard donors like isopropanol, methanol, tetrahydrofuran, acetone and dimethyl sulfoxide. The bi-exponential lifetimes in acetonitrile could be explained by the presence of two emitting species of significantly different lifetimes, attributed to partial displacement of the tridentate ligand arising from the relatively soft donors of the C≡N. It is interesting to note that, the luminescence lifetimes of **EuL1-2** were not bi-exponential decays in acetonitrile but in DMSO; whereas **SmL1-3** exhibited strictly mono-exponential decays in DMSO. It is postulated that the size difference between Sm(III) and Eu(III) ions may be the slight but distinct reason for the results, resulting in different ligand arrangements to protect the Ln(III) center from solvent molecules.

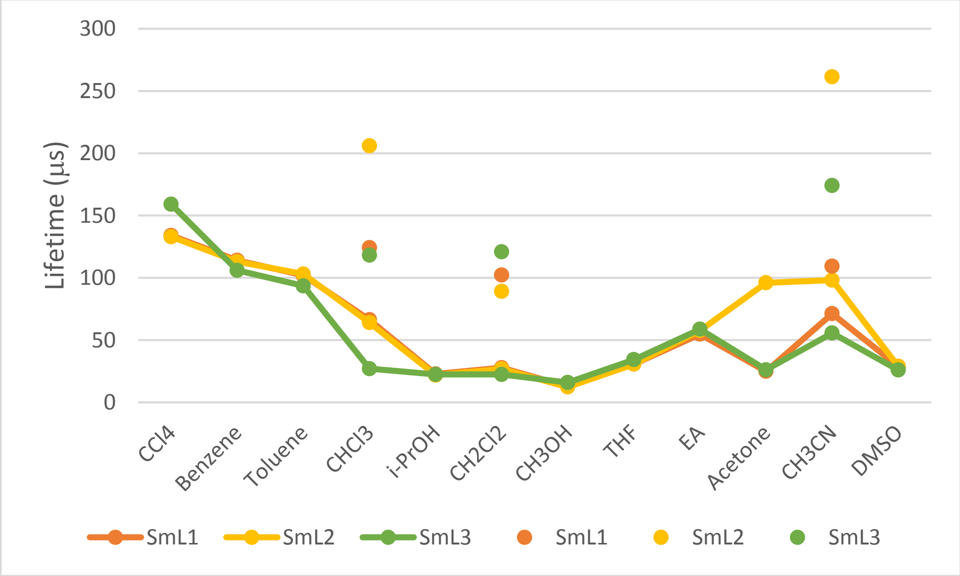

Chart 3. 7 Luminescence lifetimes of SmL1-3 in various solvents

The deuterated counterparts of three solvents with none, moderate and large dipole moments were chosen to investigate the extent of solvent coordination on the three Sm(III) complexes. For the non-polar benzene-d_6, the lifetimes measured were very similar with benzene. In the highly polar acetonitrile-d_3, two emitting species were still observed – eliminating the possibility of incidental instability – and the lifetimes were slightly variant compared to acetonitrile. However, the slight change could not rule out solvent coordination as C≡N may not be an efficient quenching of the excited state energy. The moderately polar methanol-d_4, on the other hand, gave nearly a 10-time increase in the mono-exponential lifetime, indicating only one emitting species was present and the excited energy was quenched by the O-H oscillators in methanol. Using the equation below, the *m* value for **SmL1-3** are 3.6, 3.7 and 2.8 respectively, which is much greater than the 1.9 of **EuL1**, demonstrating once again the different extent of coordination environment attributed to the slight difference in ionic radii of the two Ln(III) ions.

$$m^{\mathrm{Ln(III)}} = A[(1/\tau_{\mathrm{MeOH}})-(1/\tau_{\mathrm{MeOD}})-0.125);\ A = 0.05\ \mathrm{ms\ for\ Sm(III)}$$

Luminescence Quantum Yields (Sm(III))

The luminescence quantum yields were measured against quinine sulfate using the relative method (Table 3.7). Similar to the trend of luminescence lifetimes, the quantum yield drops gradually to a low point at isopropanol along increasing solvent polarity; a recovery was observed in tetrahydrofuran and ethyl acetate only for it to drop again at acetone. The luminescence quantum yield in acetonitrile of **SmL2** is also higher than **SmL1** and **SmL3**, the same in luminescence lifetimes, indicating less efficient quenching particularly in the ligand system with L2.

The intrinsic quantum yields could not be calculated as simply as in Eu(III) compounds so it is not presented here. The sensitization efficiencies for **EuL3** can be viewed as a reference for **SmL1-3** but only in non-polar solvents, as the *m* values calculated for the two analogous series differ, therefore with a higher extent of solvent coordination, the quenching of excited state energies may be different and the intrinsically more complicated energy levels of Sm(III) would also be a factor affecting the actual sensitization efficiency.

Table 3. 7 Relative quantum yields of SmL1-3 in under TTA excitation

Solvent	μ / D	SmL1 (%)	SmL2 (%)	SmL3 (%)
CCl_4	0	4.3	3.9	3.9
Benzene	0	4.5	4.9	3.8
Toluene	0.37	3.9	4.2	3.1
$CHCl_3$	1.04		/	
i-PrOH	1.56	0.82	0.29	0.65
CH_2Cl_2	1.6		/	
CH_3OH	1.7	0.18	0.19	0.14
THF	1.75	1.1	1.2	1.2
EA	1.78	1.4	1.4	1.4
Acetone	2.88	0.65	1.4	0.57
CH_3CN	3.92	0.50	2.3	0.31
DMSO	3.96	0.44	/	0.48

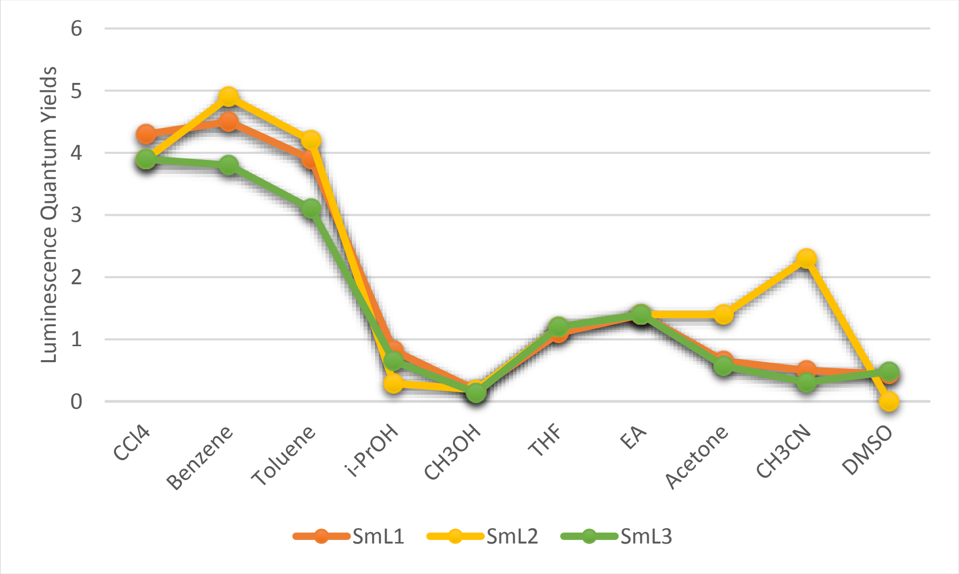

Chart 3. 8 Luminescence quantum yields of SmL1-3 in various solvents

The absolute luminescence quantum yields of **SmL1-3** were also measured with an integrating sphere and the results are summarized in Table 3.8. The excitation wavelength was chosen as the maxima of the excitation spectra corresponding to the ICLT band. The luminescence intensities of the Sm(III) complexes are much weaker than Eu(III) and the calculation of the absolute method using the software provided by Edinburgh Instruments only gave a reading of 2 decimal places, causing a greater degree of error in these measurements. Comparison with the relative quantum yield values did not give a consistent trend across the analogs and amongst the solvents, and the values in chloroform and dichloromethane were zero, therefore these data are strictly for reference only.

Table 3. 8 Absolute quantum yields of SmL1-3 in various solvents

Solvent	**μ (D)**	**SmL1 (%)**	**SmL2 (%)**	**SmL3 (%)**
CCl_4	0	1.7	2	4
Benzene	0	2.3	3	2
Toluene	0.37	0.7	4	2
$CHCl_3$	1.04	0	0	0
CH_2Cl_2	1.6	0	0	0

Instability Issue in Chlorinated Solvents

As seen in this chapter, some quantum yield data concerning chloroform and dichloromethane were left out. The issue was observed in both Eu(III) and Sm(III) complexes and is elaborated in this section. These solvents are relatively non-polar solvents without hard donor atoms, and bonding with Ln(III) ions with neutral chlorine atoms is not expected to occur; however, bi-exponential lifetimes were obtained, which is similar to the coordinating solvents. In the asymmetry ratios in **EuL3** and **SmL3**, a gradual decrease could be observed from carbon tetrachloride to chloroform to dichloromethane, whereas the asymmetry ratio for dichloroethane was similar to dichloromethane, so are their dipole moments (1.8 and 1.6 respectively). It is suspected that the increase in dipole moment would lead to an increase of coordination – due to the electrostatic nature of Ln(III) bonding interactions.

However, this idea grew more complicated in relative quantum yield measurements. In the dilution process to obtain different absorbance of sample solutions, deterioration of the ILCT absorption band is apparently serious. The stability of the complexes in chlorinated solvents is then questioned. Taking into consideration the acquisition time required for lifetime and emission spectra measurements (20 mins *vs.* 2 mins), the stability may not be quick enough – without external agitation as in the case of dilution – to be observed in the latter but more pronounced in the former results, as reflected by the bi-exponential lifetimes in chlorinated solvents. The thermodynamic stability of the complexes was investigated by means of UV-vis absorption.

The Sm(III) complexes were dissolved in selected solvents with low, moderate and high polarity and their UV-vis absorption spectra were monitored for three hours without agitation. Spectra were obtained every 30 seconds. Possible displacement of the tridentate ligand to yield the free ligand was monitored by the rise of absorption at 375 nm. Respective maxima of the ILCT absorption bands in different solvents were monitored, as well as the TTA absorption at 350 nm. Plots of the absorbances at these wavelengths against time were obtained to examine possible scenarios with the chlorinated solvents.

In non-polar solvents, the complexes were very stable, with the absorbances at different wavelengths maintaining at a similar level from t = 0 to three hours. In highly polar solvents, methanol (Figures 3.152, 3.159) and acetonitrile (Figures 3.146, 3.154, 3.161), the absorbances of the TTA and ILCT moieties were stable for the duration as well, and no obvious increase in the free ligand absorption was observed. These stability results are consistent with mono-exponential lifetimes obtained in the same solvents, confirming no solvent coordination in non-polar solvents and very quick solvent coordination – upon dissolution – by highly polar solvent molecules.

In chlorinated solvents, however, the deterioration of the ILCT band was quite consistent amongst the complexes. By monitoring the absorption peak maxima of the ILCT absorption bands, it was found that, for all the complexes, the ILCT band deteriorated to almost zero absorbance at around 30 and 100 minutes after dissolution in carbon tetrachloride (Figures 3.148, 3.156, 3.162) and chloroform (Figures 3.149, 3.163) respectively. In dichloromethane (Figures 3.150, 3.157, 3.164) the deterioration was slower and did not reach zero absorbances after three hours. These results hinted at a relationship between the number of chlorine atoms in the solvent and rate of deterioration. The bi-exponential luminescence lifetimes of **SmL1-3** in chloroform and dichloromethane corroborated with these results.

The presence of water was suspected to be displacing the tridentate ligand. Nonetheless, the complexes were stable in water-miscible solvents such as methanol and acetonitrile, and the use of calcium hydride – a common drying agent – did not resolve the issue, water was ruled out to be the cause. Due to the instability issues, the quantum yields could not be measured and thus are not reported.

It was suspected that photo-degradation of the chlorinated solvents produced hydrogen chloride, which protonates the nitrogen atoms on the tridentate ligand and causes de-complexation, leading to the rapid deterioration in ICLT absorption. Sodium bicarbonate, potassium carbonate and calcium hydride were added into the chlorinated solvents in separate trials for either three hours or overnight prior to usage. However, all three bases had negligible effects towards arresting the deterioration.

The interference of acid causing the instability was further investigated with incremental titration of acetic acid into a toluene solution of **EuL3**. The absorption and emission spectra were obtained. Upon addition of 2 μL of acetic acid into the 3 mL solution, drastic changes were observed. In the absorption spectra (Figure 3.165), addition of acid led to a quick decrease in the ILCT absorption band, with further decrease upon subsequent addition of acid until reaching a plateau in absorbance. The TTA absorption peak of **EuL3** was also blue-shifted, vindicated by comparing with a control experiment with Eu(tta)$_3$ (Figure 3.168). The absorption band with a peak at *ca.* 375 nm is assigned to the absorption of the free tridentate ligand, caused by protonation of the nitrogen atoms and losing its ability to chelate to the electropositive Eu(III).

The emission intensities upon addition of acid was also greatly affected. A considerable decrease under excitation at 350 nm and 390 nm (Figures 3.166-167) was observed, and the change of splitting patterns of the hypersensitive transition indicates a change in coordination environment of the Eu(III). Comparison with the emission spectra of Eu(tta)$_3$ in toluene, most notably the splitting of the hypersensitive transitions as well as the shape of $^5D_0 \rightarrow {}^7F_4$ transition, revealed that the new species in the acidified **EuL3** solution bears a high degree of resemblance to the acidified Eu(tta)$_3$ solution.

It could be concluded that, addition of acetic acid led to the protonation of both the nitrogen atoms of the tridentate ligand and the anionic TTA, leading to gradual decomplexation of both ligands, as demonstrated with the gradual decrease in emission intensities under 350 nm and 390 nm excitation. Furthermore, and more importantly, the decrease of the ILCT band absorption and the rise of the free ligand absorption corroborated with the stability studies of the complexes with UV-vis spectroscopy, implying that the species may indeed be identical. The most intriguing aspect lies in the introduction of acid within the solution. As pre-treating the solvents did not improve the situation, it is reasonable to suspect the acid was generated after introducing the complex. As chlorinated solvents are known to slowly oxidize into phosgene and hydrogen chloride, we propose the redox character of the readily reducible complexes promoted the oxidation to generate hydrogen chloride *in situ* to introduce acid and cause the aforemention decomplexation, resulting in the presence of multiple species as demonstrated in luminescence lifetimes.

3.3. Conclusion

Three ligands each containing an *N*,*N*-diethylaniline moiety electronically conjugated to a tridentate bis(pyrazol-1-yl)-1,3,5-triazine with different numbers of methyl arms were synthesized. The ligands were then complexed with Eu(tta)$_3$ and Sm(tta)$_3$ to give nonadentate Ln(III) compounds for detailed photophysical studies. The TTA moiety sensitizes both Eu(III) and Sm(III) – of which the accepting levels are quite close – decently with little residual ligand fluorescence. The intraligand charge transfer (ILCT) character, imparted by the aniline structure, was also found to sensitize Eu(III) and Sm(III) luminescence efficiently through a non-triplet energy transfer pathway with quantum yields higher than sensitization by TTA. Characteristic of charge transfer transitions, however, the sensitization is also polarity-dependent and is only efficient in non-polar solvents, due to the different extent of stabilization of the ground state energy level, shifting the excited energies towards or away from the optimal ΔE required for energy transfer. The modification of pyrazoles by methyl side-arms proved to be insignificant on the Ln(III) luminescence as they are too peripheral to affect the coordination environment and also play a negligible role in altering the energy levels of the TTA and ILCT chromophores.

Coordination of certain nucleophilic solvent molecules was also revealed in the photophysical properties of the complexes, causing a drastic drop in luminescence lifetimes as a result of non-radiative multiphonon quenching by high energy oscillators and a change in coordination environment evidenced by the hypersensitive $^5D_0 \rightarrow {}^7F_2$ transition of Eu(III). The number of coordinated methanol molecules were determined to be around 2 and 3.5 respectively for Eu(III) and Sm(III), a result of the discrepancy in their ionic radii.

Stability issues were found in chlorinated solvents and investigated by luminescence lifetimes and UV-vis spectroscopy. It is believed that the readily reducible complexes, especially the Eu(III) compounds, promoted oxidation of the chlorinated solvents to produce hydrogen chloride, causing decomplexation.

Nonetheless, this work is fundamentally important for optimizing the ILCT transition as an efficient energy transfer pathway for various potential applications which utilizes, non-UV excitation sources.

3.4. Appendix – Spectra and Decay Curves

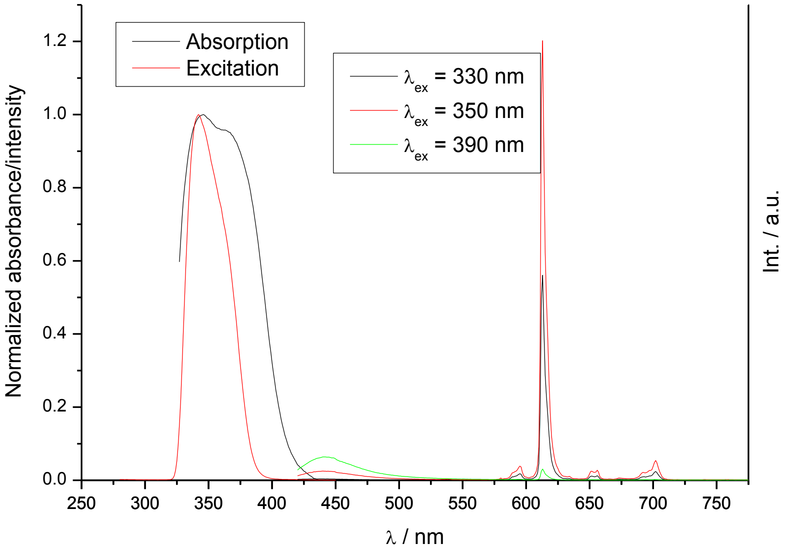

Figure 3. 7 Normalized absorption, excitation, and emission spectra of EuL1 in acetone

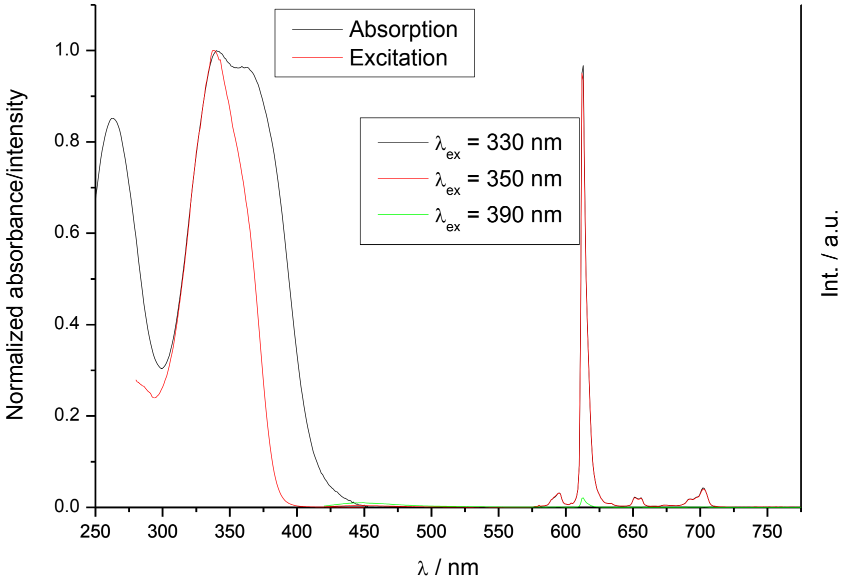

Figure 3. 8 Normalized absorption, excitation, and emission spectra of EuL1 in ACN

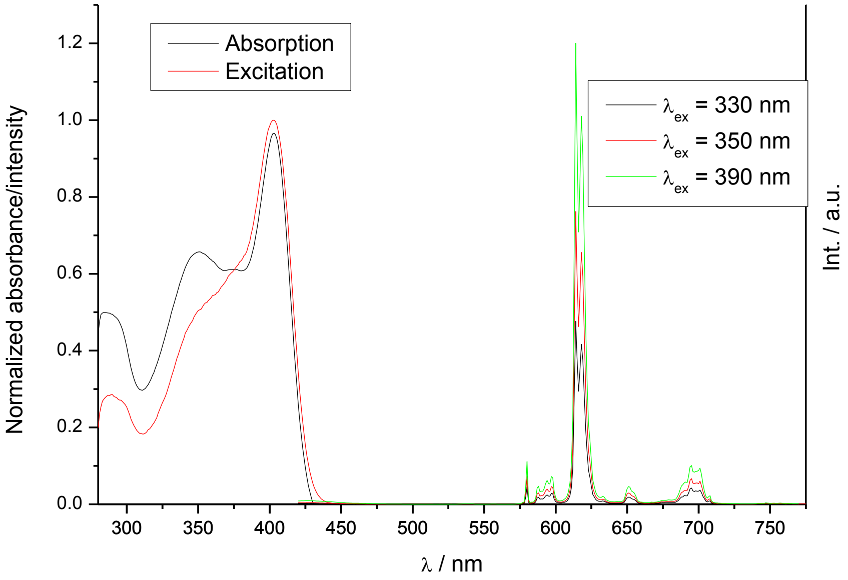

Figure 3. 9 Normalized absorption, excitation, and emission spectra of EuL1 in benzene

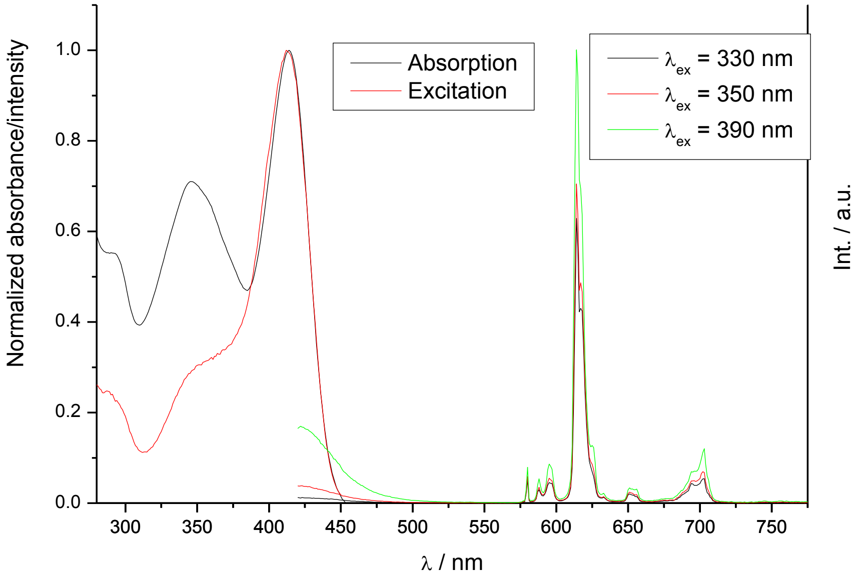

Figure 3. 10 Normalized absorption, excitation, and emission spectra of EuL1 in chloroform

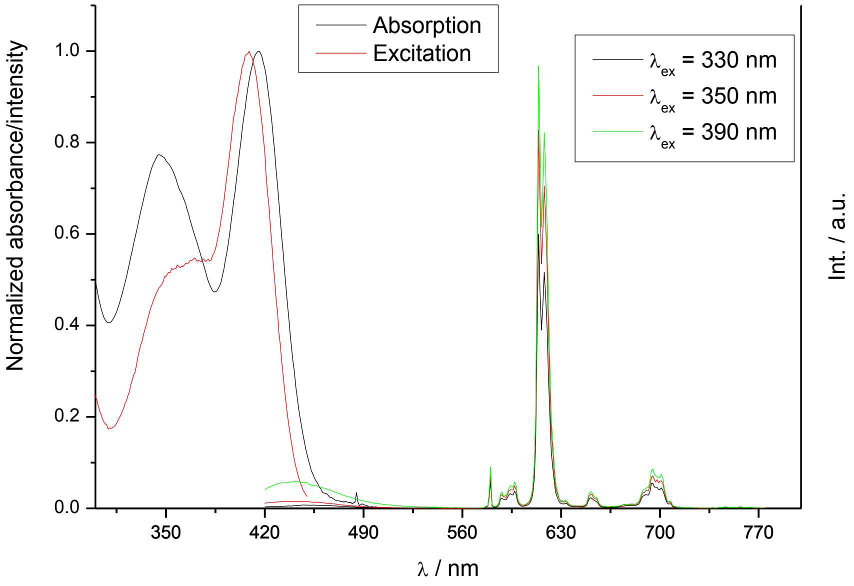

Figure 3. 11 Normalized absorption, excitation, and emission spectra of EuL1 in DCM

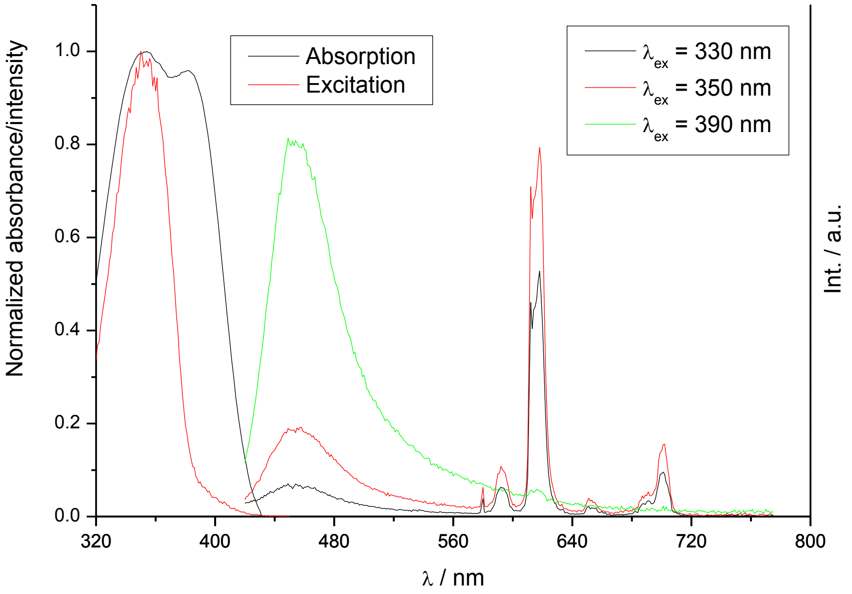

Figure 3. 12 Normalized absorption, excitation, and emission spectra of EuL1 in DMSO

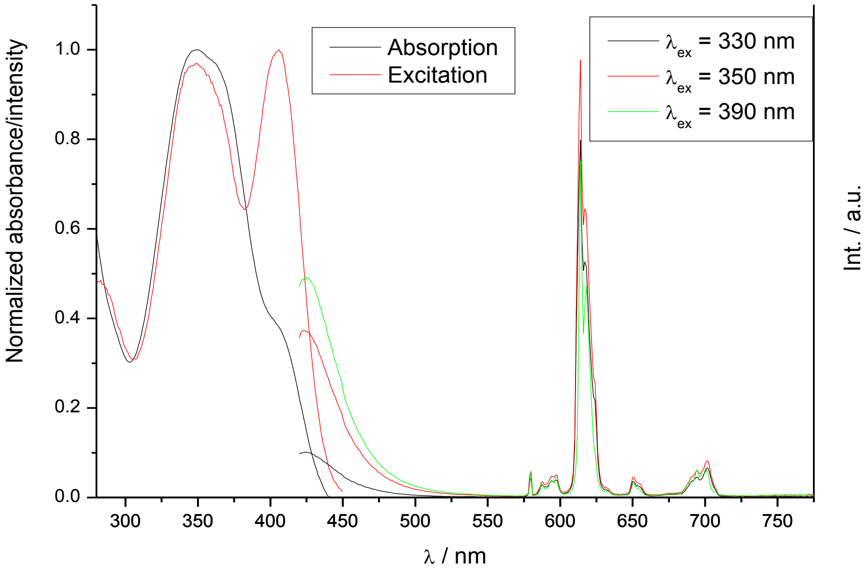

Figure 3. 13 Normalized absorption, excitation, and emission spectra of EuL1 in EA

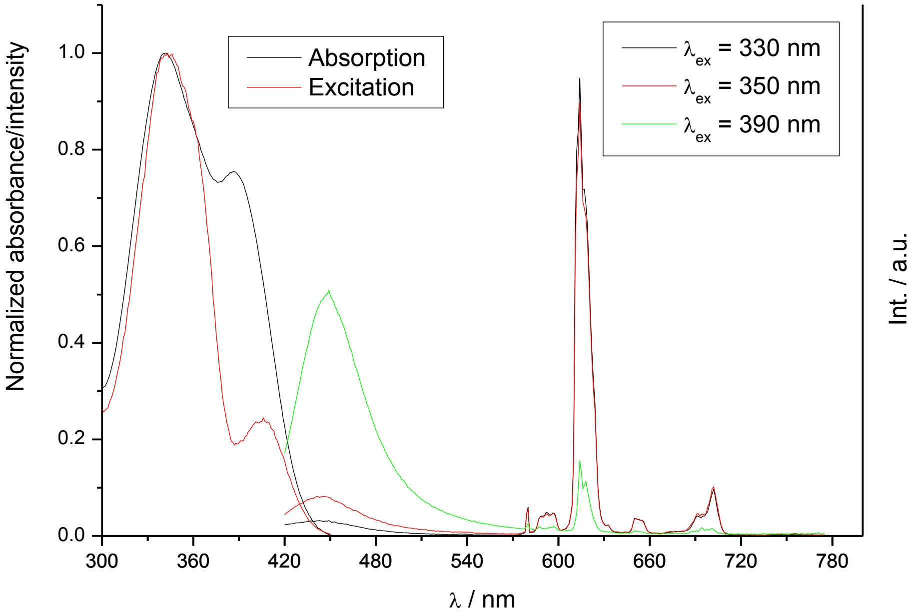

Figure 3. 14 Normalized absorption, excitation, and emission spectra of EuL1 in IPA

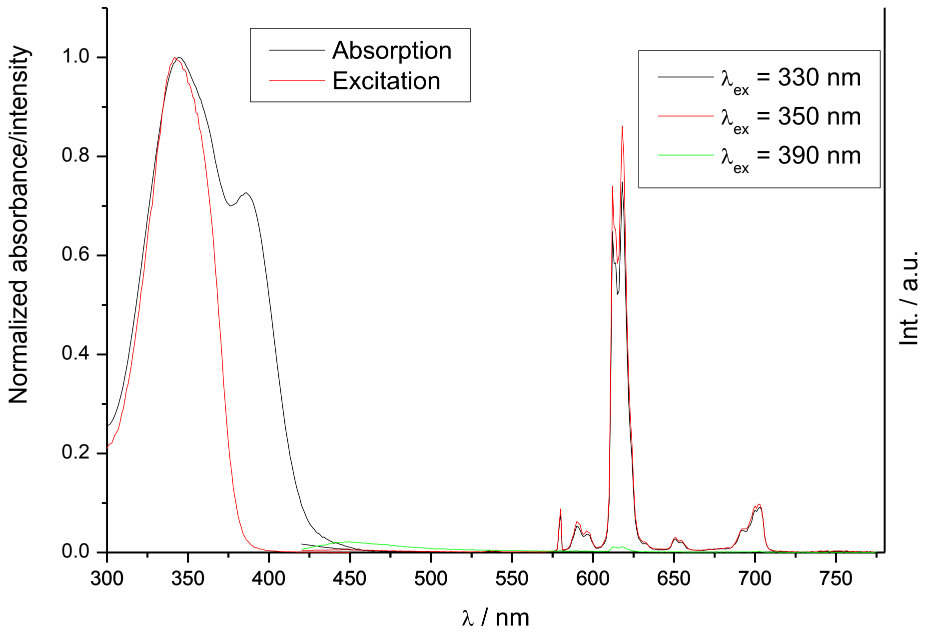

Figure 3. 15 Normalized absorption, excitation, and emission spectra of EuL1 in methanol

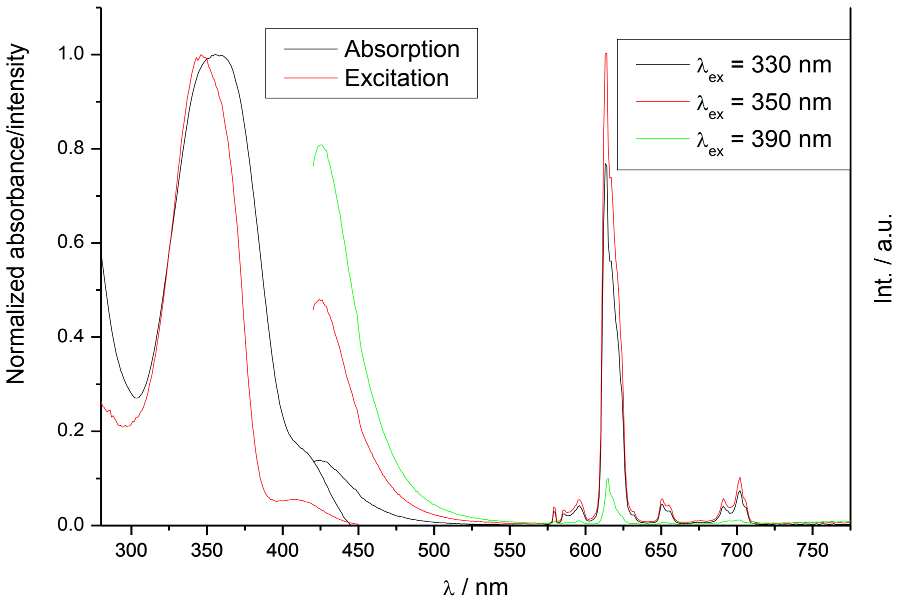

Figure 3. 16 Normalized absorption, excitation, and emission spectra of EuL1 in THF

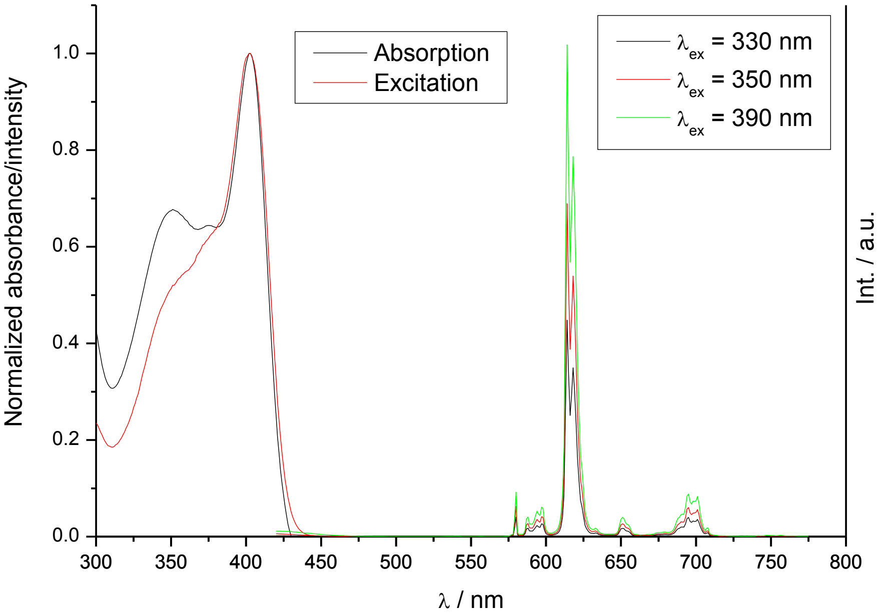

Figure 3. 17 Normalized absorption, excitation, and emission spectra of EuL1 in toluene

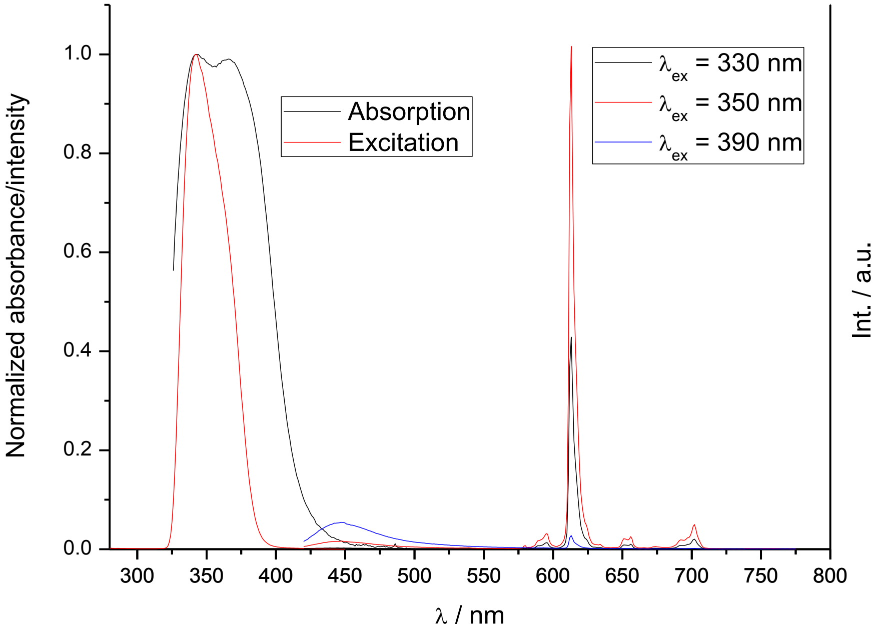

Figure 3. 18 Normalized absorption, excitation, and emission spectra of EuL2 in acetone

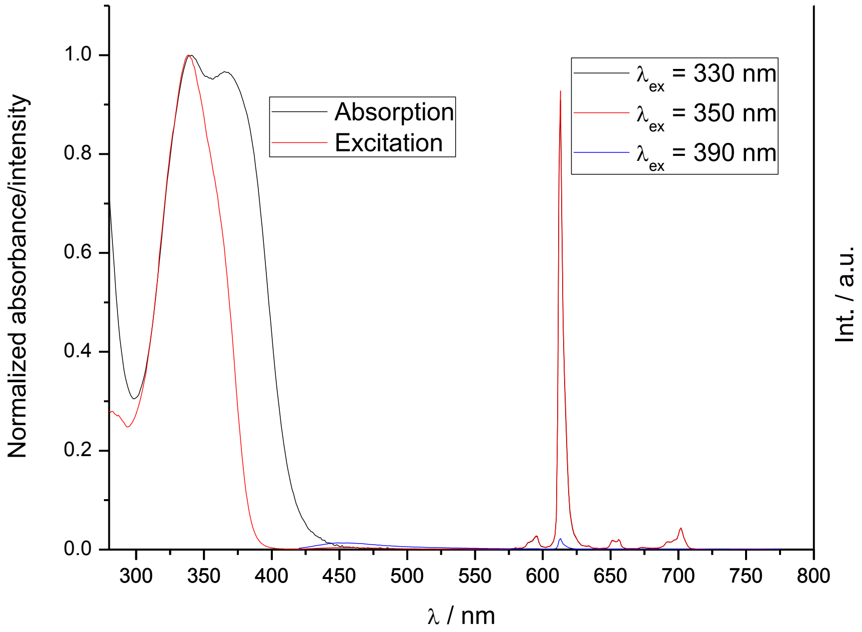

Figure 3. 19 Normalized absorption, excitation, and emission spectra of EuL2 in ACN

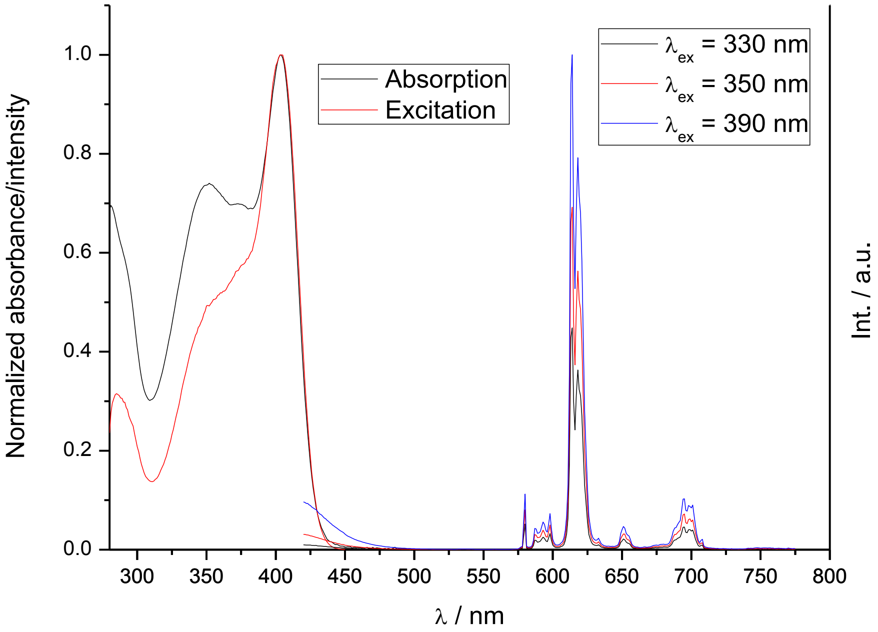

Figure 3. 20 Normalized absorption, excitation, and emission spectra of EuL2 in benzene

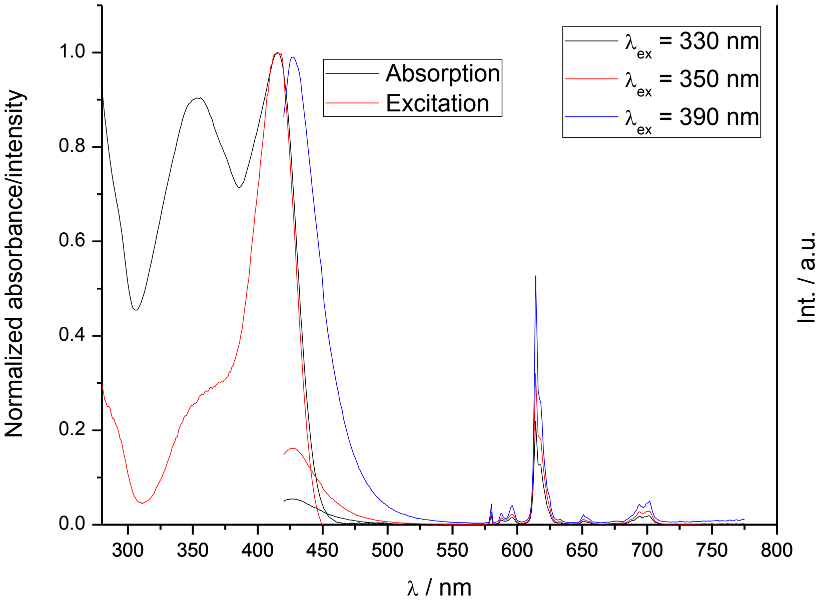

Figure 3. 21 Normalized absorption, excitation, and emission spectra of EuL2 in chloroform

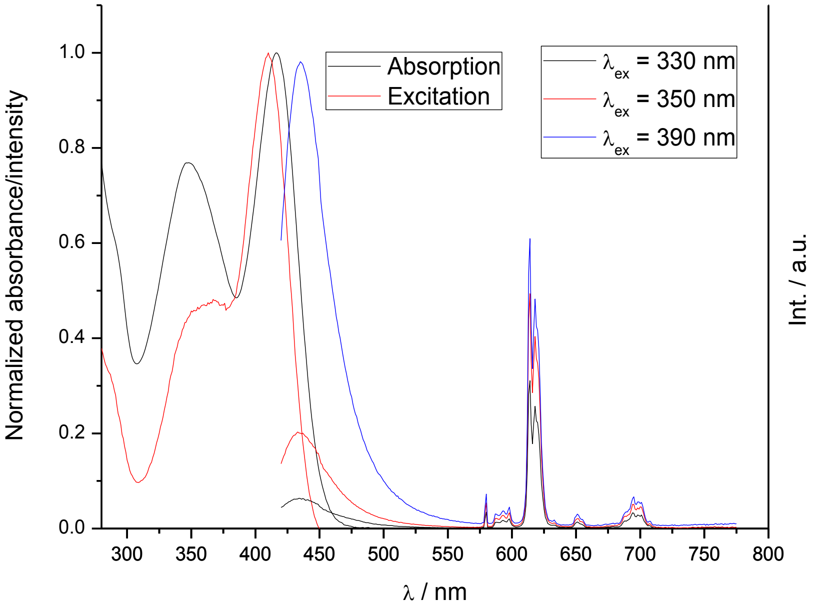

Figure 3. 22 Normalized absorption, excitation, and emission spectra of EuL2 in DCM

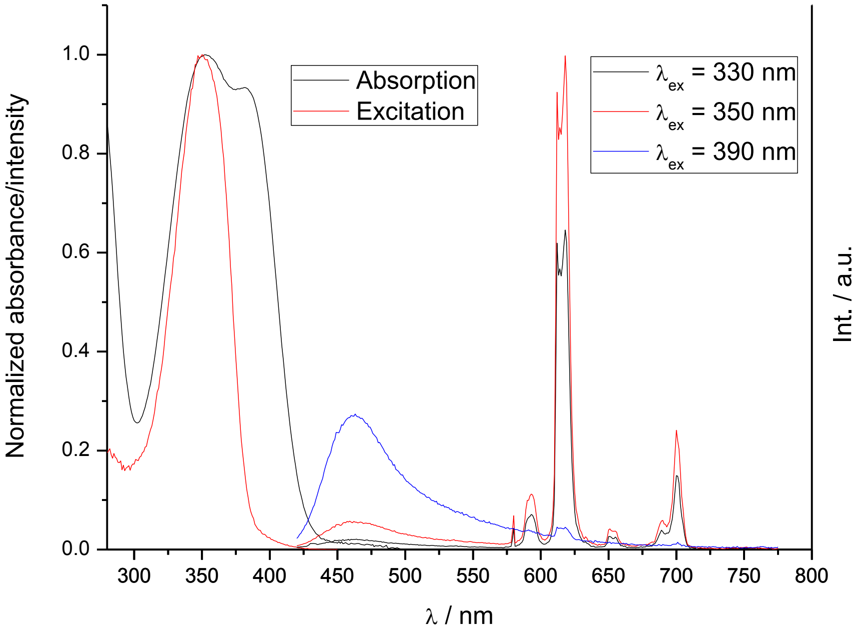

Figure 3. 23 Normalized absorption, excitation, and emission spectra of EuL2 in DMSO

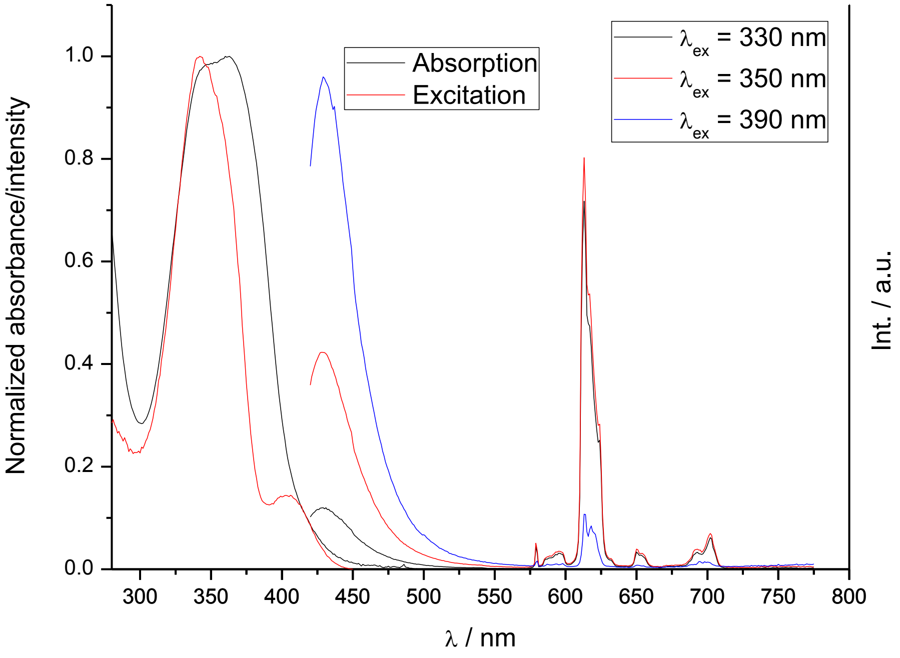

Figure 3. 24 Normalized absorption, excitation, and emission spectra of EuL2 in EA

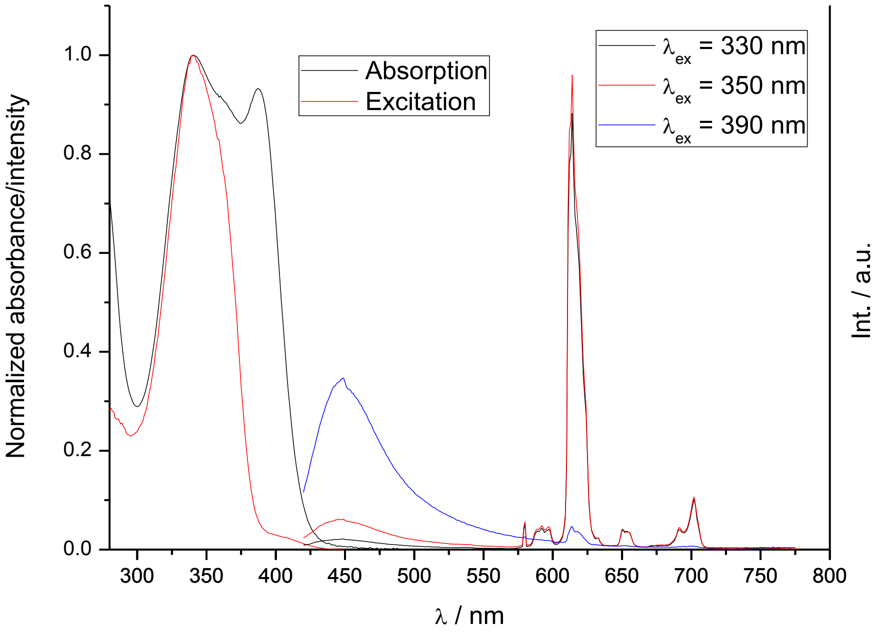

Figure 3. 25 Normalized absorption, excitation, and emission spectra of EuL2 in IPA

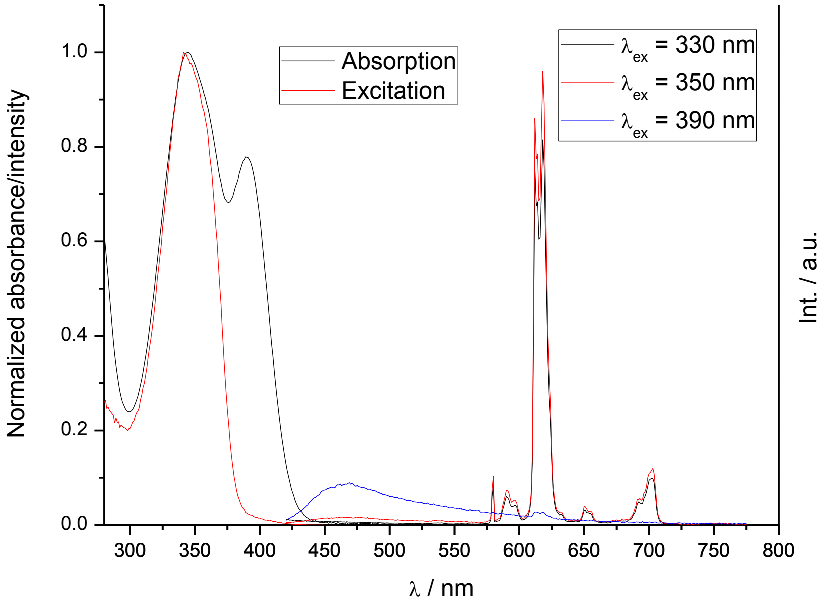

Figure 3. 26 Normalized absorption, excitation, and emission spectra of EuL2 in methanol

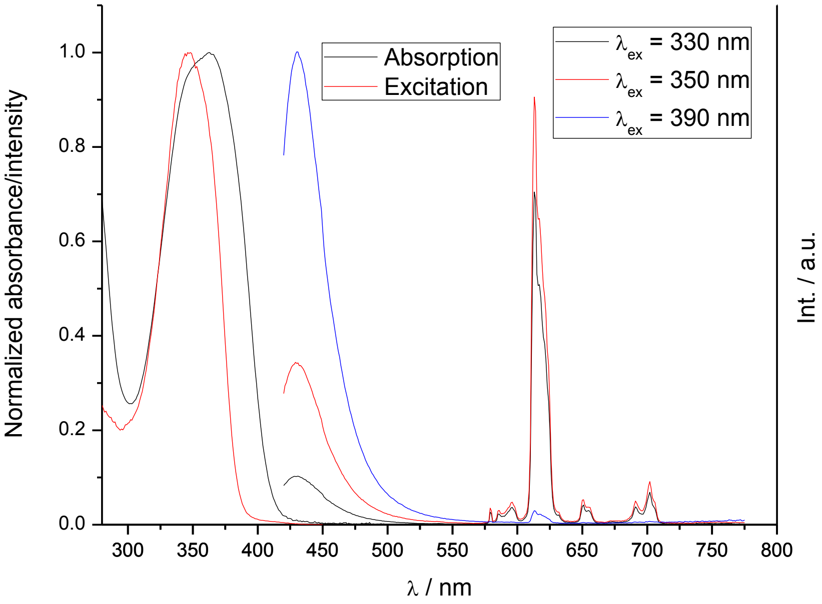

Figure 3. 27 Normalized absorption, excitation, and emission spectra of EuL2 in THF

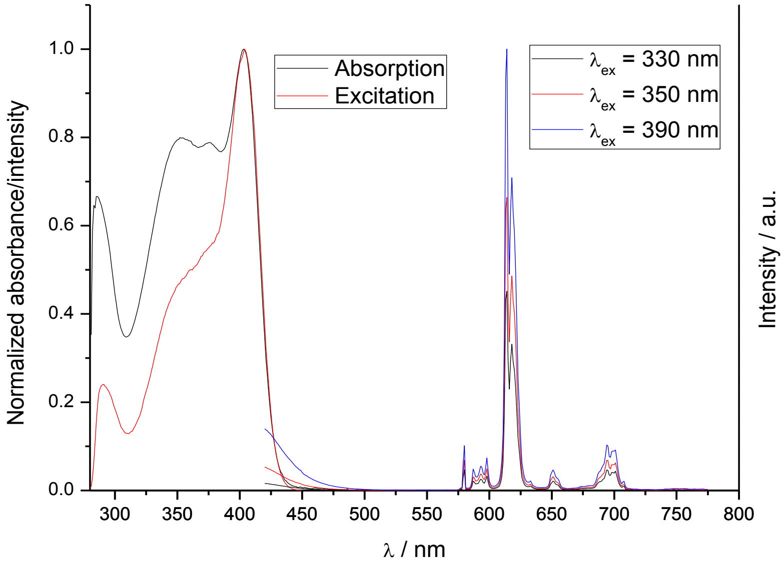

Figure 3. 28 Normalized absorption, excitation, and emission spectra of EuL2 in toluene

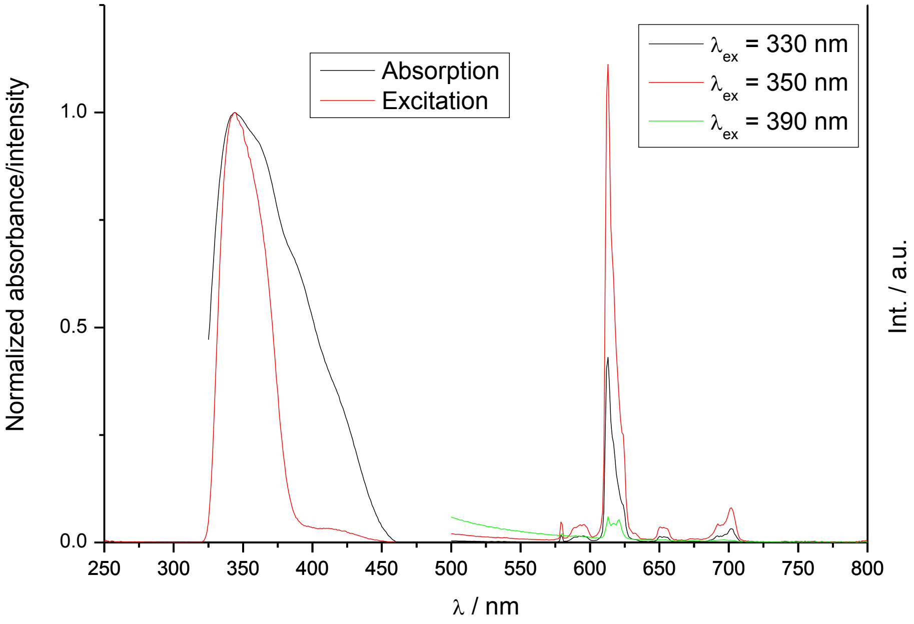

Figure 3. 29 Normalized absorption, excitation, and emission spectra of EuL3 in acetone

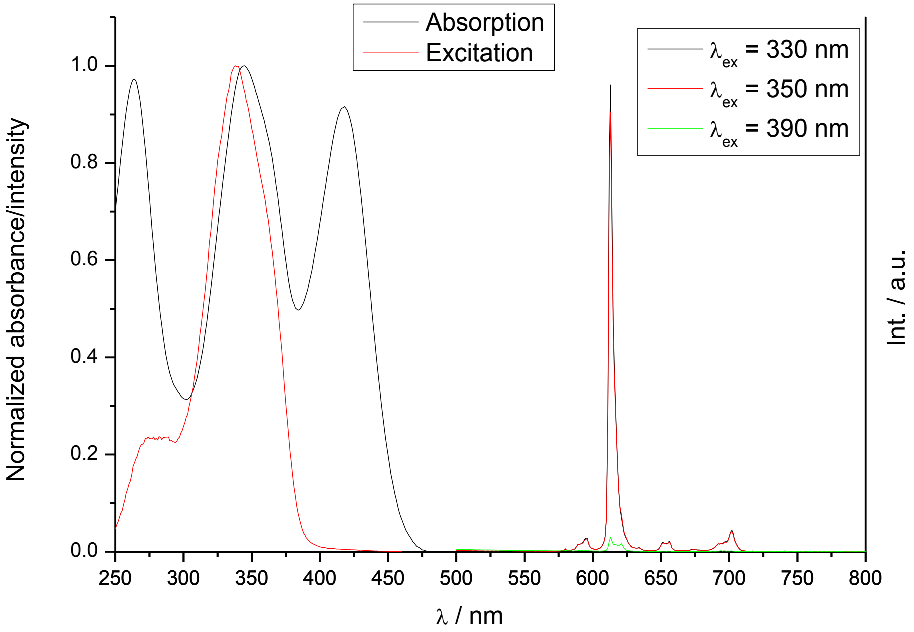

Figure 3. 30 Normalized absorption, excitation, and emission spectra of EuL3 in ACN

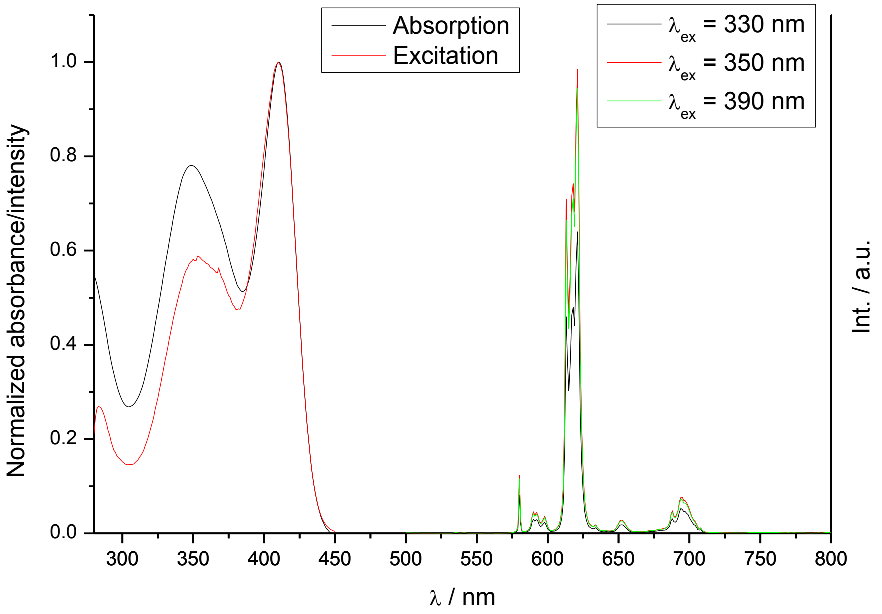

Figure 3. 31 Normalized absorption, excitation, and emission spectra of EuL3 in benzene

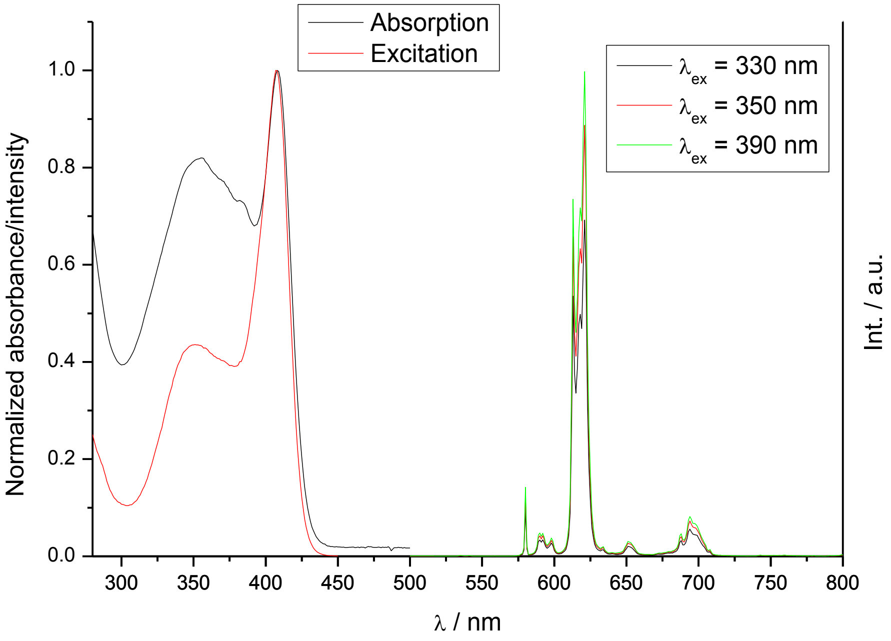

Figure 3. 32 Normalized absorption, excitation, and emission spectra of EuL3 in CCl4

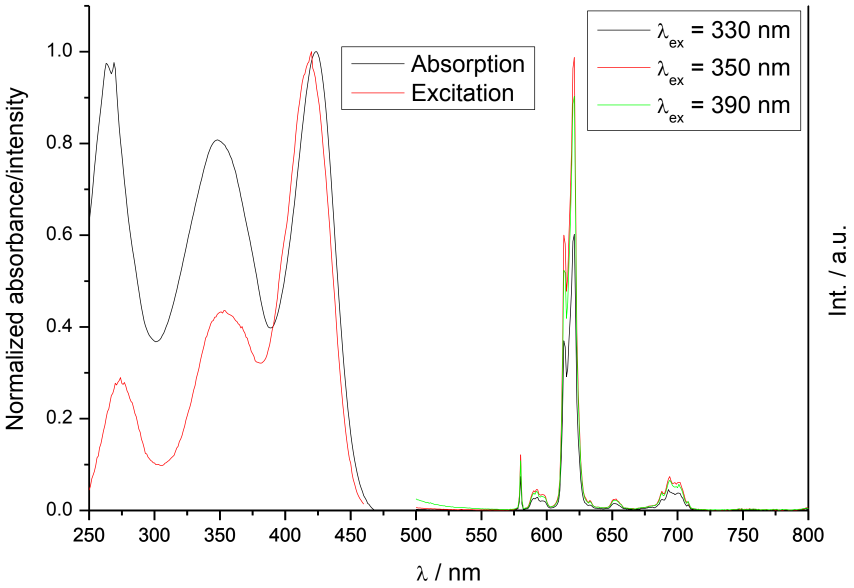

Figure 3. 33 Normalized absorption, excitation, and emission spectra of EuL3 in chloroform

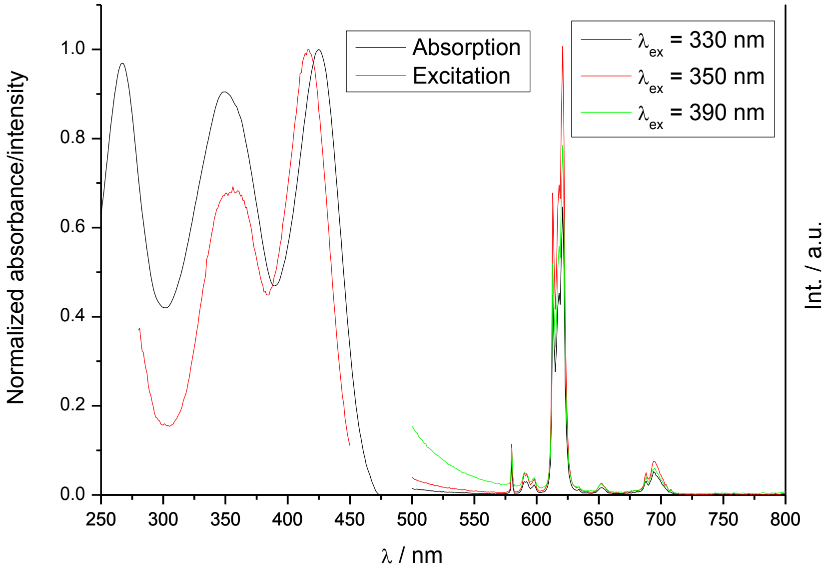

Figure 3. 34 Normalized absorption, excitation, and emission spectra of EuL3 in 1,2-dichloroethane

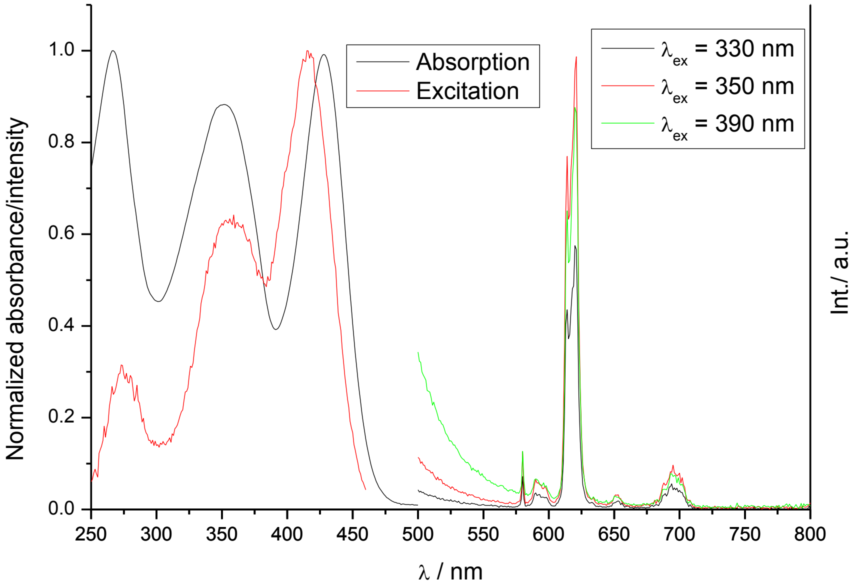

Figure 3. 35 Normalized absorption, excitation, and emission spectra of EuL3 in DCM

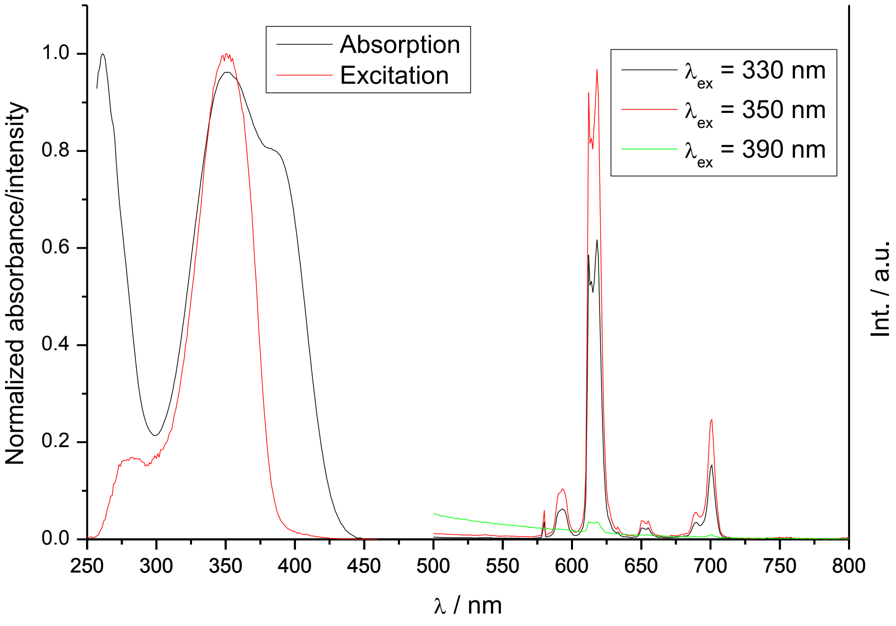

Figure 3. 36 Normalized absorption, excitation, and emission spectra of EuL3 in DMSO

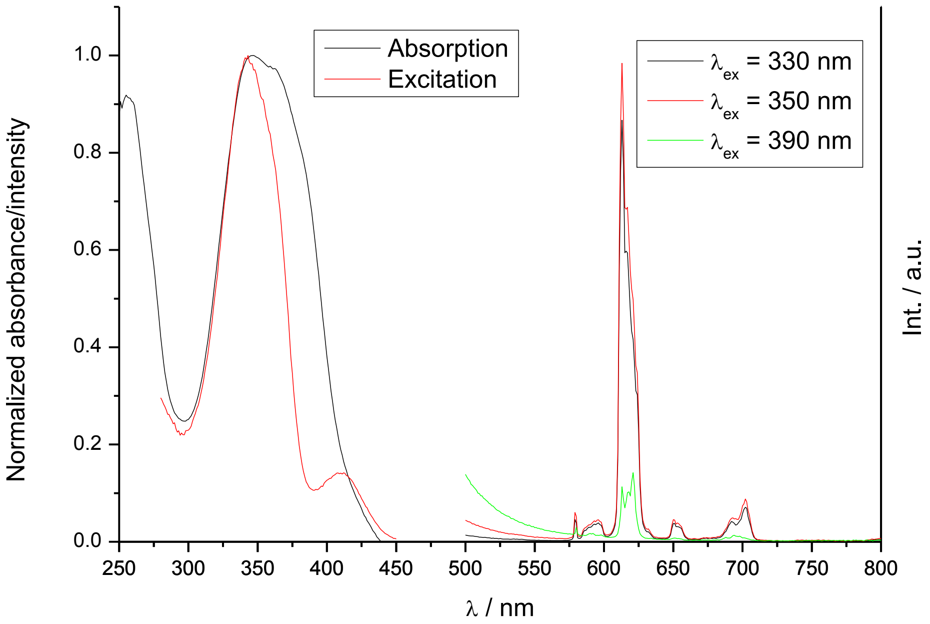

Figure 3. 37 Normalized absorption, excitation, and emission spectra of EuL3 in EA

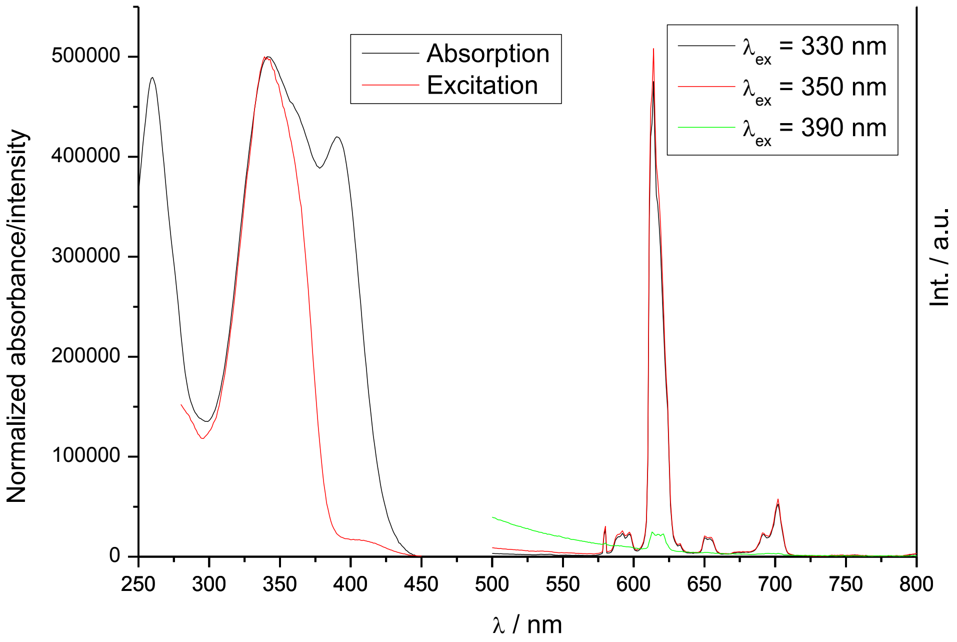

Figure 3. 38 Normalized absorption, excitation, and emission spectra of EuL3 in IPA

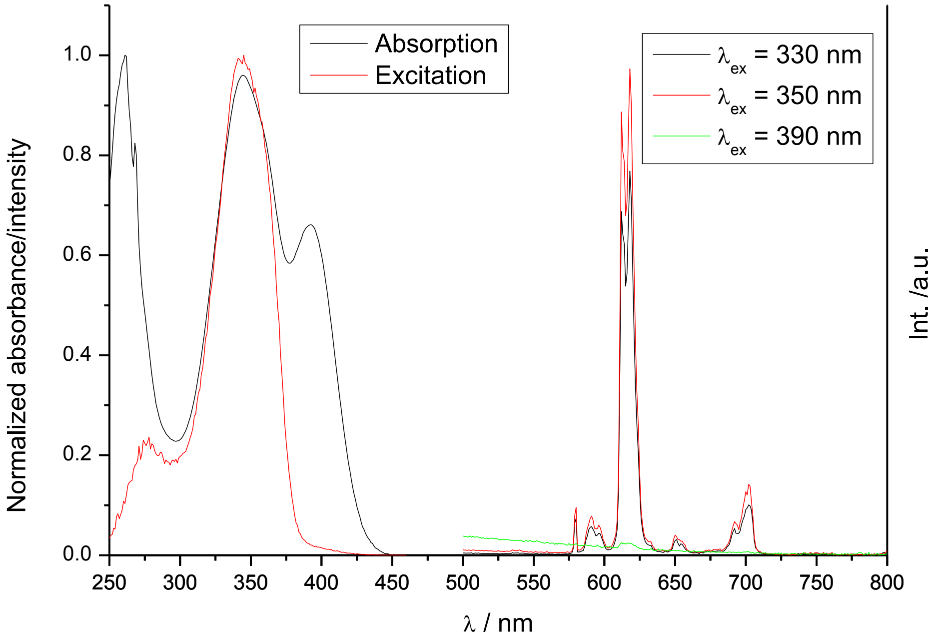

Figure 3. 39 Normalized absorption, excitation, and emission spectra of EuL3 in methanol

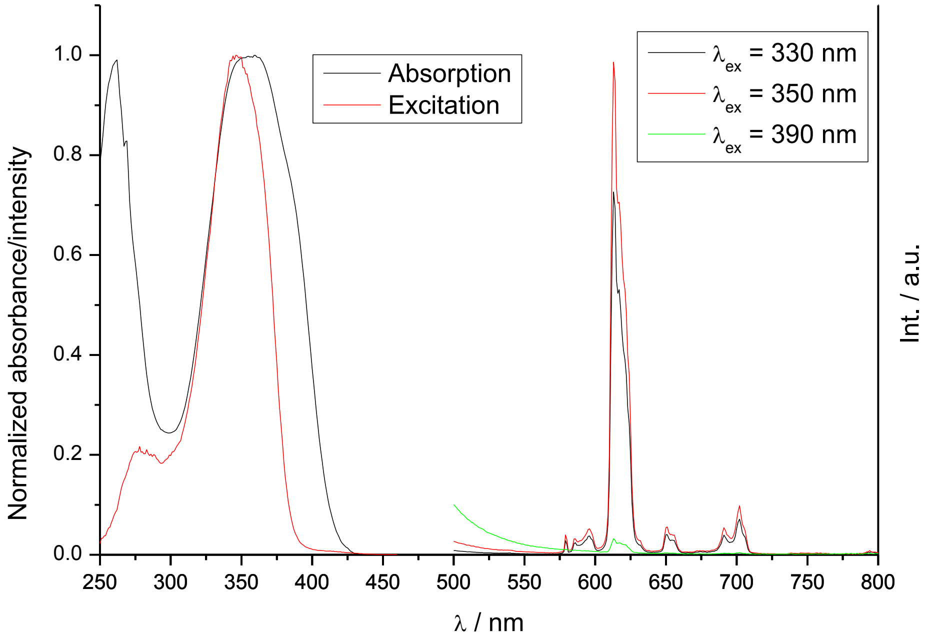

Figure 3. 40 Normalized absorption, excitation, and emission spectra of EuL3 in THF

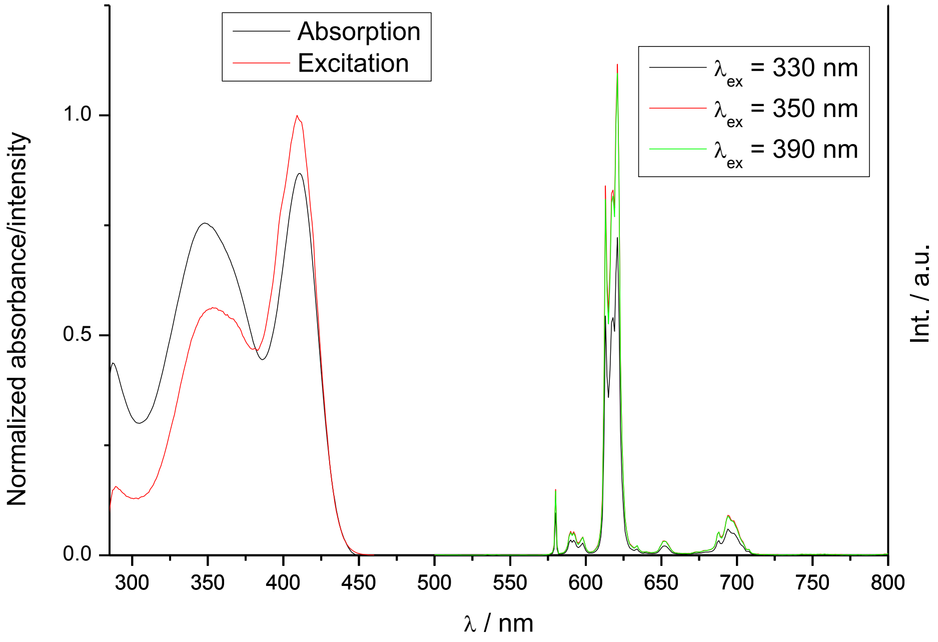

Figure 3. 41 Normalized absorption, excitation, and emission spectra of EuL3 in toluene

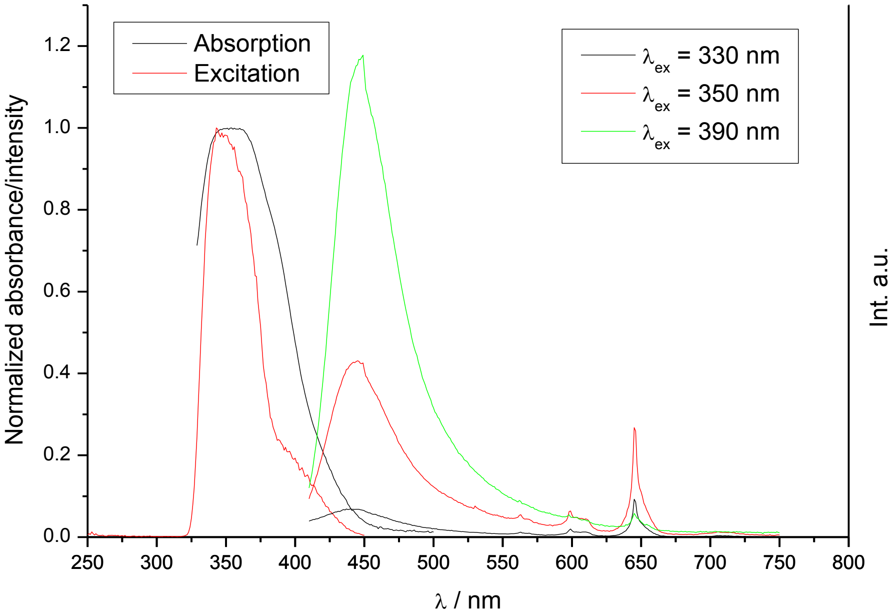

Figure 3. 42 Normalized absorption, excitation, and emission spectra of SmL1 in acetone

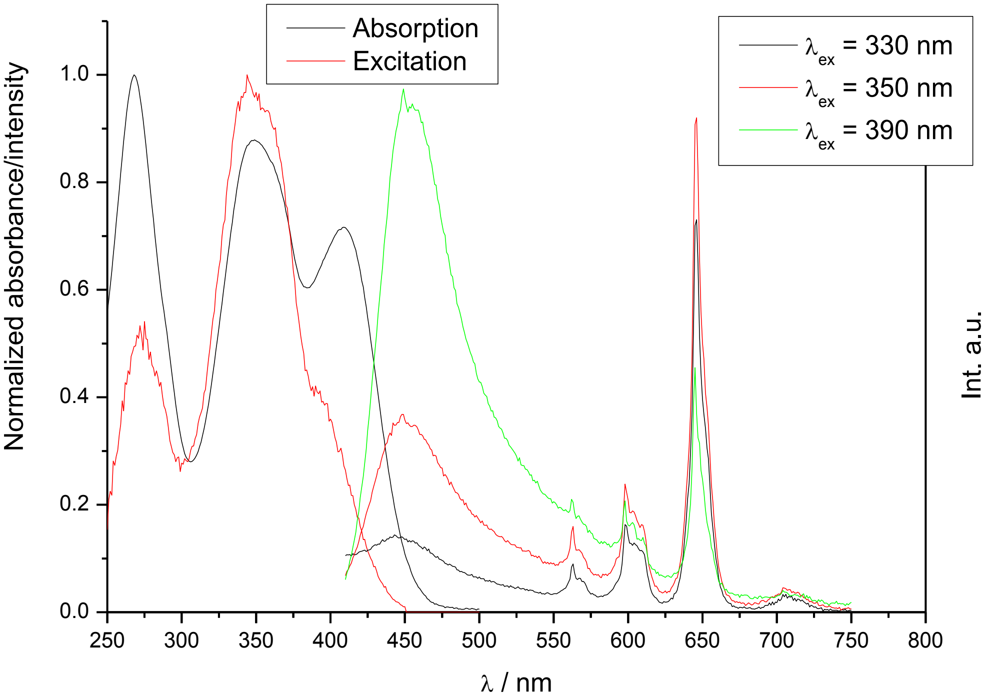

Figure 3. 43 Normalized absorption, excitation, and emission spectra of SmL1 in ACN

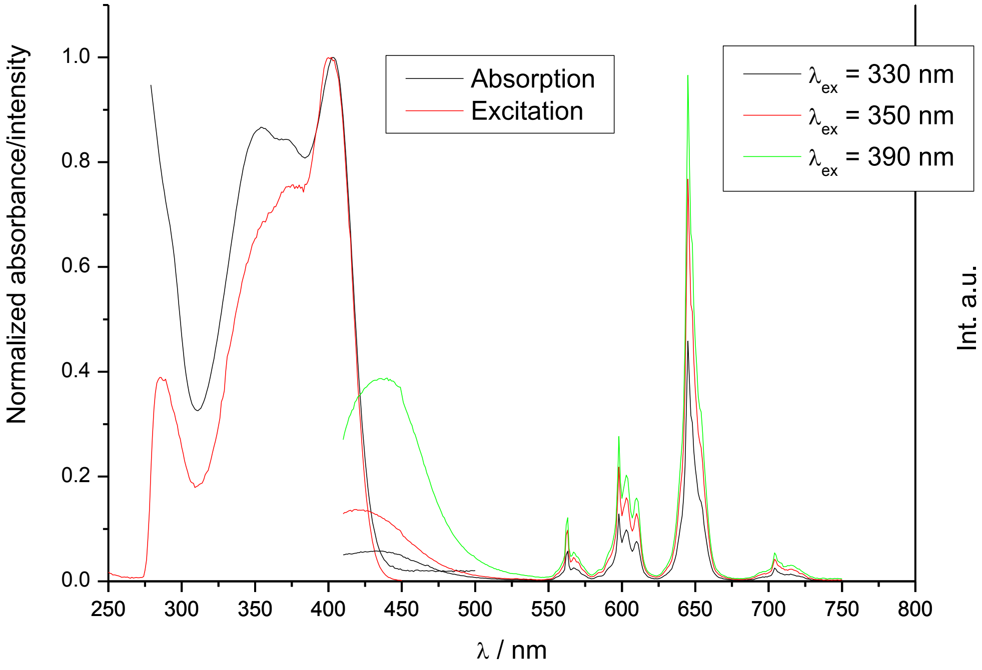

Figure 3. 44 Normalized absorption, excitation, and emission spectra of SmL1 in benzene

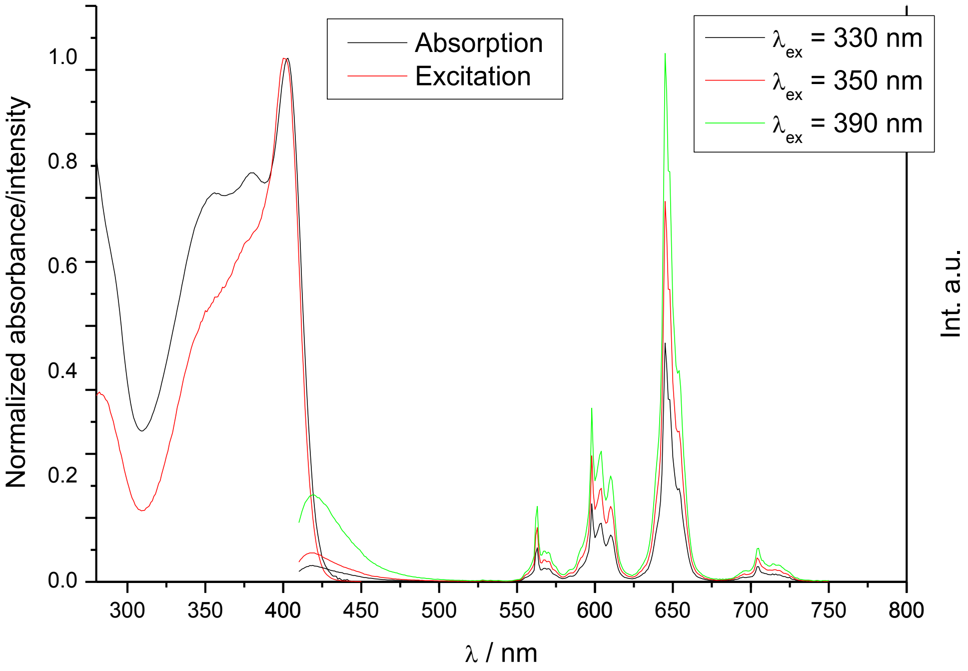

Figure 3. 45 Normalized absorption, excitation, and emission spectra of SmL1 in CCl_4

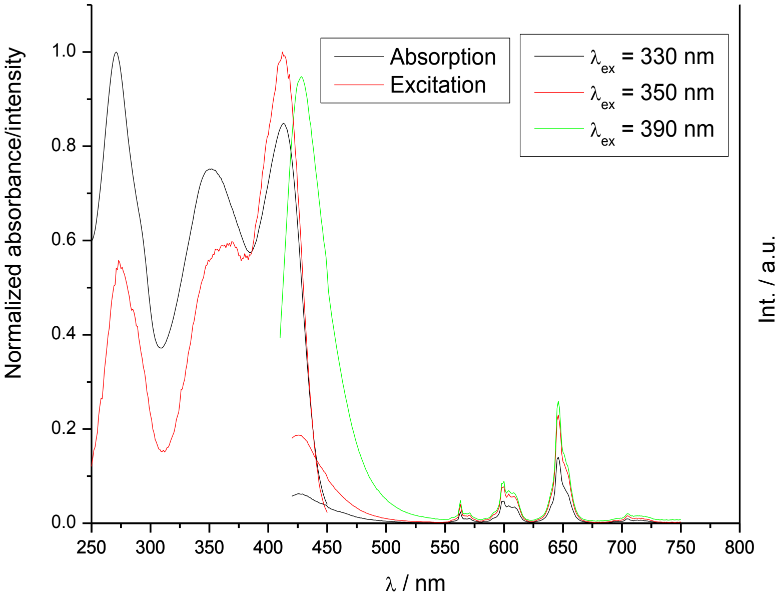

Figure 3. 46 Normalized absorption, excitation, and emission spectra of SmL1 in chloroform

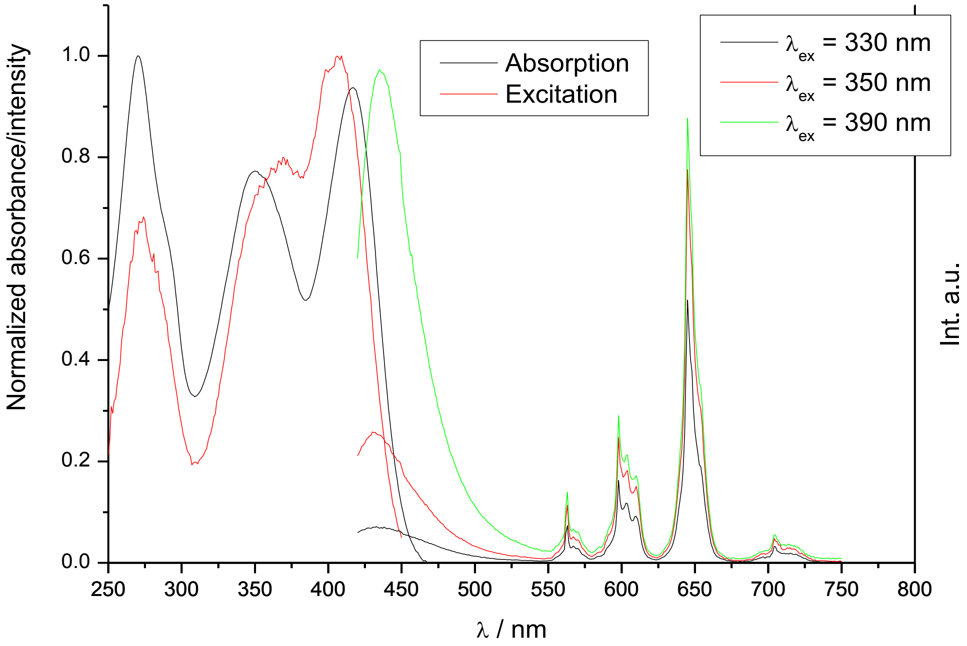

Figure 3. 47 Normalized absorption, excitation, and emission spectra of SmL1 in DCM

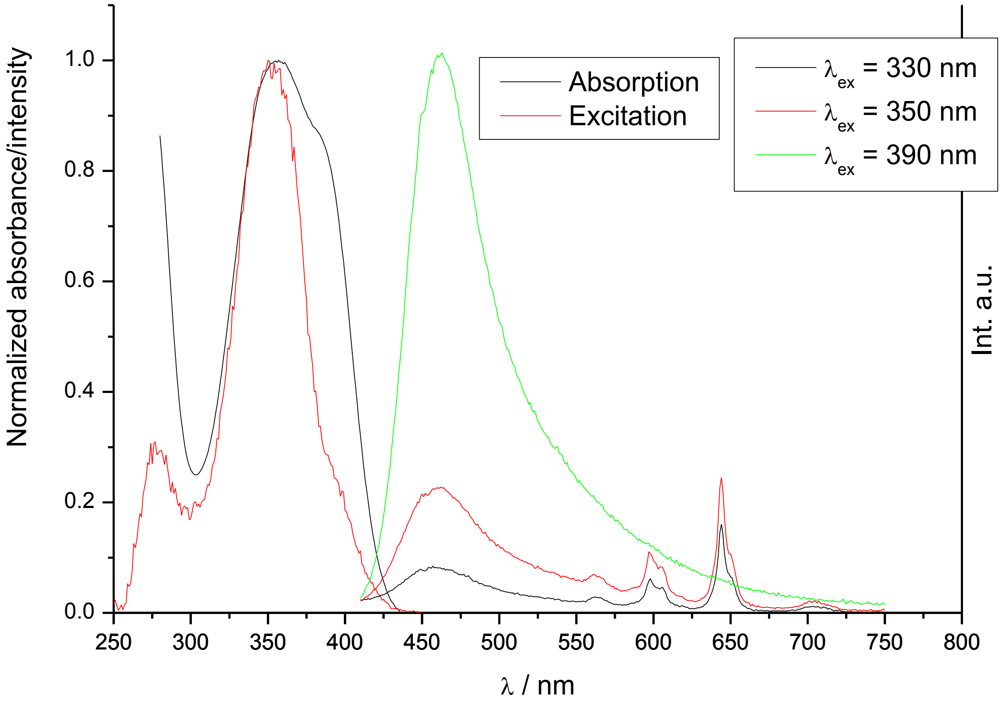

Figure 3. 48 Normalized absorption, excitation, and emission spectra of SmL1 in DMSO

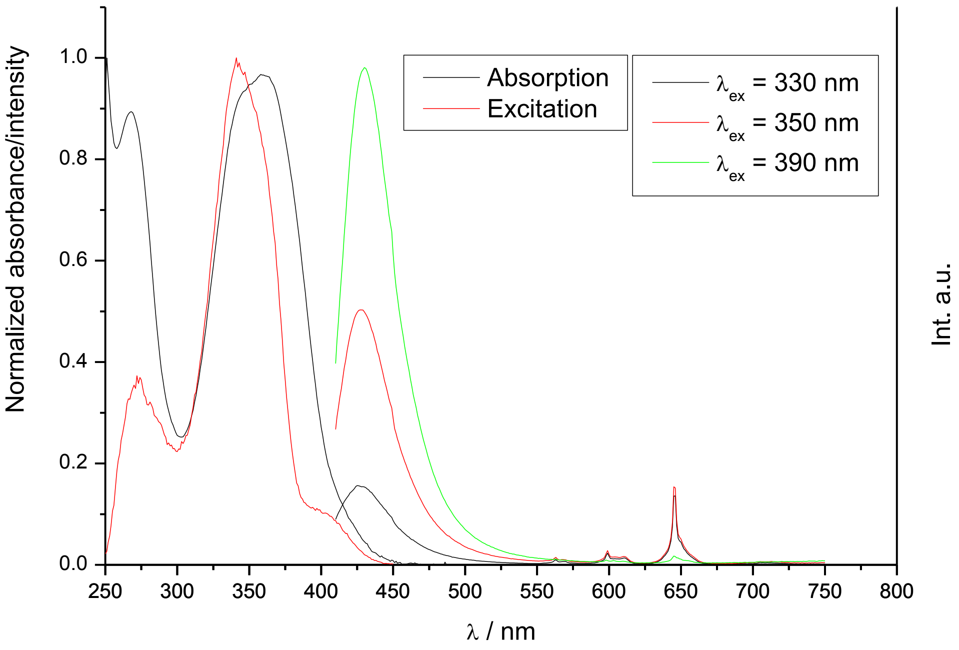

Figure 3. 49 Normalized absorption, excitation, and emission spectra of SmL1 in EA

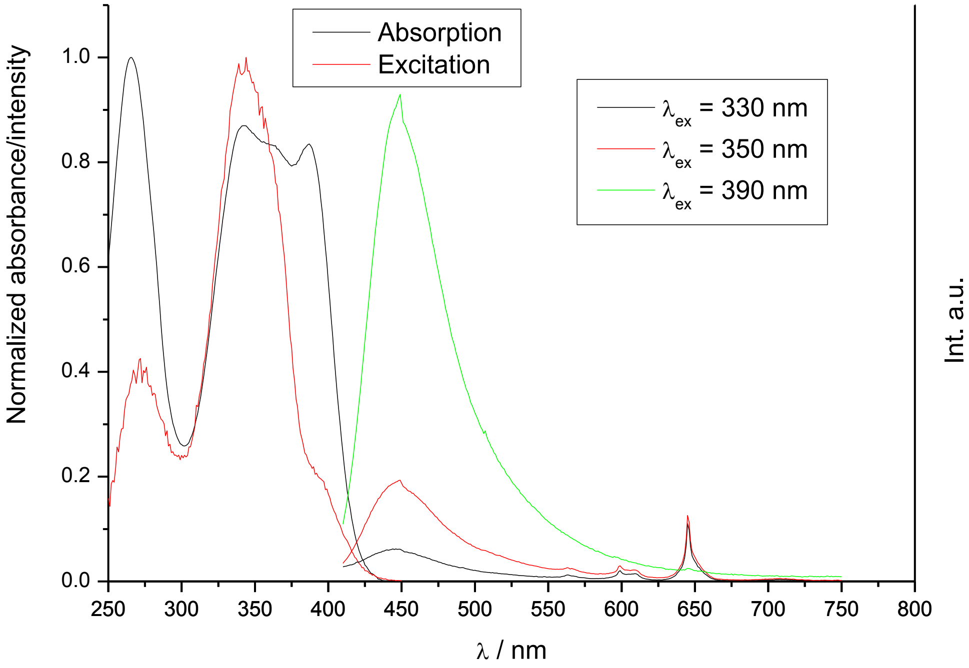

Figure 3. 50 Normalized absorption, excitation, and emission spectra of SmL1 in IPA

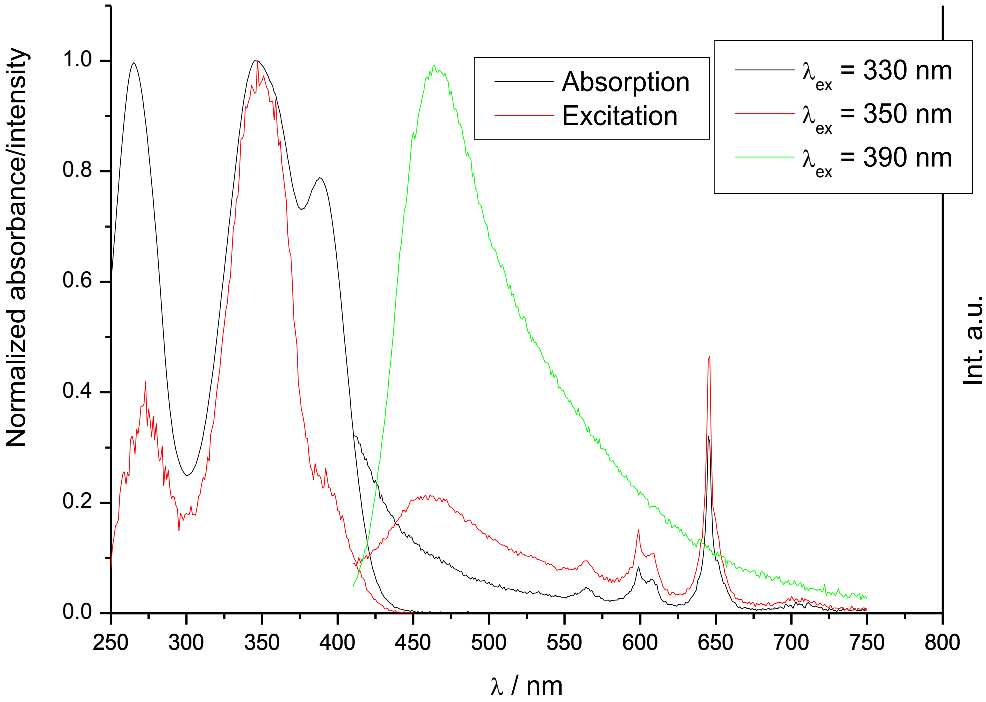

Figure 3. 51 Normalized absorption, excitation, and emission spectra of SmL1 in methanol

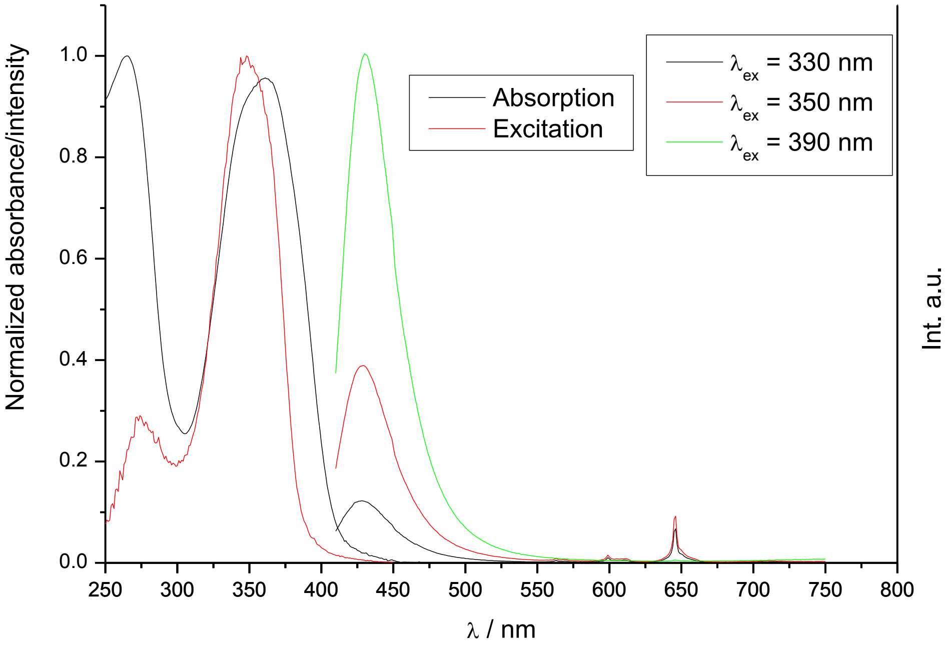

Figure 3. 52 Normalized absorption, excitation, and emission spectra of SmL1 in THF

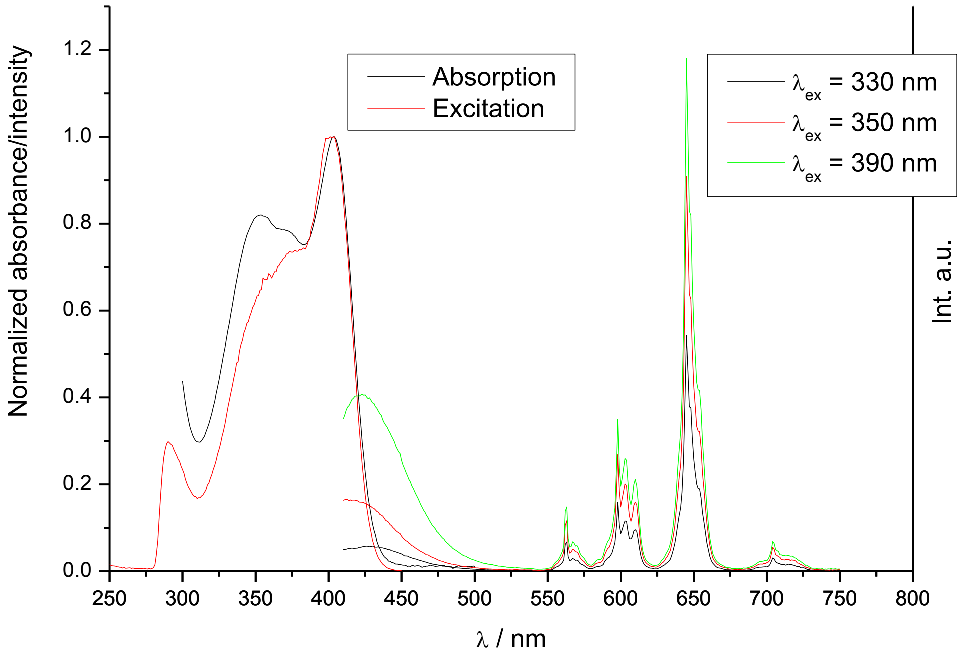

Figure 3. 53 Normalized absorption, excitation, and emission spectra of SmL1 in toluene

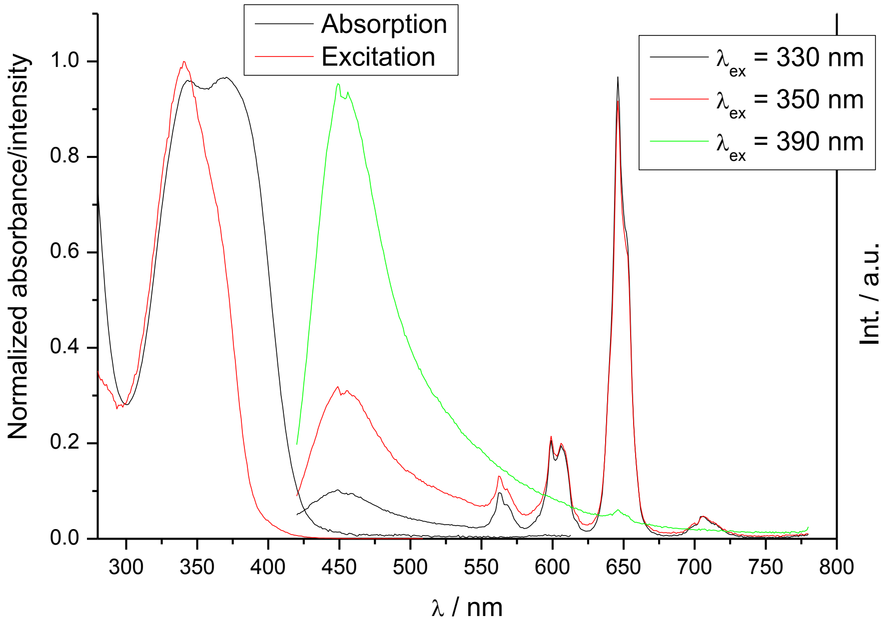

Figure 3. 54 Normalized absorption, excitation, and emission spectra of SmL2 in acetone

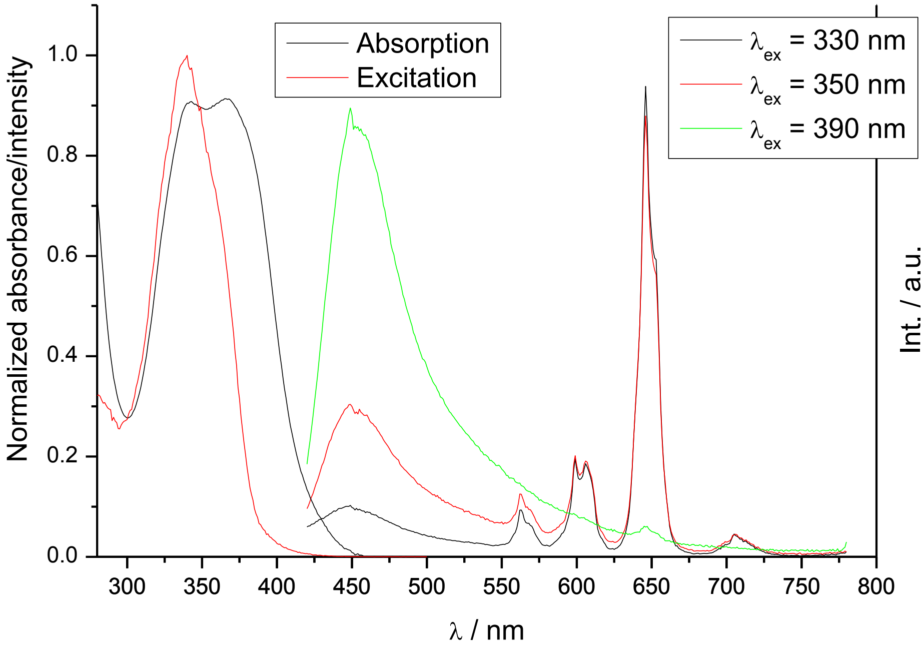

Figure 3. 55 Normalized absorption, excitation, and emission spectra of SmL2 in ACN

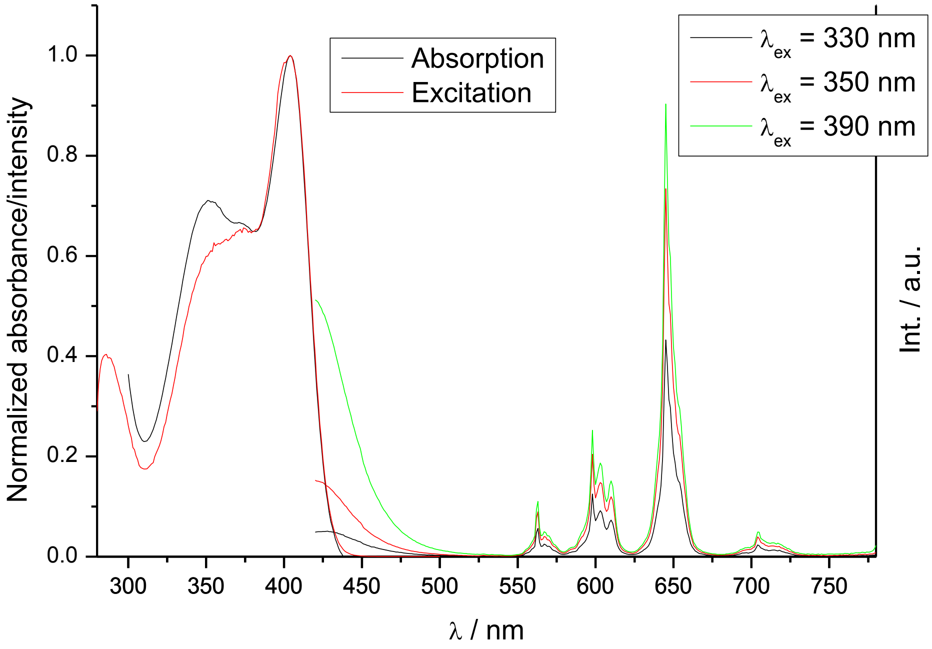

Figure 3. 56 Normalized absorption, excitation, and emission spectra of SmL2 in benzene

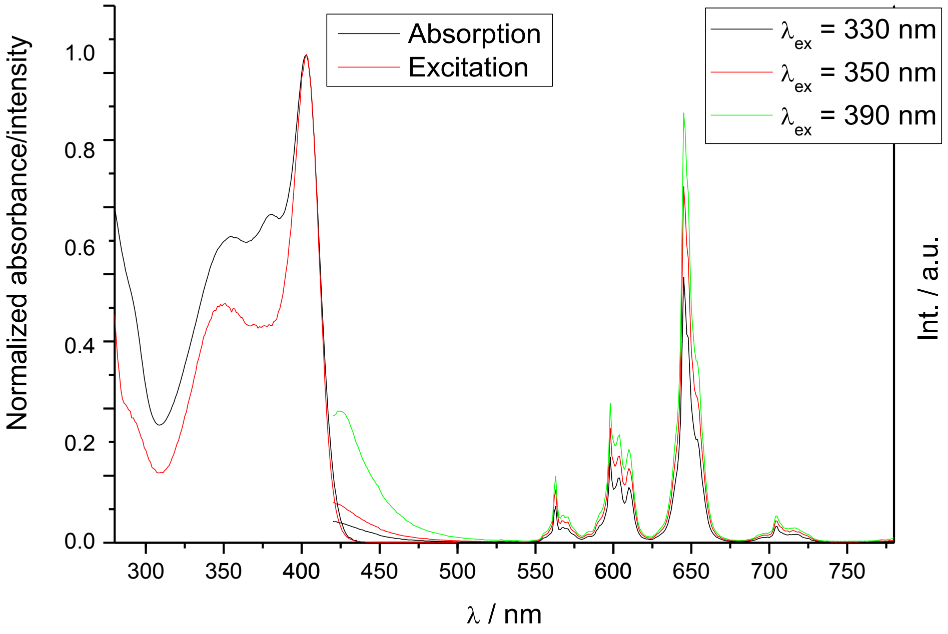

Figure 3. 57 Normalized absorption, excitation, and emission spectra of SmL2 in CCl_4

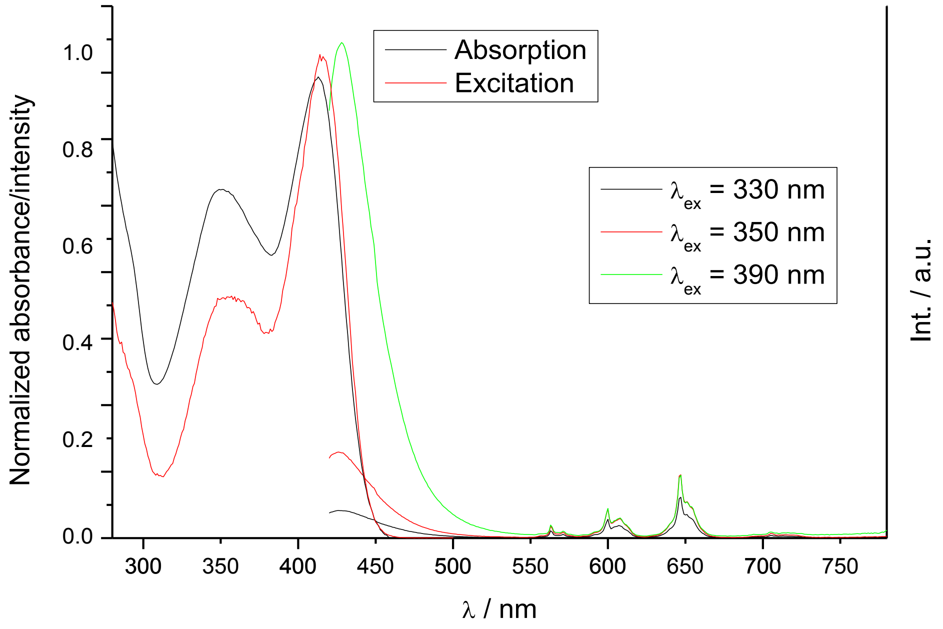

Figure 3. 58 Normalized absorption, excitation, and emission spectra of SmL2 in chloroform

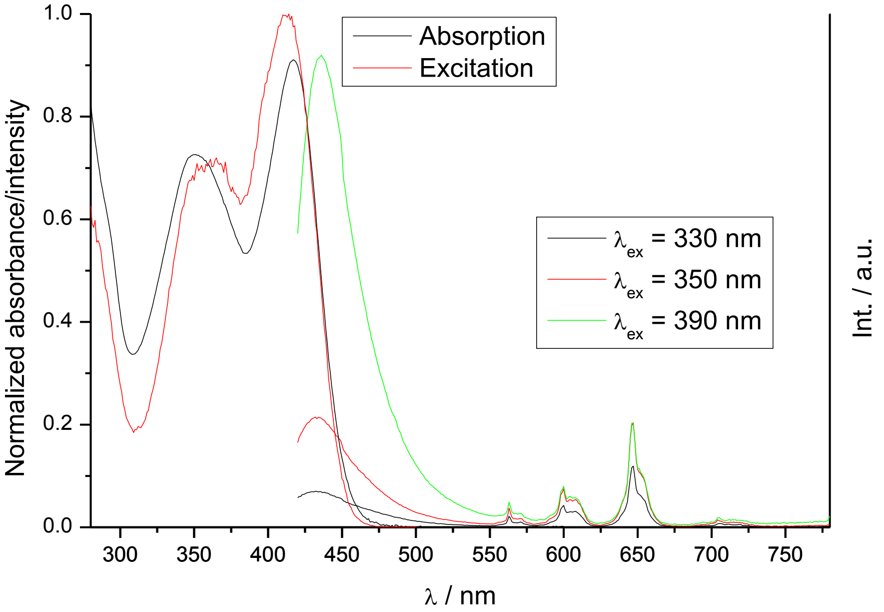

Figure 3. 59 Normalized absorption, excitation, and emission spectra of SmL2 in DCM

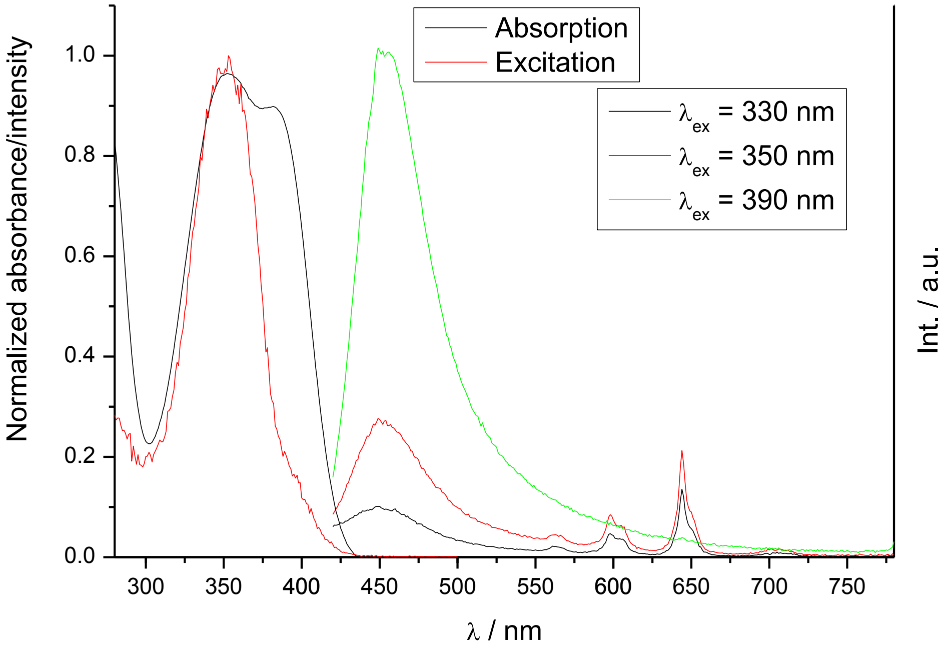

Figure 3. 60 Normalized absorption, excitation, and emission spectra of SmL2 in DMSO

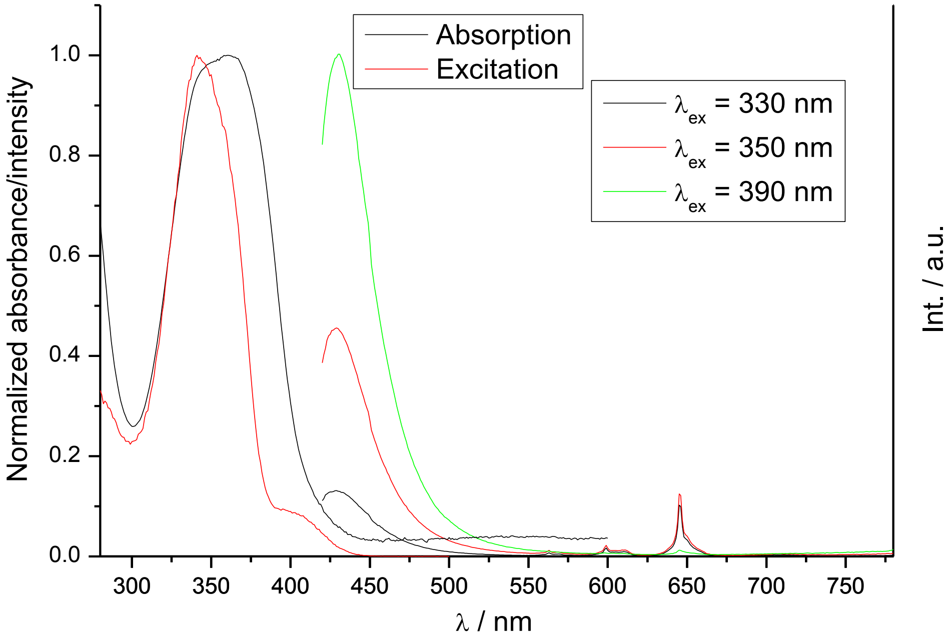

Figure 3. 61 Normalized absorption, excitation, and emission spectra of SmL2 in EA

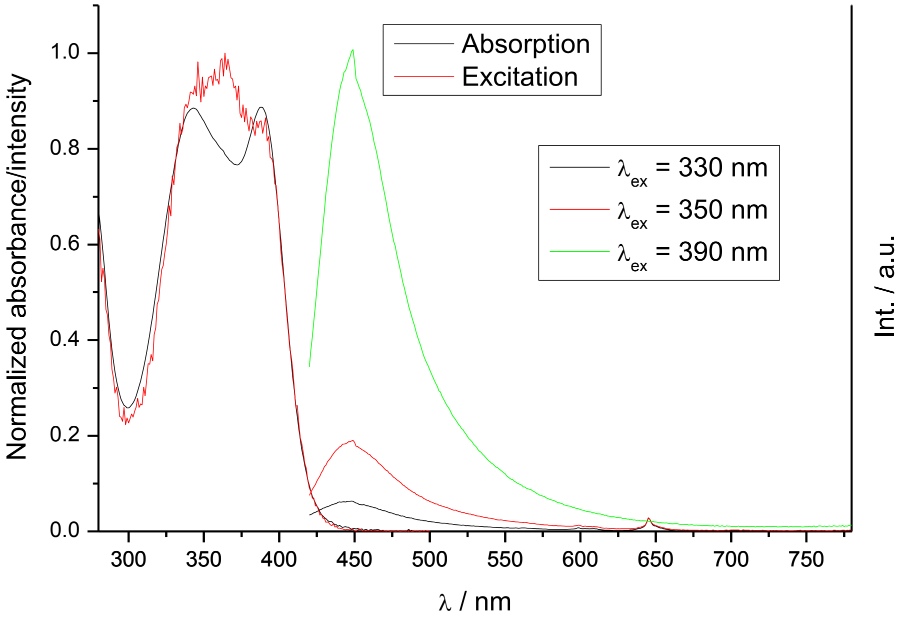

Figure 3. 62 Normalized absorption, excitation, and emission spectra of SmL2 in IPA

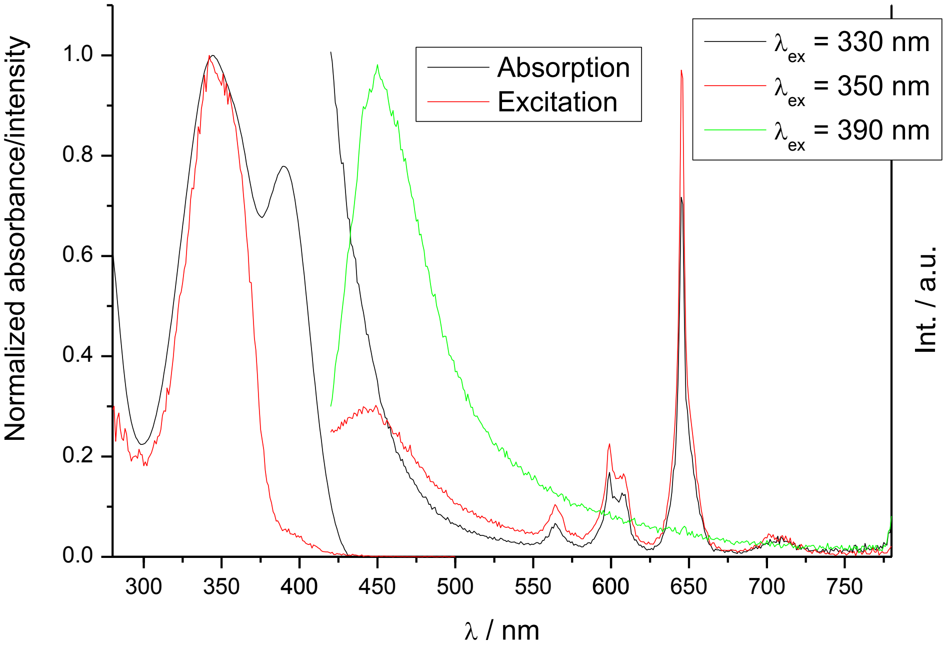

Figure 3. 63 Normalized absorption, excitation, and emission spectra of SmL2 in methanol

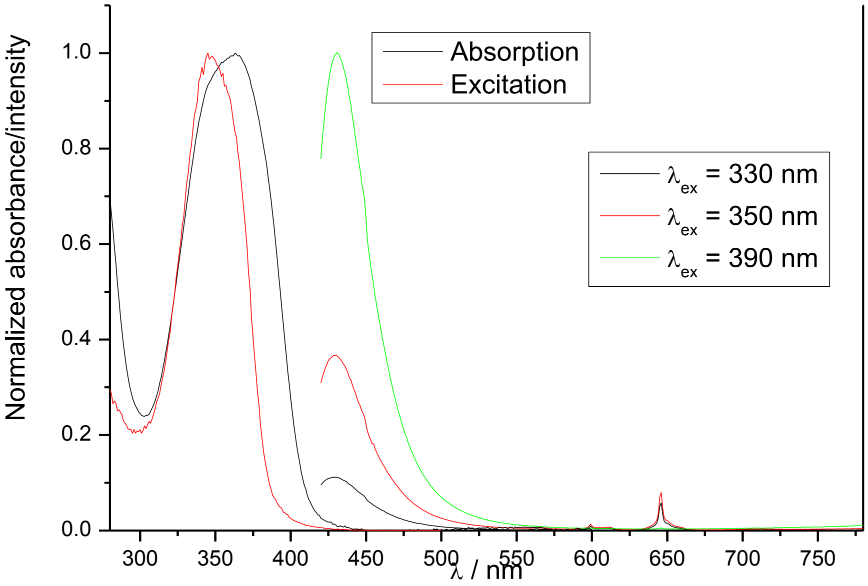

Figure 3. 64 Normalized absorption, excitation, and emission spectra of SmL2 in THF

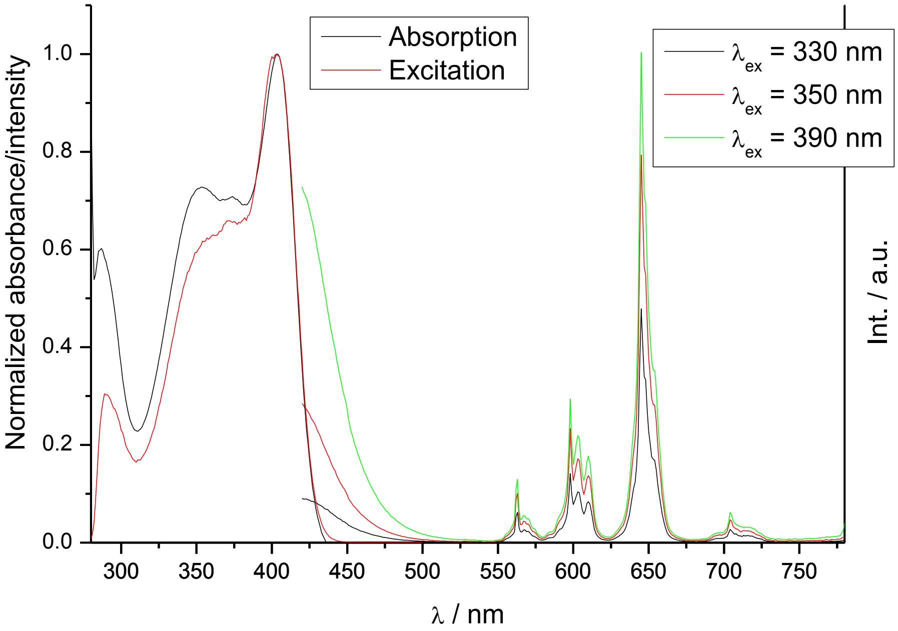

Figure 3. 65 Normalized absorption, excitation, and emission spectra of SmL2 in toluene

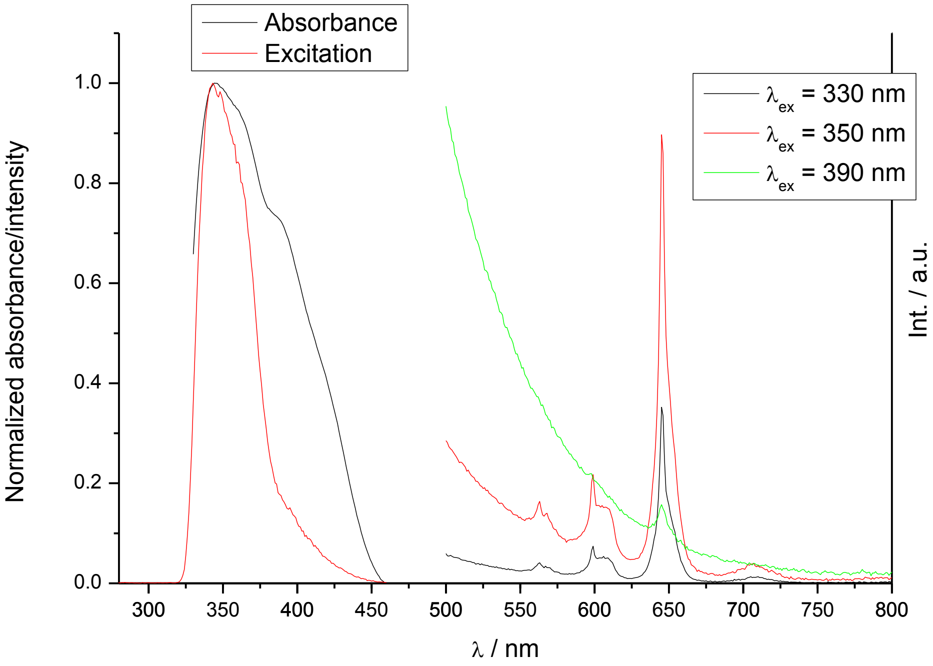

Figure 3. 66 Normalized absorption, excitation, and emission spectra of SmL3 in acetone

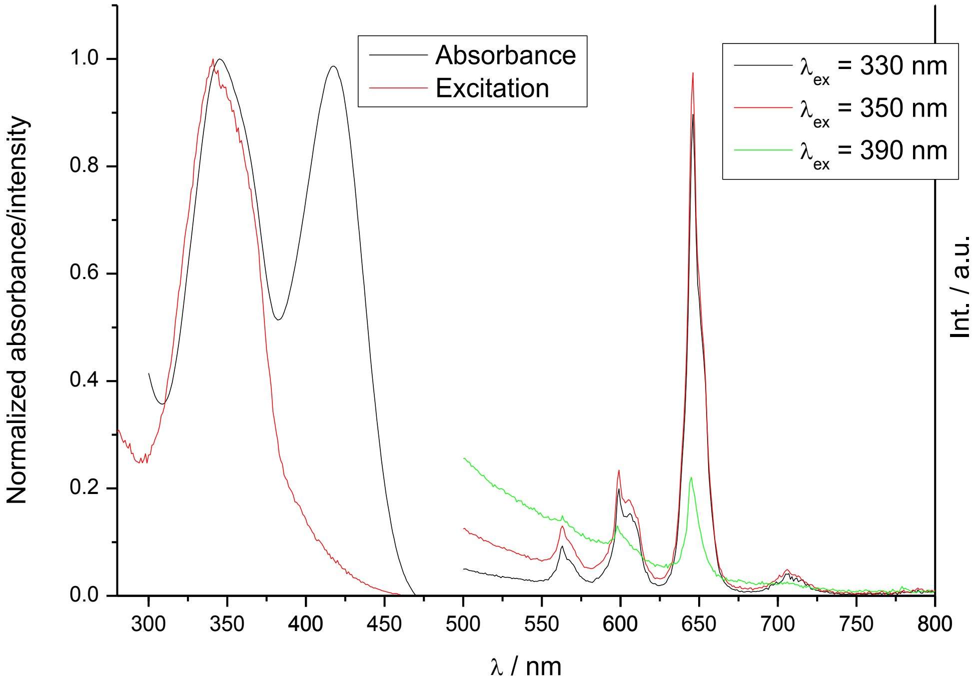

Figure 3. 67 Normalized absorption, excitation, and emission spectra of SmL3 in ACN

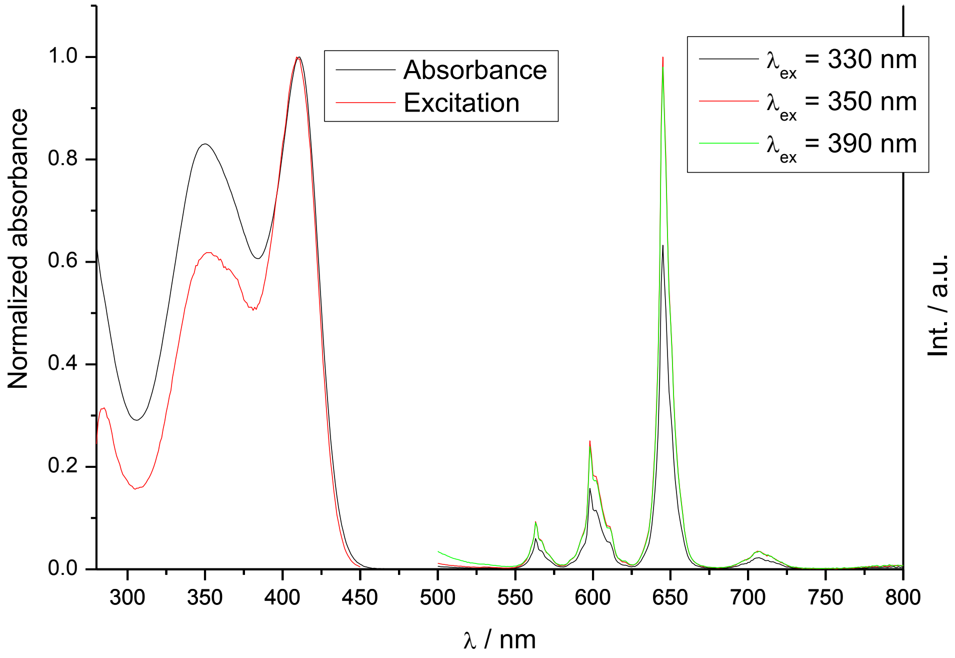

Figure 3. 68 Normalized absorption, excitation, and emission spectra of SmL3 in benzene

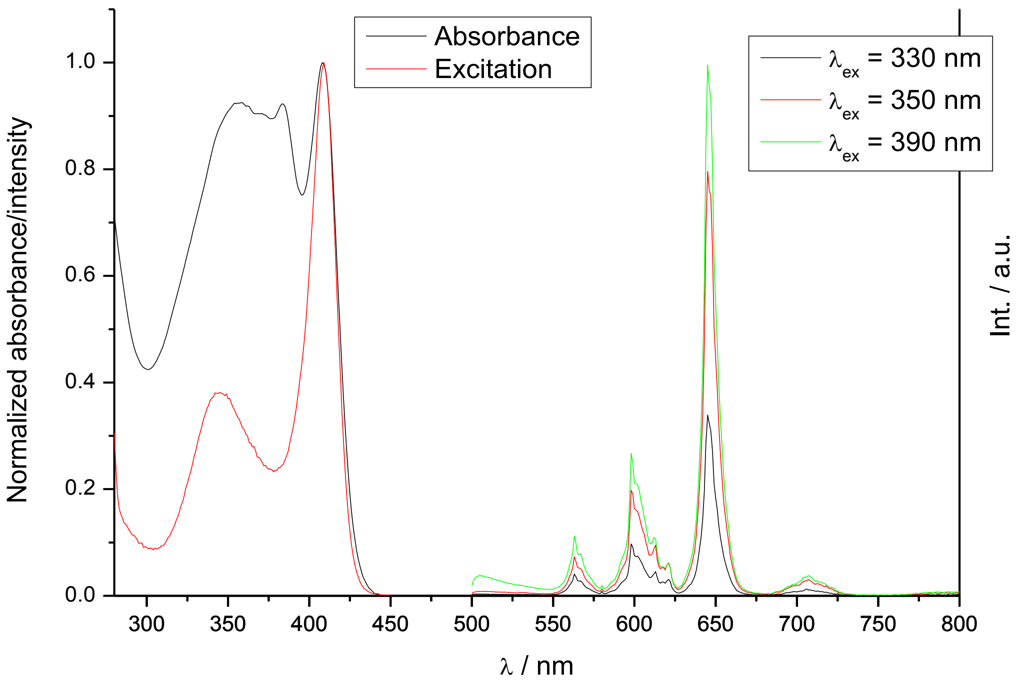

Figure 3. 69 Normalized absorption, excitation, and emission spectra of SmL3 in CCl_4

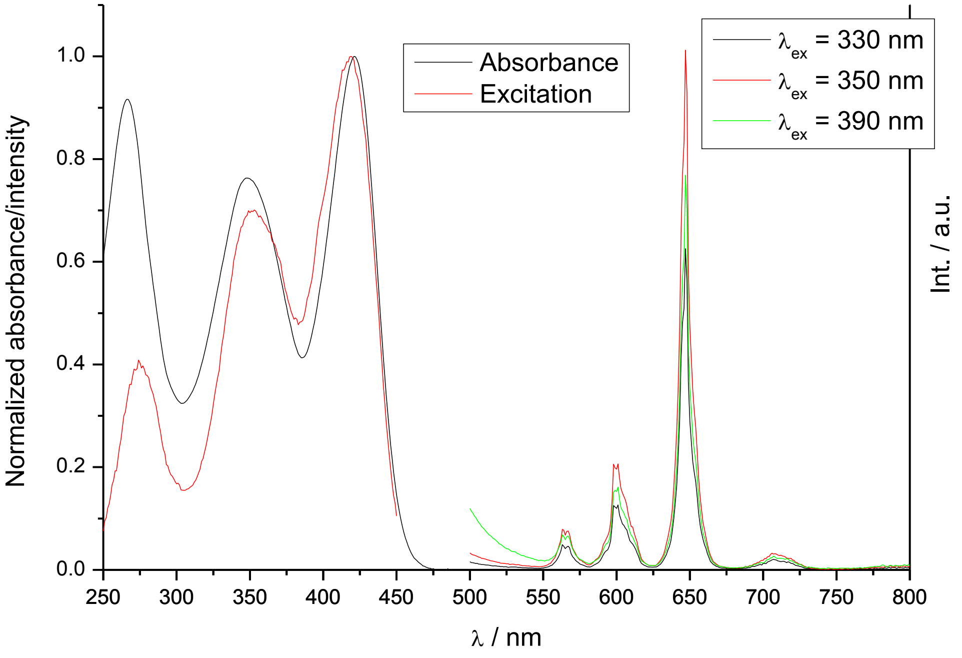

Figure 3. 70 Normalized absorption, excitation, and emission spectra of SmL3 in chloroform

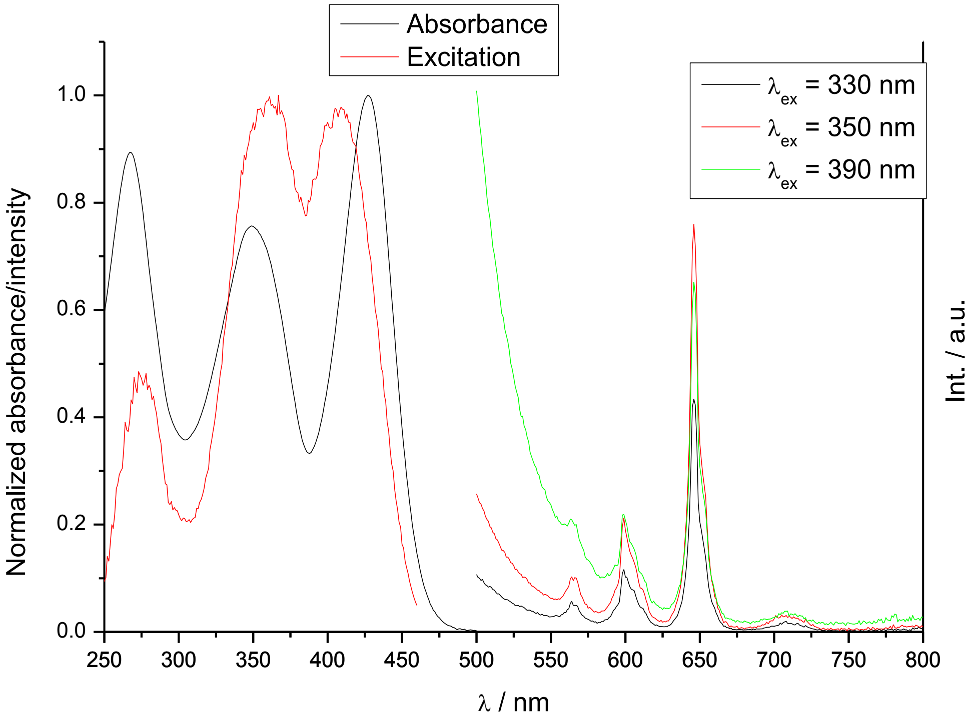

Figure 3. 71 Normalized absorption, excitation, and emission spectra of SmL3 in DCM

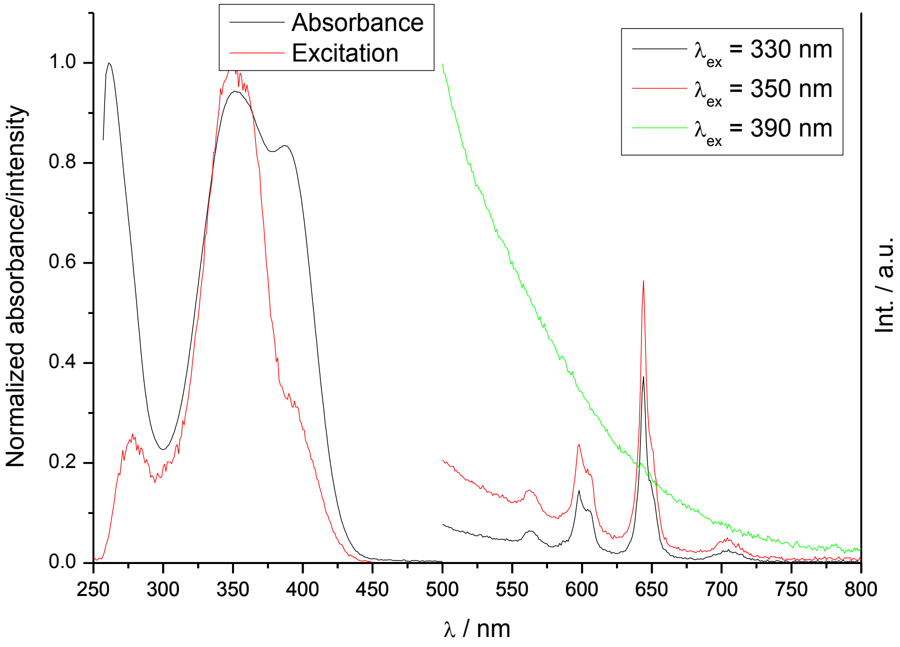

Figure 3. 72 Normalized absorption, excitation, and emission spectra of SmL3 in DMSO

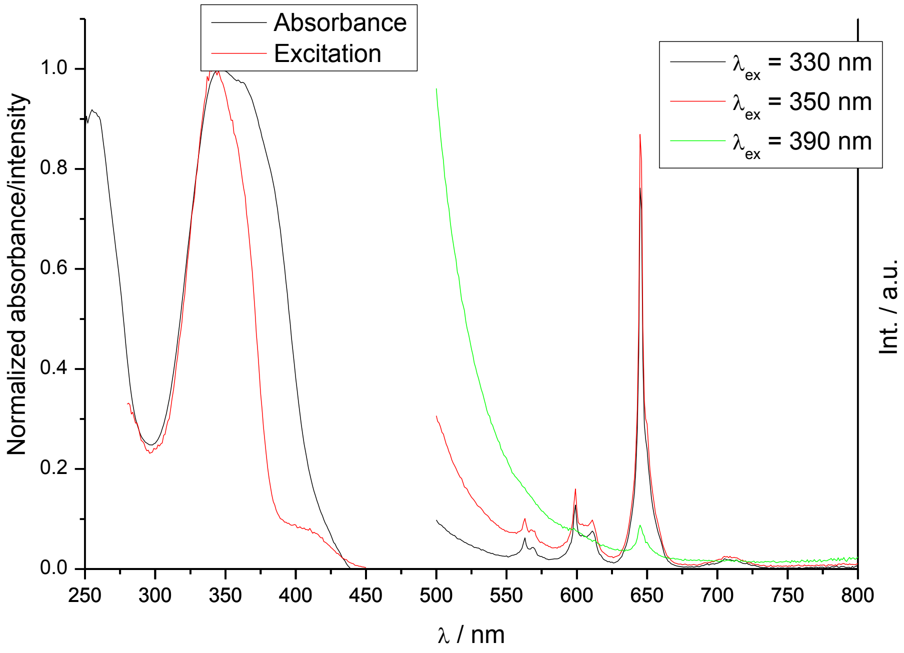

Figure 3. 73 Normalized absorption, excitation, and emission spectra of SmL3 in EA

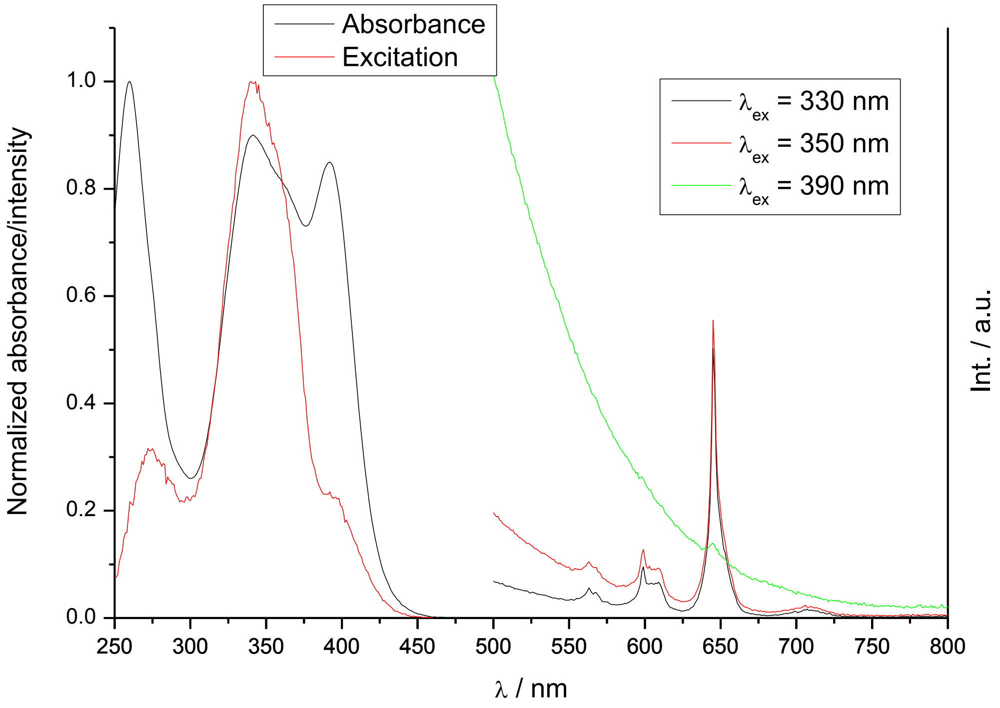

Figure 3. 74 Normalized absorption, excitation, and emission spectra of SmL3 in IPA

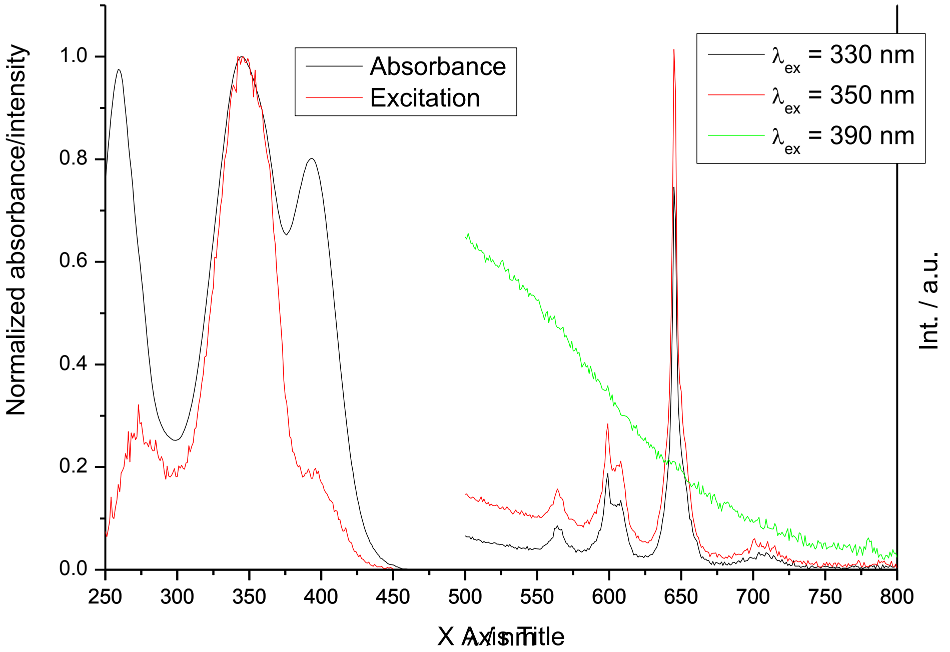

Figure 3. 75 Normalized absorption, excitation, and emission spectra of SmL3 in methanol

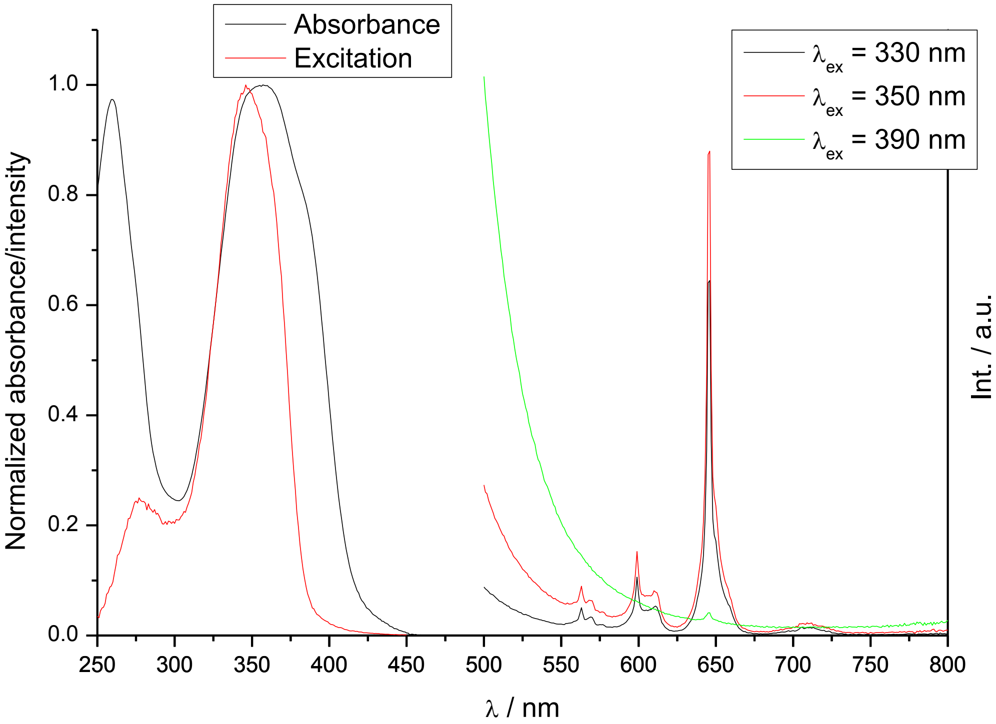

Figure 3. 76 Normalized absorption, excitation, and emission spectra of SmL3 in THF

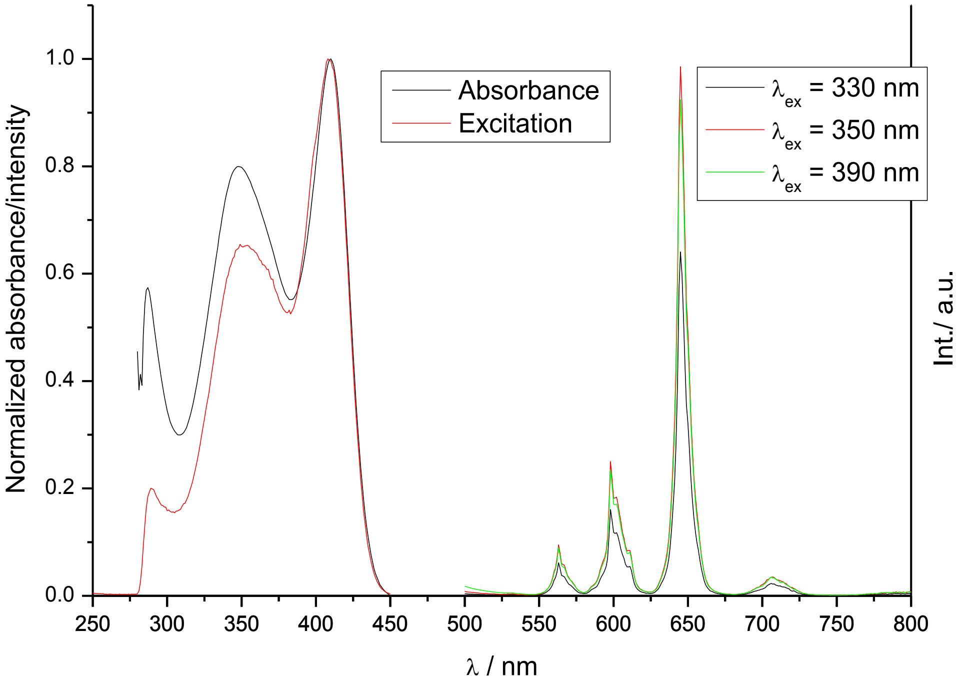

Figure 3. 77 Normalized absorption, excitation, and emission spectra of SmL3 in toluene

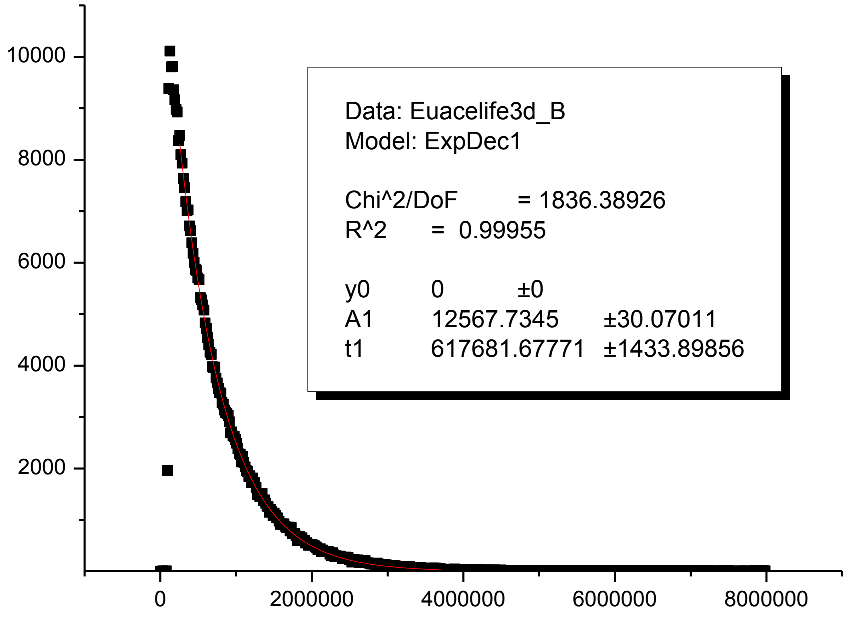

Figure 3. 78 Decay curve of luminescence lifetime measurement of EuL1 in acetone

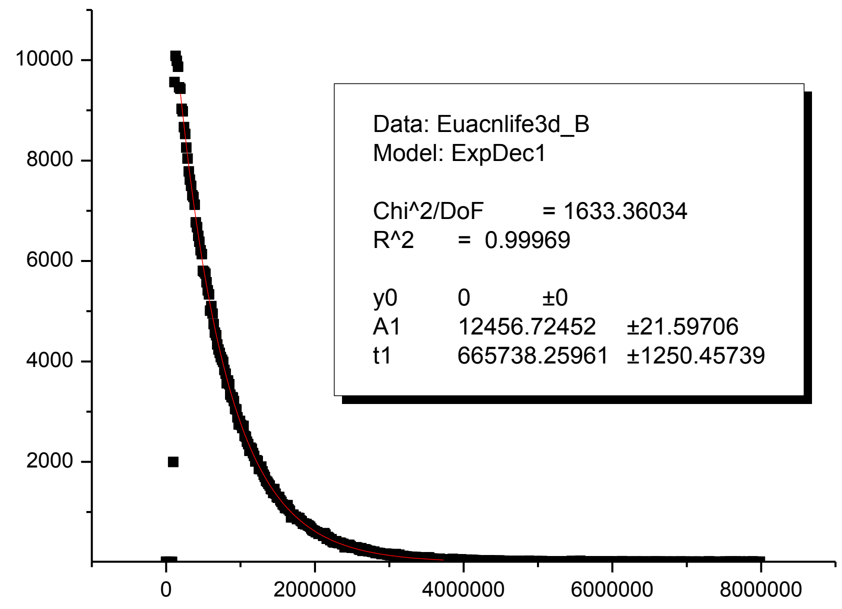

Figure 3. 79 Decay curve of luminescence lifetime measurement of EuL1 in acetonitrile

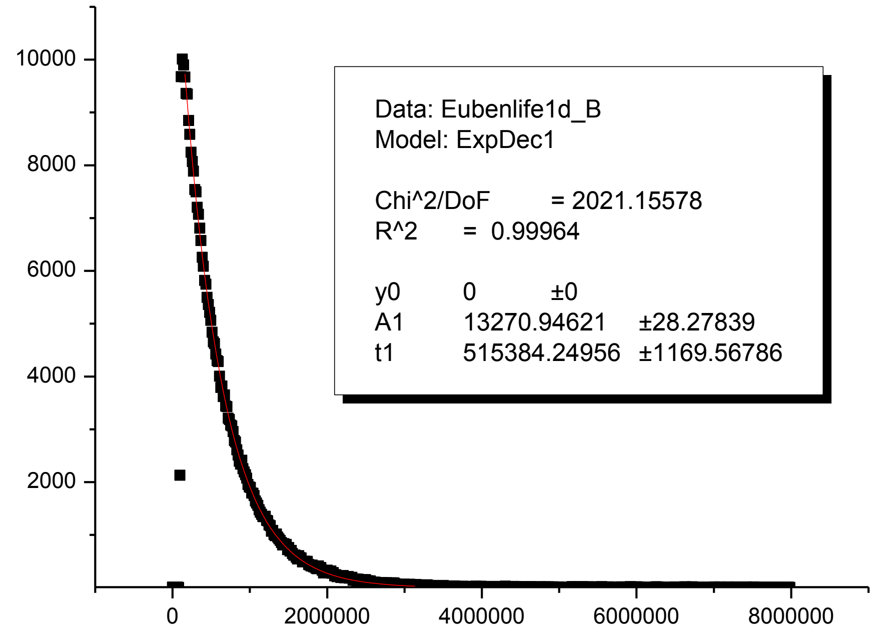

Figure 3. 80 Decay curve of luminescence lifetime measurement of EuL1 in benzene

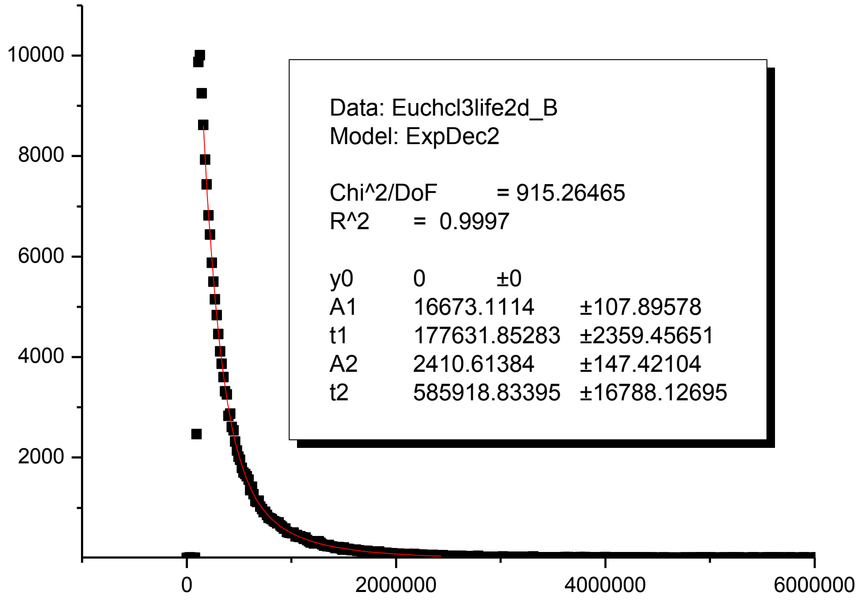

Figure 3. 81 Decay curve of luminescence lifetime measurement of EuL1 in chloroform

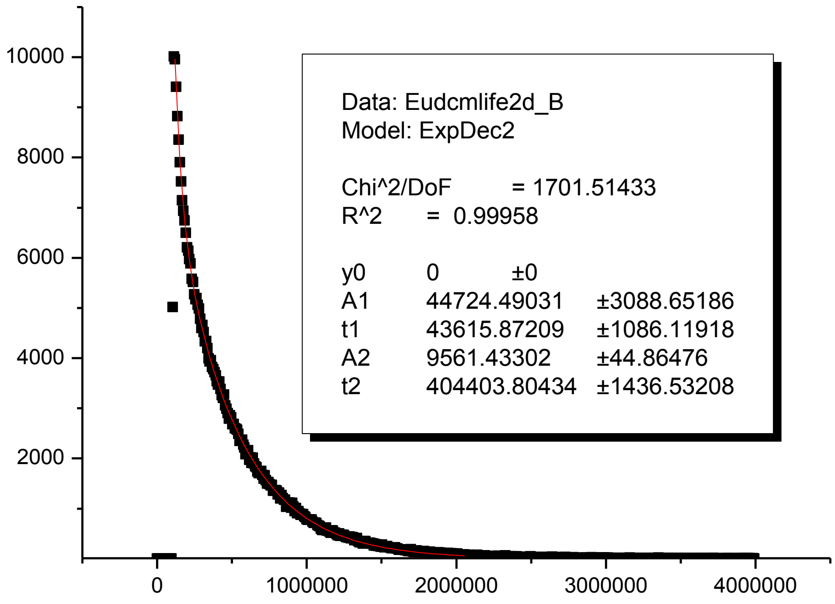

Figure 3. 82 Decay curve of luminescence lifetime measurement of EuL1 in dichloromethane

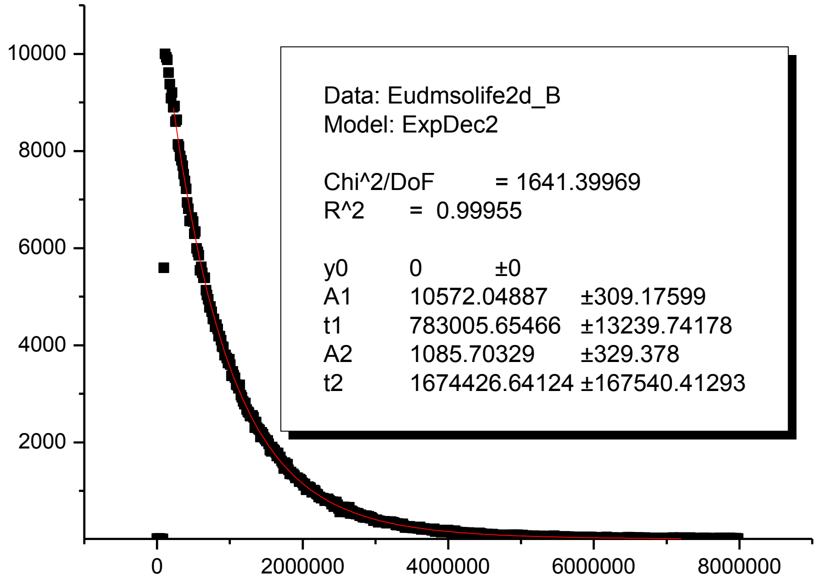

Figure 3. 83 Decay curve of luminescence lifetime measurement of EuL1 in dimethyl sulfoxide

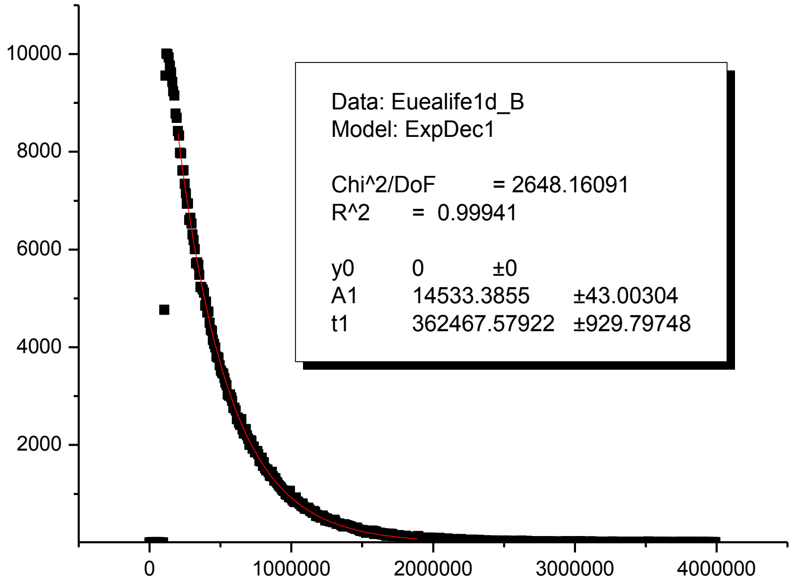

Figure 3. 84 Decay curve of luminescence lifetime measurement of EuL1 in ethyl acetate

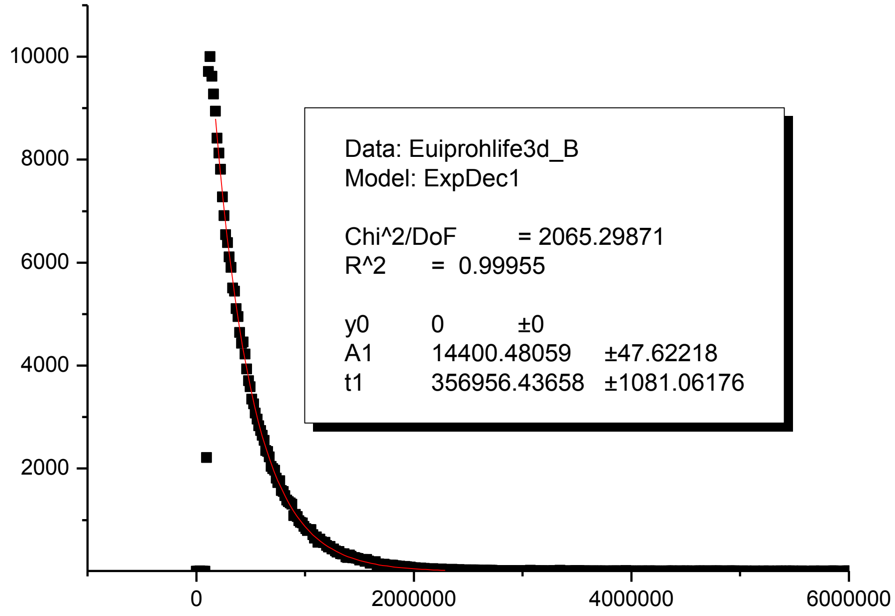

Figure 3. 85 Decay curve of luminescence lifetime measurement of EuL1 in isopropanol

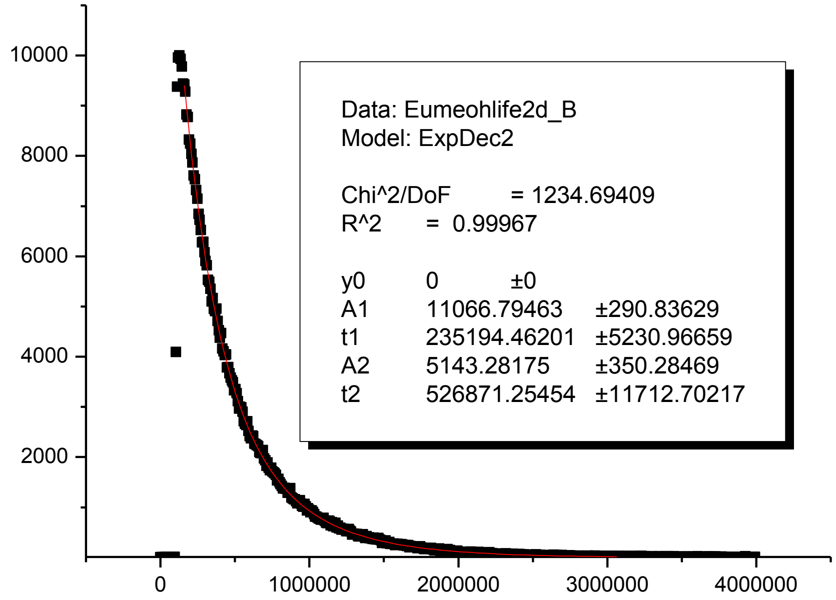

Figure 3. 86 Decay curve of luminescence lifetime measurement of EuL1 in methanol

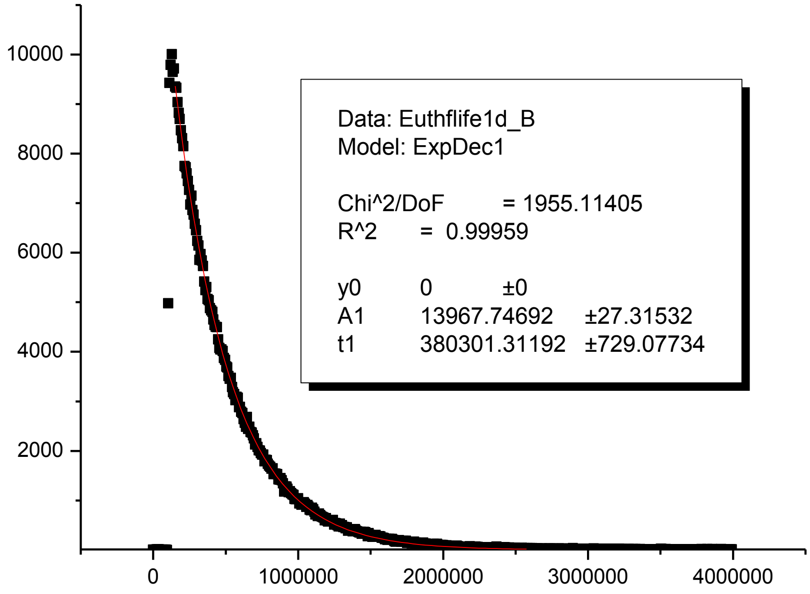

Figure 3. 87 Decay curve of luminescence lifetime measurement of EuL1 in tetrahydrofuran

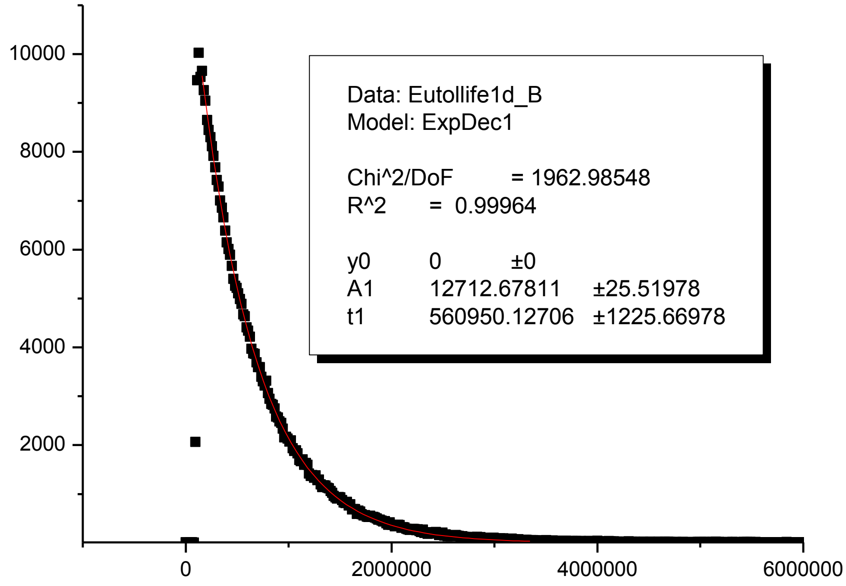

Figure 3. 88 Decay curve of luminescence lifetime measurement of EuL1 in toluene

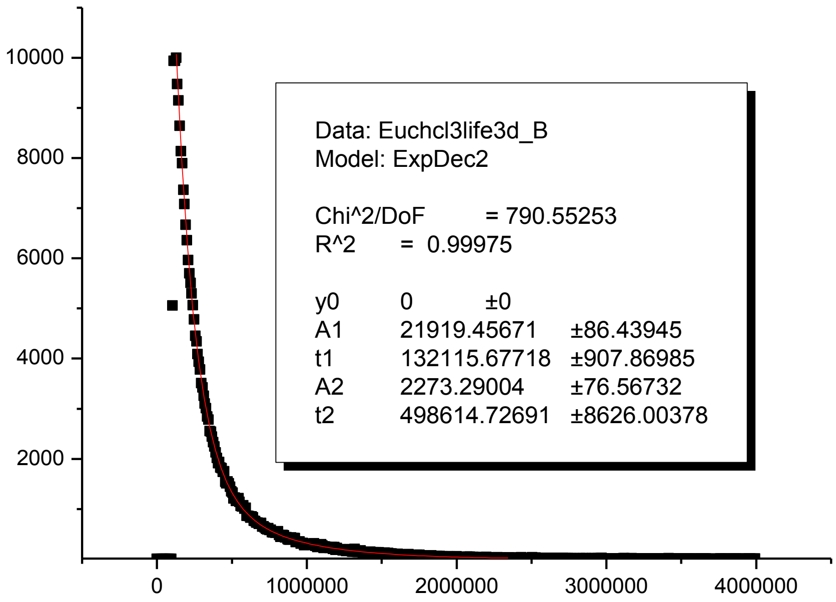

Figure 3. 89 Decay curve of luminescence lifetime measurement of EuL2 in chloroform

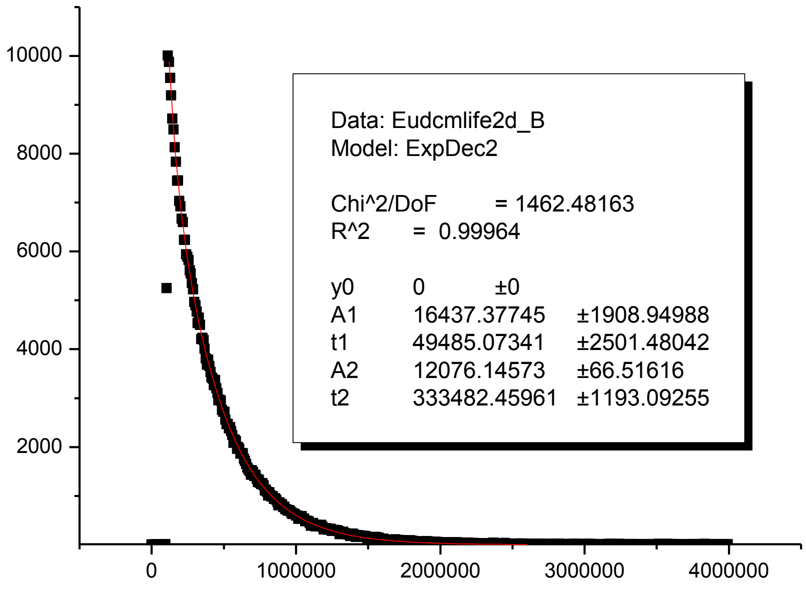

Figure 3. 90 Decay curve of luminescence lifetime measurement of EuL2 in dichloromethane

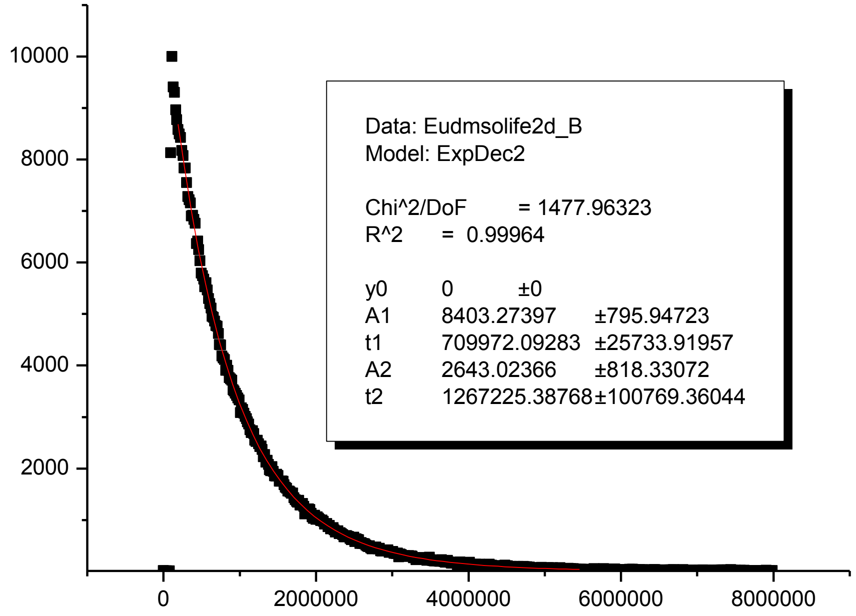

Figure 3. 91 Decay curve of luminescence lifetime measurement of EuL2 in dimethyl sulfoxide

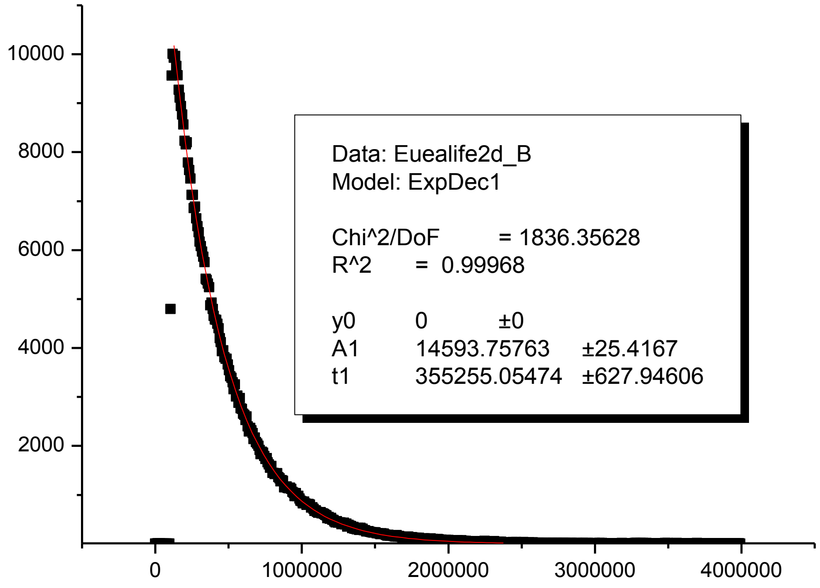

Figure 3. 92 Decay curve of luminescence lifetime measurement of EuL2 in ethyl acetate

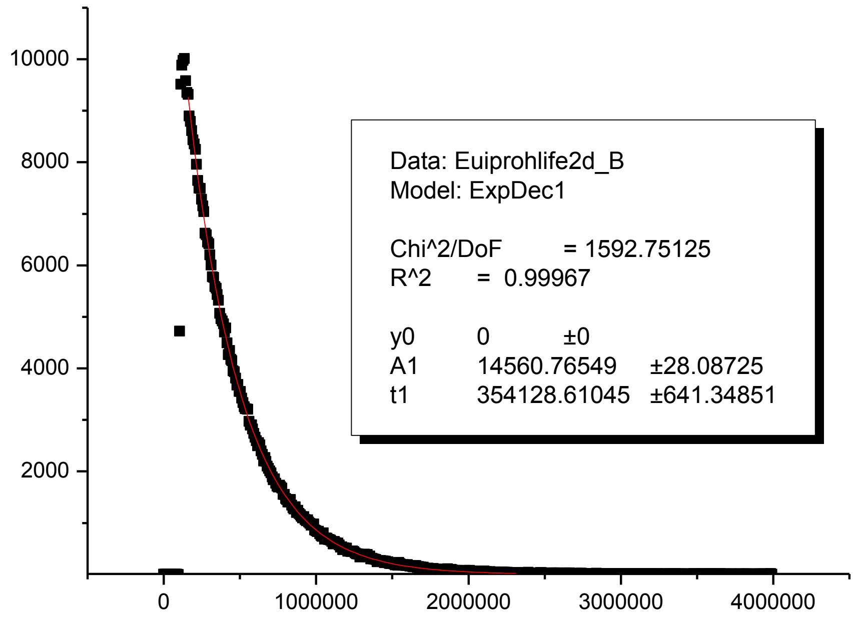

Figure 3. 93 Decay curve of luminescence lifetime measurement of EuL2 in isopropanol

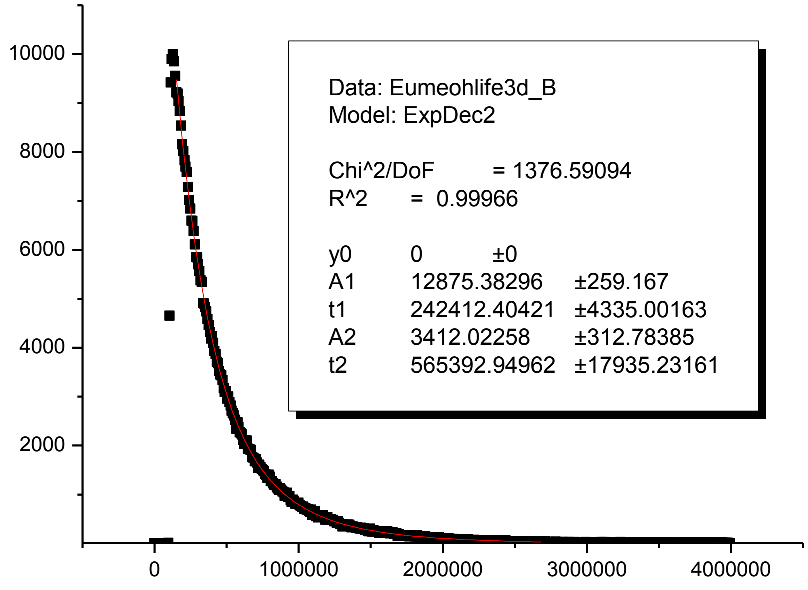

Figure 3. 94 Decay curve of luminescence lifetime measurement of EuL2 in methanol

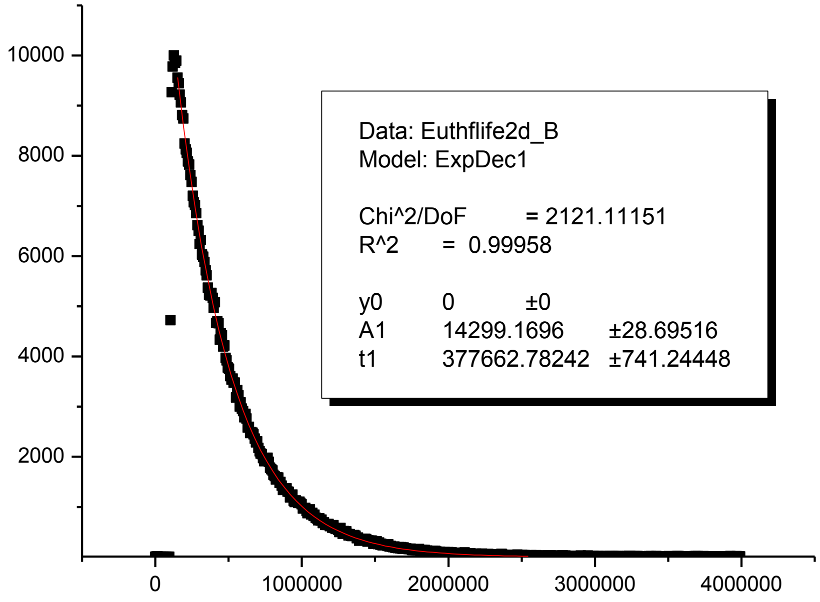

```
Data: Euthflife2d_B
Model: ExpDec1

Chi^2/DoF        = 2121.11151
R^2      =  0.99958

y0        0           ±0
A1        14299.1696       ±28.69516
t1        377662.78242   ±741.24448
```

Figure 3. 95 Decay curve of luminescence lifetime measurement of EuL2 in THF

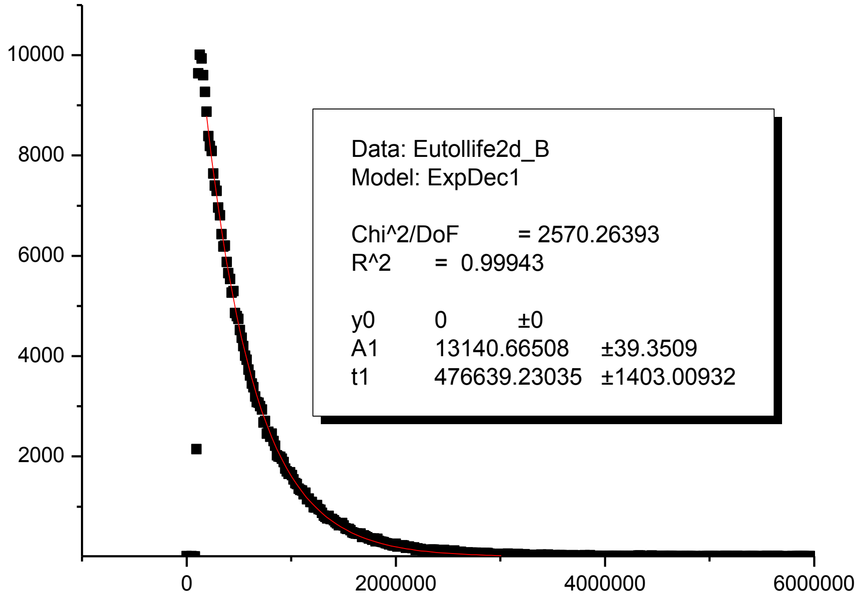

```
Data: Eutollife2d_B
Model: ExpDec1

Chi^2/DoF        = 2570.26393
R^2      =  0.99943

y0        0           ±0
A1        13140.66508     ±39.3509
t1        476639.23035   ±1403.00932
```

Figure 3. 96 Decay curve of luminescence lifetime measurement of EuL2 in toluene

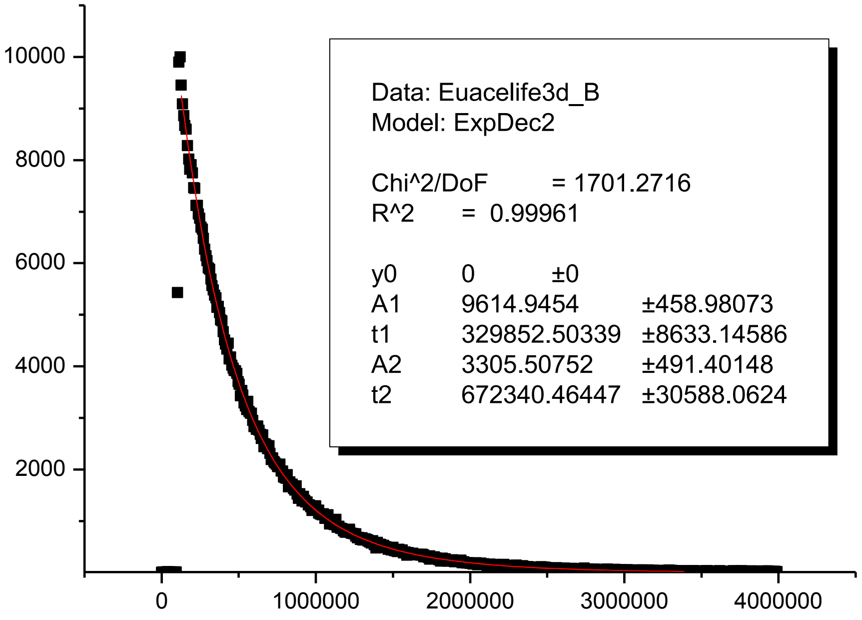

Figure 3. 97 Decay curve of luminescence lifetime measurement of EuL3 in acetone

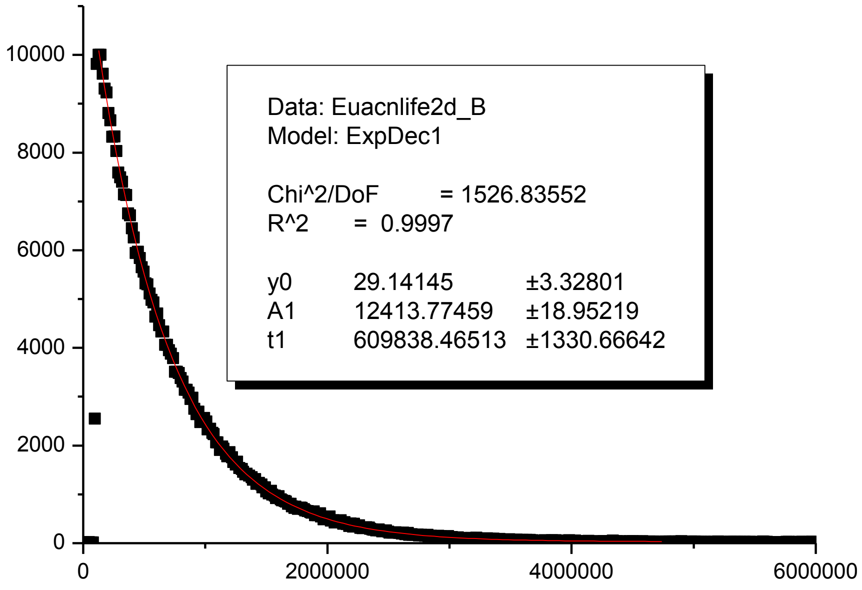

Figure 3. 98 Decay curve of luminescence lifetime measurement of EuL3 in acetonitrile

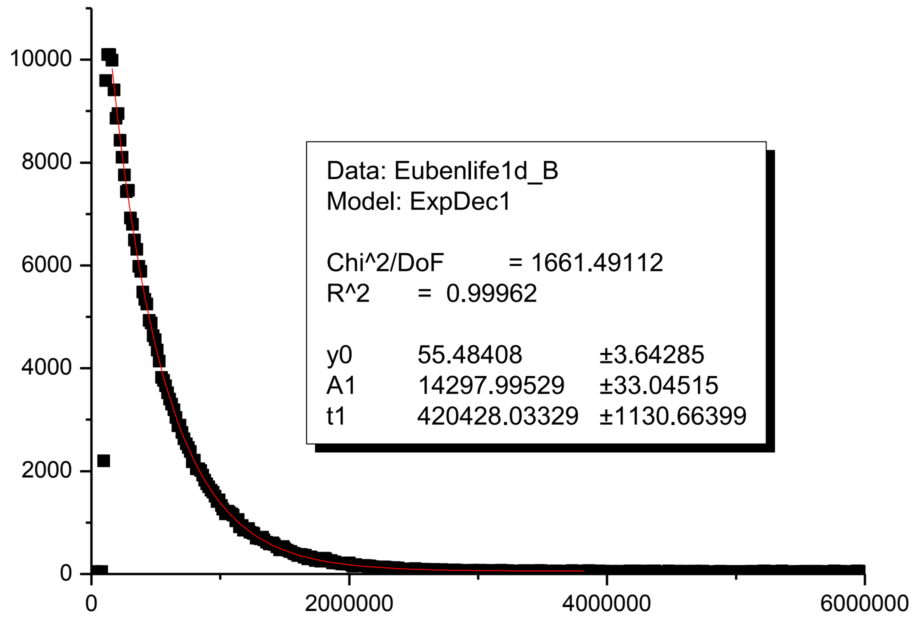

Figure 3. 99 Decay curve of luminescence lifetime measurement of EuL3 in benzene

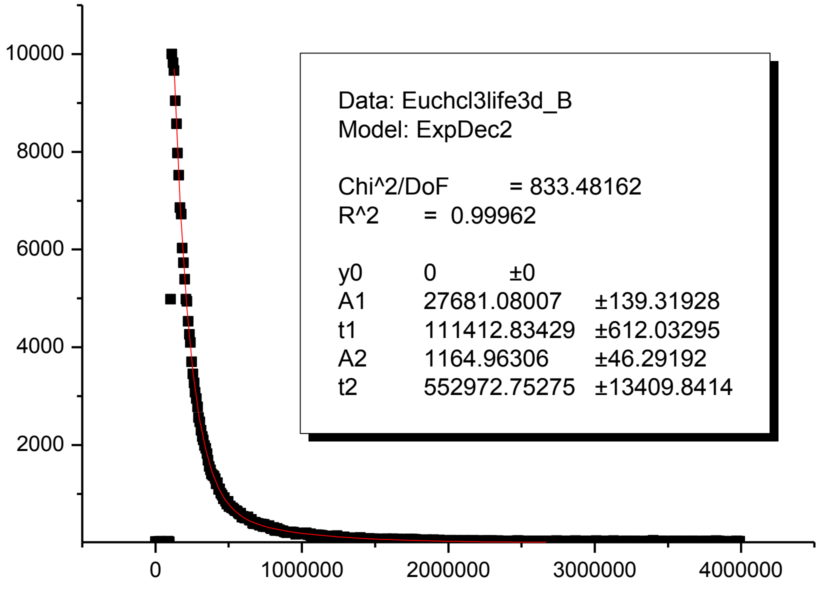

Figure 3. 100 Decay curve of luminescence lifetime measurement of EuL3 in chloroform

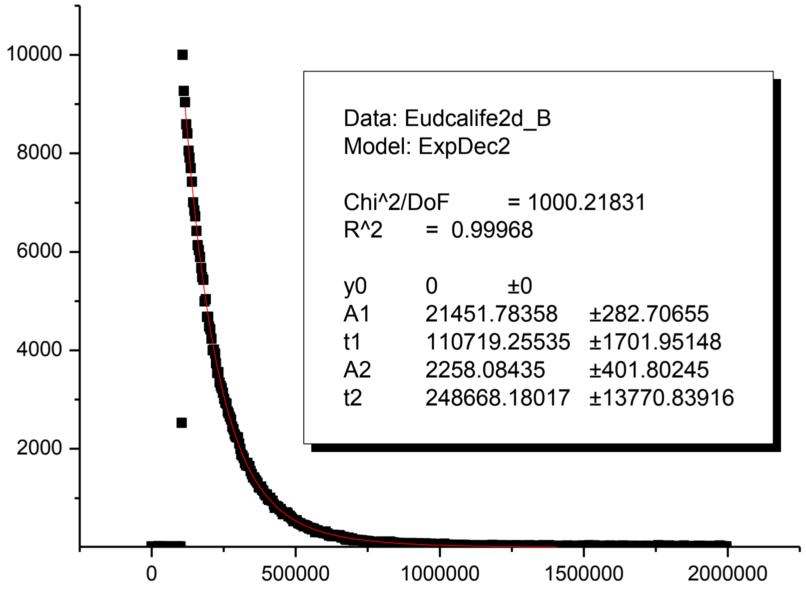

Figure 3. 101 Decay curve of luminescence lifetime measurement of EuL3 in 1,2-dichloroethane

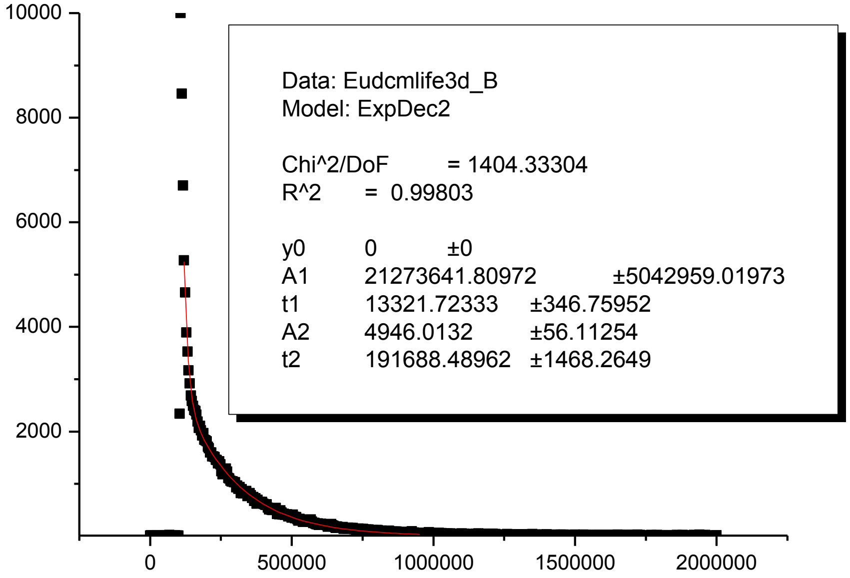

Figure 3. 102 Decay curve of luminescence lifetime measurement of EuL3 in dichloromethane

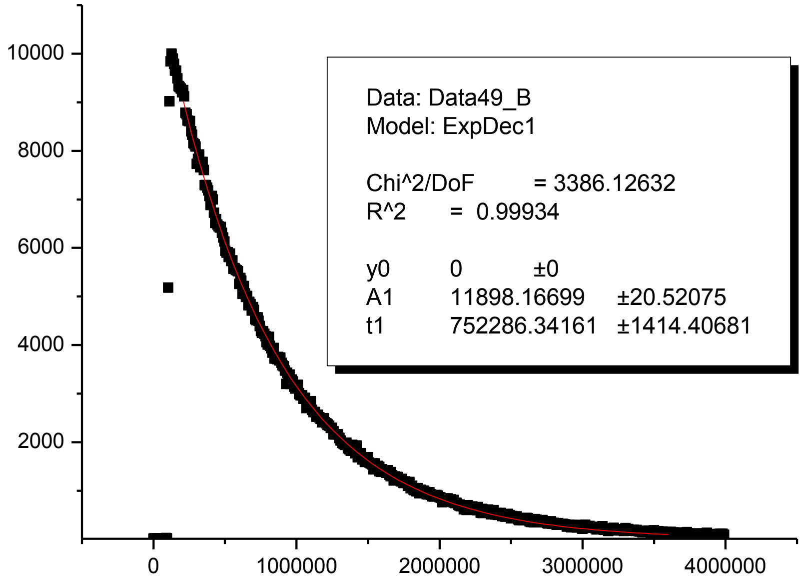

Figure 3. 103 Decay curve of luminescence lifetime measurement of EuL3 in dimethyl sulfoxide

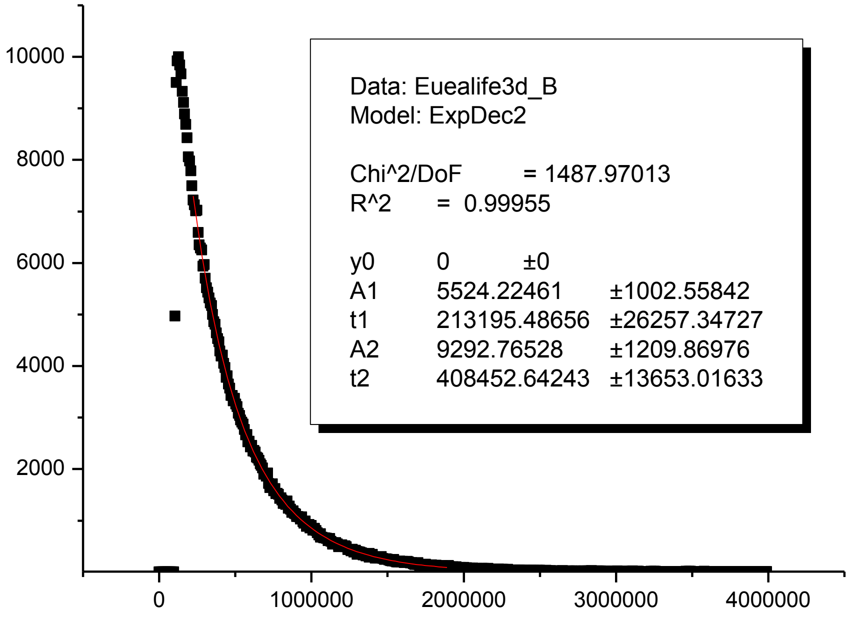

Figure 3. 104 Decay curve of luminescence lifetime measurement of EuL3 in ethyl acetate

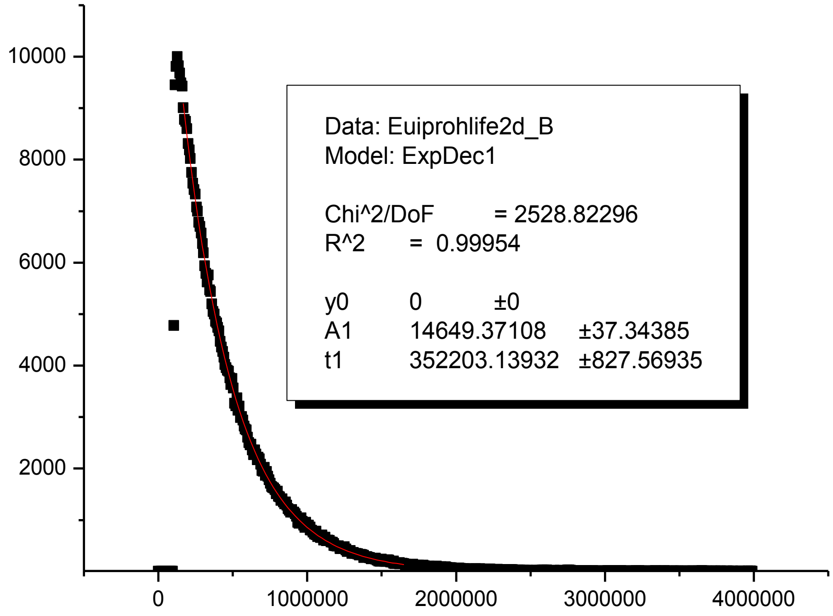

Figure 3. 105 Decay curve of luminescence lifetime measurement of EuL3 in isopropanol

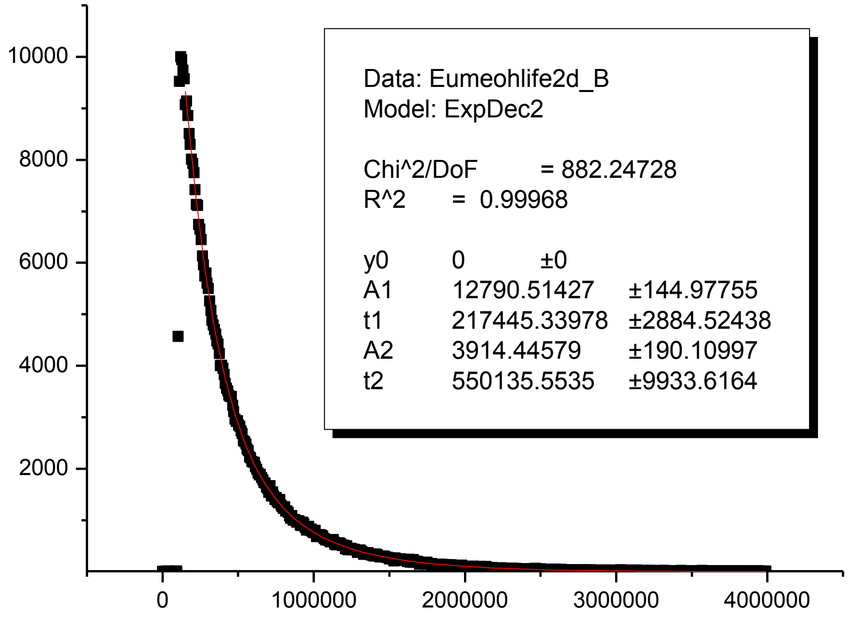

Figure 3. 106 Decay curve of luminescence lifetime measurement of EuL3 in methanol

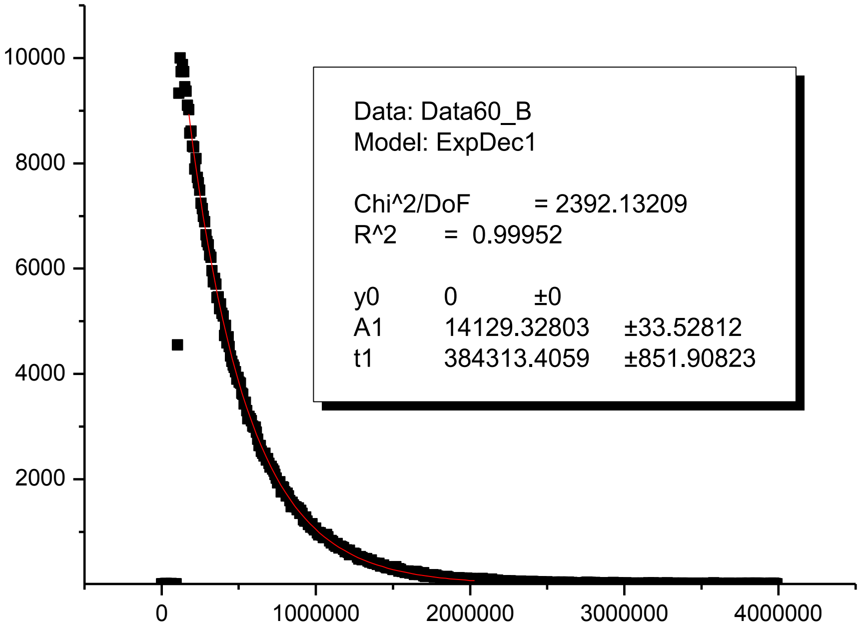

Figure 3. 107 Decay curve of luminescence lifetime measurement of EuL3 in THF

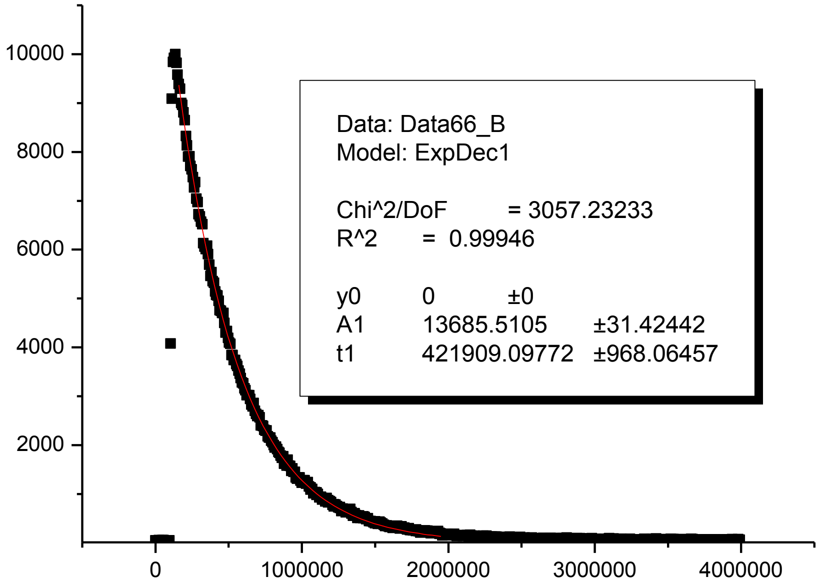

Figure 3. 108 Decay curve of luminescence lifetime measurement of EuL3 in toluene

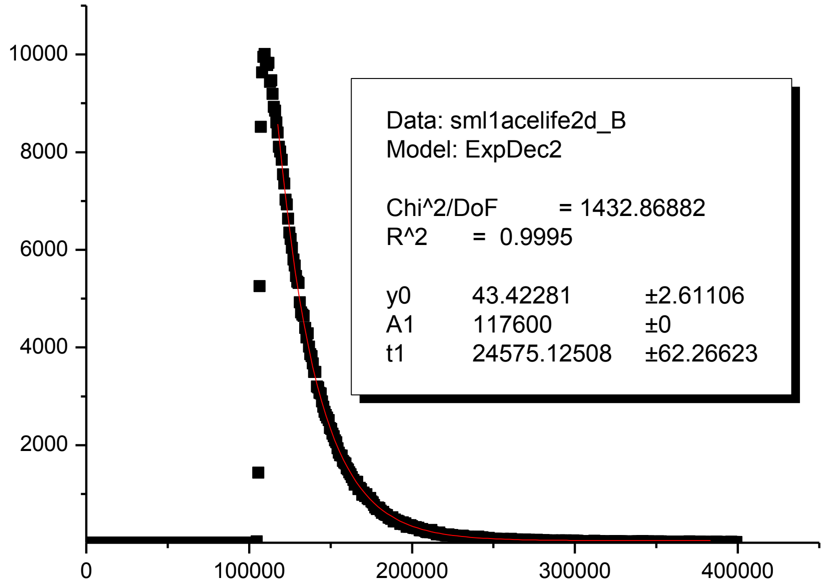

Figure 3. 109 Decay curve of luminescence lifetime measurement of SmL1 in acetone

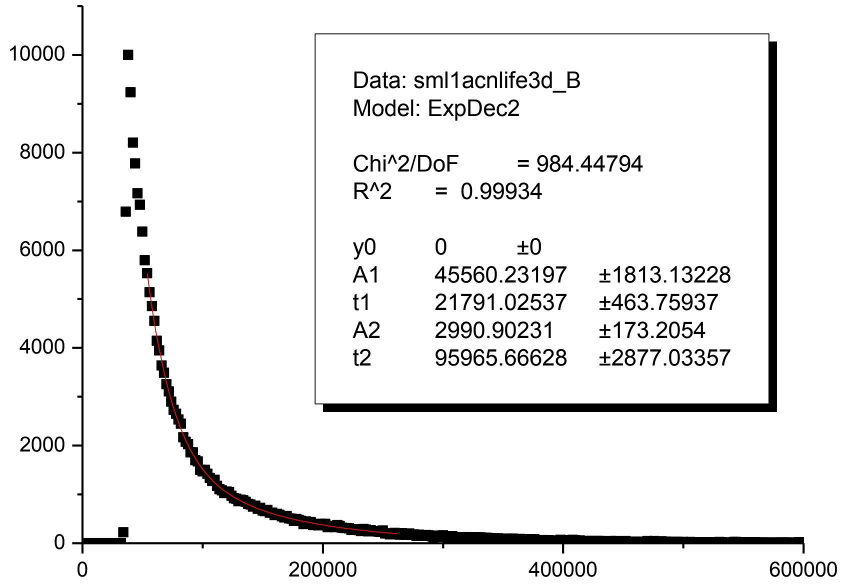

Figure 3. 110 Decay curve of luminescence lifetime measurement of SmL1 in acetonitrile

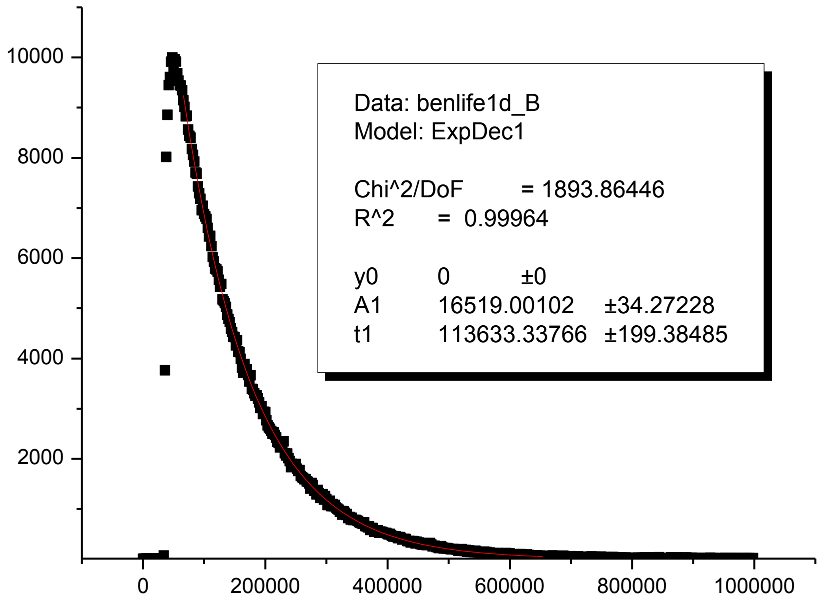

Figure 3. 111 Decay curve of luminescence lifetime measurement of SmL1 in benzene

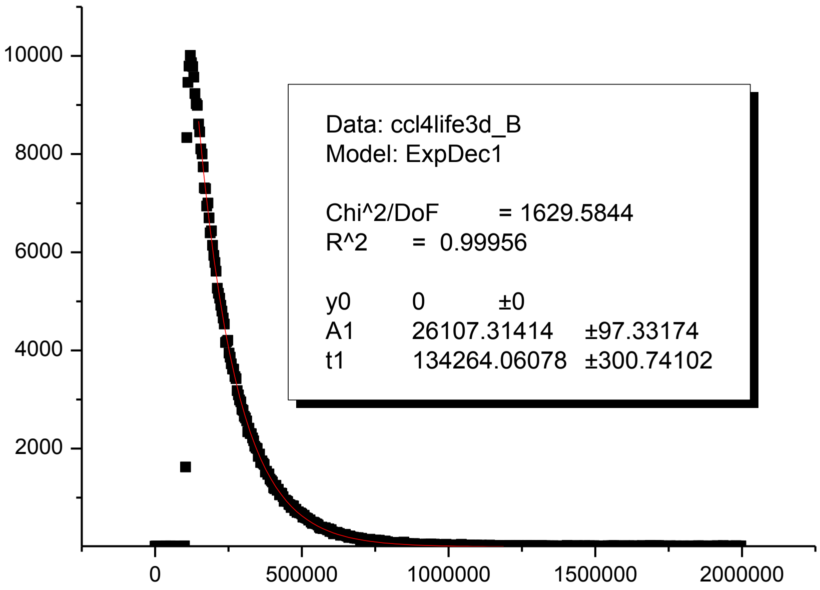

Figure 3. 112 Decay curve of luminescence lifetime measurement of SmL1 in carbon tetrachloride

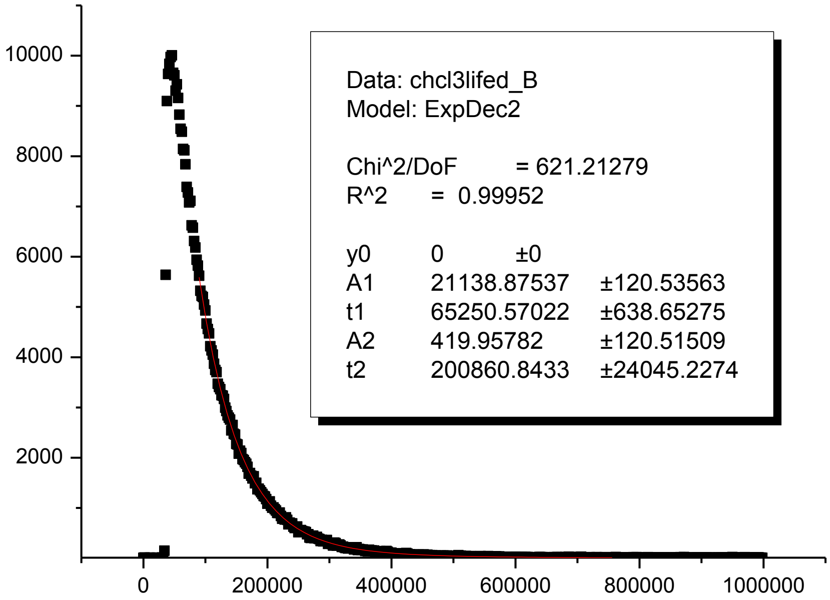

Figure 3. 113 Decay curve of luminescence lifetime measurement of SmL1 in chloroform

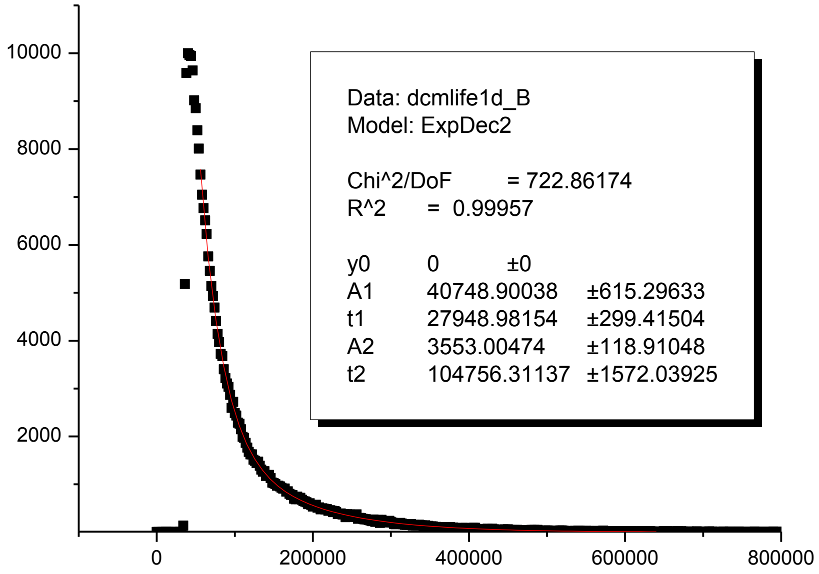

Figure 3. 114 Decay curve of luminescence lifetime measurement of SmL1 in dichloromethane

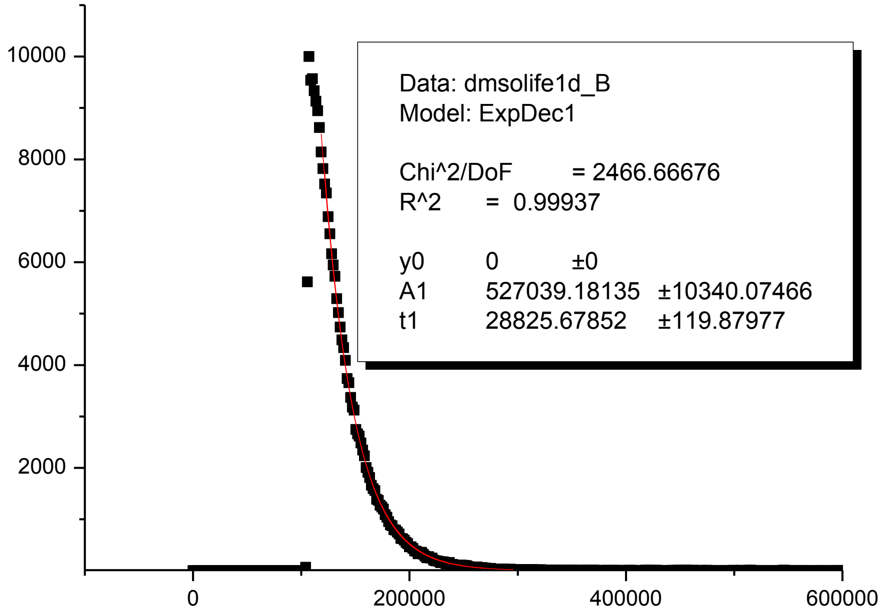

Figure 3. 115 Decay curve of luminescence lifetime measurement of SmL1 in DMSO

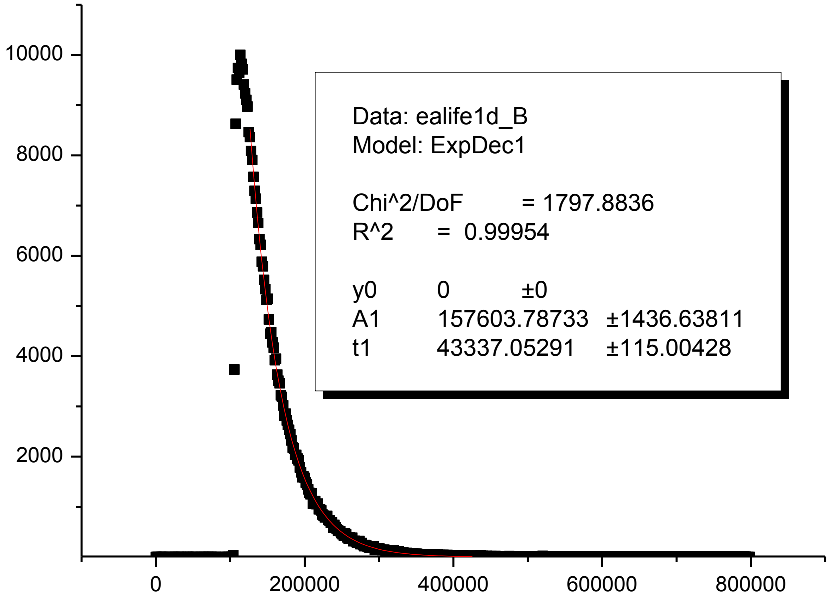

Figure 3. 116 Decay curve of luminescence lifetime measurement of SmL1 in ethyl acetate

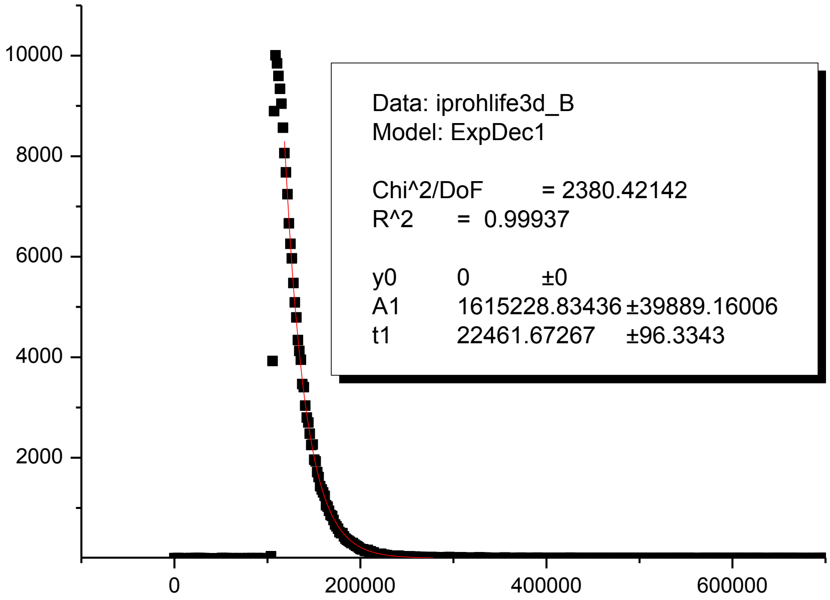

Figure 3. 117 Decay curve of luminescence lifetime measurement of SmL1 in isopropanol

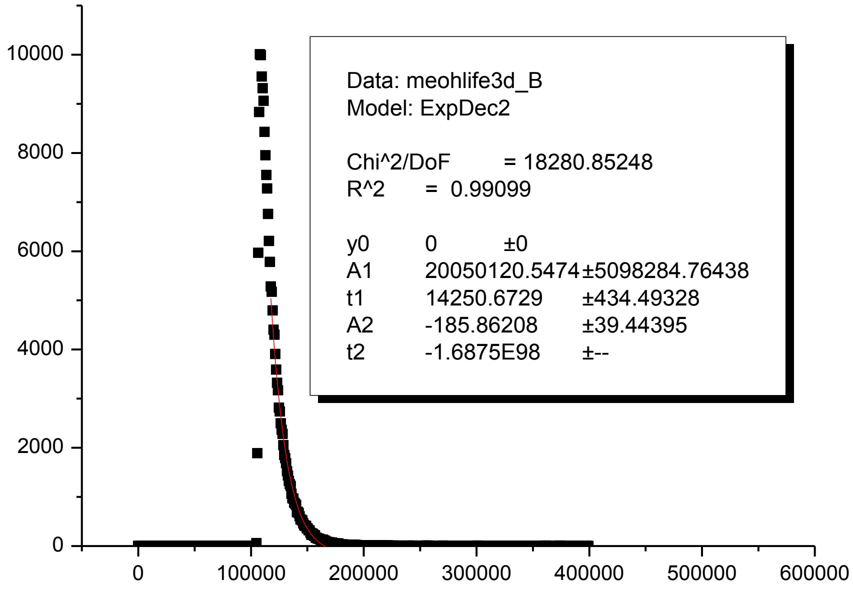

Figure 3. 118 Decay curve of luminescence lifetime measurement of SmL1 in methanol

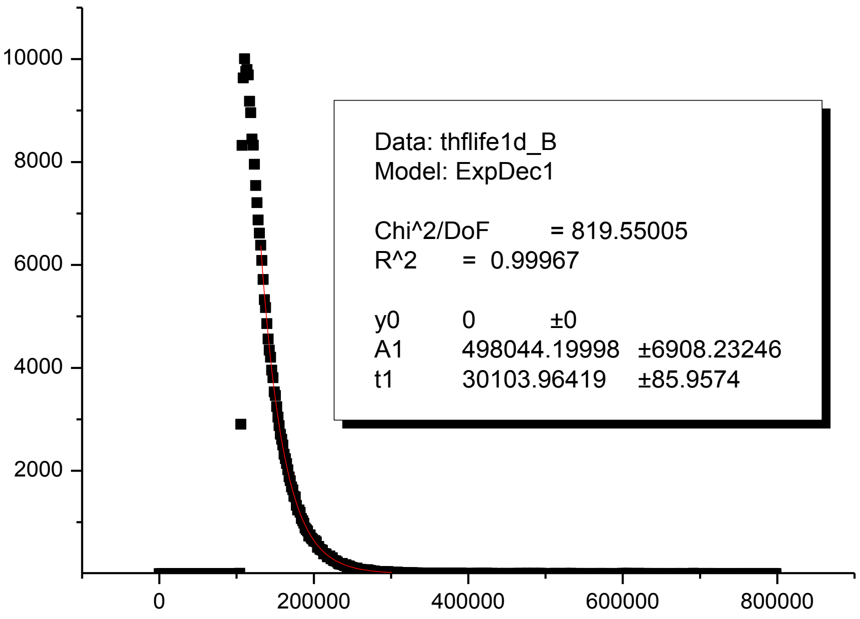

Figure 3. 119 Decay curve of luminescence lifetime measurement of SmL1 in THF

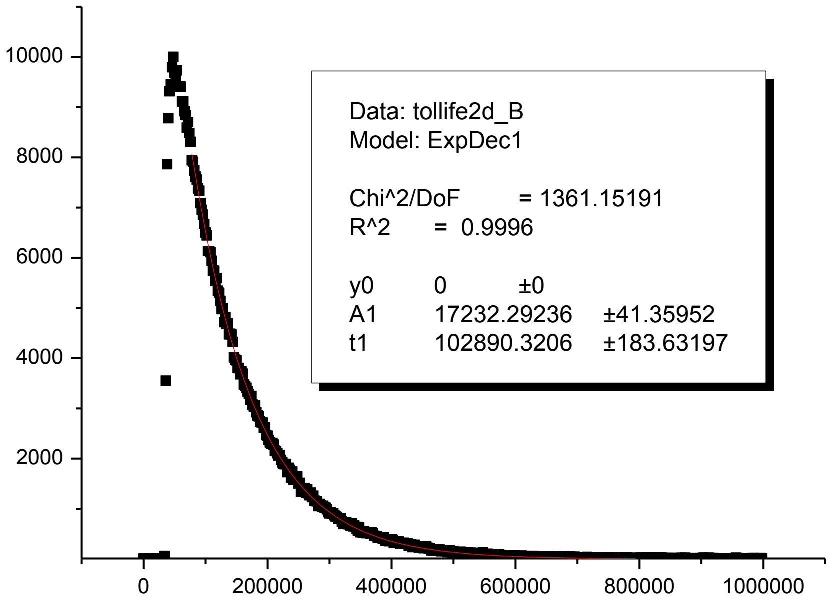

Figure 3. 120 Decay curve of luminescence lifetime measurement of SmL1 in toluene

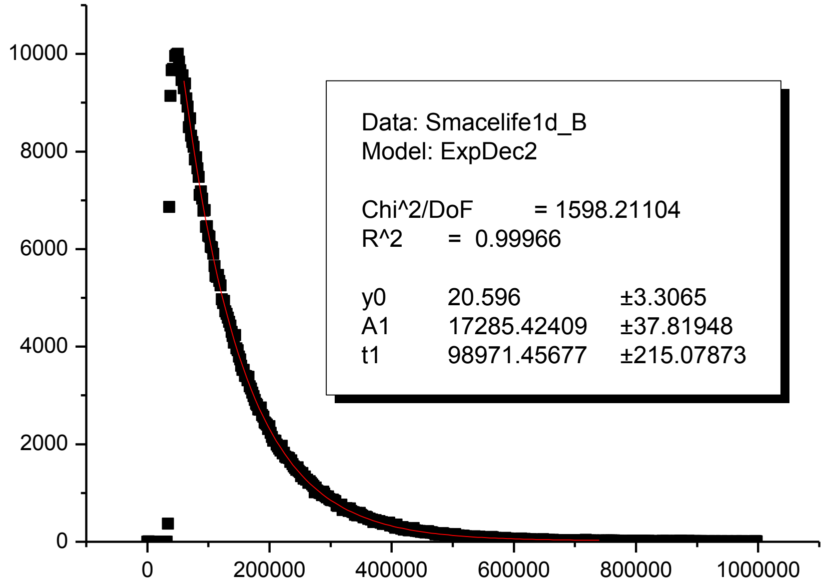

Figure 3. 121 Decay curve of luminescence lifetime measurement of SmL2 in acetone

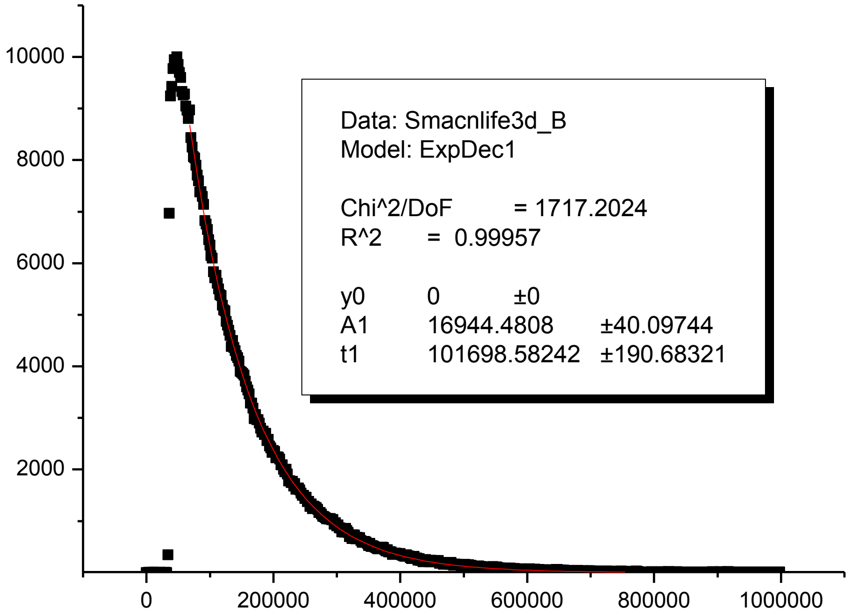

Figure 3. 122 Decay curve of luminescence lifetime measurement of SmL2 in acetonitrile

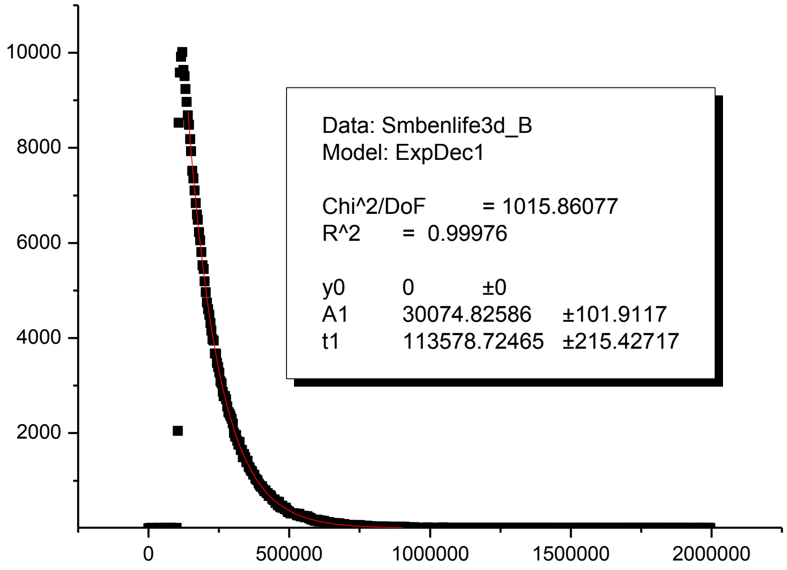

Figure 3. 123 Decay curve of luminescence lifetime measurement of SmL2 in benzene

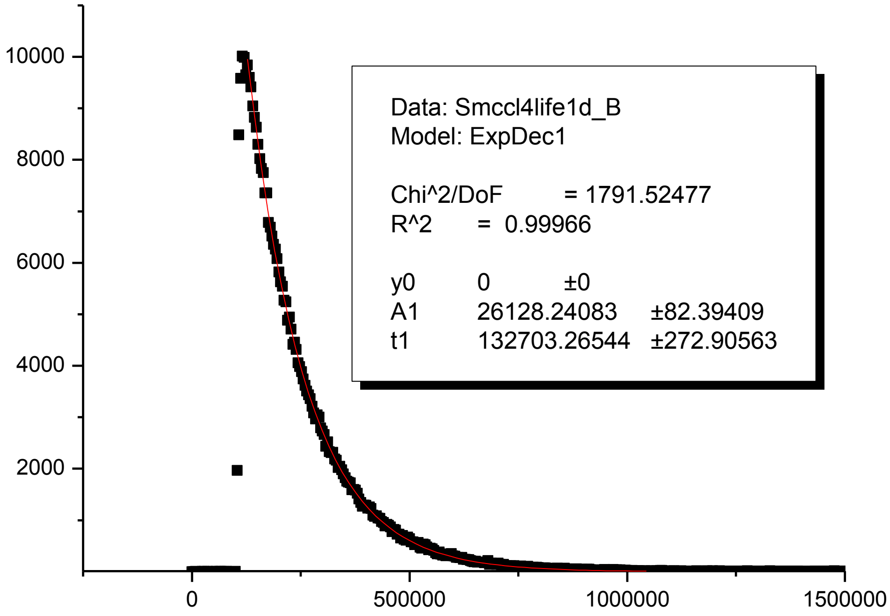

Figure 3. 124 Decay curve of luminescence lifetime measurement of SmL2 in carbon tetrachloride

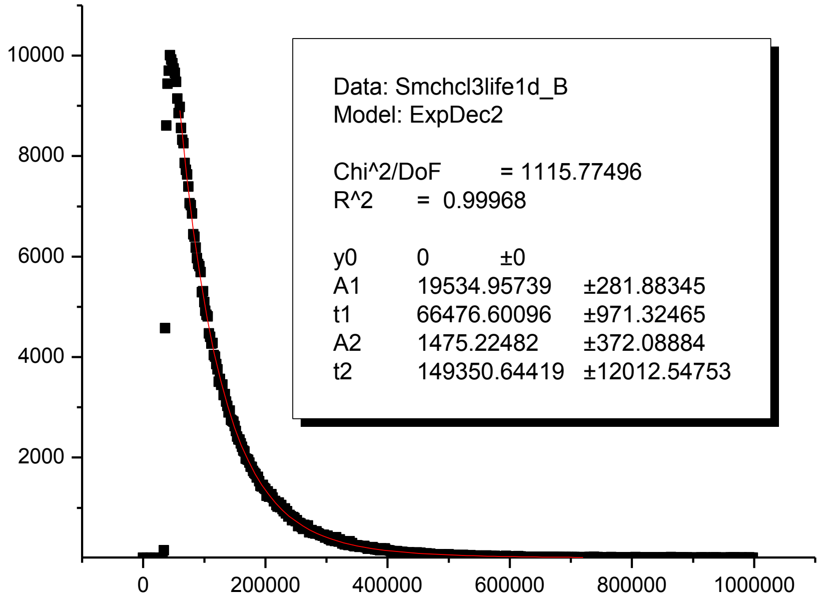

Data: Smchcl3life1d_B
Model: ExpDec2

Chi^2/DoF = 1115.77496
R^2 = 0.99968

y0	0	±0
A1	19534.95739	±281.88345
t1	66476.60096	±971.32465
A2	1475.22482	±372.08884
t2	149350.64419	±12012.54753

Figure 3. 125 Decay curve of luminescence lifetime measurement of SmL2 in chloroform

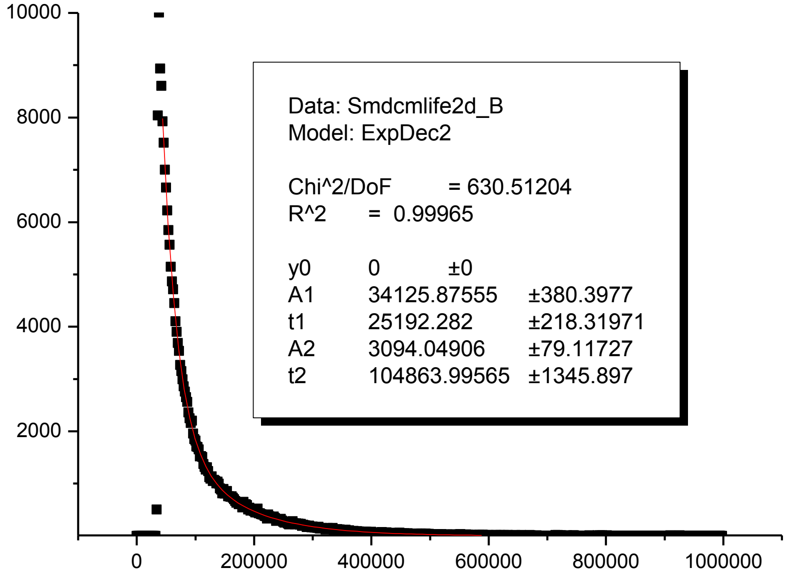

Data: Smdcmlife2d_B
Model: ExpDec2

Chi^2/DoF = 630.51204
R^2 = 0.99965

y0	0	±0
A1	34125.87555	±380.3977
t1	25192.282	±218.31971
A2	3094.04906	±79.11727
t2	104863.99565	±1345.897

Figure 3. 126 Decay curve of luminescence lifetime measurement of SmL2 in dichloromethane

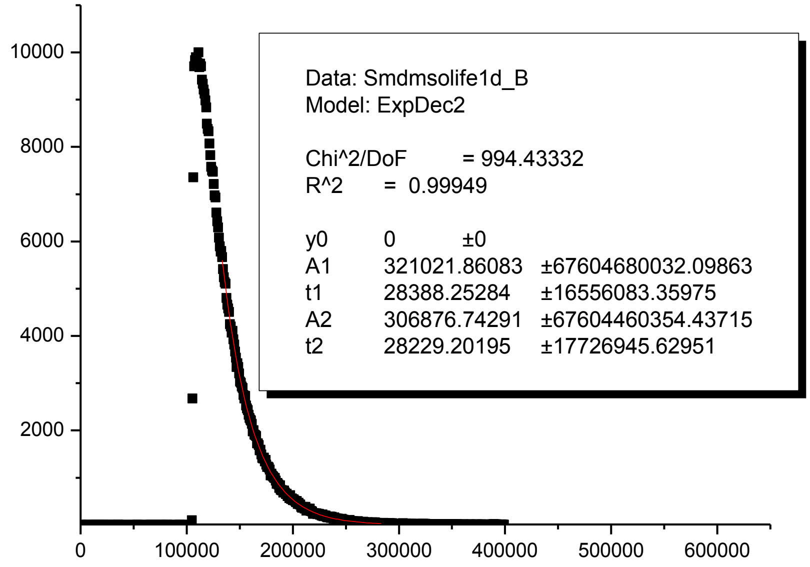

Figure 3. 127 Decay curve of luminescence lifetime measurement of SmL2 in dimethyl sulfoxide

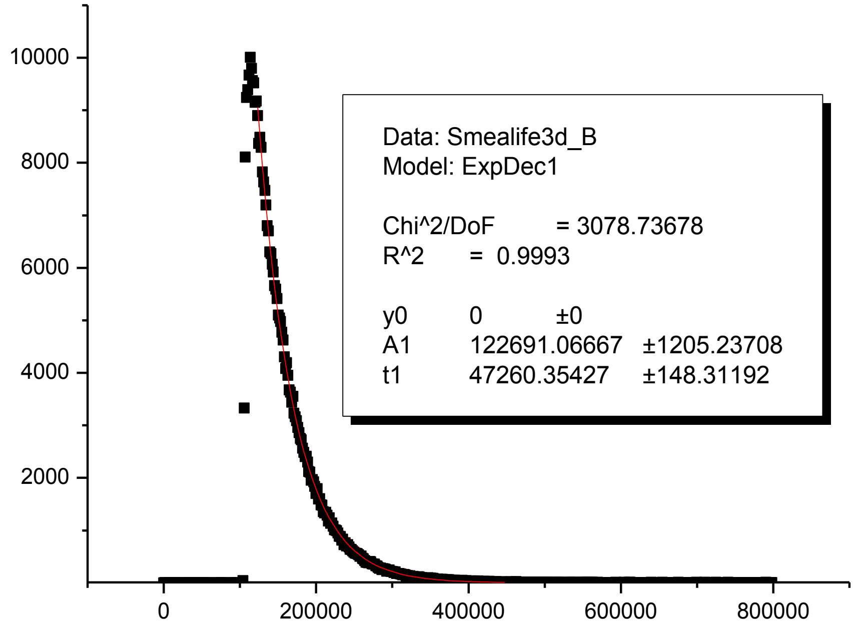

Figure 3. 128 Decay curve of luminescence lifetime measurement of SmL2 in ethyl acetate

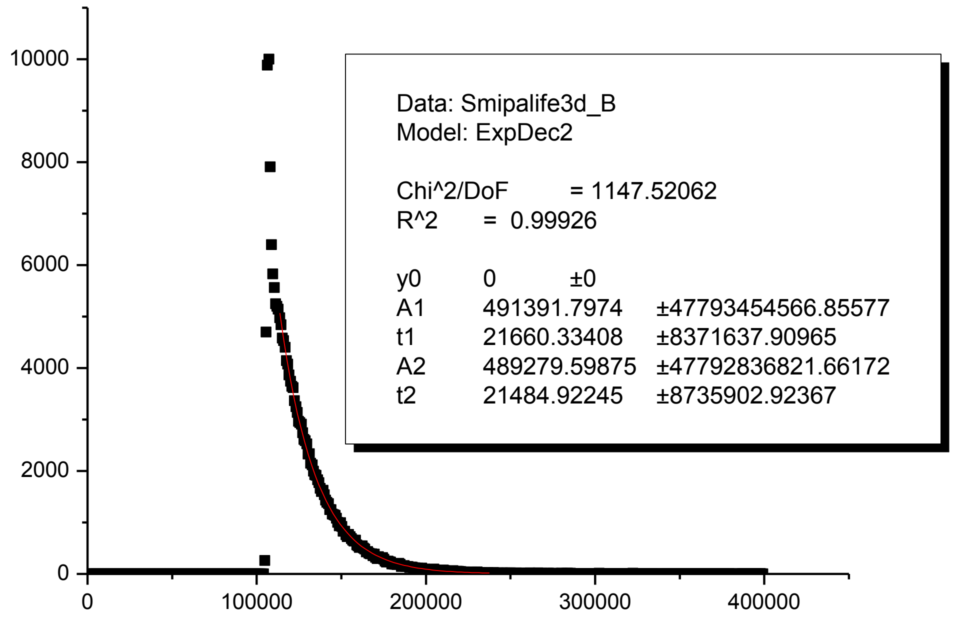

Figure 3. 129 Decay curve of luminescence lifetime measurement of SmL2 in isopropanol

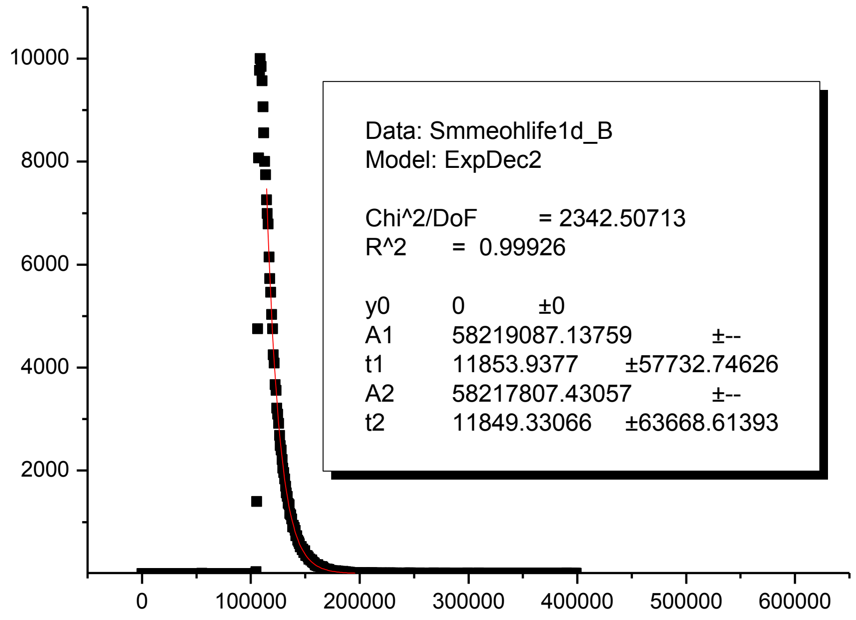

Figure 3. 130 Decay curve of luminescence lifetime measurement of SmL2 in methanol

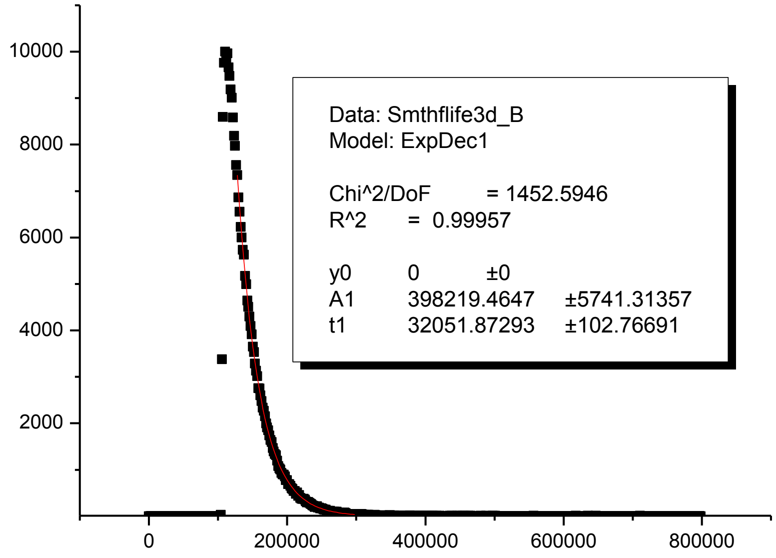

Figure 3. 131 Decay curve of luminescence lifetime measurement of SmL2 in tetrahydrofuran

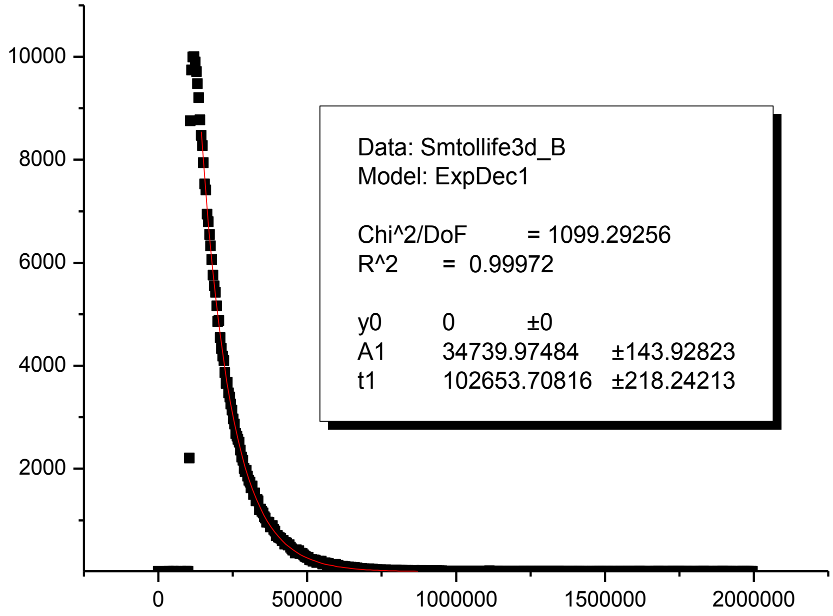

Figure 3. 132 Decay curve of luminescence lifetime measurement of SmL2 in toluene

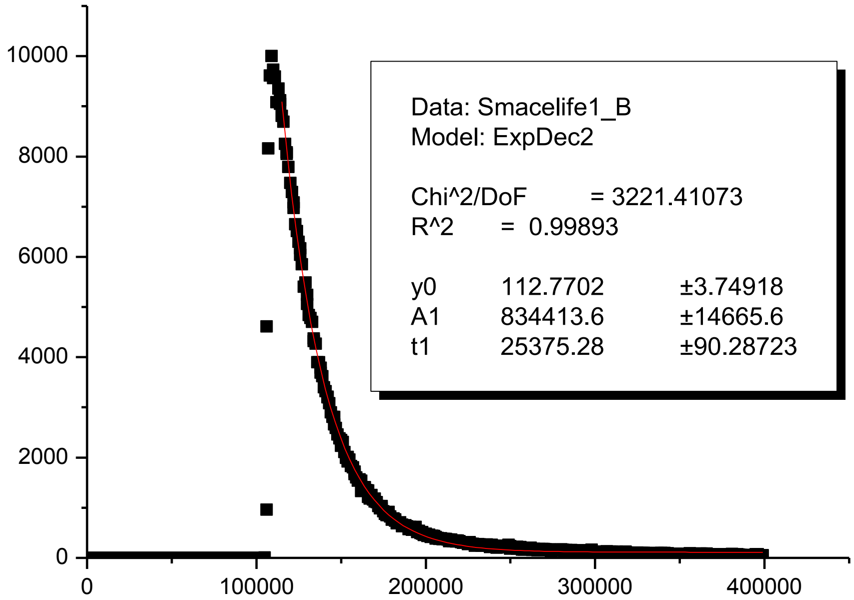

Figure 3. 133 Decay curve of luminescence lifetime measurement of SmL3 in acetone

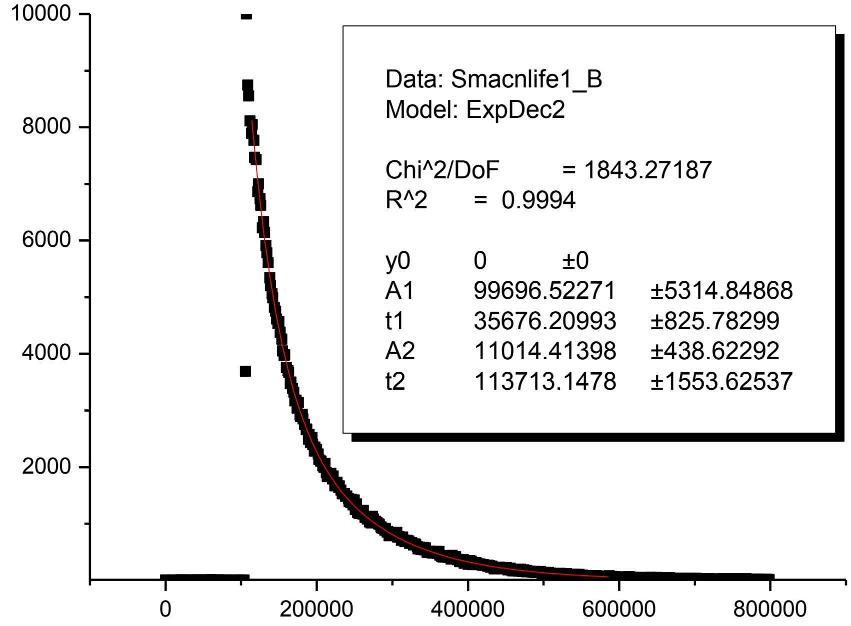

Figure 3. 134 Decay curve of luminescence lifetime measurement of SmL3 in acetonitrile

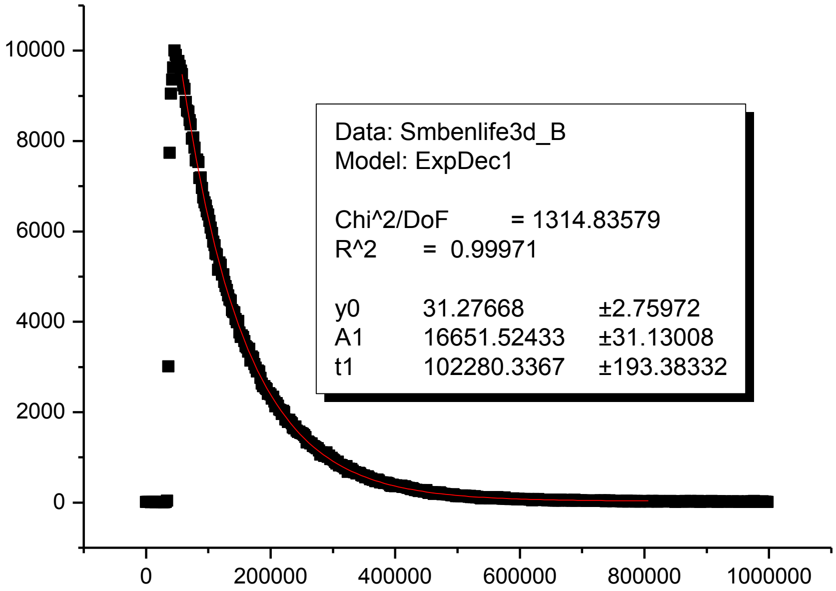

Figure 3. 135 Decay curve of luminescence lifetime measurement of SmL3 in benzene

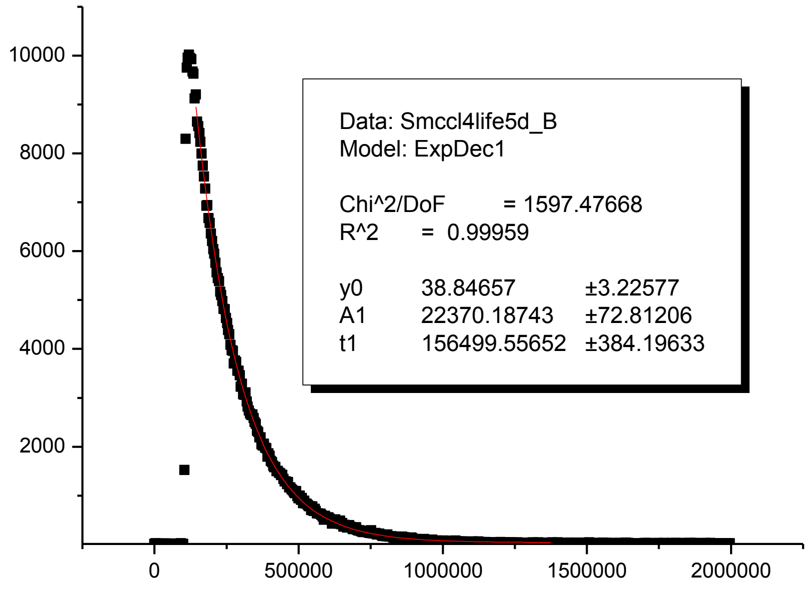

Figure 3. 136 Decay curve of luminescence lifetime measurement of SmL3 in carbon tetrachloride

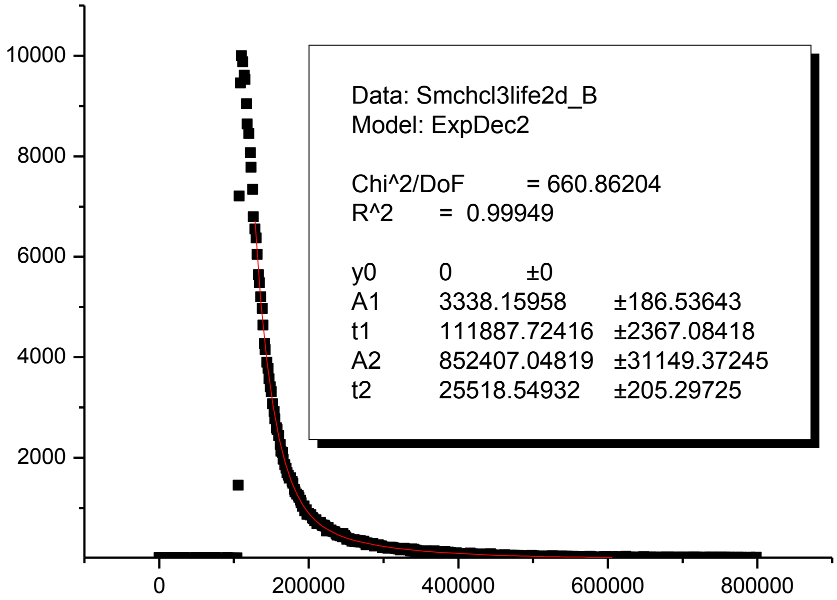

Figure 3. 137 Decay curve of luminescence lifetime measurement of SmL3 in chloroform

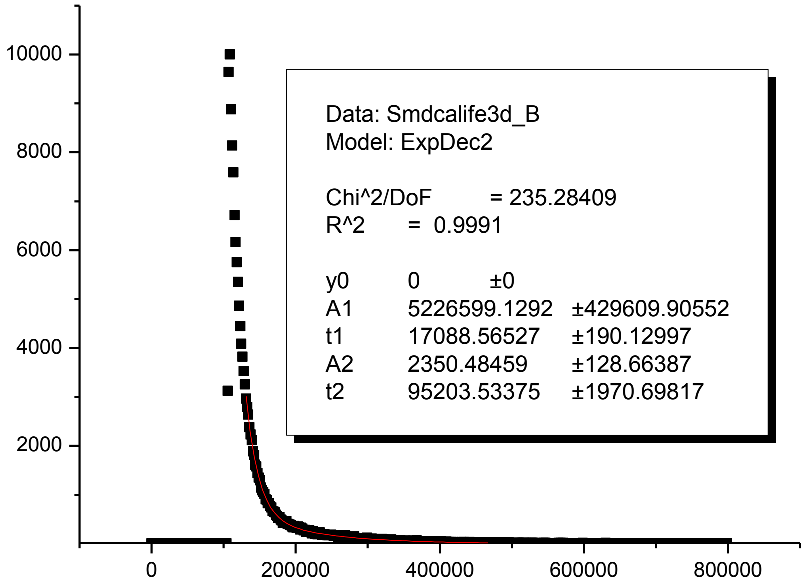

Figure 3. 138 Decay curve of luminescence lifetime measurement of SmL3 in 1,2-dichloroethane

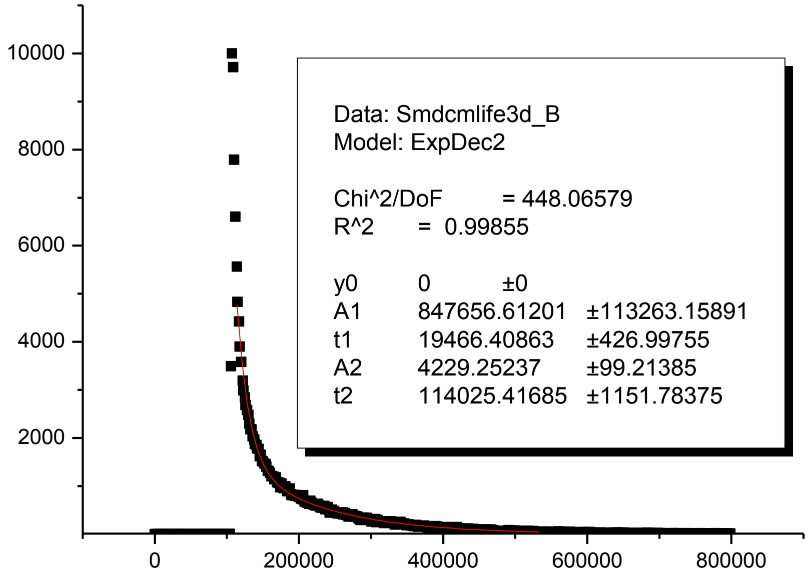

Figure 3. 139 Decay curve of luminescence lifetime measurement of SmL3 in dichloromethane

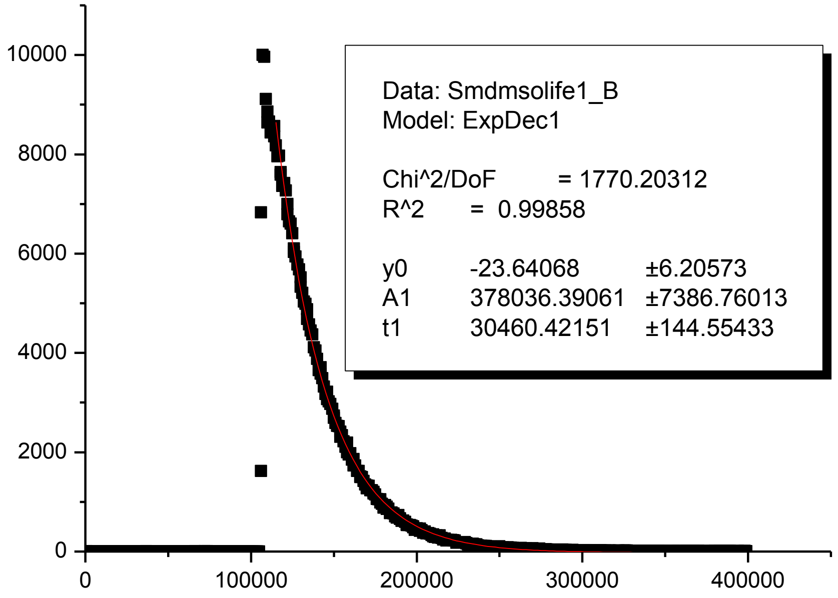

Figure 3. 140 Decay curve of luminescence lifetime measurement of SmL3 in dimethyl sulfoxide

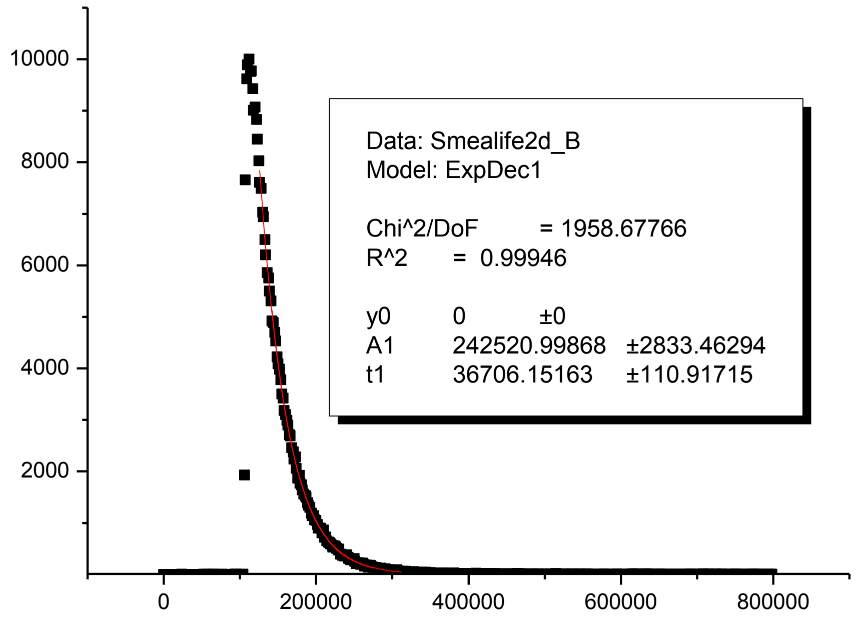

Figure 3. 141 Decay curve of luminescence lifetime measurement of SmL3 in ethyl acetate

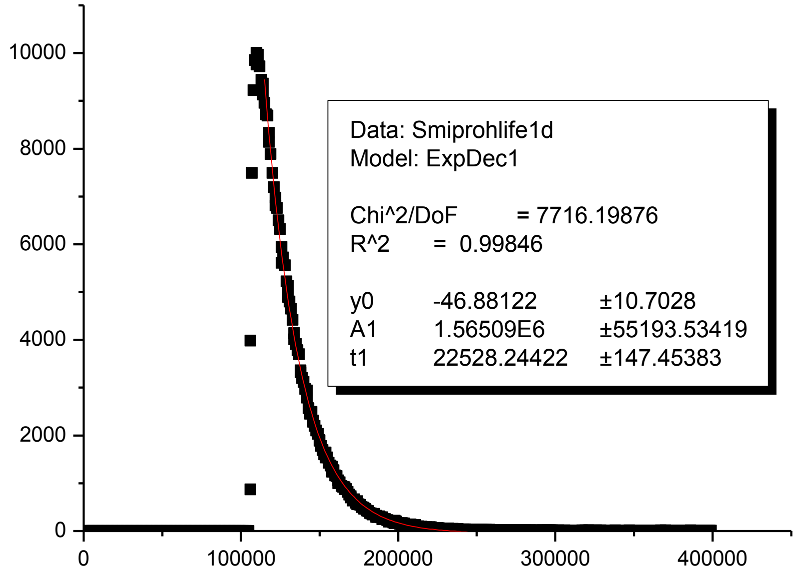

Figure 3. 142 Decay curve of luminescence lifetime measurement of SmL3 in isopropanol

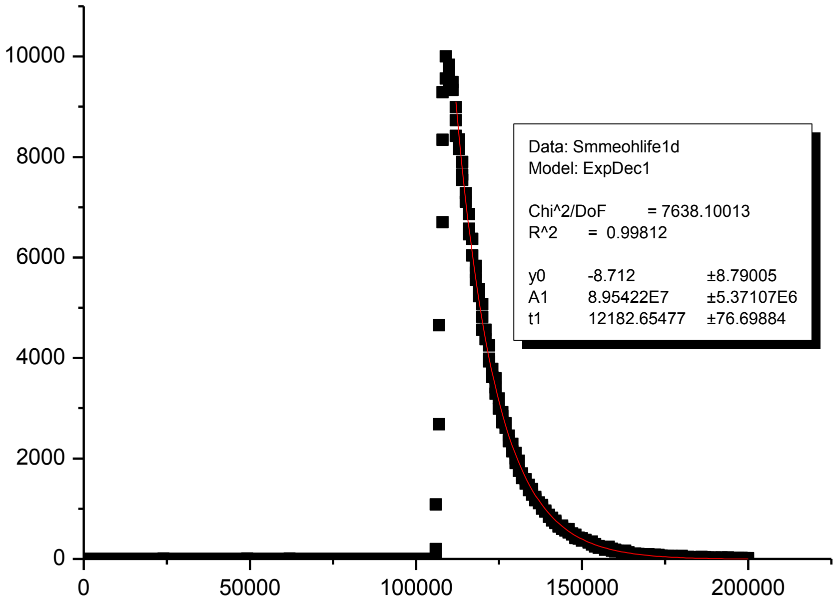

Figure 3. 143 Decay curve of luminescence lifetime measurement of SmL3 in methanol

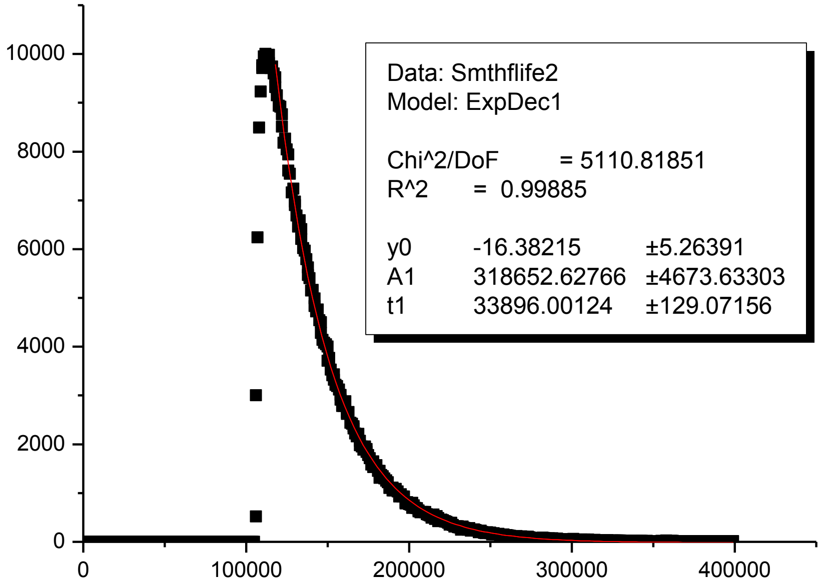

Figure 3. 144 Decay curve of luminescence lifetime measurement of SmL3 in tetrahydrofuran

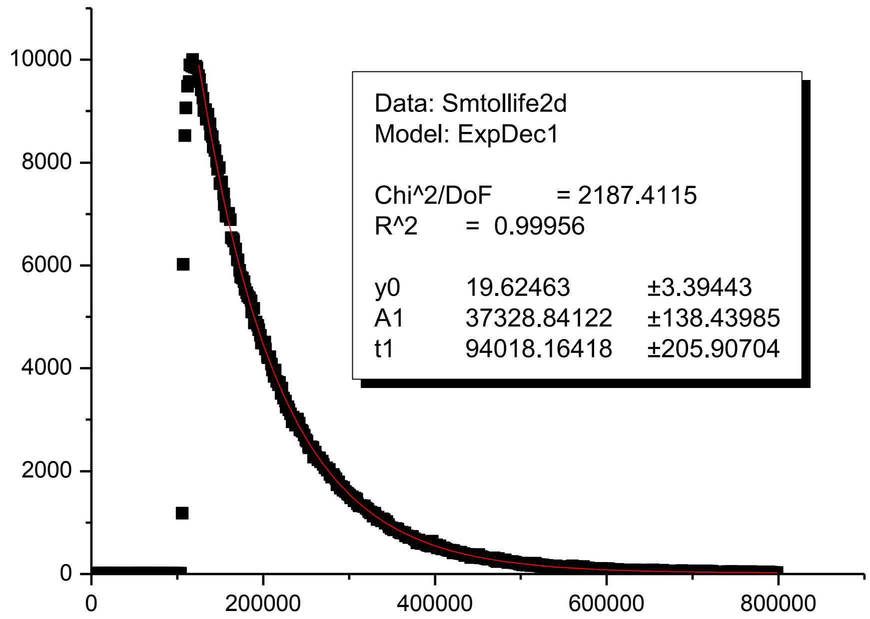

Figure 3. 145 Decay curve of luminescence lifetime measurement of SmL3 in toluene

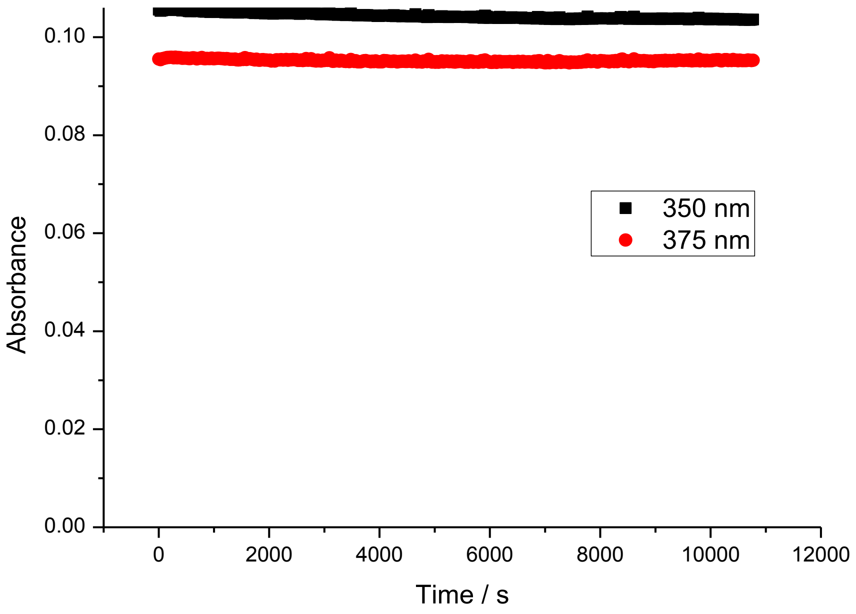

Figure 3. 146 Graph of selected absorbances against time of SmL1 in acetonitrile

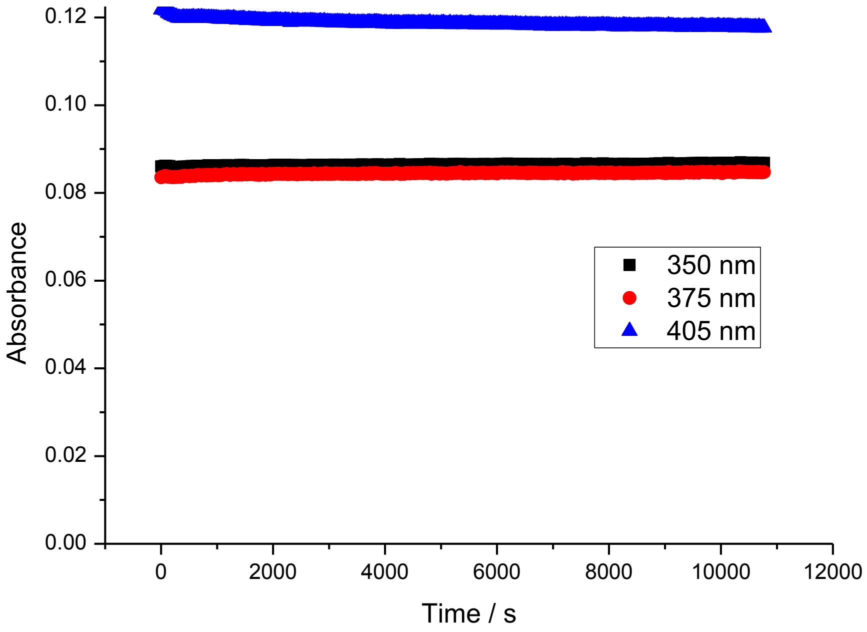

Figure 3. 147 Graph of selected absorbances against time of SmL1 in benzene

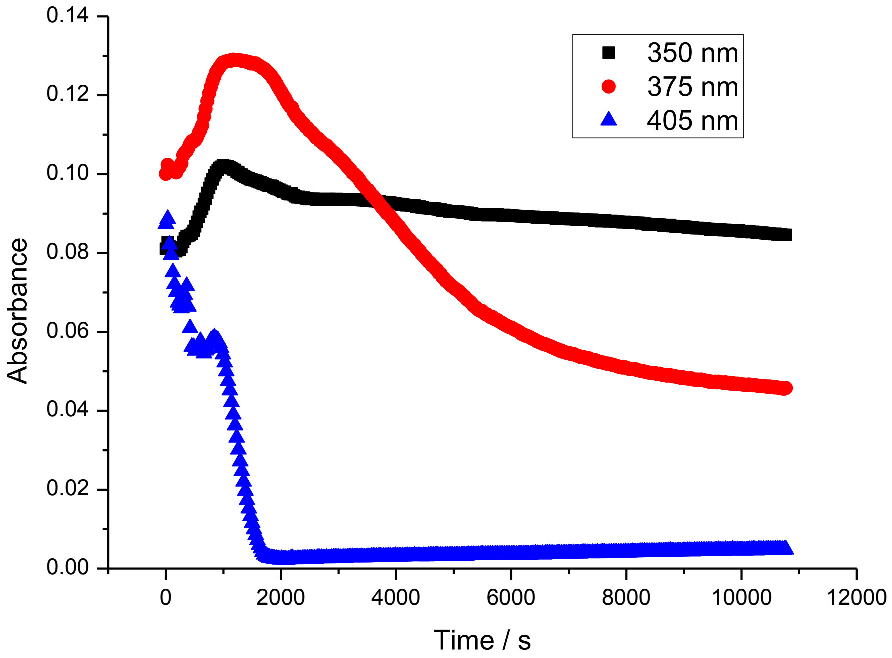

Figure 3. 148 Graph of selected absorbances against time of SmL1 in carbon tetrachloride

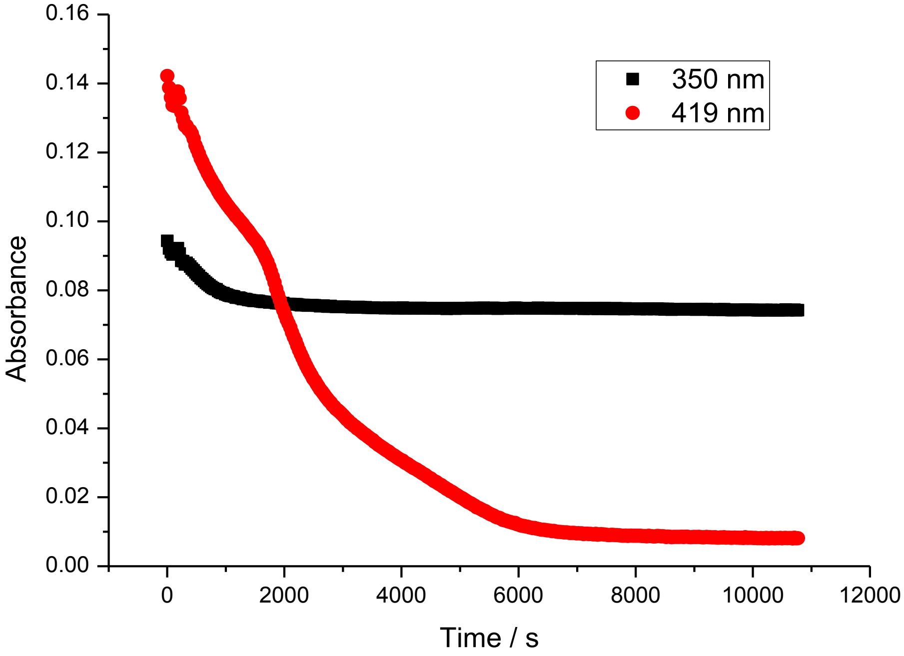

Figure 3. 149 Graph of selected absorbances against time of SmL1 in chloroform

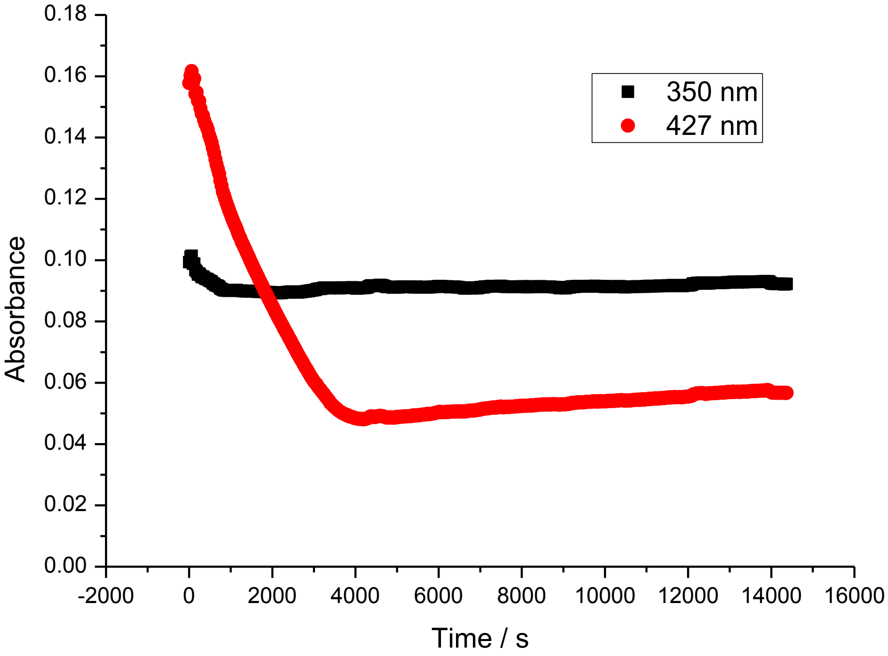

Figure 3. 150 Graph of selected absorbances against time of SmL1 in dichloromethane

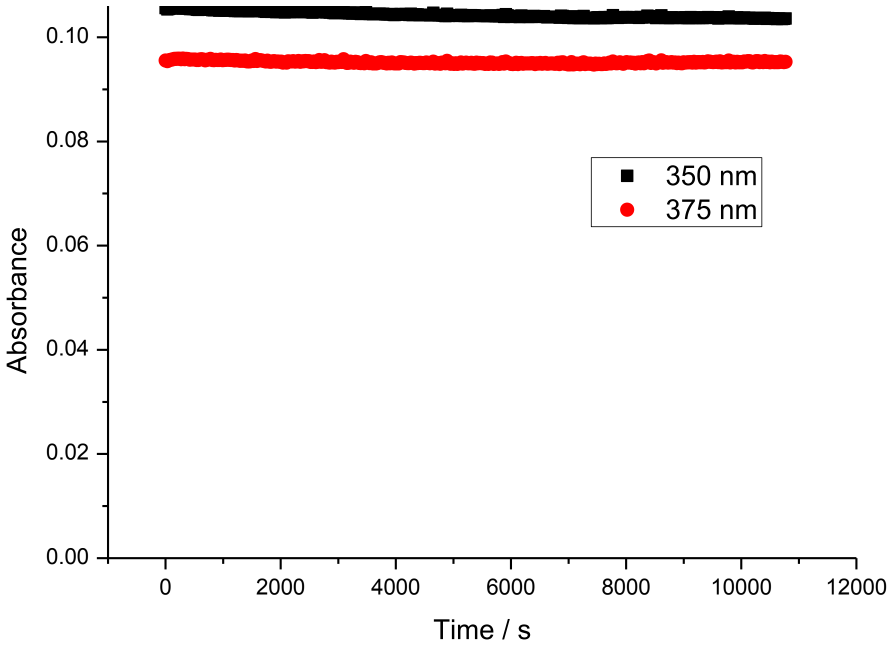

Figure 3. 151 Graph of selected absorbances against time of SmL1 in ethyl acetate

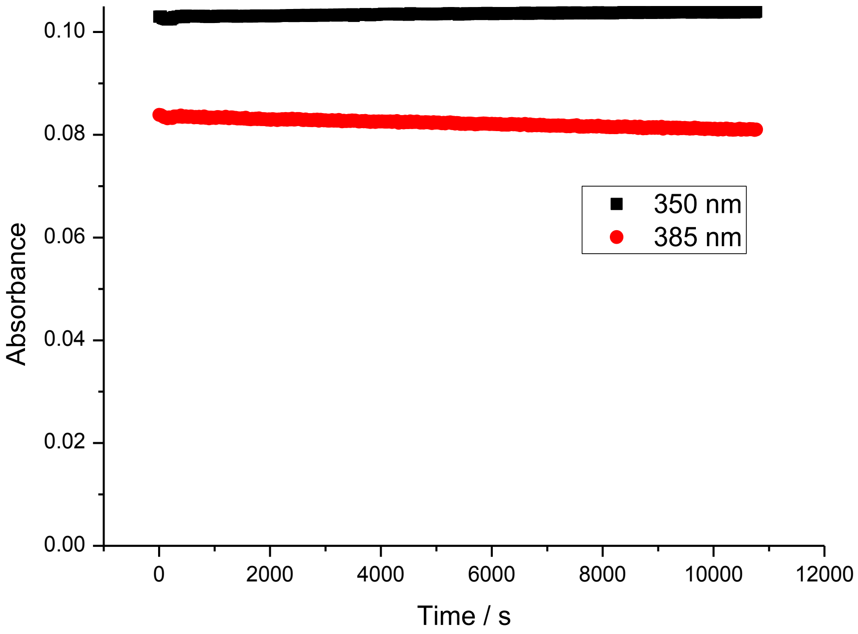

Figure 3. 152 Graph of selected absorbances against time of SmL1 in methanol

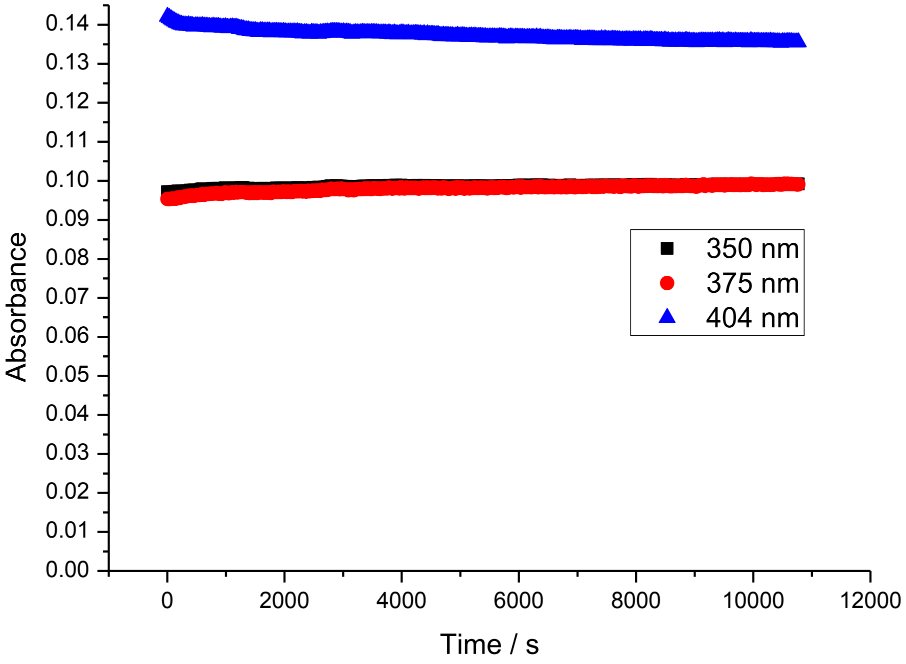

Figure 3. 153 Graph of selected absorbances against time of SmL1 in toluene

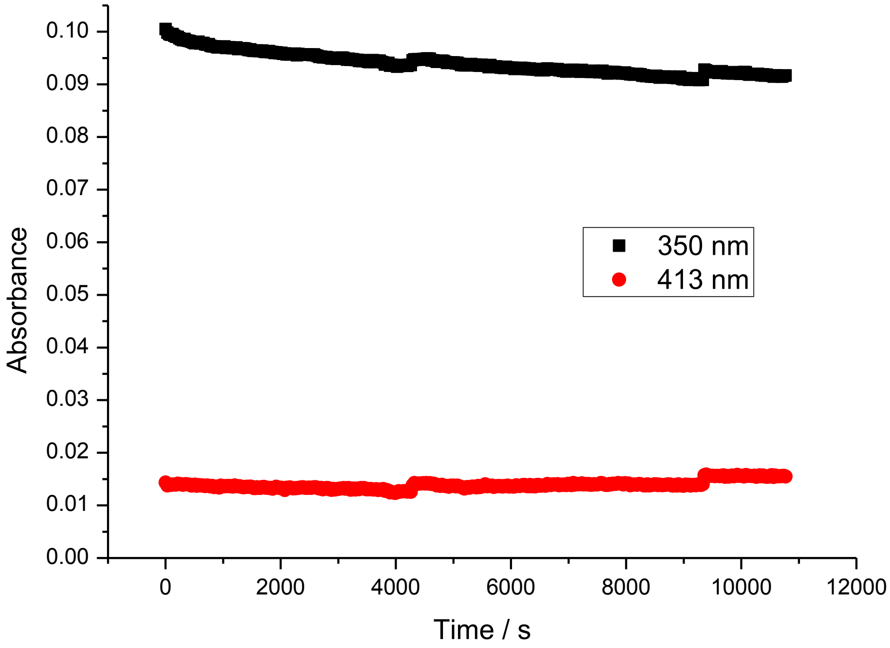

Figure 3. 154 Graph of selected absorbances against time of SmL2 in acetonitrile

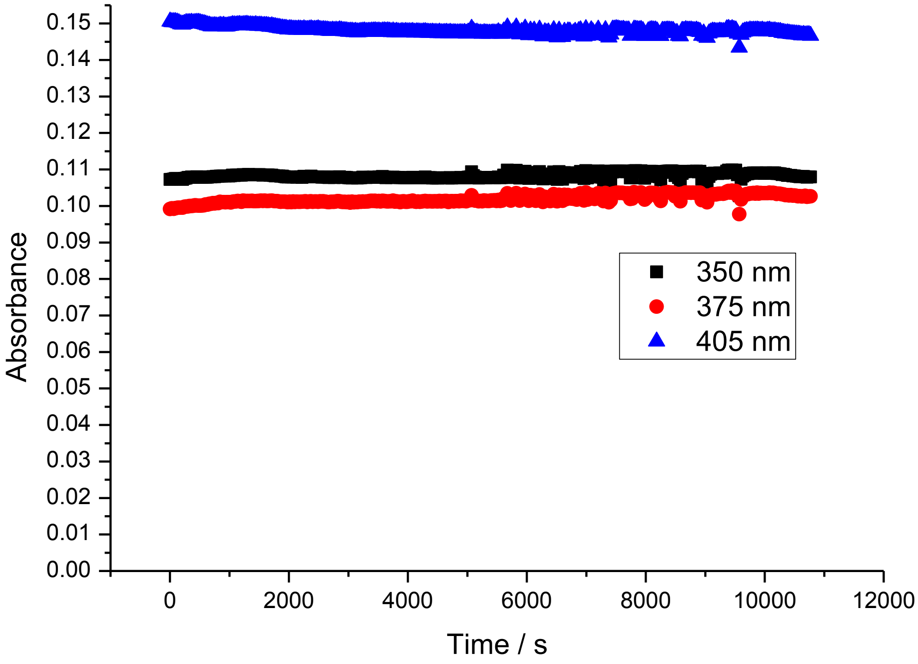

Figure 3. 155 Graph of selected absorbances against time of SmL2 in benzene

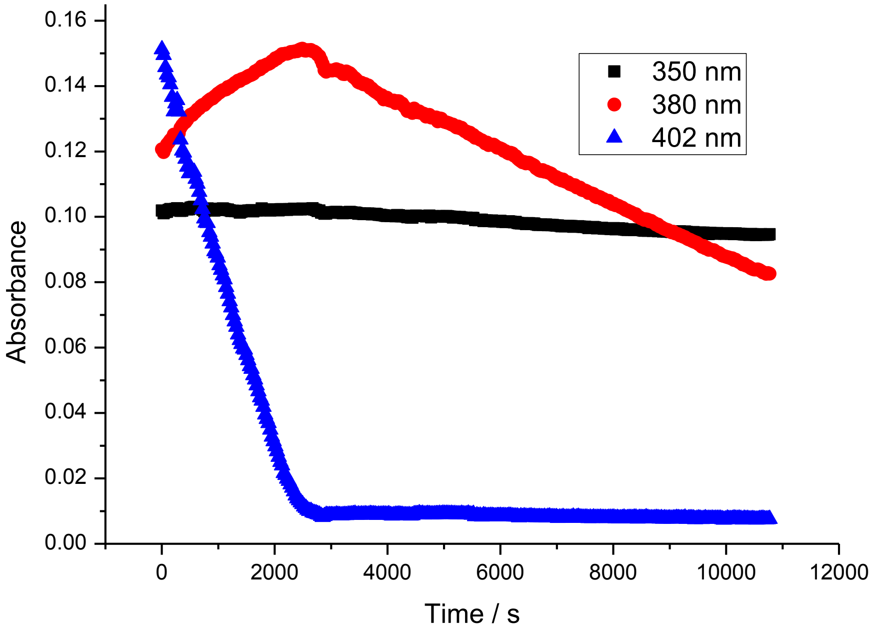

Figure 3. 156 Graph of selected absorbances against time of SmL2 in carbon tetrachloride

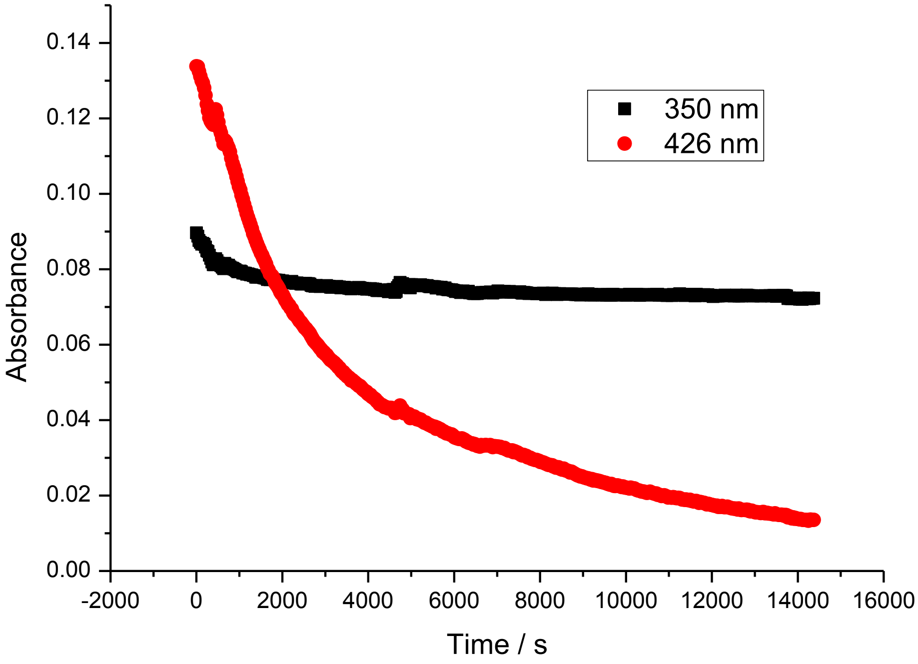

Figure 3. 157 Graph of selected absorbances against time of SmL2 in dichloromethane

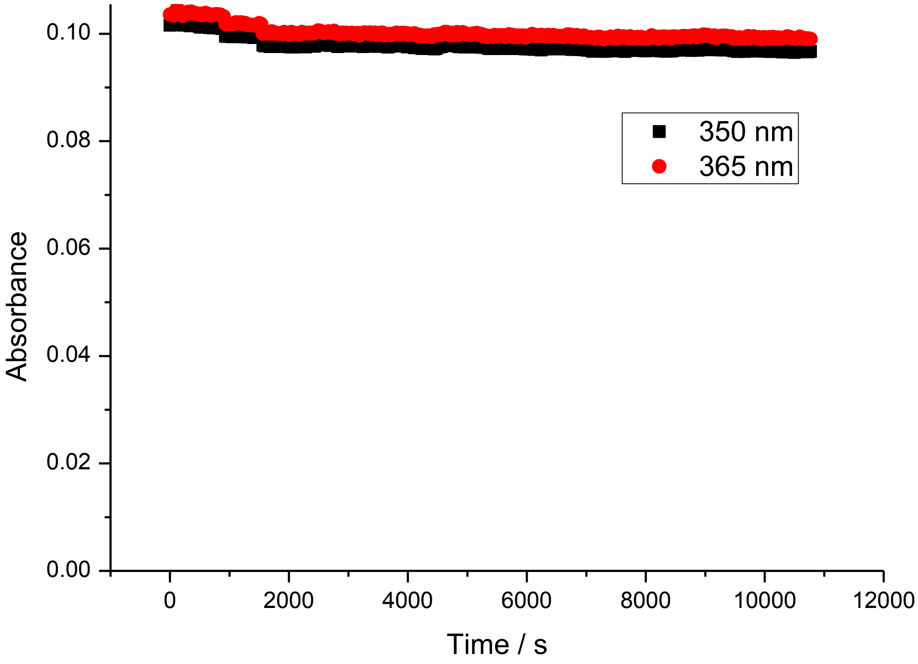

Figure 3. 158 Graph of selected absorbances against time of SmL2 in ethyl acetate

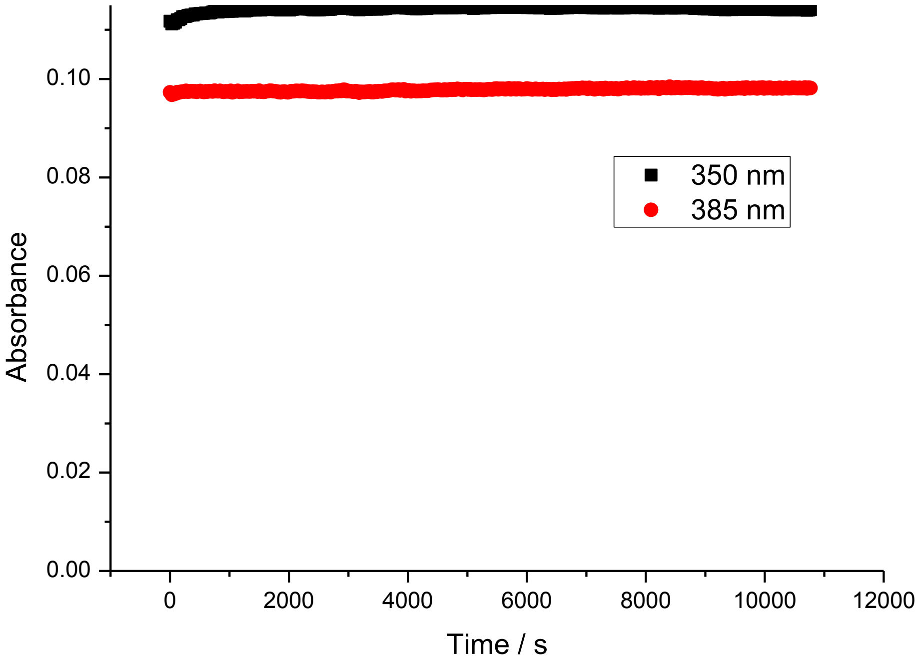

Figure 3. 159 Graph of selected absorbances against time of SmL2 in methanol

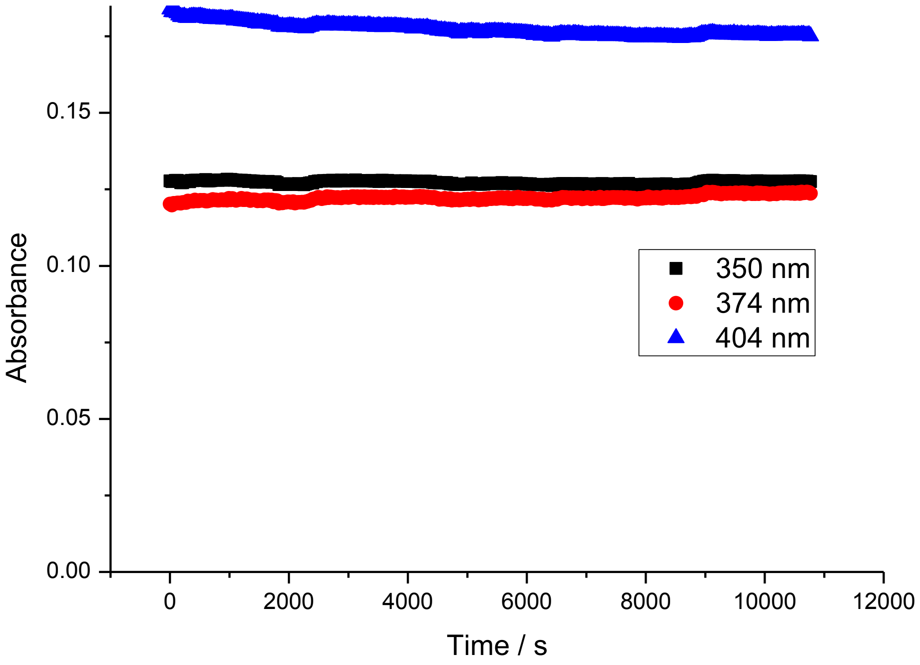

Figure 3. 160 Graph of selected absorbances against time of SmL2 in toluene

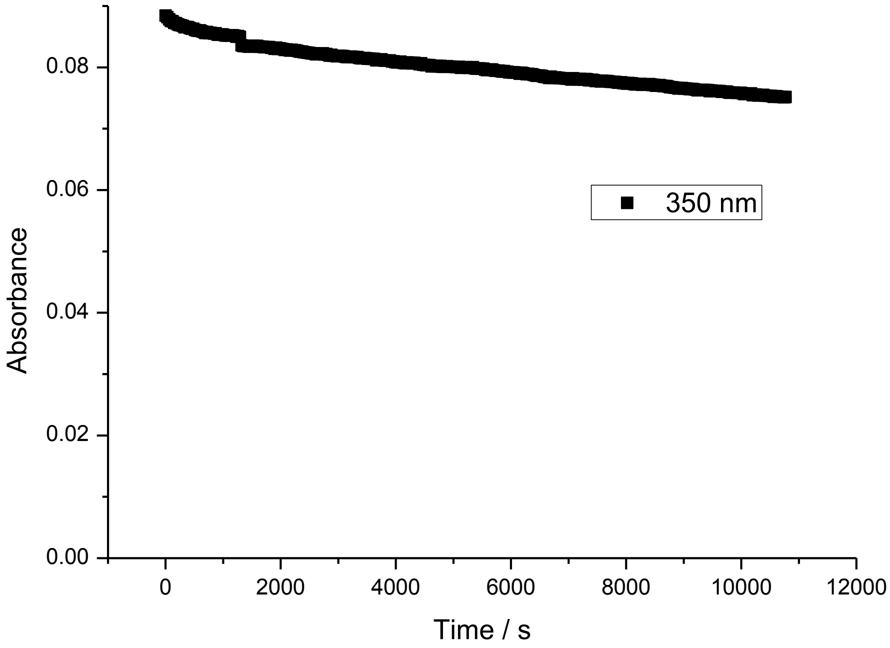

Figure 3. 161 Graph of selected absorbances against time of SmL3 in acetonitrile

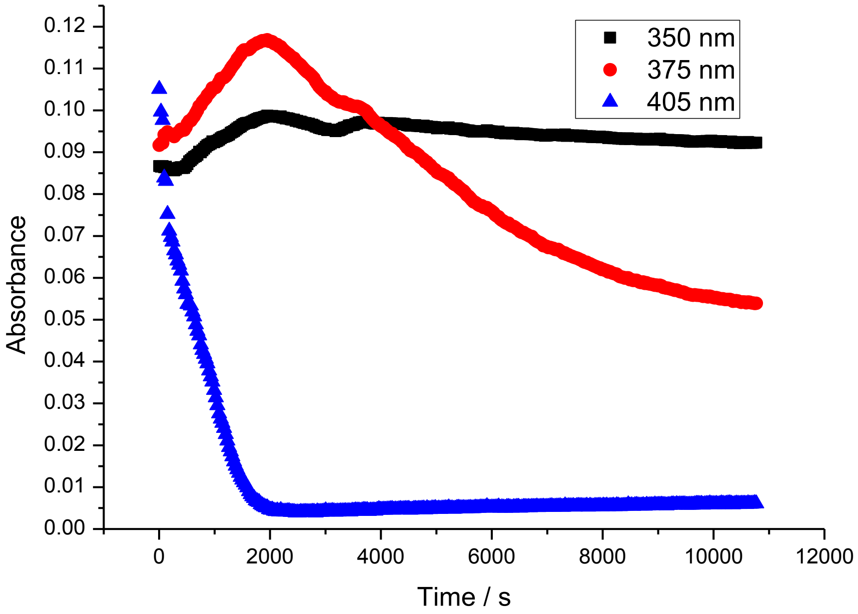

Figure 3. 162 Graph of selected absorbances against time of SmL3 in carbon tetrachloride

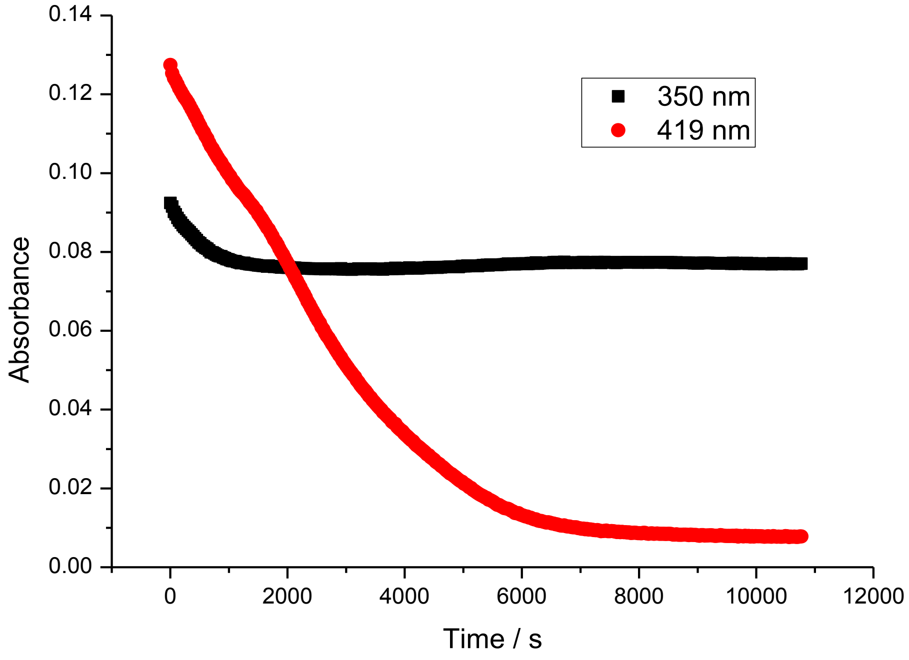

Figure 3. 163 Graph of selected absorbances against time of SmL3 in chloroform

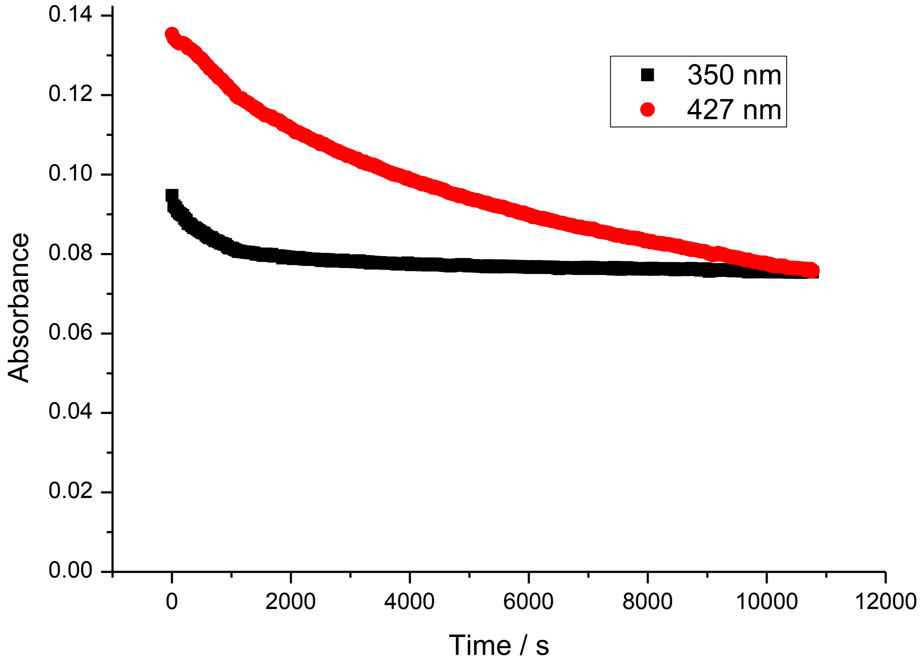

Figure 3. 164 Graph of selected absorbances against time of SmL3 in dichloromethane

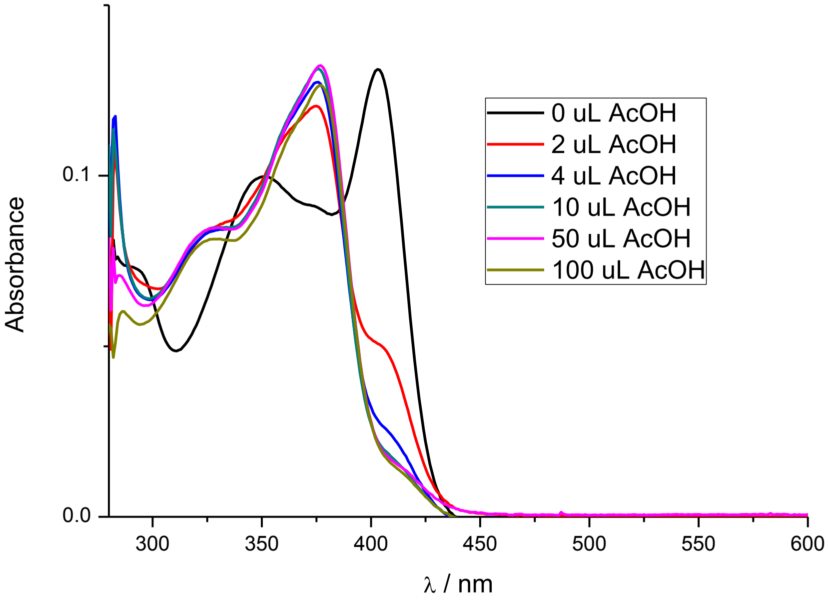

Figure 3. 165 Absorption spectra of EuL3 in toluene with incremental addition of AcOH

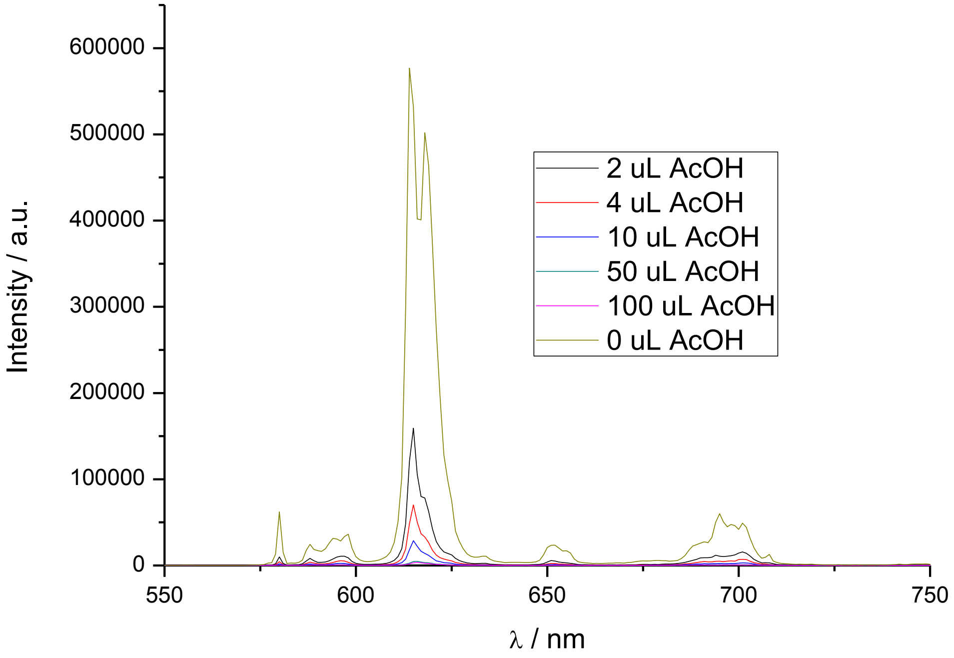

Figure 3. 166 Emission spectra of EuL3 in toluene with incremental addition of AcOH, excitation at 350 nm

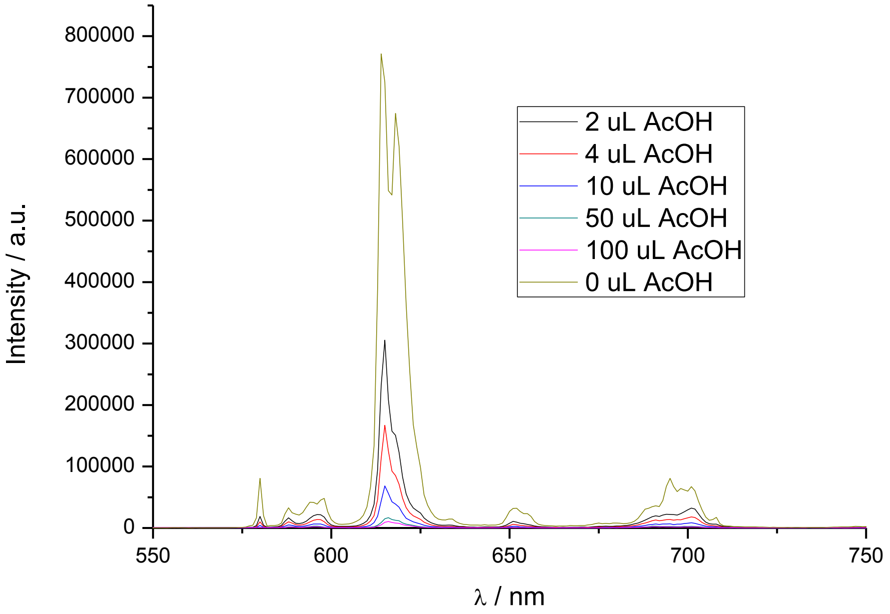

Figure 3. 167 Emission spectra of EuL3 in toluene with incremental addition of AcOH, excitation at 390 nm

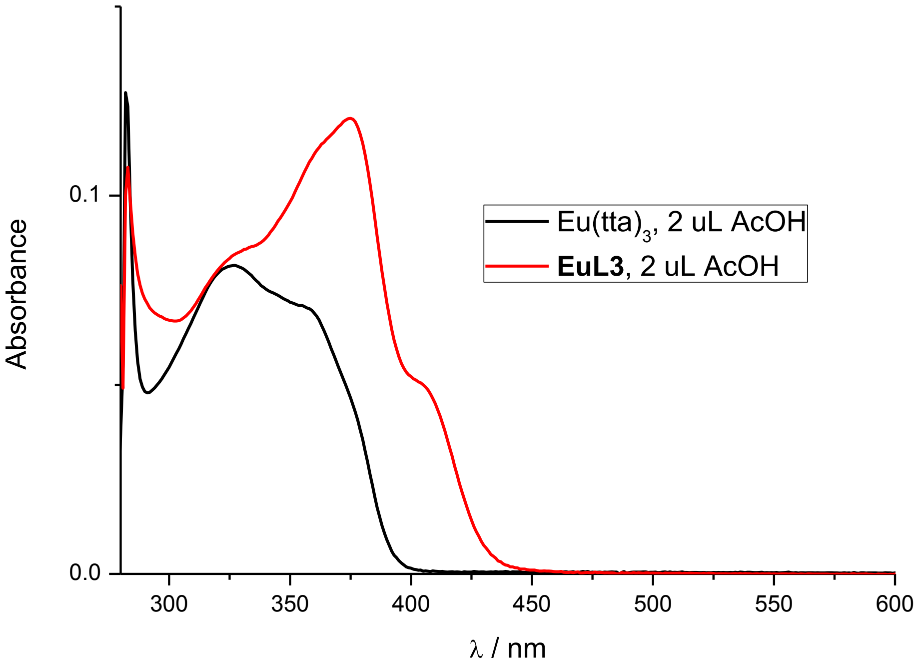

Figure 3. 168 Absorption spectra of Eu(tta)$_3$ and EuL3 in toluene with 2 μL AcOH added

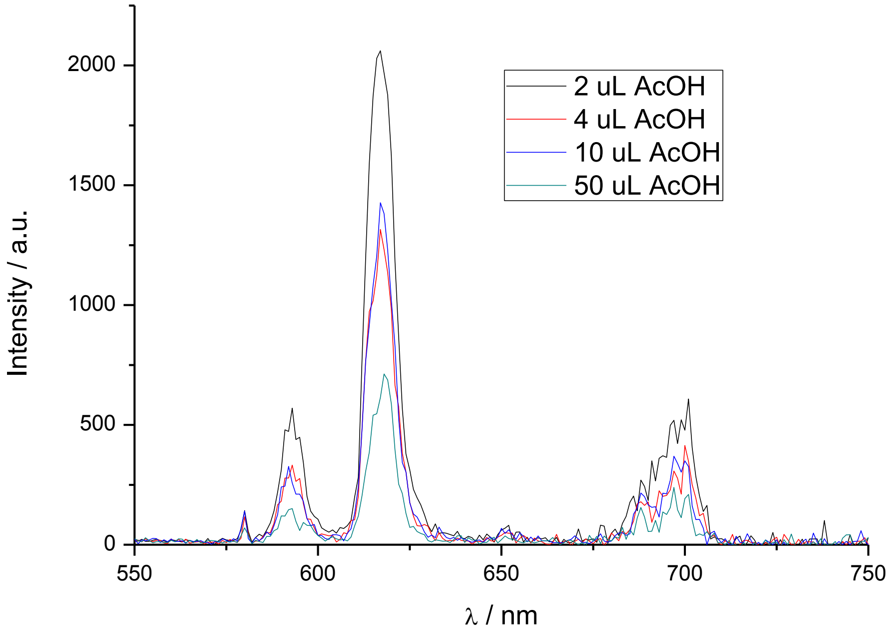

Figure 3. 169 Emission spectra of Eu(tta)$_3$ in toluene with incremental addition of AcOH, excitation at 350 nm

4. Non-Triplet Intraligand Charge Transfer Sensitization of Near-Infrared Luminescence of Samarium(III) and Ytterbium(III) Complexes

4.1. Introduction on Near-Infrared Luminescence of Lanthanide(III) Complexes

The previous chapter focused on the sensitization of Eu(III) and Sm(III) compounds which emit light in the visible region. A plethora of applications of lanthanide(III) have focused on their luminescence in the visible region, such as optical imaging agents with bright green and red light from Tb(III) and Eu(III), anti-counterfeiting features of bank notes with europium(III) and OLEDs with separate or a mixture of Ln(III) ions etc. Near-infrared-emitting lanthanides, nevertheless, have found utilization in other aspects.

Er(III), with its characteristic emission at around 1530 – 1540 nm ($^4I_{13/2} \rightarrow {}^4I_{15/2}$ transition), is doped into silica optical fibers and have become prominent in telecommunication applications, as well as the $^1G_4 \rightarrow {}^3H_5$ transition of Pr(III) at around 1300 – 1330 nm. In Nd:YAG lasers, the Nd(III) is optically pumped due to their relatively decent absorption ability (≈ 10 L $mol^{-1}cm^{-1}$) to emit mainly at 1060 nm ($^4F_{3/2} \rightarrow {}^4I_{11/2}$ transition), which could be efficiently frequency doubled to produce green laser at 532 nm or quadrupled to give UV laser at 266 nm. The development of Yb(III) and Sm(III) complexes, and lanthanide-doped upconversion nanocrystals[101,102] as optical imaging agents have also gathered pace,[2,42, 45, 47,104] thanks to the low signal-to-noise ratio brought about by NIR emission as it penetrates living tissue well and the absence of NIR-auto-fluorescent entities. Ln(III) ions also play a role in enhancing solver energy conversion by reducing the mismatch with the entire solar spectrum by upconversion and downconversion,[105-107] due to the many energy levels present – an advantage over semiconductors.

Lanthanide(III) ions capable of emitting in the NIR region usually have abundant energy levels, thus creating more gaps with lower energies (Figure 4.1). As a result, their quantum efficiencies are often quite low as the smaller ΔE with the next lower energy level is more susceptible towards non-radiative multiphonon deactivation. Sensitization of Ln(III) NIR luminescence is no different to visible luminescence, relying on antenna effect from light-harvesting chromophores, transition metal complexes, other Ln(III) and d-state of transition metal ions (forming heterometallic complexes) and charge-transfer states (see Chapter 1). The numerous energy levels cause multiple emitting and accepting states, leading to much more f-f transitions. Some Ln(III), consequently, are dual-emissive – capable of emitting in both the visible and NIR region: Sm(III), Dy(III), Ho(III), Er(III), Tm(III). The main NIR transitions are summarized in Table 4.1.

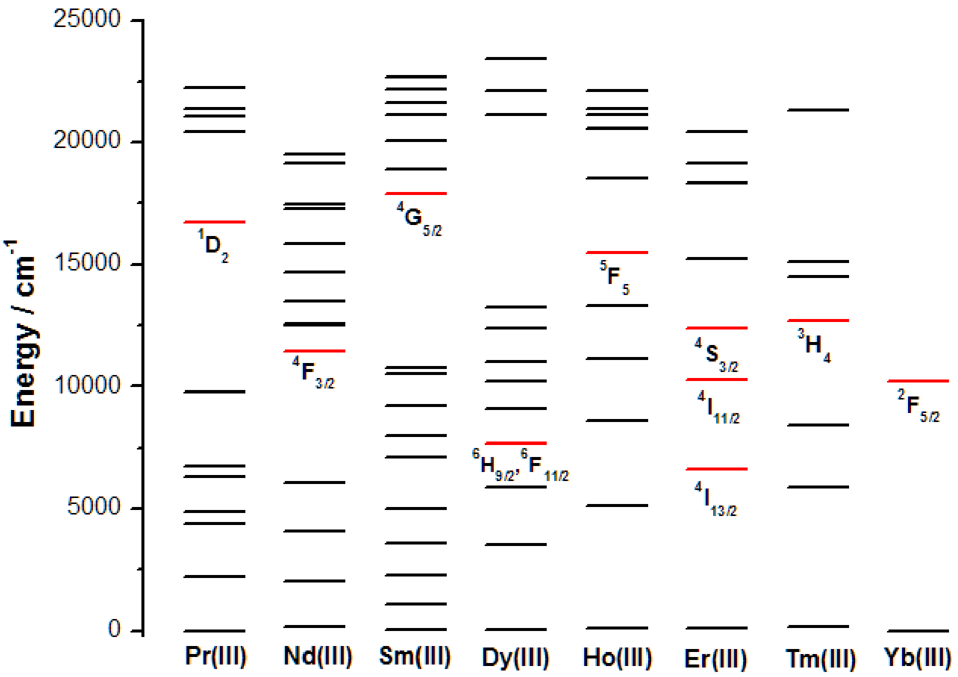

Figure 4. 1 Energy levels (< 25000 cm^{-1}) of NIR-emitting Ln^{3+}(aq) and their main emissive states (highlighted in red)[108]

Table 4. 1 Selected NIR and IR-B (1400 – 3000 nm) f-f transitions of Ln(III)[109]

Ln(III)	Emitting State	Final State	Emission Wavelength (nm)
Pr	$^1D_2$	$^3F_4$	1010 – 1040
		$^1G_4$	1440
	$^1G_4$	$^3H_5$	1300 – 1330[a]
Nd	$^4F_{3/2}$	$^4I_{9/2}$	870 – 920
		$^4I_{11/2}$	1060 – 1090
		$^4I_{13/2}$	1320 – 1390
		$^4I_{15/2}$	1840 – 1860
Sm	$^4G_{5/2}$	$^6F_{1/2}$	880
		$^6F_{7/2}$	1020 – 1040
		$^6F_{9/2}$	1160 – 1170
Dy	$^6H_{9/2}$, $^6F_{11/2}$[b]	$^6H_{15/2}$	1280 – 1340
	$^6H_{11/2}$		1700 – 1800
Ho	$^5F_5$	$^5I_6$	1480 – 1510
	$^5I_5$	$^5I_7$	1630 – 1680
	$^5I_6$	$^5I_8$	1160 – 1190
	$^5I_7$		1980 – 2100[c]

Er	${}^4S_{3/2}$	${}^4I_{9/2}$	1700[c]
	${}^4I_{11/2}$	${}^4I_{13/2}$	2700[c]
	${}^4I_{13/2}$	${}^4I_{15/2}$	1540[a]
Tm	${}^3H_4$	${}^3H_5$	2330
	${}^3F_4$	${}^3H_6$	1750 – 1900
Yb	${}^2F_{5/2}$	${}^2F_{7/2}$	980 – 1000

[a] Telecommunication application; [b] Very closely spaced, both with energy of 7700 cm^{-1}; [c] Laser application

Cyclen-based macrocycles remain popular chelates for NIR-emitting Ln(III) as they produce stable and kinetically inert complexes and provide saturation of the first and second coordination spheres from solvent molecules. Examples could be found in references 110-113. Porphyrinates are also widely used to form Yb(III) complexes not least due to their low-energy levels (14000-15000 cm^{-1}) and ability to absorb UV-vis light efficiently,[114,115] but the planar structure is not ideal for sufficiently protecting the coordination sphere. Wong and co-workers[116] developed a Yb(III) porphyrinate complex capped with a cobalt(II) cyclopentadienyl-based tripodal moiety to saturation coordination, and sensitization of Yb(III) NIR luminescence was achieved by photoexcitation of the Soret band at low energy (430 nm). Its luminescence quantum yield of 2.5 % in water is among the highest recorded.

This chapter set out to investigate the sensitization of NIR luminescence of Sm(III) and Yb(III) by both the TTA and the ILCT state *via* the triplet and non-triplet pathways respectively. The energy transfer mechanism of **YbL3** will also be discussed.

4.2. Results and Discussion

SmL3 and **YbL3** were synthesized to construct a Ln(III) complex system with two chromophoric moieties for comparing the sensitization pathways. The methyl groups on the pyrazoles had negligible effect on the luminescence properties and are thus excluded from discussion.

Sensitization of visible luminescence of **SmL3** was demonstrated to be quite good in the previous chapter and it would be interesting to find out whether NIR luminescence would also give decent results. Given the low luminescence quantum yields of Yb(III) compounds in the past, the potential of using the ILCT state as excited energy donor is explored and the nature of energy transfer from the ILCT state were investigated. The solvatochromism properties of the complexes were studied and, last but not least, effort was devoted into elucidating the non-radiative quenching processes of **SmL3** and **YbL3**.

4.2.1. Photophysical Studies

Absorption and Excitation Spectra

As expected and inferred from the results in the previous chapter, the absorption spectra are quite similar to those of **EuL3** and **SmL3**. The π-π* absorption of the triazine-core base could be found before 300 nm and the peak maximum of the π-π* absorption of TTA is at 340 nm. The broad ILCT absorption bands exhibit a blue shift with increasing solvent polarity, even merging with the TTA absorption in highly polar solvents. The absorption spectra of **YbL3**, however, were quite different from those of **EuL3** and **SmL3**. The ILCT absorption band was not distinctly visible in terms of peak position and band shape, even in non-polar solvents. In benzene (Figure 4.11) and toluene (Figure 4.22), in which the ILCT absorption of **SmL3** is intense and distinct, the ILCT transition appeared rather as a shoulder of the broader TTA absorption band without a clear peak maximum.

The excitation spectra of **SmL3** and **YbL3** were monitored at the $^4G_{5/2} \rightarrow {}^4F_{5/2}$ and $^2F_{5/2} \rightarrow {}^2F_{7/2}$ NIR transitions respectively. In non-polar solvents, the ILCT excitation bands of **SmL3** overlay perfectly with the absorption band, indicating efficient antenna effect with intensities higher than the TTA – given the molecular ratio between the *N*,*N*-diethylanilinyl moiety and TTA is 1:3. As polarity increases, the ILCT excitation bands diminish drastically and eventually become irrelevant in the alcoholic and polar solvents. Comparing the excitation spectra of the visible and NIR transitions gave unsurprisingly very similar results, as both transitions originate from the same emissive state. The excitation spectra of **YbL3** are more similar among the series than the absorption spectra, with the ILCT transition clearly visible and with higher intensities in non-polar solvents.

NIR Emission Spectra of SmL3 and YbL3

Due to the weak signals from **SmL3** and **YbL3**, the emission spectra for **YbL3** were not corrected to detector responses as the correction file would over-amplify the noise to mask the emission bands, and the emission spectra for SmL3 were only measured up to 1050 to avoid interference from the corrected noise. Uncorrected emission spectra of **SmL3** showing $^4G_{5/2} \rightarrow {}^4F_{5/2}$ transition were obtained for quantum yield measurements.

The emission spectra were obtained under three excitations: 330, 350 and 390 nm in order to compare between exciting different chromophores. In view of the instability issues of chlorinated solvents, chlorobenzene (Figures 4.19, 4.33) was added into the list of solvent along with dimethylformamide (DMF) to confirm the results in DMSO.

The near-infrared transitions of **SmL3** are located around 790, 885 and 950 nm, corresponding to the $^4G_{5/2} \rightarrow {}^6H_{13/2}$ and $^4G_{5/2} \rightarrow {}^4F_J$ transitions ($J = 1/2, 3/2$) respectively.

The *J* = 5/2 transition at around 1050 is quite weak and not observable in the full spectra spanning from 550 to 1030 nm, which were obtained in one run in order to compare the relative intensities between visible and NIR luminescence. The emission slits were at 10 nm, therefore to avoid detecting the second order of the excitation light, spectral acquisition discontinued at 1030 nm.

In non-polar solvents, such as benzene (Figure 4.11), toluene (Figure 4.22) and fluorobenzene (Figure 4.20), excitation at 390 nm – which does not excite TTA – gave greater overall luminescence intensities than excitation at 350 and 330 nm for both the visible and NIR regions. This is expected as the transitions originate from the same emissive state, as mentioned above. In chlorinated solvents, such as chloroform (Figure 4.12), dichloromethane (Figure 4.13) and chlorobenzene (Figure 4.19), excitation of the ILCT band also gave the most intense luminescence, consistent with the excitation spectra. Residual ligand fluorescence dominates the emission spectra when **SmL3** was excited at 390 nm in polar solvents, and despite little visible luminescence, negligible NIR luminescence was recorded.

The $^2F_{5/2} \rightarrow {}^2F_{7/2}$ transition of Yb(III) could be found as a broad peak with a peak maximum at around 980 nm. The unusual broad f-f transition of Yb(III) is attributed to the ligand-field effect[117-121] which splits both the ground and excited states into Stark components. Excitation at 330 and 350 nm gave decent results, as TTA is known to sensitize Yb(III) and $Yb(tta)_3$ is a commonly used quantum yield standard[38] for NIR measurements. On the other hand, excitation of the ILCT band at 390 nm was also able to induce antenna effect efficiently in non-polar solvents – in particular chlorobenzene

(Figure 4.33) which was markedly stronger than TTA excitation – while insignificant intensities were measured in polar solvents. The results corroborate within the series.

NIR Luminescence Quantum Yields of SmL3 and YbL3

The luminescence of the NIR transitions were too weak for luminescence lifetime measurements due to technical restrictions, so the quantum yields were determined and discussed. The quantum yields of both complexes were measured relative to Yb(tta)$_3$ in toluene (λ_{ex} = 340 nm, Φ = 0.35%). Some values were not determined for **SmL3** as the emission intensities were negligible and dominated by background.

Table 4. 2 NIR luminescence quantum yields of SmL3 and YbL3 in various solvents

Solvent	**μ (D)**	**SmL3 Φ (%)**	**YbL3 Φ (%)**
Benzene	0	6.09	0.43
Toluene	0.37	4.72	1.22
***i*-PrOH**	1.56	0.71	0.05
Fluorobenzene	1.66	5.33	0.18
CH_3OH	1.7	[b]	0.02
THF	1.75	0.97	0.20
EA	1.78	1.43	0.57
Acetone	2.88	0.77	0.07
DMF	3.82	/	/
CH_3CN	3.92	0.69	0.31
DMSO	3.96	/	0.52

The quantum yields of the **SmL3** and **YbL3** exhibit a similar trend with decreasing quantum yield with increasing solvent polarity, with the exception of fluorobenzene (Table 4.2). It is believed that steric factors hinder the coordination of the fluorobenzene molecule towards the Ln(III) and the aromaticity would impart sufficient rigidity via π-π interactions with the planar ligand backbone to allow efficient energy transfer. The quantum yields of tetrahydrofuran and ethyl acetate are slightly higher amongst the polar solvents, whereas those in DMSO and DMF are hardly measurable.

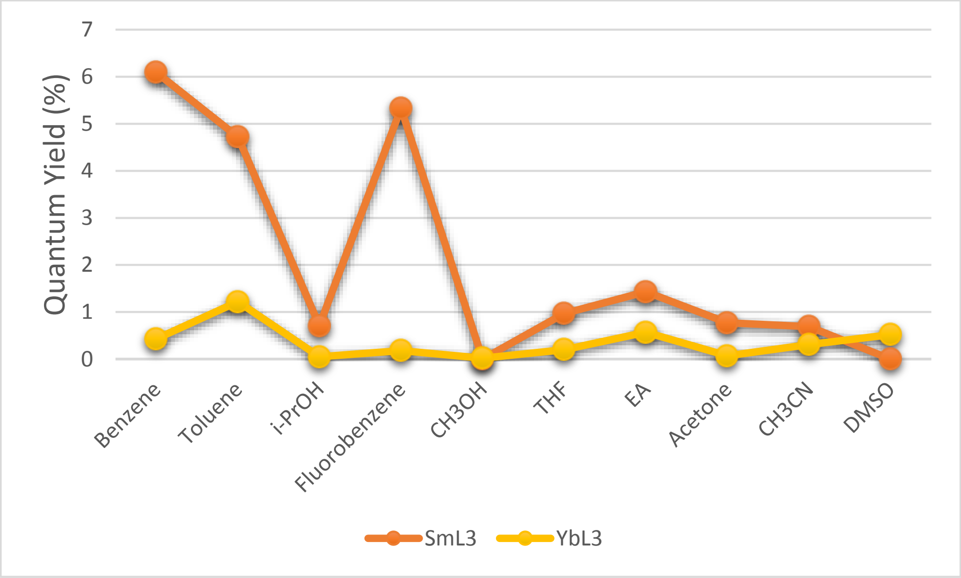

Figure 4. 2 Relative NIR luminescence quantum yields of SmL3 and YbL3

While the *m* value – number of coordinated methanol molecules – could not be calculated from the NIR luminescence lifetimes, coordination of solvent molecule is still expected and quantum yield measurements were carried out in deuterated solvents for verification (Table 4.3). Given the smaller gaps between the energy states of the NIR transitions, the deuteration of aliphatic and aromatic C-H oscillators were investigated in addition to O-H oscillators.

In methanol-d_4, the quantum yield of **SmL3** was a decent 1.37 %, compared to the immeasurable value in ordinary methanol. In the previous chapter, the *m* value for **SmL3** was determined to be around 4, hence the drastic enhancement is not a surprise. On the other hand, the ionic radius of Yb(III) is 86.8 pm compared to the 95.8 pm of Sm(III). In view of the non-directional and electrostatic nature of lanthanide-ligand interaction, it is completely possible that even more solvent molecules would coordinate to Yb(III). That is demonstrated in the scale of increase in quantum yield of **YbL3** in methanol-d_4: a fifty-time increase from 0.02 % to 1.05 %.

Methanol-d_1 (CH_3OD) was also introduced to compare the quenching efficiencies of C-H and O-H oscillators. In **YbL3**, deuteration of O-H only would lead to a seventeen-time increase while further deuteration of the methyl C-H oscillators would give a further three-time increase. Deuterated acetonitrile also gave a 50 % increase in quantum yield. These results indicate that the excited state of Yb(III), $^2F_{5/2}$, is more efficiently quenched by the harmonics of O-H oscillators than C-H. Replacing CH_3 with CD_3 in **SmL3** resulted in more than eleven times the quantum yield of methanol-d_1. While it could not be compared with ordinary methanol, C-H oscillators seem to have a more detrimental quenching effect towards Sm(III) than Yb(III).

Table 4. 3 NIR luminescence quantum yields of SmL3 and YbL3 in deuterated solvents

Solvent	μ (D)	SmL3 Φ (%)	YbL3 Φ (%]
Benzene-d_6	0	2.69%	0.52%
Toluene-d_8	0.37	3.42%	0.99%
CH_3OD	1.7	0.12%	0.34%
CD_3OD	1.7	1.37%	1.05%
CD_3CN	3.92	n/a	1.74%

However, in benzene-d_6 and toluene-d_8, a general decrease – except for **YbL3** in benzene-d_6 – was observed was observed for both complexes. This is contrary to the general idea of having an increase in lifetimes and quantum yields with deuteration of high energy oscillators. Nevertheless, compared to the luminescence lifetime of the visible $^4G_{5/2} \rightarrow {}^6H_{9/2}$ transition, a slight increase was observed in deuterated benzene (106 μs *vs.* 123.9 μs, see Chapter 3, Table 3.6). Hence it is believed that certain processes have selectively quenched the NIR transitions and not the visible ones by affecting the final states of the transitions since the same emissive state was involved.

Is the Energy Gap Law Still Valid?

The energy gap law[20,122,123] (EGL) states that the rate of non-radiative decay increases exponentially when the energy gap between the excited state and the next lower energy state of a fluorescent molecule decreases. High-energy vibrational overtones that match well with the energy gap would efficiently quench the excited energy by a multiphonon energy transfer process analogous to the Förster resonance energy transfer (FRET) and exhibit a distance-dependent relationship towards the reciprocal of d^6 – where d is the distance between the excited fluorophore and quencher. Originally developed for simple organic molecules, the EGL has also been commonly applied to explain the quenching of lanthanide(III) luminescence, as the energy levels of Ln(III) ions remain insensitive to coordination environments.

In order to demonstrate the EGL, the luminescence quantum yield results of **SmL3** and **YbL3** were revisited. The energy gap between the (only) two energy levels of Yb(III), $\Delta E(^4G_{5/2} \rightarrow {}^6F_{11/2})$, is ≈10250 cm^{-1}. The second vibrational overtone of the O-H oscillator – ≈10500 cm^{-1} – matches well with the gap and thus, when the oscillator is brought to proximity through solvent coordination, the excited energy is effectively quenched, resulting in the drastic difference in lifetimes between methanol and methanol-d_1. The comparatively slight increase when C-H was deuterated could also be explained by the EGL, as neither the second nor third vibrational overtone of C-H (≈8700 and 11600 cm^{-1} respectively) is in good resonance with the ΔE, therefore the increase was not too significant.

Alternatively, the energy gap between the emissive $^4G_{5/2}$ state and next lower $^6F_{11/2}$ state of **SmL3** is ≈7400 cm^{-1}. The second and third vibrational overtones of C-H are at ≈8700 cm^{-1} and ≈11600 cm^{-1} respectively and are quite distant from the energy difference. The first vibrational overtone of O-H oscillator, though, comes closest to matching with the ΔE at ≈7000 cm^{-1}, but is still not good enough due to quantized amount of energies. As a result, the quantum yield of the NIR transitions of **SmL3** did not give a significant increase in methanol-d_1.

However, as mentioned previously, the increase of quantum yields from methanol-d_1 to methanol-d_4 for **SmL3** is much greater than **YbL3**. This implied that the C-H oscillators still play an important role[124] in non-radiative quenching yet do not follow the EGL. A closer examination of the energy levels of Sm(III) would reveal a close match between the second C-H overtone (≈8700 cm^{-1}) with the energy difference between $^4G_{5/2}$ and $^4F_{9/2}$ states – the second lower state – at ≈8600 cm^{-1}, resulting in efficient quenching of that particular ΔE. One may also refute by stating that the third vibrational overtone of C-D (≈8400 cm^{-1}) also has a good match with the energy gap. This deactivation pathway requires four quanta of phonons compared to that of three of C-H oscillators, and with the additional 100 cm^{-1} energy difference, the efficiency of this quenching process is therefore understandably lower, but it could not be completely ruled out, too.

Seitz and co-workers[125] have suggested that the EGL is not '*universally relevant*' in explaining the quenching of lanthanide luminescence, due to the law's neglect of the Franck-Condon principle, which governs the intensity of vibronic transitions. The claim is particularly pronounced in complex systems such as Sm(III), with many electronic states, and also explains why NIR-emitting Ln(III) ions have very low quantum yields: the more electronic states, the more possible quenching pathways.

4.3. Energy Transfer Mechanism

The ILCT transition was shown to sensitize Eu(III), Sm(III) and Yb(III) efficiently. Time-resolved lifetime measurements by Wang's group[92,93] revealed the transition undergoes a non-triplet energy transfer pathway which is different from the conventional triplet-mediated pathway taken by common organic chromophores, such as TTA, allowing lower energy excitation by circumventing the triplet state.

In this section, low temperature measurements were carried out to learn more about the role the transition plays in antenna effect. The ILCT transition in the ligand system was found to sensitize Eu(III), Sm(III) and Yb(III) efficiently in non-polar solvents, and sometimes better than three molecules of TTA. **GdL1** was synthesized and the luminescence spectra of **GdL3** and $Gd(tta)_3$ were measured in 2-methyltetrahydrofuran at 77 K.

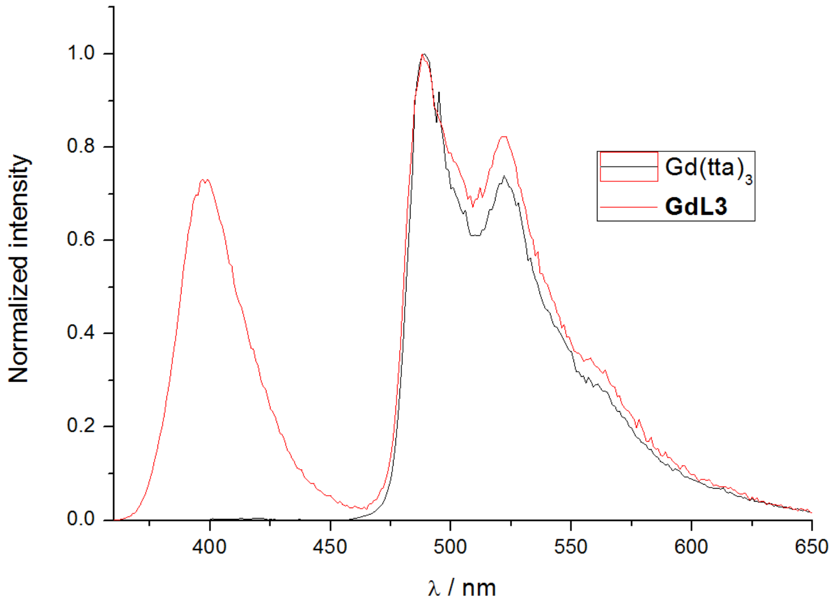

Figure 4. 3 Normalized emission spectra of GdL3 and Gd(tta)$_3$ cooled at 77 K for 180 mins

2-Methyltetrahydrofuran was chosen as the solvent for the cryogenic experiments as it forms a glass matrix and does not crystallize below its melting point, as well as having a relatively low dipole moment of 1.38 D amongst other solvents exhibiting the same property such as DMSO.

The low temperature emission spectrum of Gd(tta)$_3$ was measured at 350 nm excitation to help identify the TTA phosphorescence band in the spectrum of **GdL3** and assign the ILCT transition (Figure 4.3). The broad emission band beyond 450 nm was thus identified as TTA phosphorescence and its identity was further confirmed by lifetime measurements: 3.62 ms for the two peaks at 488 and 522 nm. The emission band with peak maximum at around 400 nm only appeared in the spectrum of **GdL3** but not Gd(tta)$_3$, therefore we could assign that to the *N*,*N*-diethylanilinyl chromophore. The emission lifetime of that band at 77 K was measured and a bi-exponential decay (3.6 and 10 μs) was observed.

A change in excitation wavelength to 390 nm did not cause a large change in the peak position of the ILCT emission (Figure 4.4). The emission lifetimes at the peak maximum at around 400 nm (1.8 and 9.3 μs) and the shoulder at around 422 nm (1.6 and 10 μs) were measured and are quite similar to the lifetime measured at 350 nm excitation, except for the shorter lifetime which was halved when the excitation was shifted. Comparison with the room temperature emission spectrum of **GdL3** with excitation at 390 nm revealed that the emission band of the ILCT transition is broader and has a peak maximum at a lower energy at a higher temperature (Figure 4.5). These results reinforce the idea that the ILCT transition of **LnL3** has a non-triplet donor energy level as the energy of emission is higher at low temperature, whereas for in TTA, decreasing the temperature would greatly hinder thermally-promoted back energy transfer in the reverse direction of intersystem crossing and the triplet state would be prominent.

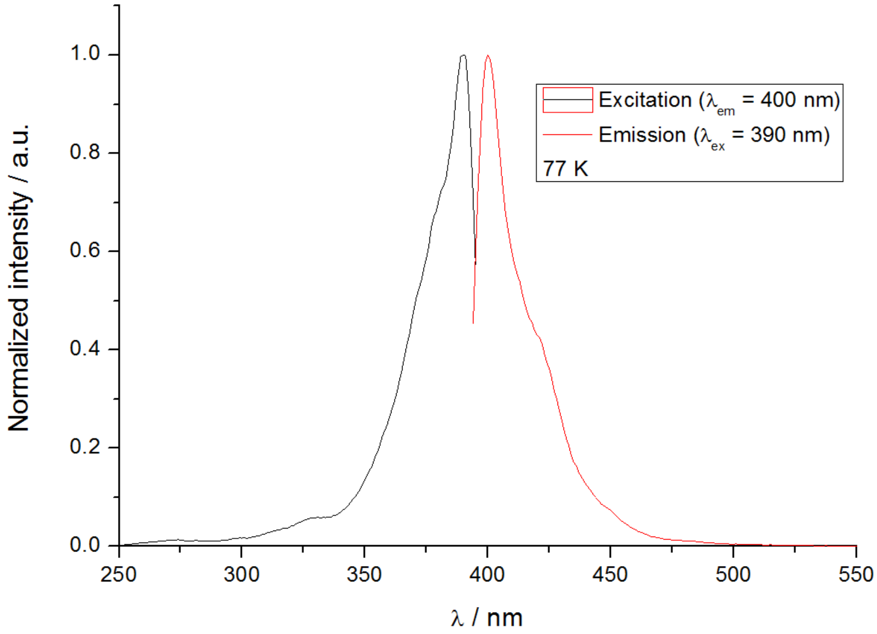

Figure 4. 4 Normalized low temperature excitation (λ_{em} = 415 nm) and emission spectra (λ_{ex} = 390 nm) of GdL3 in 2-methyltetrahydrofuran

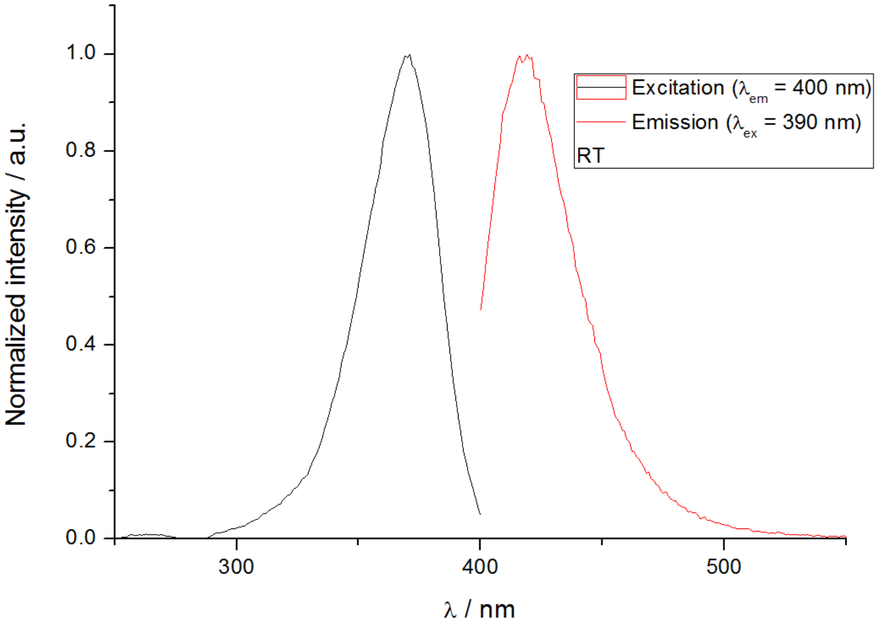

Figure 4. 5 Normalized room temperature excitation (λ$_{em}$ = 400 nm) and emission spectra (λ$_{ex}$ = 390 nm) of GdL3 in 2-methyltetrahydrofuran

As mentioned earlier, this ILCT moiety exhibits negative solvatochromism – emission blue-shifts with increasing polarity, so the polar ground state is stabilized to a greater extent than the excited state. It is therefore worth noting that the energy level estimated in 2-methyltetrahydrofuran is not universally applicable to all solvents.

The energy level of the ILCT band is estimated to be at around 23900 cm^{-1} from the room temperature emission spectrum of **GdL3**, as the energy level best represents the actual energy level taking part in the sensitization process. The $^5D_1$ and $^5D_0$ accepting levels of Eu(III) are situated at 19200 and 17200 cm^{-1} respectively, which is at a good distance with the ILCT energy level to prevent back energy transfer. From the inset Figure 4.6, the $^5D_1 \rightarrow {}^7F_J$ (J = 1,2) transitions could be seen in the emission spectrum of benzene, confirming that 5D1 was involved as an accepting state. The transitions could also be observed in other non-polar solvents as well. The $^4G_{5/2}$ level of Sm(III) at around 17900 cm^{-1} is also well-positioned for energy transfer as well, vindicated by the sensitized visible and NIR luminescence.

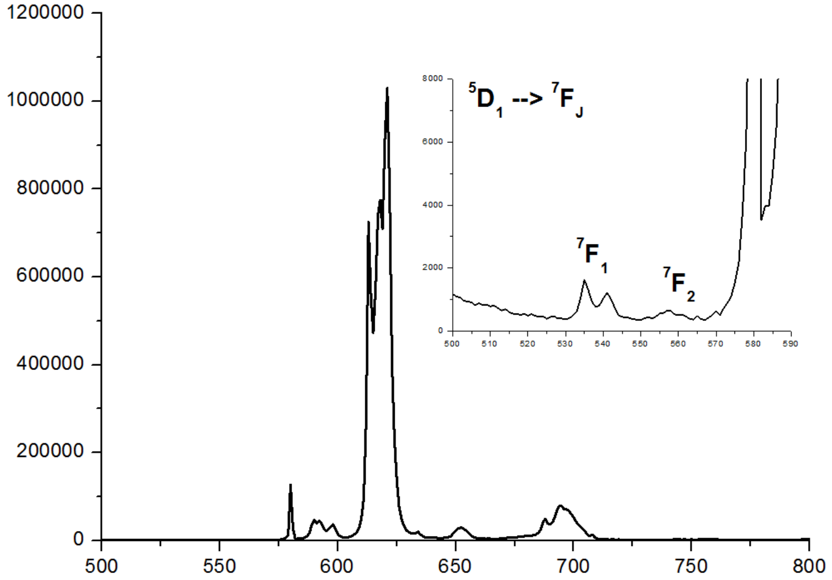

Figure 4. 6 Emission spectrum of EuL3 in benzene with 390 nm excitation

The excited state of Yb(III), though, is much lower in energy at around 10200 cm^{-1}. Figure 4.7 presents an energy level diagram showing the three Ln(III) ions, energy level of the ILCT band and triplet donor state of TTA. The two main energy transfer mechanisms are the Förster and Dexter mechanisms. The former requires spectral overlap between the donor and acceptor and these conditions are partially fulfilled by Eu(III) and Sm(III). The huge ΔE implies minimal overlap between the emission spectra of both the TTA and ILCT transition and the $^2F_{5/2}$ excited state of Yb(III), effectively ruling out the Förster mechanism. However, numerous literature reports[126-128] and this chapter has already demonstrated decent sensitization of Yb(III) luminescence.

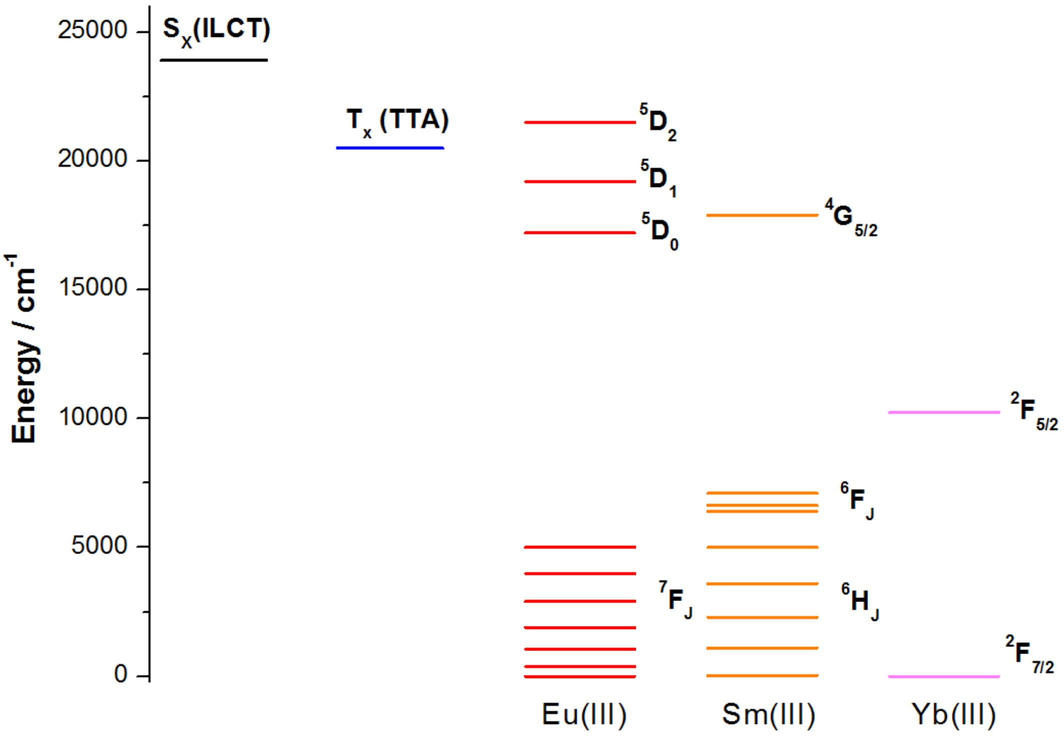

Figure 4. 7 Energy level diagram of Eu(III), Sm(III), Yb(III), ILCT band and triplet state of TTA

The selection rule[129,130] of the Dexter energy transfer mechanism are restricted to $|\Delta J| = 0, 1$ between the accepting and ground state (see Chapter 1). For Yb(III), ΔJ is 1 is obeys the selection rule. The Dexter mechanism does not require spectral overlap but instead necessitates physical orbital overlap between the donor and acceptor.

Horrocks Jr's[117] work in 1997 proposed a long range electron transfer process for the sensitization of Yb(III) luminescence in a protein containing tryptophan. Upon photoexcitation, the excited state of tryptophan reduced Yb(III) to Yb(II) and was quickly followed by the oxidation of Yb(II) back to Yb(III) by the strongly oxidizing tryptophan radical cation, a process which has a greater driving force than the $^2F_{5/2}$ excited state of Yb(III), and result in probable excited energy transfer. This mechanism is favorable towards Yb(III) as it is the second most readily reduced ion among the Ln(III) series behind Eu(III) with a reduction potential of -1.05 V in water *vs.* NHE. In Eu(III), the same mechanism proceeds but could not sensitize Eu(III) due to the $^5D_0$ level occupying a higher energy position.

To evaluate the feasibility of this two-step electron transfer mechanism, the free energy on electron transfer (ΔG_{ET}) of the complex system was calculated from the extended Rehm-Weller equation:[131,132]

$$\Delta G_{ET} = (E_{ox} - E_{red}) - E_s - e_o^2/\varepsilon_a$$

From cyclic voltammetry experiments, the oxidation potential (E_{ox}) of the donor (ILCT ligand) and reduction potential (E_{red}) of the acceptor (Yb(III)) was determined to be 0.77 and -1.55 V respectively. The singlet state energy (E_s) of the zero-zero transition of the ligand was determined by averaging the longest excitation maximum and the shortest emission maximum measured at 77 K to be 3.1 eV. The columbic attraction (e_0^2/ε_a) experienced by radical ion pair is taken as 0.15 eV with reference to literature.[133-134] The ΔG_{ET} is then determined, with the above formula and values, to be -0.93 eV, indicating that the double electron transfer process is feasible.[135]

Similarly, the ΔG_{ET} for **EuL3** and **SmL3** were found to be -0.94 and -0.65 respectively. The reduction potential for Eu(III) is -0.35 V vs NHE and thus its high driving force for the energy transfer mechanism is expected. Sm(III), the third readily reduced Ln(III), has a reduction potential of -1.55 V, could also be sensitized by the double electron transfer mechanism, as seen in luminescence measurements.

The weak sensitization when the **LnL3** complexes were excited at 390 nm could be attributed to the hindering the electron transfer of the redox mechanism by alcoholic and highly polar solvent molecules. The previous chapter discussed about shifting the energy levels according to solvent polarity, resulting in higher mismatch of energy levels for excited energy transfer or the displacement of the chromophore leading to poor energy transfer. These, however, are factors concerning the Förster resonance energy transfer mechanism. The role solvent plays in the aforementioned internal redox mechanism puts emphasis on the lone-pair electrons on the anilinyl moiety, as alcoholic solvents are capable to form a hydrogen bond and restrict electron transfer and highly polar solvents may hinder electron transfer by strong dipole-dipole interactions.

Nevertheless, the results presented do not suggest exclusivity of the double electron transfer mechanism at 390 nm excitation, especially in **EuL3** and **SmL3** where the ΔE between the ILCT state is not too far away from the accepting states of Eu(III) and Sm(III), as observed in the weaker luminescence at 390 nm excitation in polar solvents.

4.4. Control Experiments

LnL4-6 were synthesized to confirm the ILCT character imparted by the *N*,*N*-diethylamino group in comparison with **LnL1-3**. Without the electron-donating group, the push-pull extent on the planar tridentate molecule is much decreased and the solvatochromism is not expected. The methyl substituents are not expected to have any effect on the photophysical properties as well.

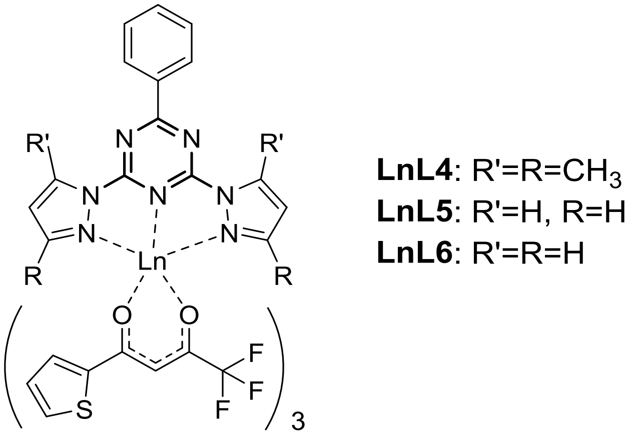

Figure 4. 8 Structures of LnL4-6 used in this work

4.4.1. Photophysical Studies

UV-vis spectroscopy is the most straightforward way to see if the ILCT transition is present, as it is generally a broad, structureless band sensitive to solvent polarity. As seen in the absorption spectra of **Ln4-6** in toluene – the solvent which the ILCT transition was distinctly observable for **LnL1-3**, only two absorption bands are observed: the high energy absorption band (peak maximum at around 290 nm) of the triazine core – which was sometimes interfered by solvent absorption – and the signature TTA absorption band centered at 340 nm. In methanol, in spite of the poor sensitization in the highly polar environment, the ILCT absorption band was still apparent in **EuL2**; however, only two peaks still were observed for **EuL5** in methanol, confirming once again the absence of any ILCT transitions. The same were observed for **SmL2** and **SmL5** as well.

Luminescence spectra were recorded in toluene with excitation at 390 nm and compared against with excitation at a TTA-only wavelength, 330 nm. The luminescence intensity of the latter was much higher, expectedly so, and is significantly weaker than the ILCT counterparts. According to the hypersensitive $^5D_0 \rightarrow {}^7F_2$ transition, it is revealed that both excitation wavelengths gave rise to two emitting species of very similar, if not identical, coordination environment. Coupled with the information obtained from the absorption and excitation spectra, it is reasonable to suggest that one emitting species was present, as 390 nm excitation would still be exciting the TTA.

The luminescence lifetimes of **EuL5** and **SmL5** were measured, at their most intense transitions, in methanol and toluene under excitation at 350 nm, and were found to be quite similar to those of **EuL2** and **SmL2**. The *m* values calculated for **EuL5** and **SmL5** are 3.8 and 3.0 respectively. Solvent coordination is expected as removing the *N*,*N*-diethylamino group will not have much effect on the chelating strength of the tridentate ligand. The values are slightly different to those of **EuL2** (1.9) and **SmL2** (3.7) and the discrepancy in **EuL5** is a result of the difference in coordination geometry and decrease in steric hindrance because of removing the electron-rich ILCT group, leading to less protection of the Eu(III) center.

Table 4. 4 Luminescence lifetimes of EuL5 and SmL5 compared with EuL2 and SmL2

Solvents	EuL5 τ (ms)	SmL5 τ (μs)	EuL2 τ (ms)	SmL2 τ (μs)
MeOH	0.262	14.5	0.239	12.3
CD_3OD	0.474	137	/	132
Toluene	0.321	97	0.485	103

The luminescence quantum yields were measured relative to quinine sulfate (Φ = 0.577, λ_{ex} = 340 nm). In methanol, due to solvent coordination, the quantum yields are low as a result of quenching by solvent oscillators. In toluene, however, it is also markedly lower than the analogs with the ILCT moiety. The difference is attributed to the partial excitation of the ILCT transition – which is a good excited energy donor state – that is absent in these analogs, therefore resulting in poorer values. The results are particularly pronounced in **SmL5**, which is only 10 % of the quantum yield of **SmL2**, vindicating the efficiency of the ILCT transition in sensitizing the $^4G_{5/2}$ excited state of Sm(III).

Table 4. 5 Relative quantum yields of EuL5 and SmL5

Solvents	EuL5 Φ (ms)	SmL5 Φ (μs)
MeOH	3.4	0.2
CD_3OD	/	/
Toluene	15.1	0.4

Since excitation at 350 nm would be able to partially excite the ILCT band and, for non-polar solvents, promote antenna effect for sensitization, it is therefore understandable that the NIR luminescence of both **YbL5** and **SmL5** are very weak. The luminescence of **SmL5** was hardly observable even at a concentration of 0.3 absorbance at 340 nm. Yb(III) emission was moderate and the quantum yield was measured relative to $Yb(tta)_3$ (λ_{ex} = 340 nm, Φ = 0.35 %) and presented in Table 4.6. The value of 0.38 % is closer to that of the standard than the ILCT analog **YbL2**.

Table 4. 6 Relative quantum yields of YbL5 and YbL2

Solvents	YbL5 Φ (%)	YbL2 Φ (%)
Toluene	0.38	1.22

4.5. Conclusion

NIR luminescence of Sm(III) and Yb(III) were well sensitized by an ILCT band, with intensities greater than the antenna effect of three TTAs. The absolute quantum yields of ILCT excitation were not measured to quantify the comparison due to technical constrains. Examination of the relative quantum yields under excitation of TTA revealed different extents of quenching efficiencies by O-H and C-H oscillators. Results obtained in partial and fully deuterated measurements were able to selectively investigate the quenchers and the various degrees of enhancement were explained in details by studying the energy levels of the Ln(III), in which the commonly used Energy Gap Law was also found to be inadequate to predict the probability of quenching in emitting systems with complex energy levels such as Sm(III).

The energy transfer mechanism involved in sensitizing **YbL3** was investigated as cryogenic measurements revealed a huge energy gap between the non-triplet energy level of the ILCT transition and the $^2F_{5/2}$ excited state of Yb(III), effectively excluding the Förster energy transfer mechanism. Cyclic voltammetry experiments were carried out and suggested that a double electron transfer mechanism for populating the $^2F_{5/2}$ state is energetically feasible but not necessarily exclusive.

Comparison between the ILCT *N*,*N*-diethylamino series (**LnL1-3**) and the non-ILCT phenyl series (**LnL4-6**) provided further proof that the ILCT transition is capable of, particularly efficiently in non-polar environments, sensitizing **LnL1-3**. In addition to the tridentate ligand acting as an auxiliary ligand to prevent the coordination of solvent molecule, the broad absorption ILCT band could also be partially excited by light of 350 nm and therefore result in higher luminescence quantum yields.

4.6. Appendix

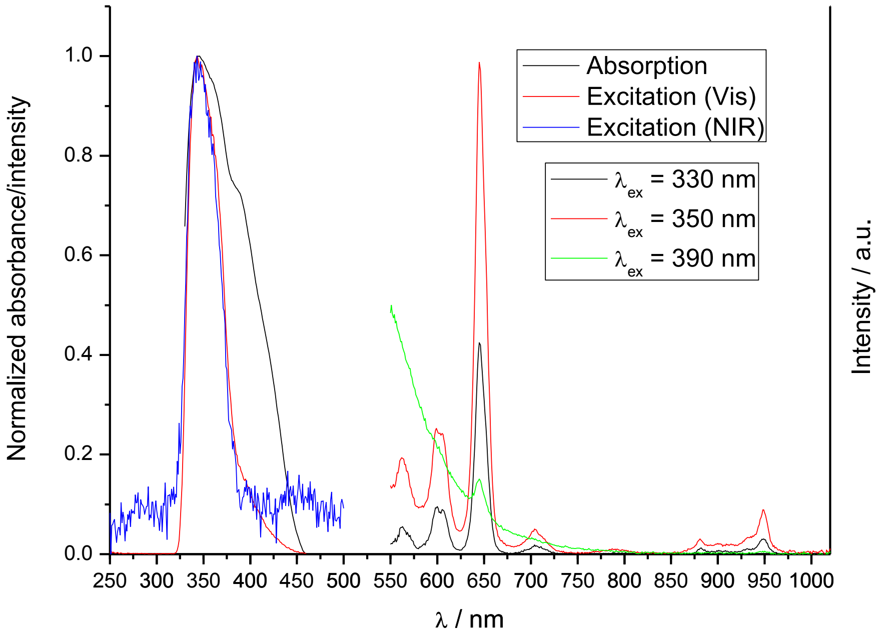

Figure 4. 9 Normalized absorption, excitation, and emission spectra of SmL3 in acetone

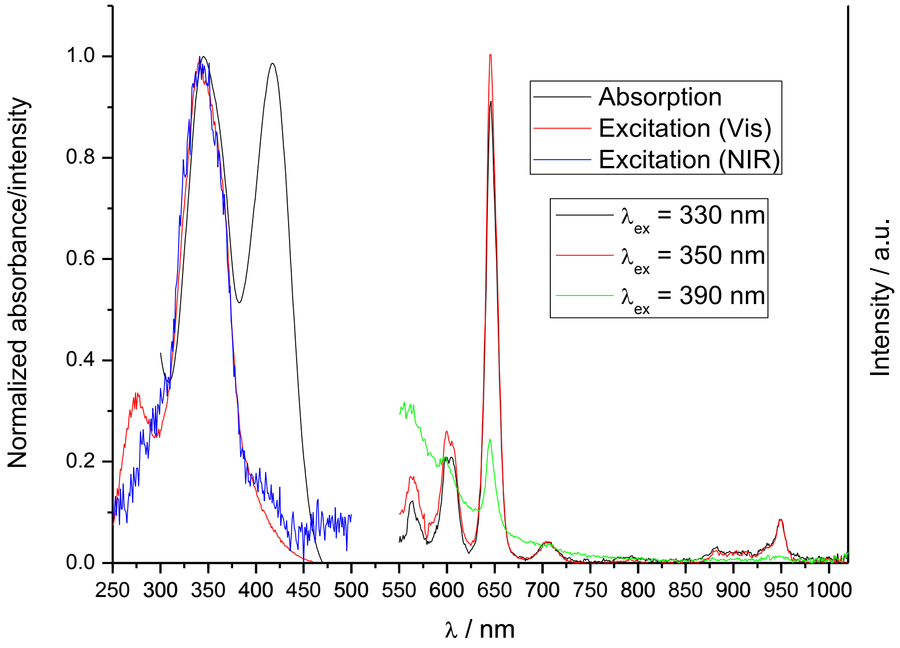

Figure 4. 10 Normalized absorption, excitation, and emission spectra of SmL3 in ACN

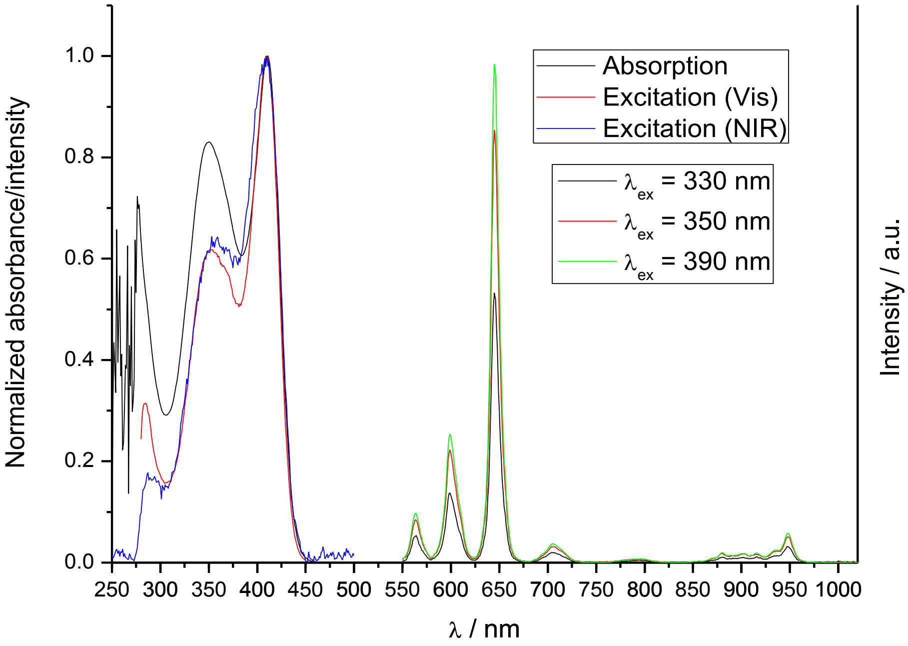

Figure 4. 11 Normalized absorption, excitation, and emission spectra of SmL3 in benzene

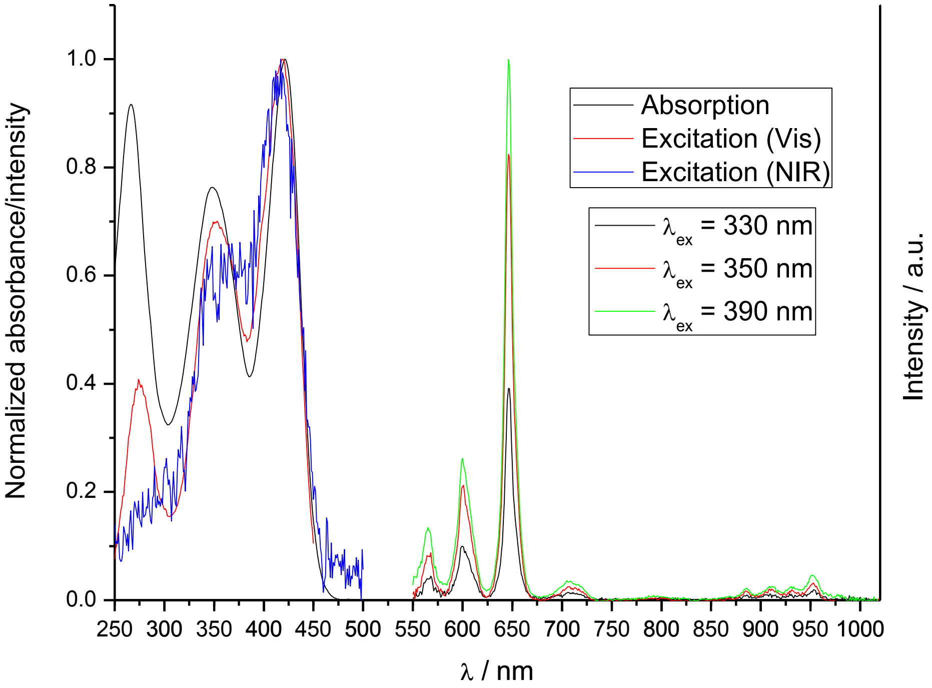

Figure 4. 12 Normalized absorption, excitation, and emission spectra of SmL3 in $CHCl_3$

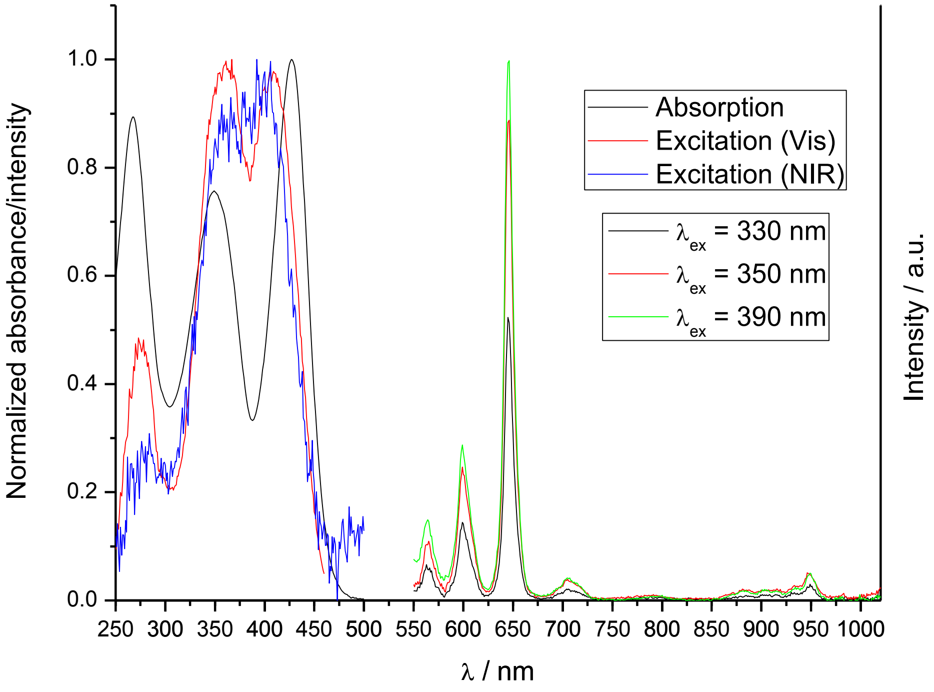

Figure 4. 13 Normalized absorption, excitation, and emission spectra of SmL3 in DCM

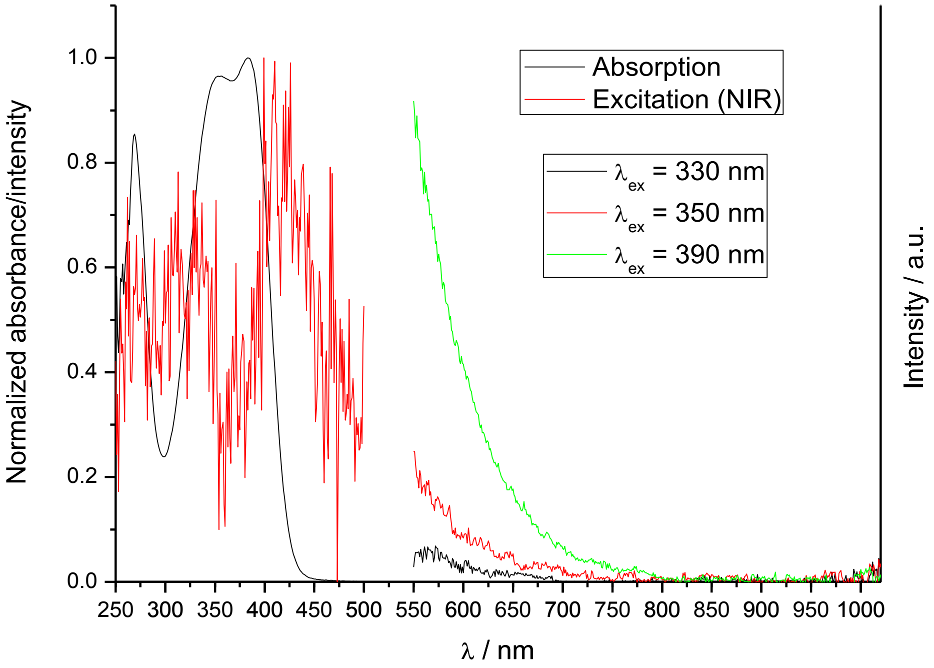

Figure 4. 14 Normalized absorption, excitation, and emission spectra of SmL3 in DMF

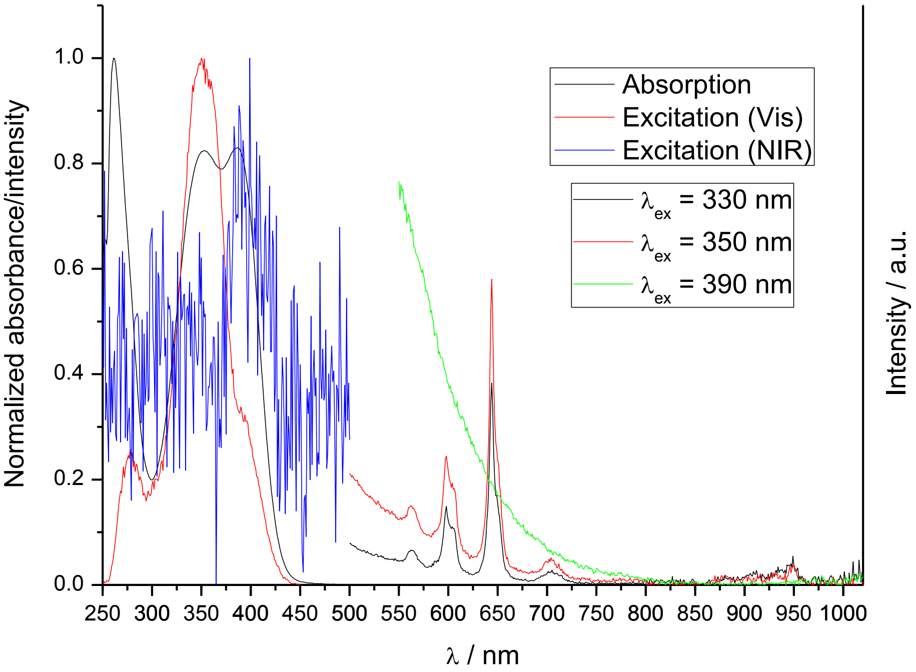

Figure 4. 15 Normalized absorption, excitation, and emission spectra of SmL3 in DMSO

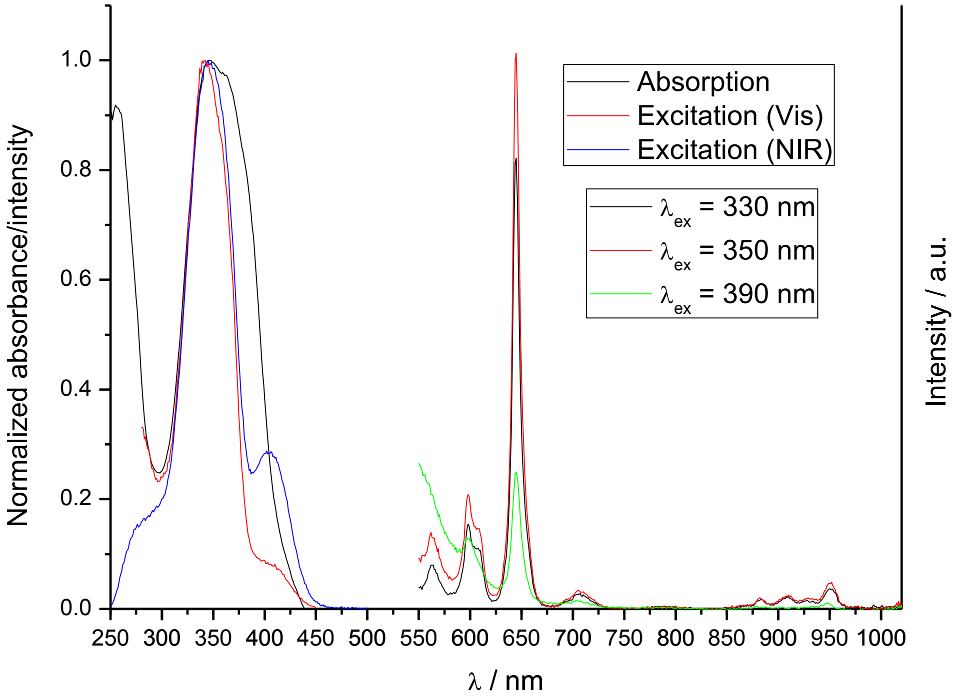

Figure 4. 16 Normalized absorption, excitation, and emission spectra of SmL3 in EA

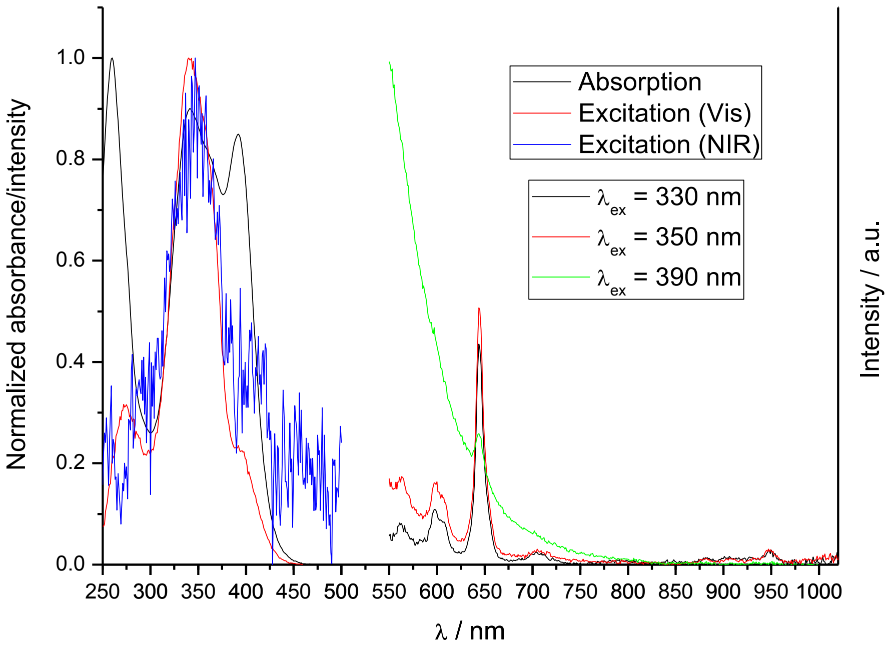

Figure 4. 17 Normalized absorption, excitation, and emission spectra of SmL3 in IPA

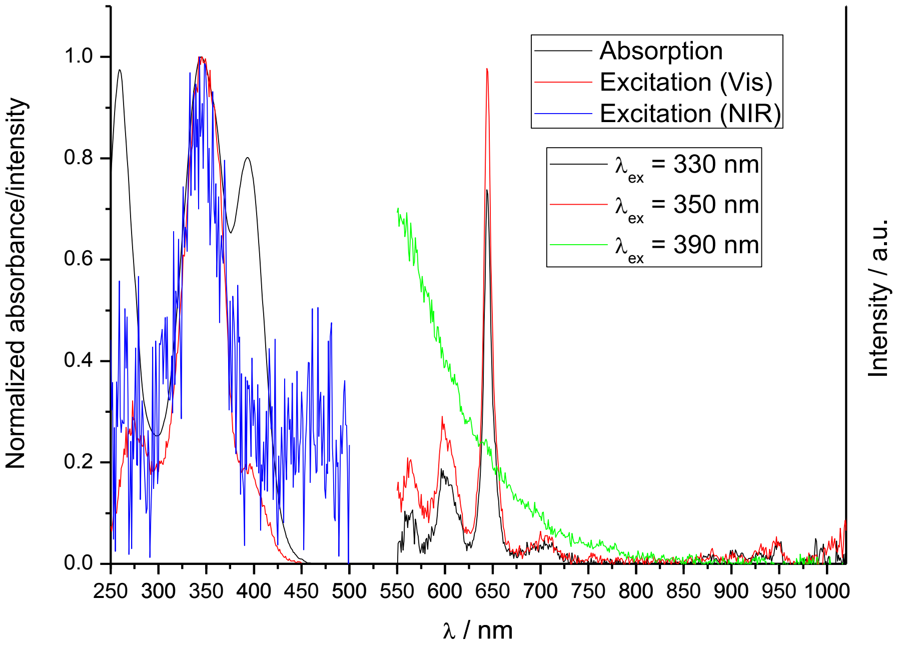

Figure 4. 18 Normalized absorption, excitation, and emission spectra of SmL3 in methanol

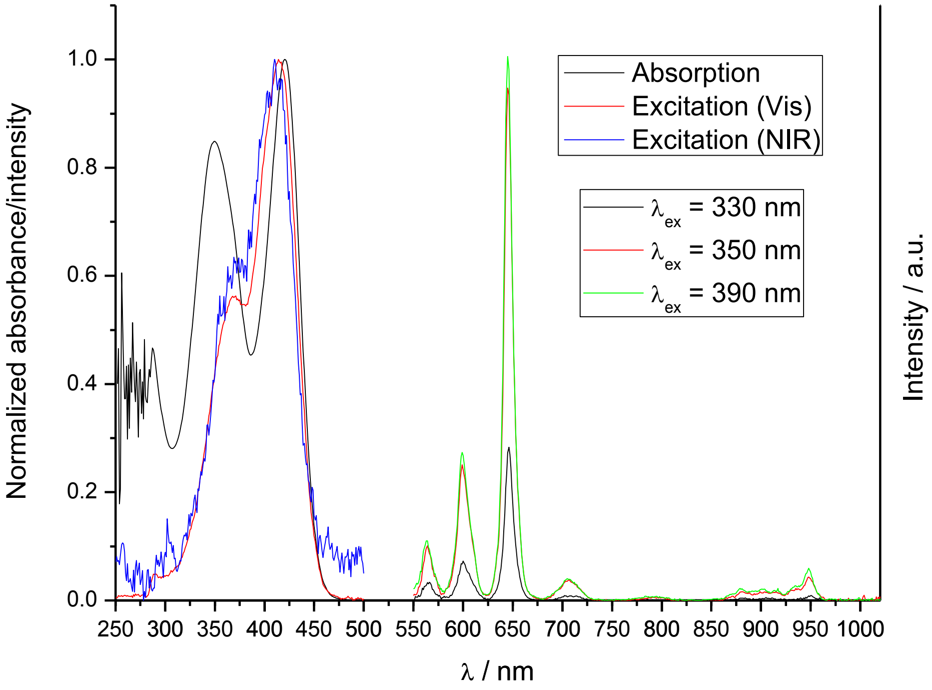

Figure 4. 19 Normalized absorption, excitation, and emission spectra of SmL3 in PhCl

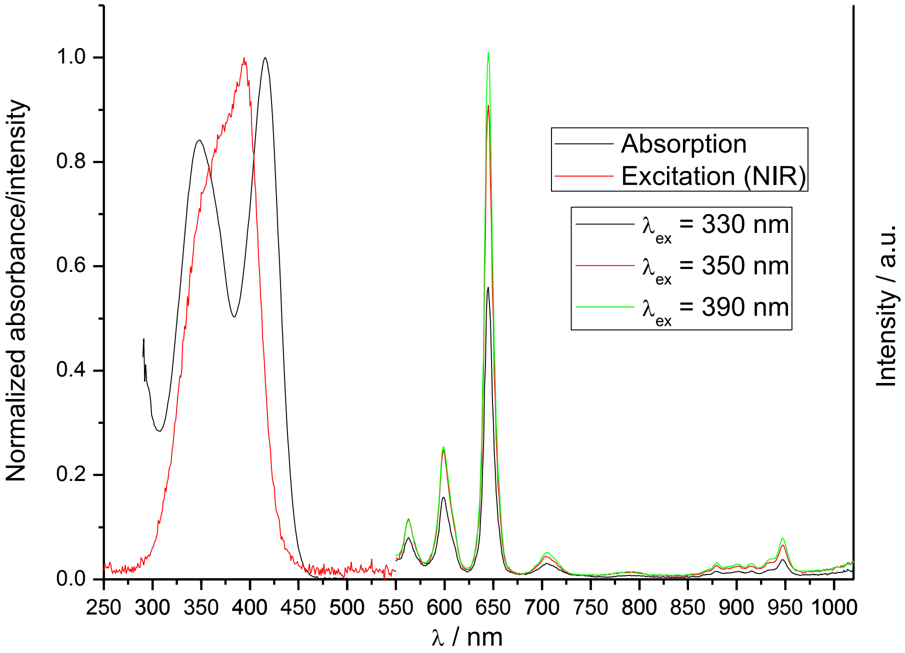

Figure 4. 20 Normalized absorption, excitation, and emission spectra of SmL3 in PhF

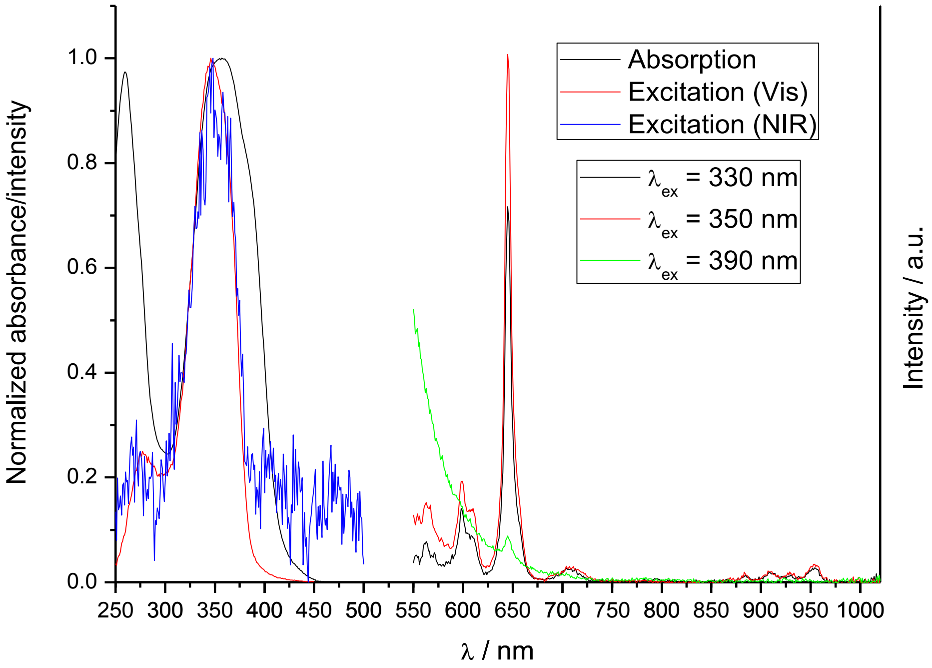

Figure 4. 21 Normalized absorption, excitation, and emission spectra of SmL3 in THF

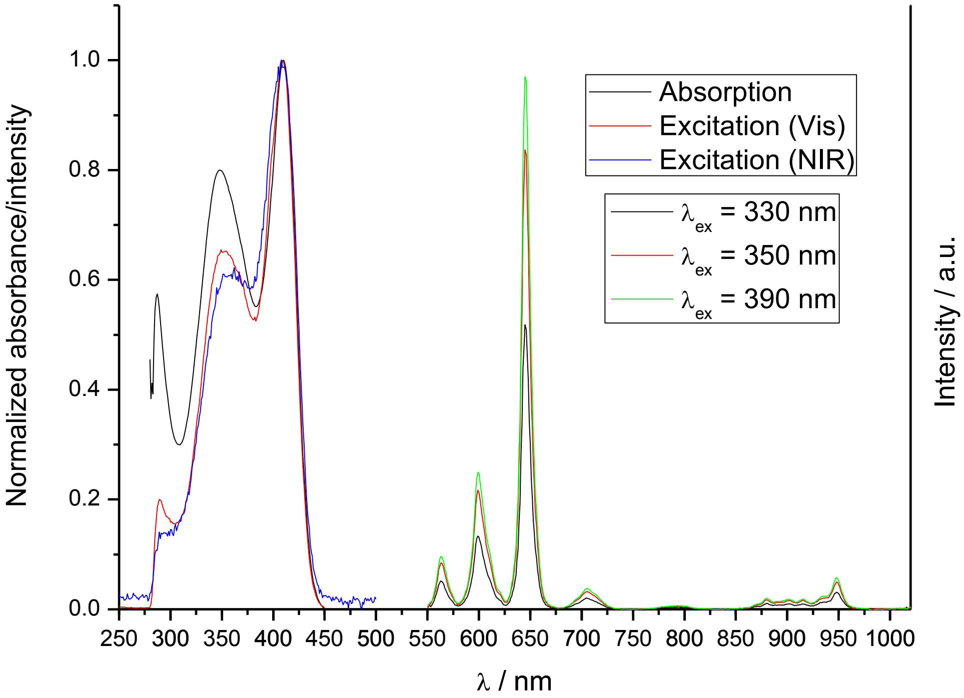

Figure 4. 22 Normalized absorption, excitation, and emission spectra of SmL3 in toluene

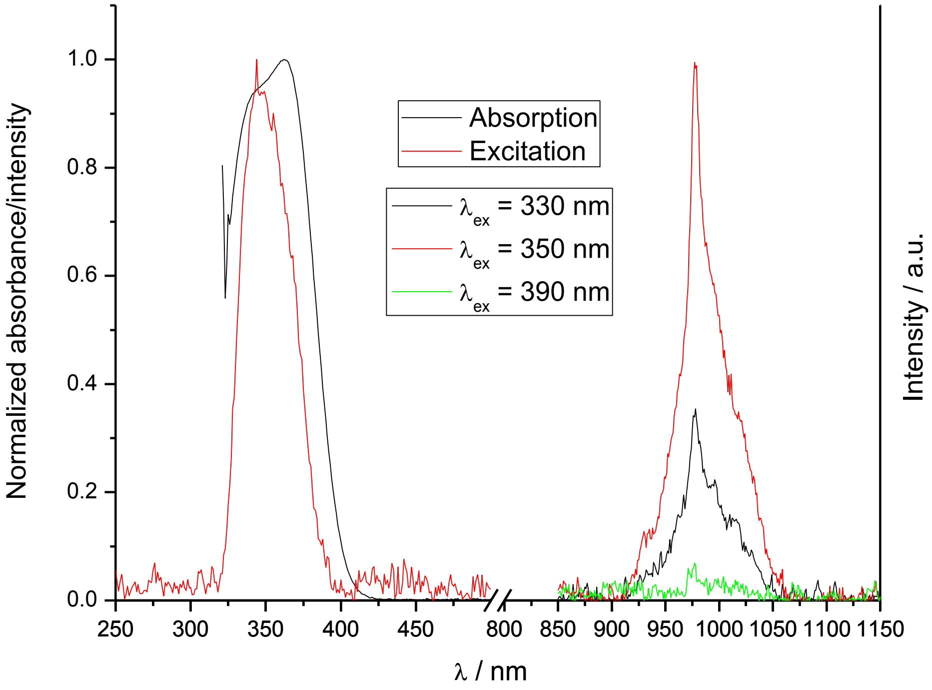

Figure 4. 23 Normalized absorption, excitation, and emission spectra of YbL3 in acetone

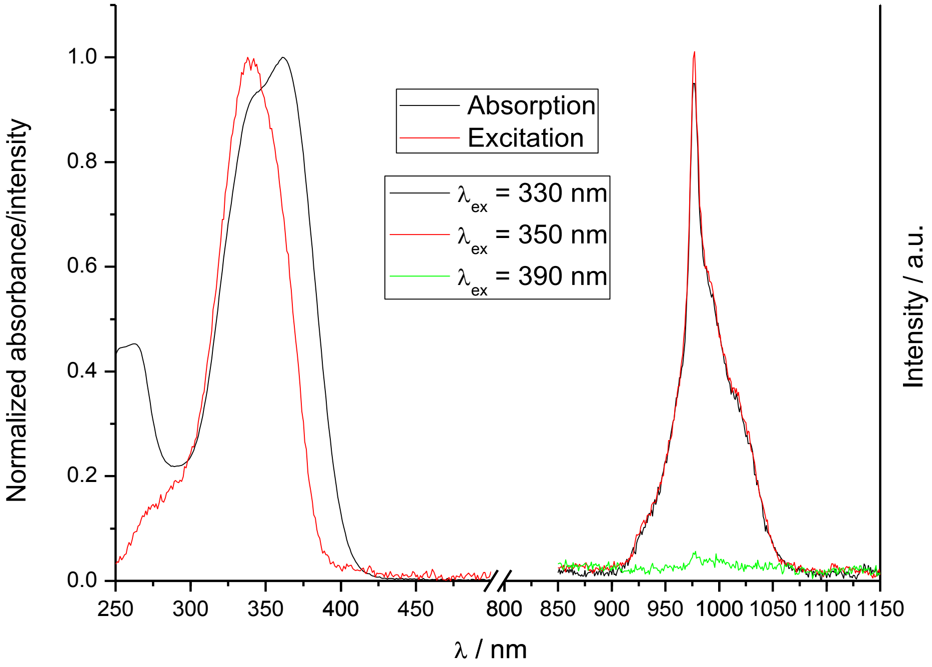

Figure 4. 24 Normalized absorption, excitation, and emission spectra of YbL3 in ACN

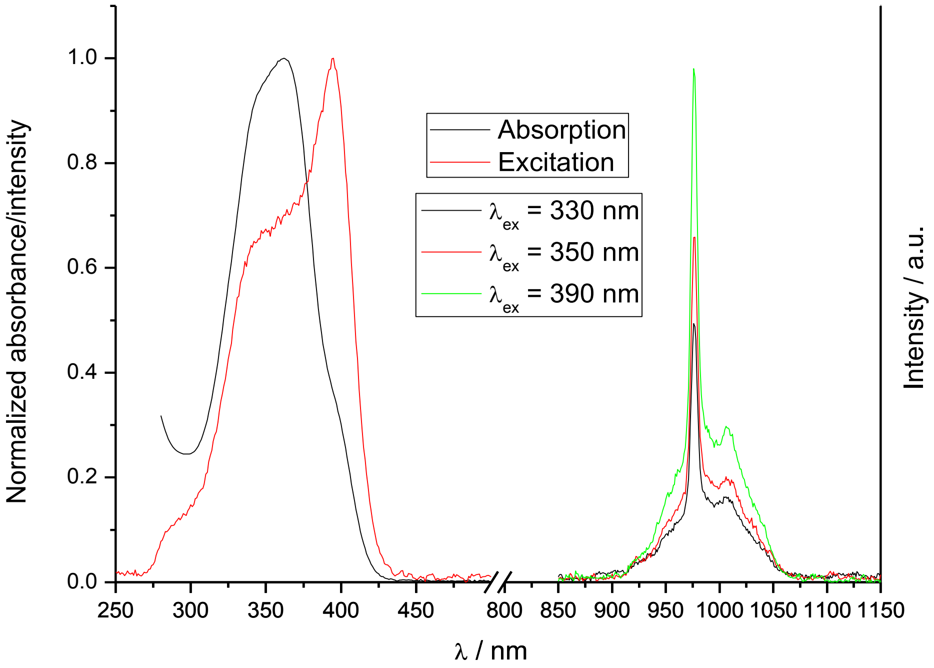

Figure 4. 25 Normalized absorption, excitation, and emission spectra of YbL3 in benzene

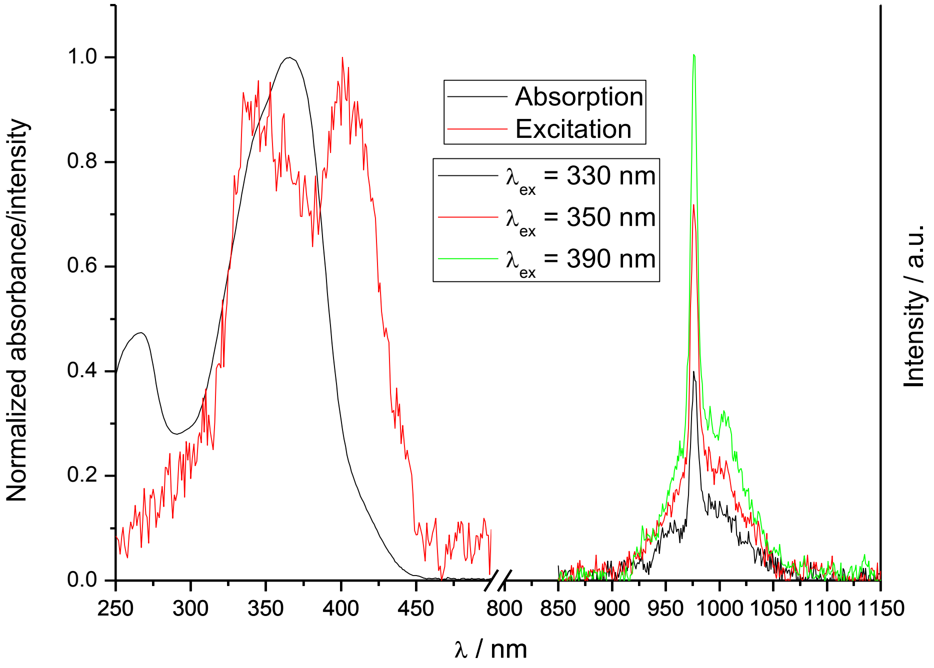

Figure 4. 26 Normalized absorption, excitation, and emission spectra of YbL3 in $CHCl_3$

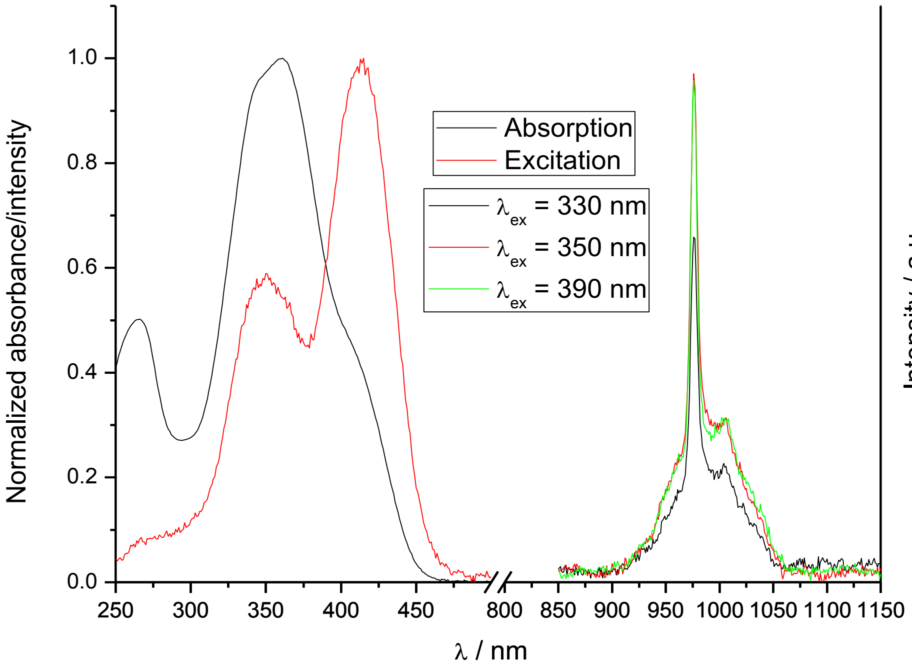

Figure 4. 27 Normalized absorption, excitation, and emission spectra of YbL3 in DCM

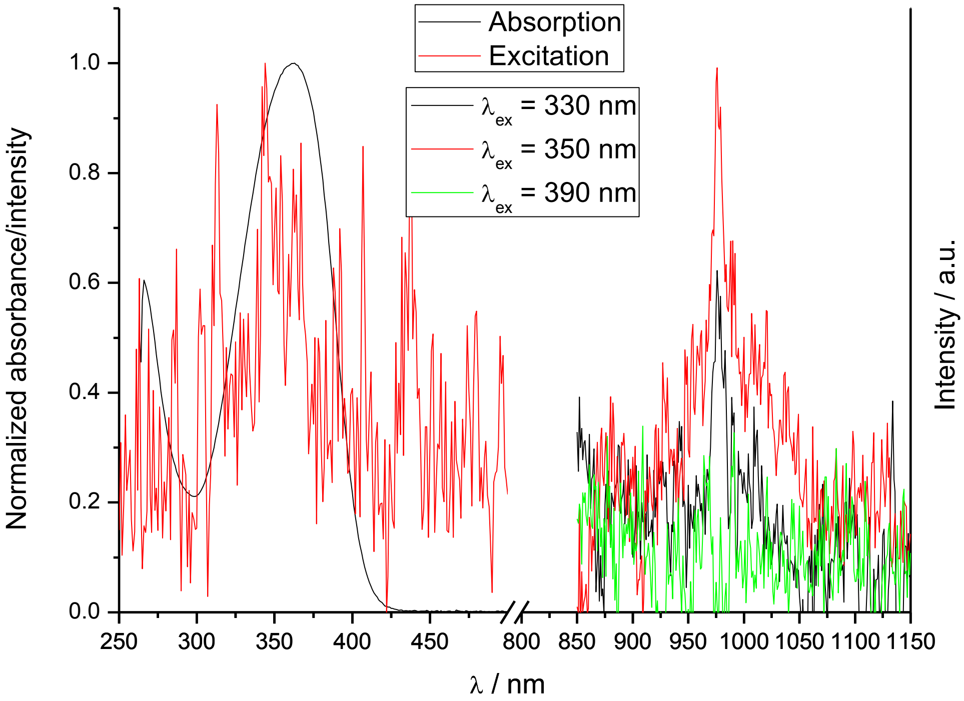

Figure 4. 28 Normalized absorption, excitation, and emission spectra of YbL3 in DMF

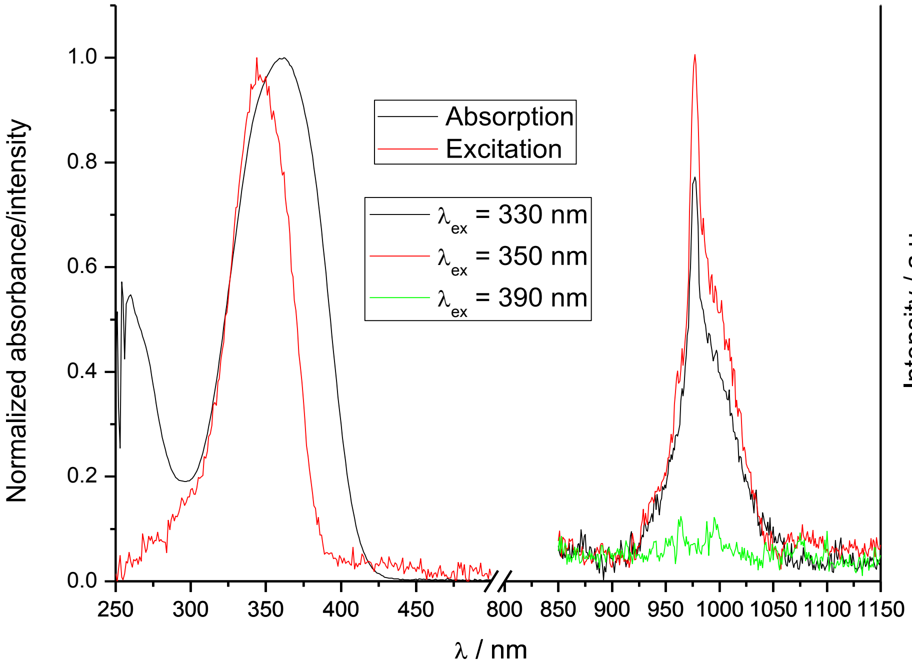

Figure 4. 29 Normalized absorption, excitation, and emission spectra of YbL3 in DMSO

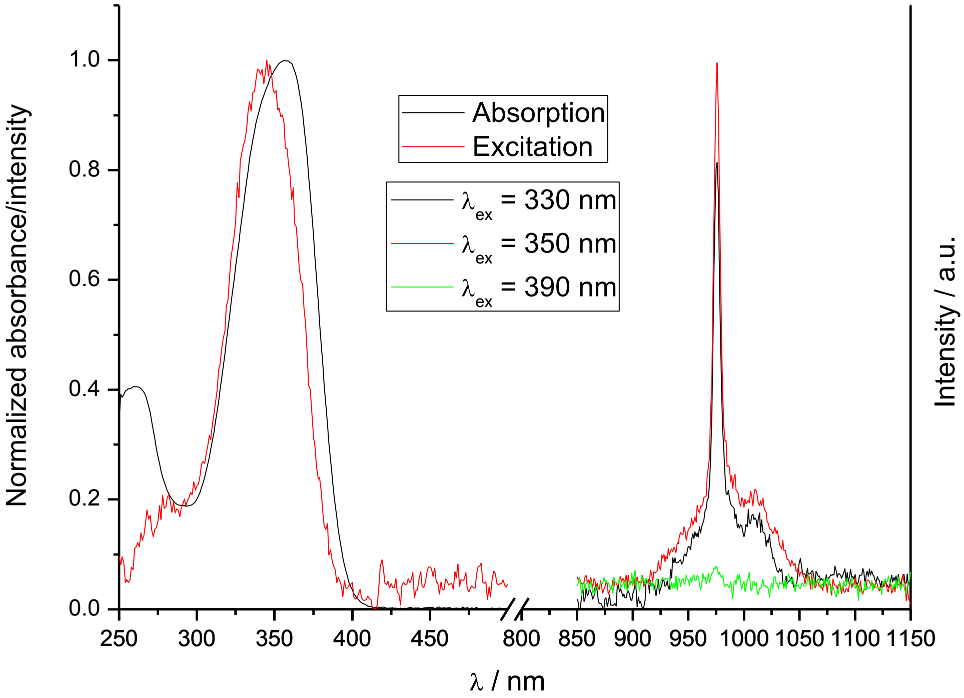

Figure 4. 30 Normalized absorption, excitation, and emission spectra of YbL3 in EA

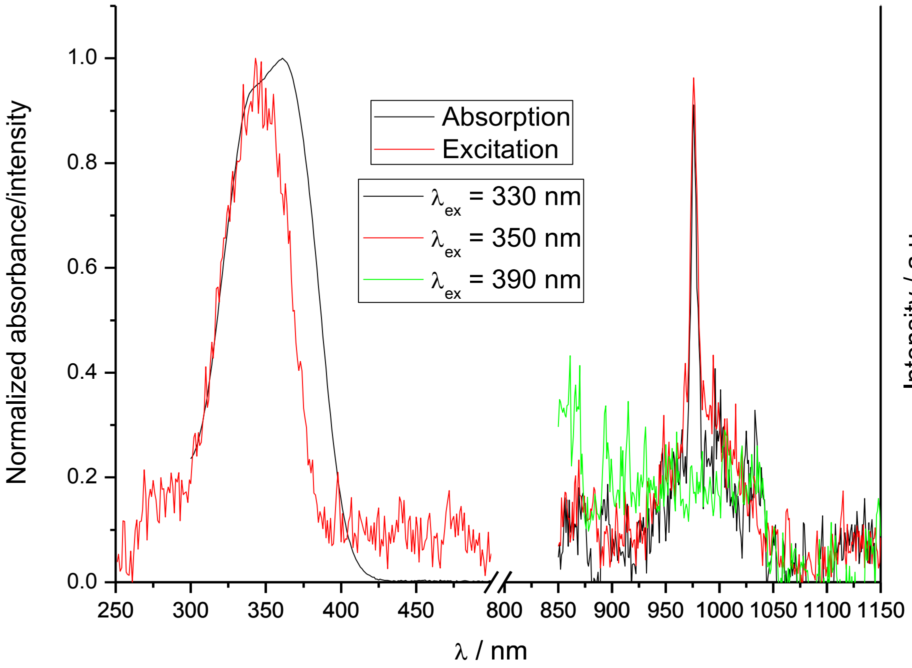

Figure 4. 31 Normalized absorption, excitation, and emission spectra of YbL3 in IPA

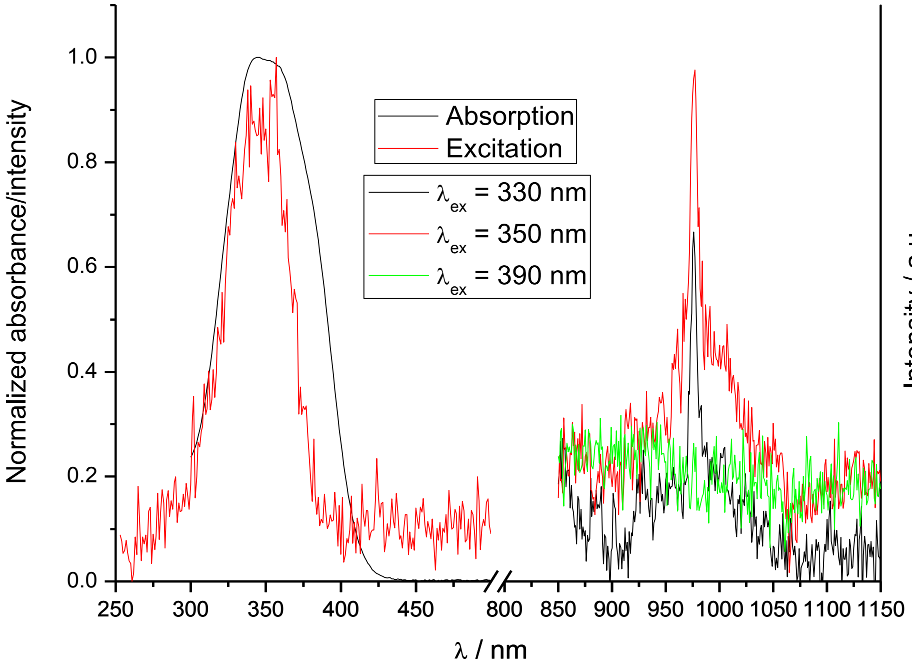

Figure 4. 32 Normalized absorption, excitation, and emission spectra of YbL3 in methanol

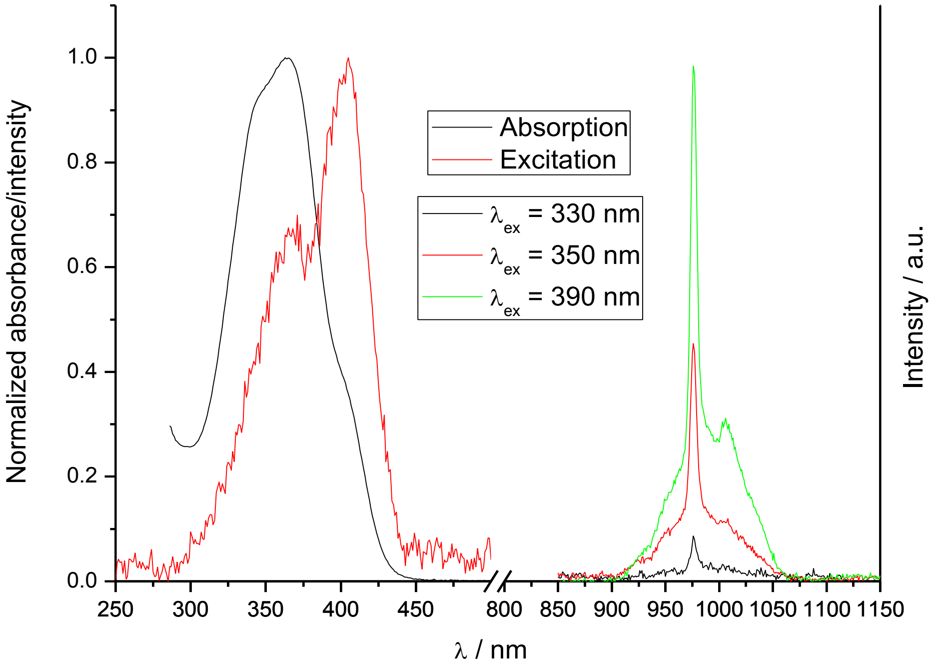

Figure 4. 33 Normalized absorption, excitation, and emission spectra of YbL3 in PhCl

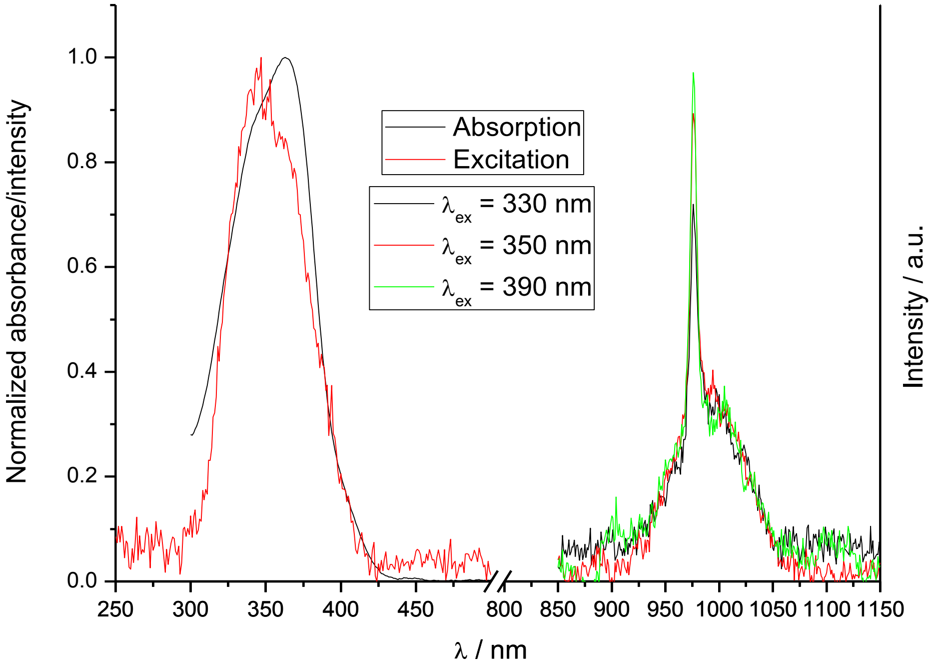

Figure 4. 34 Normalized absorption, excitation, and emission spectra of YbL3 in PhF

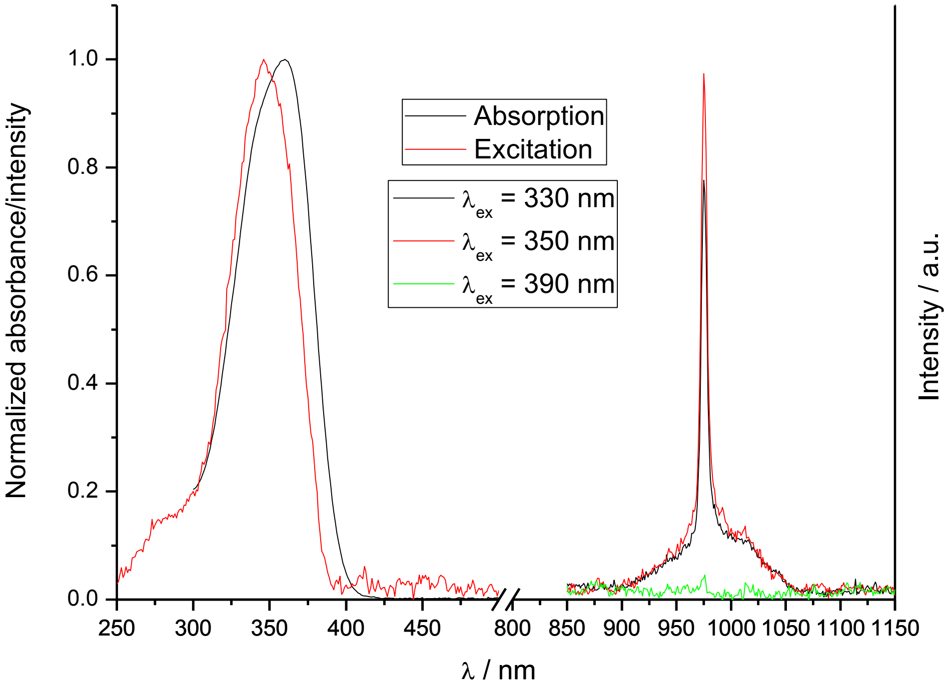

Figure 4. 35 Normalized absorption, excitation, and emission spectra of YbL3 in THF

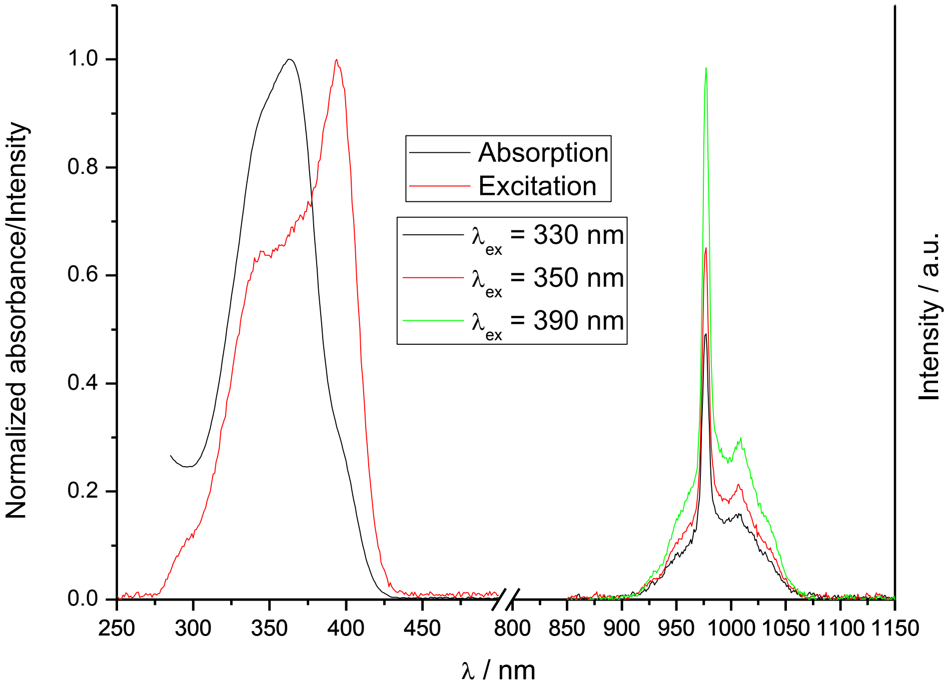

Figure 4. 36 Normalized absorption, excitation, and emission spectra of YbL3 in toluene

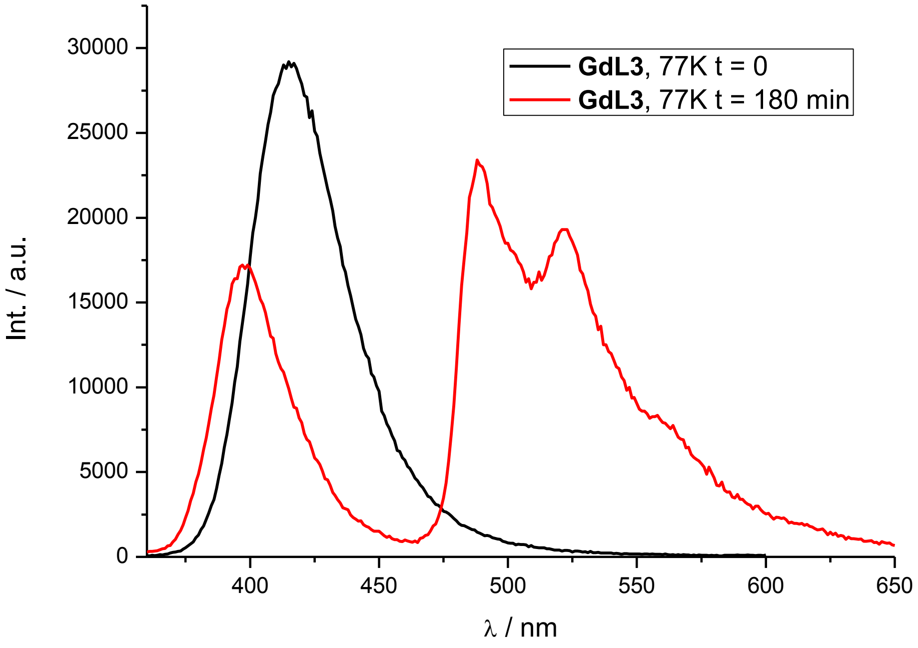

Figure 4. 37 Emission spectra of GdL3 at RT and cooled at 77 K for 180 mins (λ_{ex} = 350 nm)

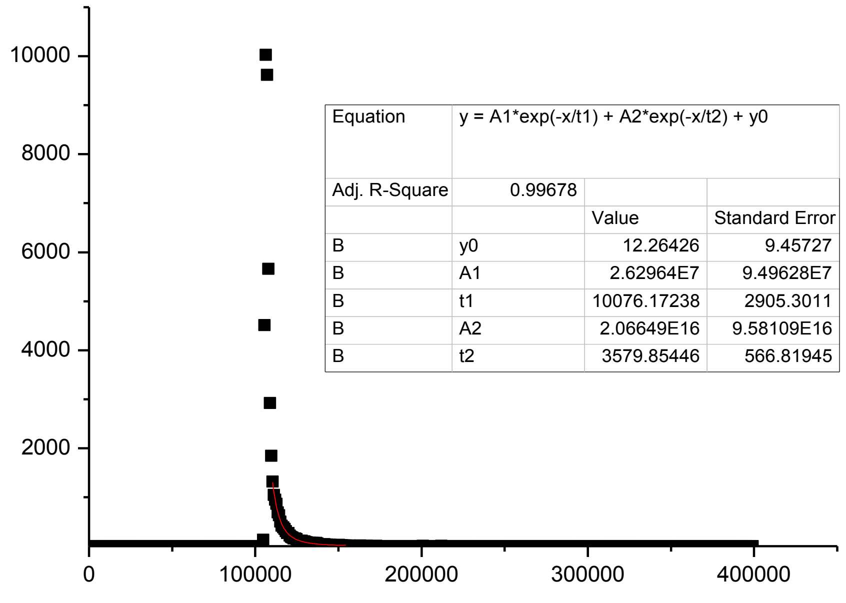

Equation	y = A1*exp(-x/t1) + A2*exp(-x/t2) + y0		
Adj. R-Square	0.99678		
		Value	Standard Error
B	y0	12.26426	9.45727
B	A1	2.62964E7	9.49628E7
B	t1	10076.17238	2905.3011
B	A2	2.06649E16	9.58109E16
B	t2	3579.85446	566.81945

Figure 4. 38 Decay curve of emission lifetime of GdL3 at 77 K (λ_{ex} = 350 nm, λ_{em} = 397 nm)

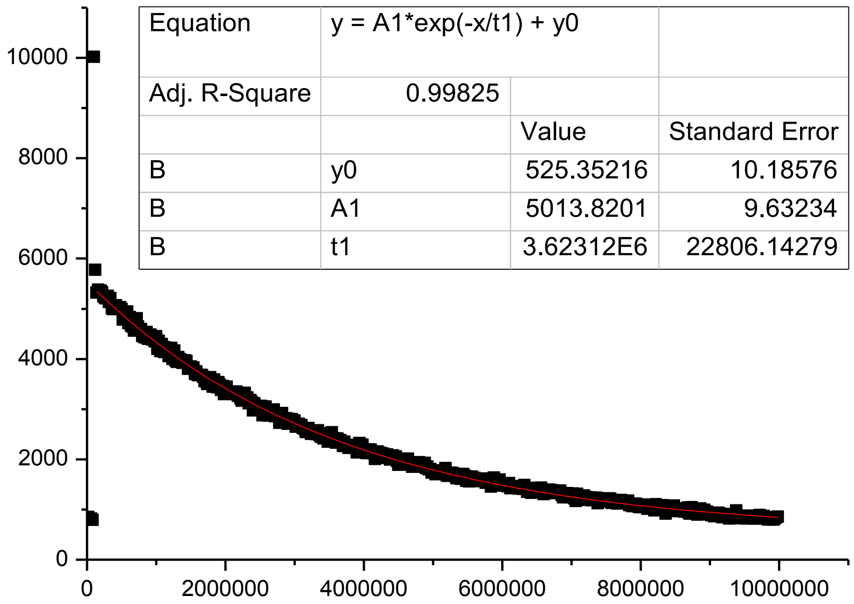

Equation	y = A1*exp(-x/t1) + y0		
Adj. R-Square	0.99825		
		Value	Standard Error
B	y0	525.35216	10.18576
B	A1	5013.8201	9.63234
B	t1	3.62312E6	22806.14279

Figure 4. 39 Decay curve of emission lifetime of GdL3 at 77 K (λ_{ex} = 350 nm, λ_{em} = 488 nm)

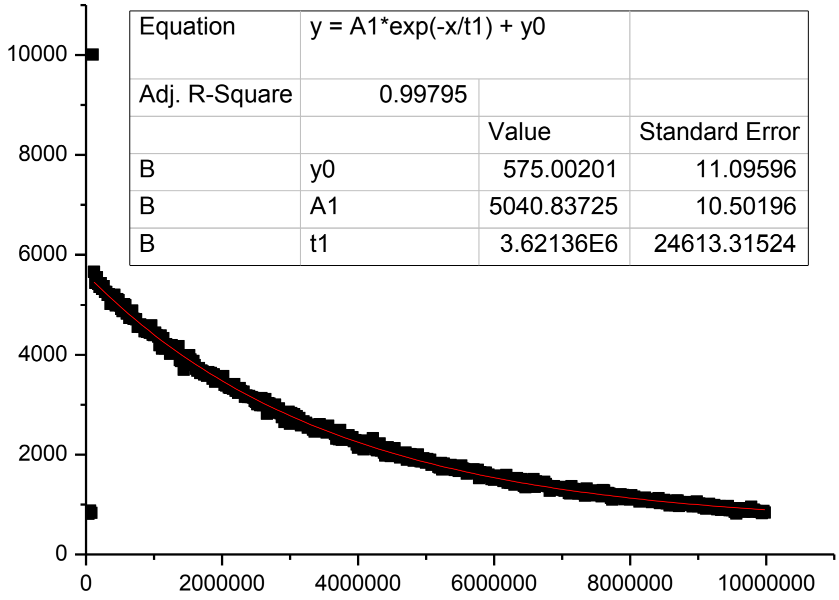

Equation	y = A1*exp(-x/t1) + y0		
Adj. R-Square	0.99795		
		Value	Standard Error
B	y0	575.00201	11.09596
B	A1	5040.83725	10.50196
B	t1	3.62136E6	24613.31524

Figure 4. 40 Decay curve of emission lifetime of GdL3 at 77 K (λ_{ex} = 350 nm, λ_{em} = 522 nm)

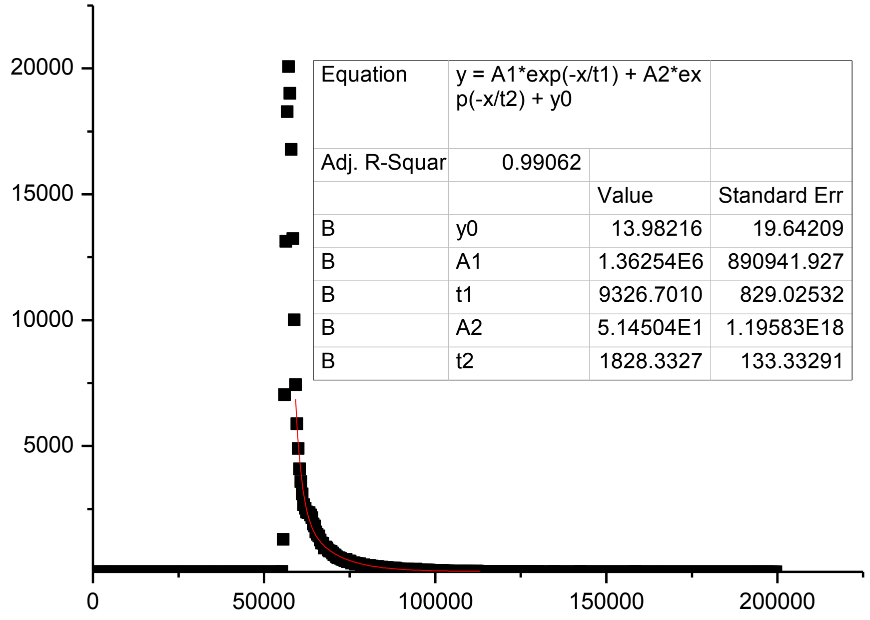

Equation	y = A1*exp(-x/t1) + A2*ex p(-x/t2) + y0		
Adj. R-Squar	0.99062		
		Value	Standard Err
B	y0	13.98216	19.64209
B	A1	1.36254E6	890941.927
B	t1	9326.7010	829.02532
B	A2	5.14504E1	1.19583E18
B	t2	1828.3327	133.33291

Figure 4. 41 Decay curve of emission lifetime of GdL3 at 77 K (λ_{ex} = 390 nm, λ_{em} = 400 nm)

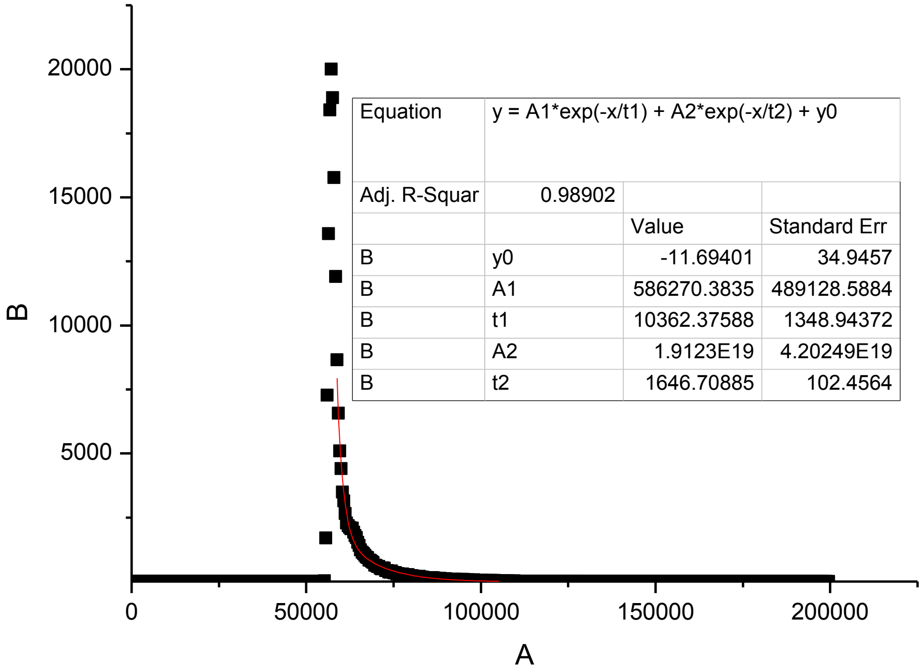

Equation	y = A1*exp(-x/t1) + A2*exp(-x/t2) + y0		
Adj. R-Squar	0.98902		
		Value	Standard Err
B	y0	-11.69401	34.9457
B	A1	586270.3835	489128.5884
B	t1	10362.37588	1348.94372
B	A2	1.9123E19	4.20249E19
B	t2	1646.70885	102.4564

Figure 4. 42 Decay curve of emission lifetime of GdL3 at 77 K (λ_{ex} = 390 nm, λ_{em} = 422 nm)

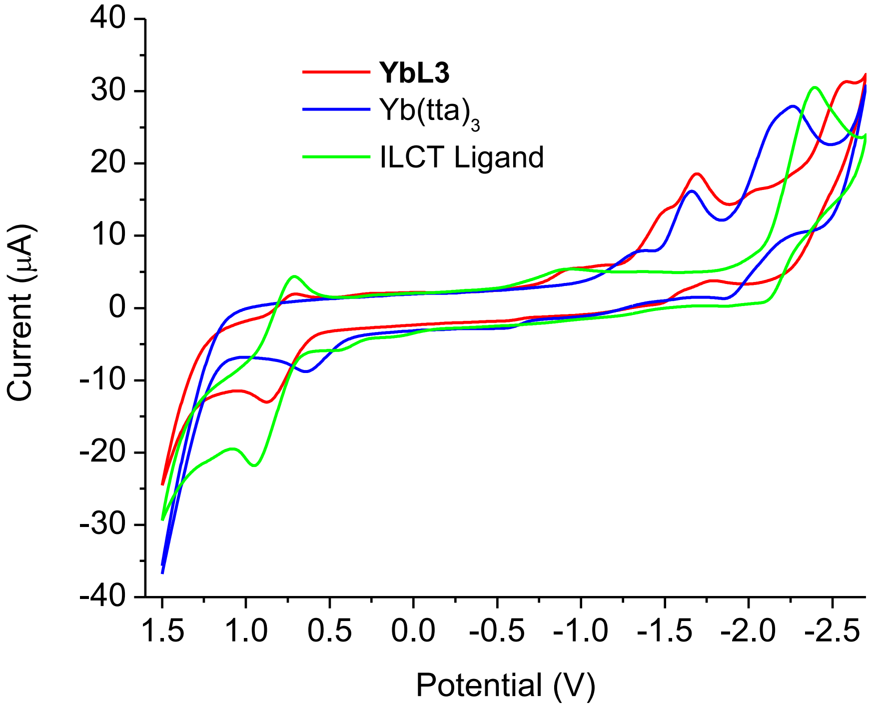

Figure 4. 43 Cyclic voltammagram of YbL3, Yb(tta)$_3$ and free ligand with ILCT character

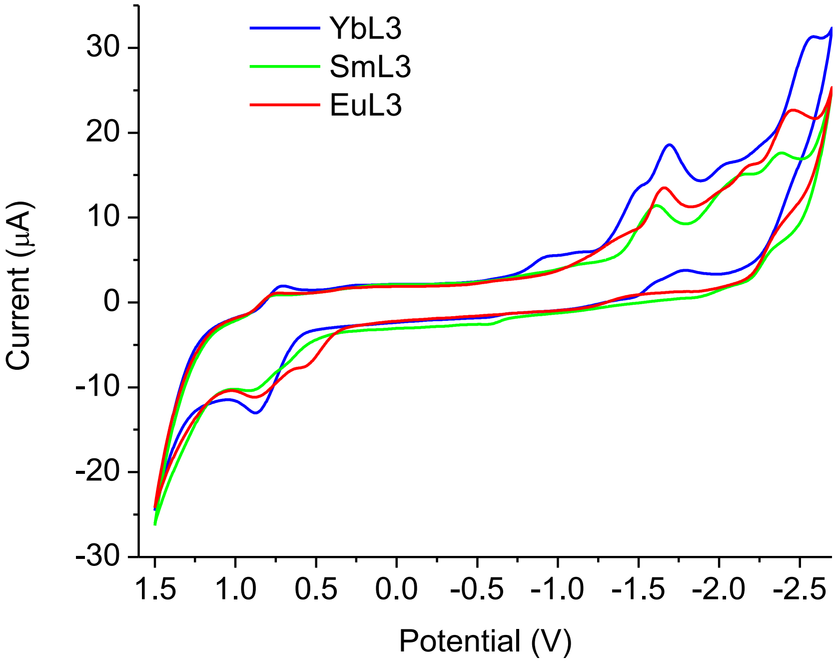

Figure 4. 44 Cyclic voltammagram of YbL3, SmL3, EuL3

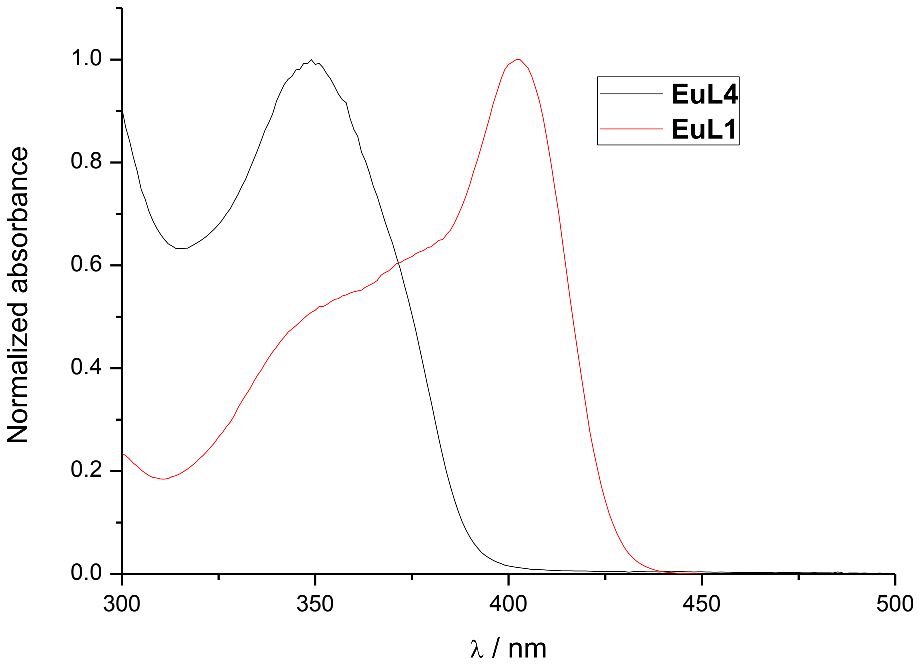

Figure 4. 45 Absorption spectra of EuL4 and EuL1 in toluene

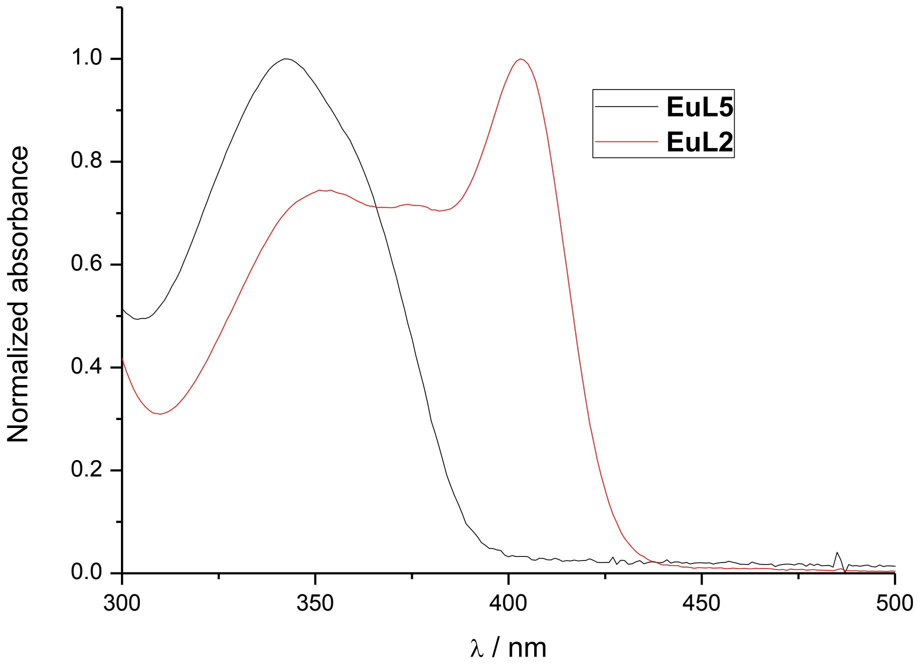

Figure 4. 46 Absorption spectra of EuL5 and EuL2 in toluene

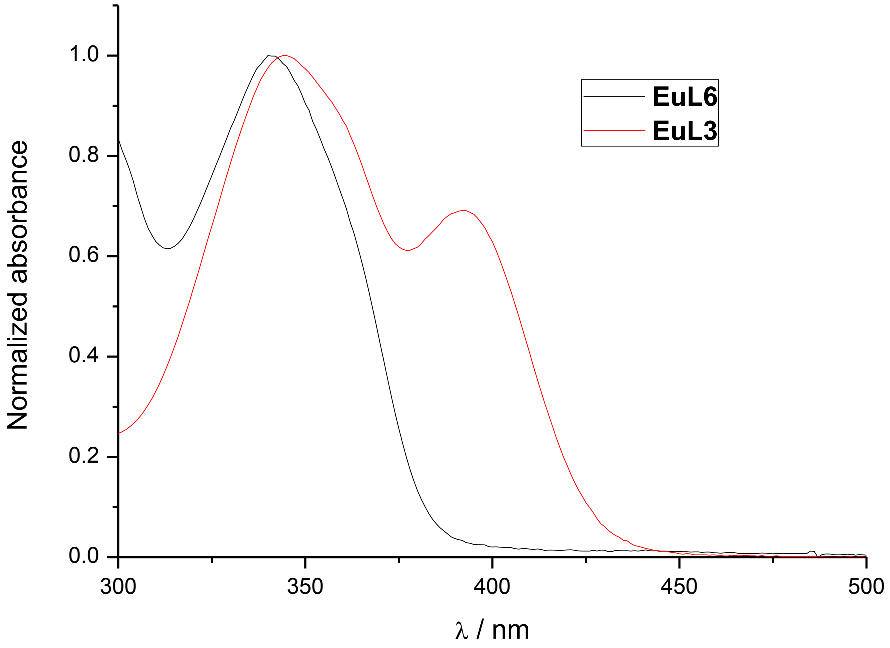

Figure 4. 47 Absorption spectra of EuL6 and EuL3 in toluene

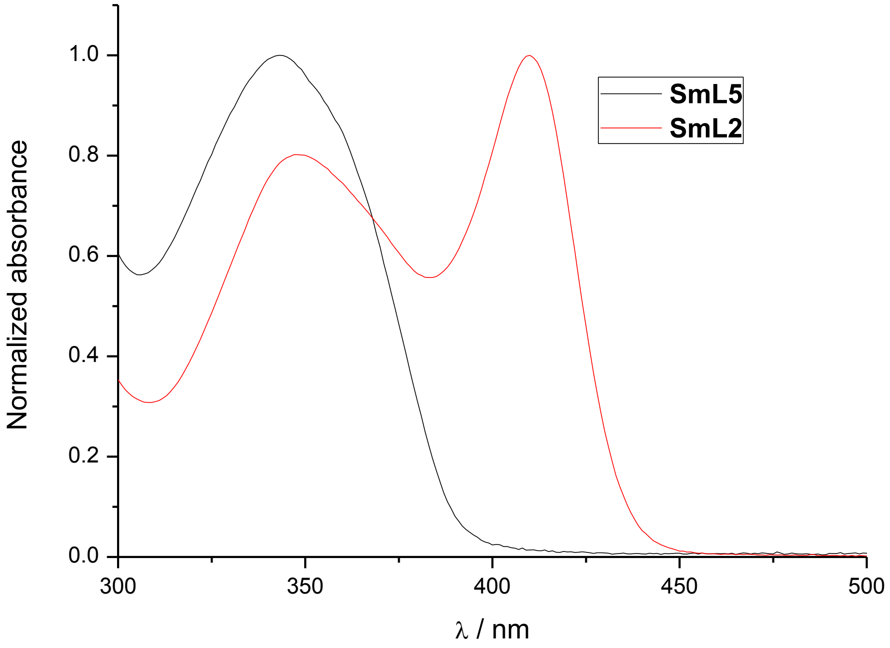

Figure 4. 48 Absorption spectra of SmL5 and SmL2 in toluene

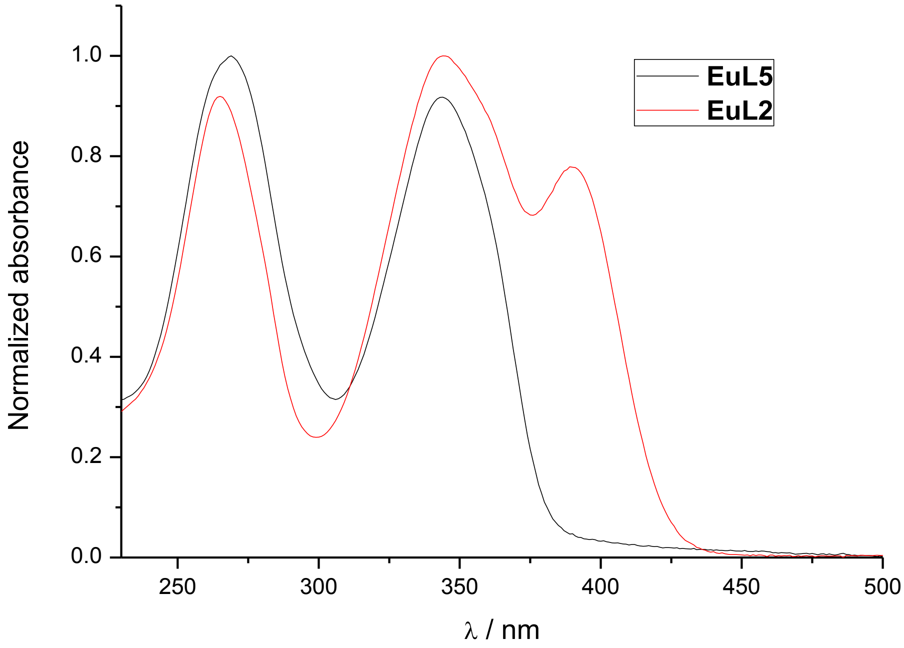

Figure 4. 49 Absorption spectra of EuL5 and EuL2 in methanol

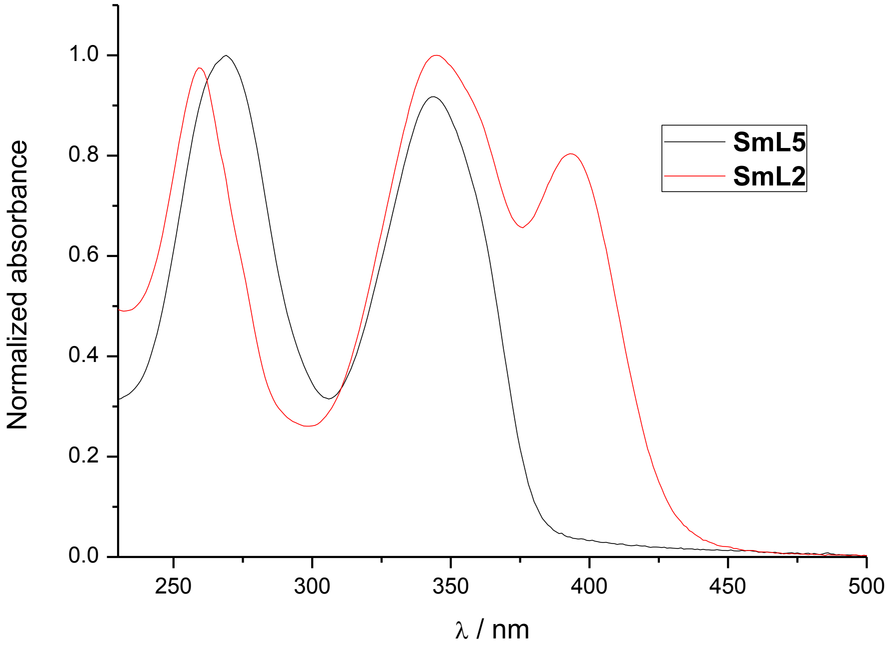

Figure 4. 50 Absorption spectra of SmL5 and SmL2 in methanol

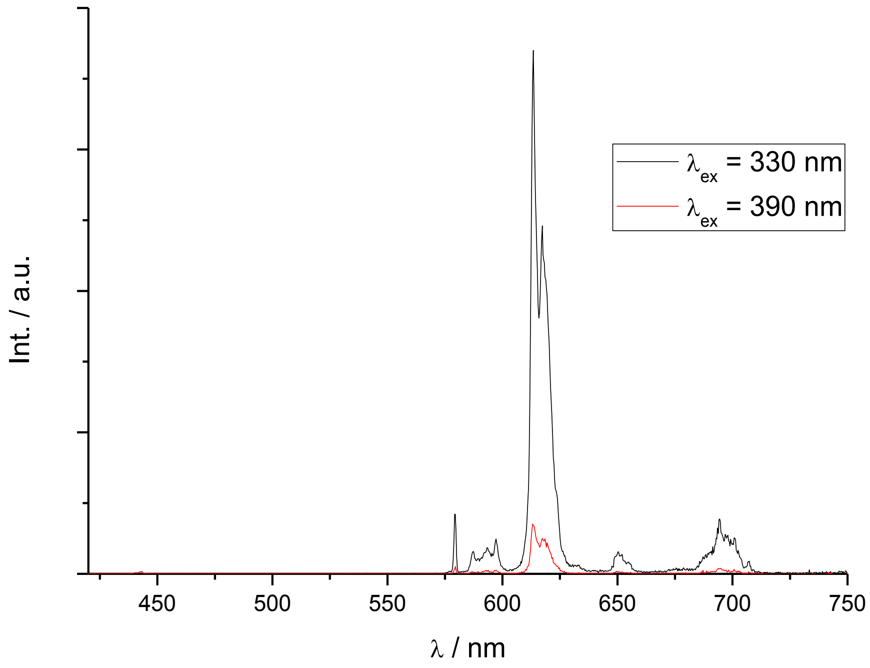

Figure 4. 51 Emission spectra of EuL4 in toluene at different excitations

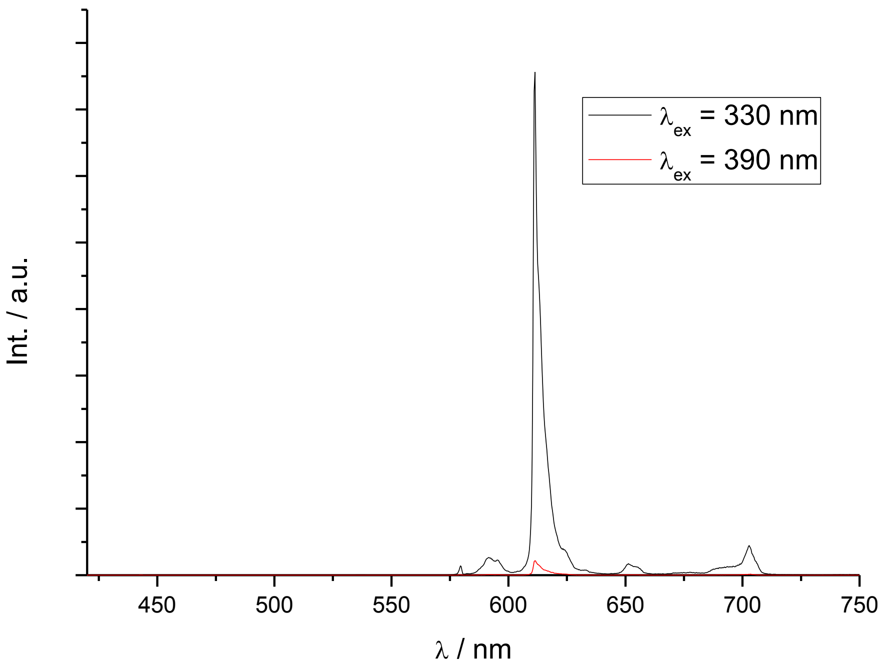

Figure 4. 52 Emission spectra of EuL6 in toluene at different excitations

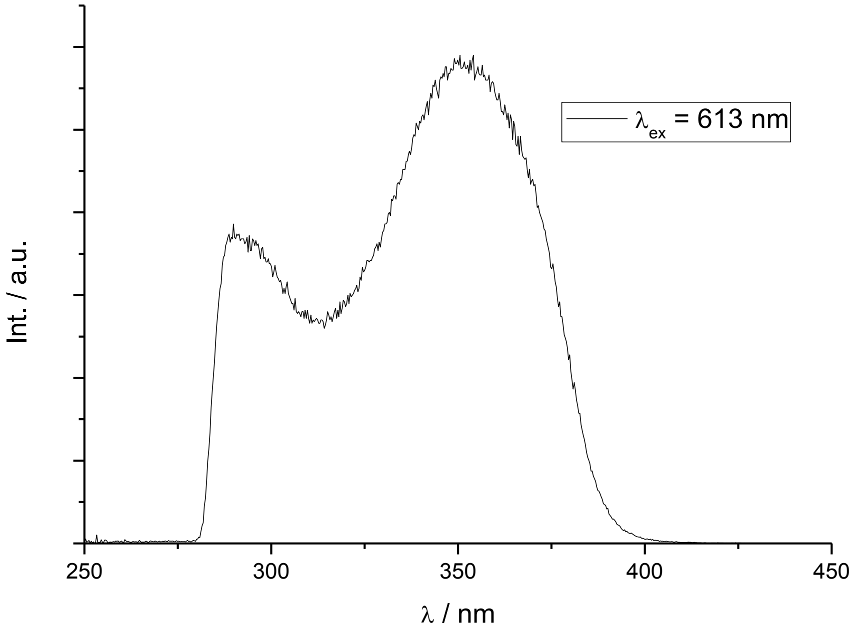

Figure 4. 53 Excitation spectrum of EuL4 in toluene

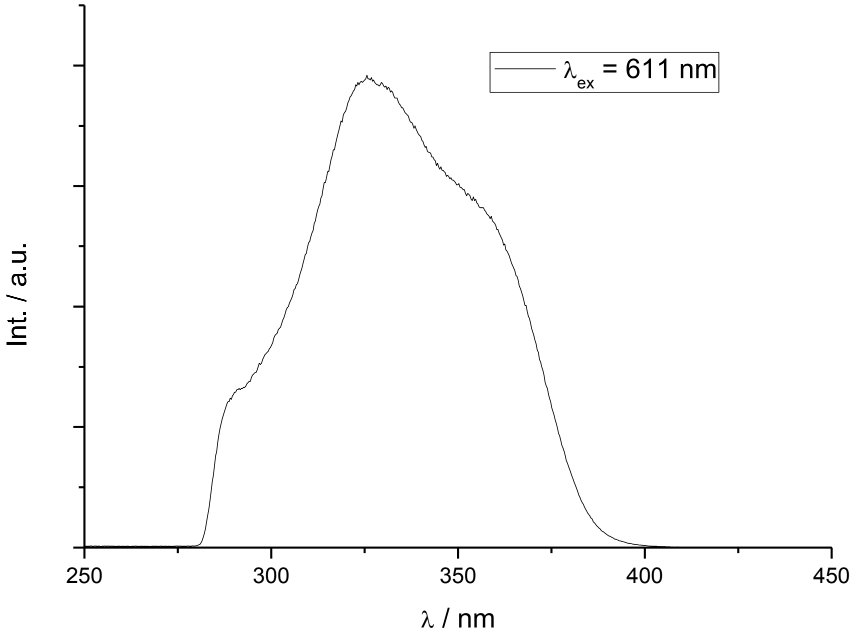

Figure 4. 54 Excitation spectrum of EuL6 in toluene

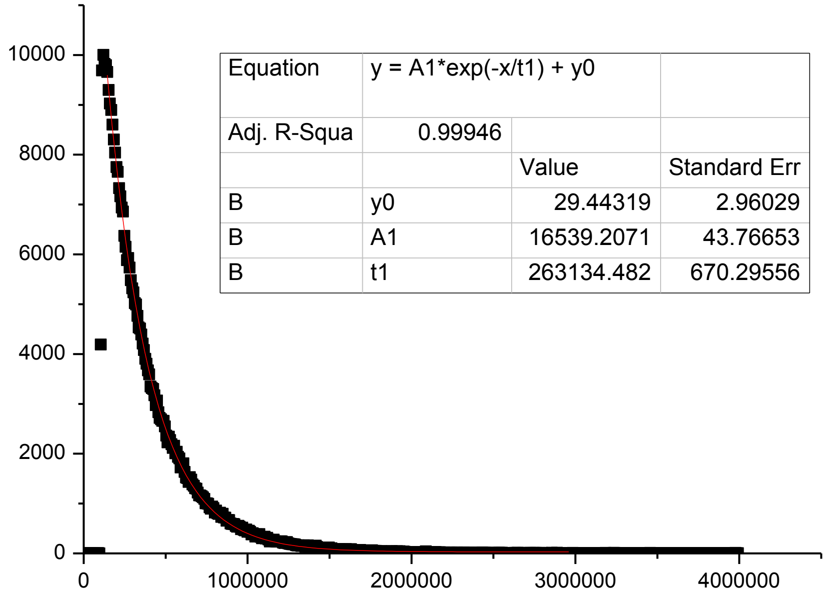

Equation	y = A1*exp(-x/t1) + y0		
Adj. R-Squa	0.99946		
		Value	Standard Err
B	y0	29.44319	2.96029
B	A1	16539.2071	43.76653
B	t1	263134.482	670.29556

Figure 4. 55 Decay curve of luminescence lifetime of EuL5 in methanol

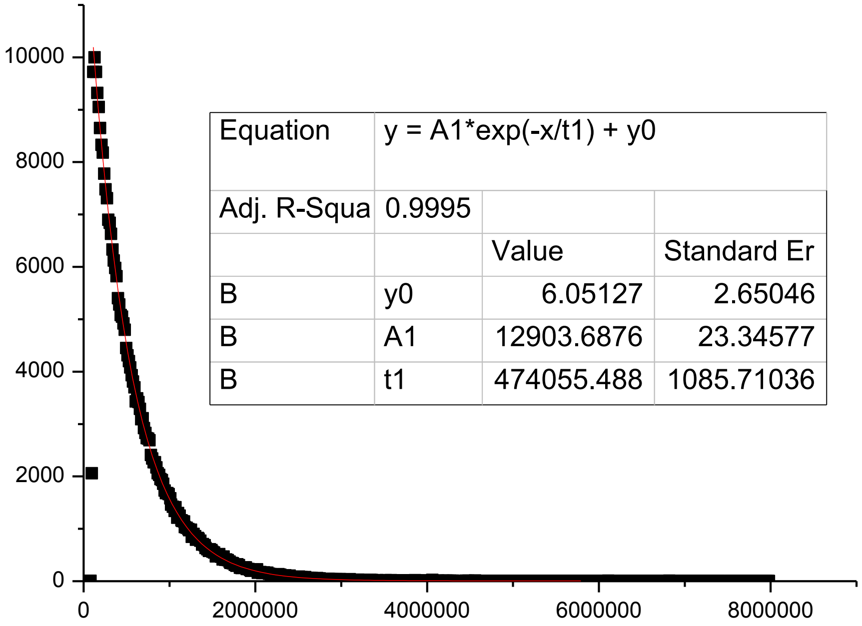

Equation	y = A1*exp(-x/t1) + y0		
Adj. R-Squa	0.9995		
		Value	Standard Er
B	y0	6.05127	2.65046
B	A1	12903.6876	23.34577
B	t1	474055.488	1085.71036

Figure 4. 56 Decay curve of luminescence lifetime of EuL5 in methanol-d_4

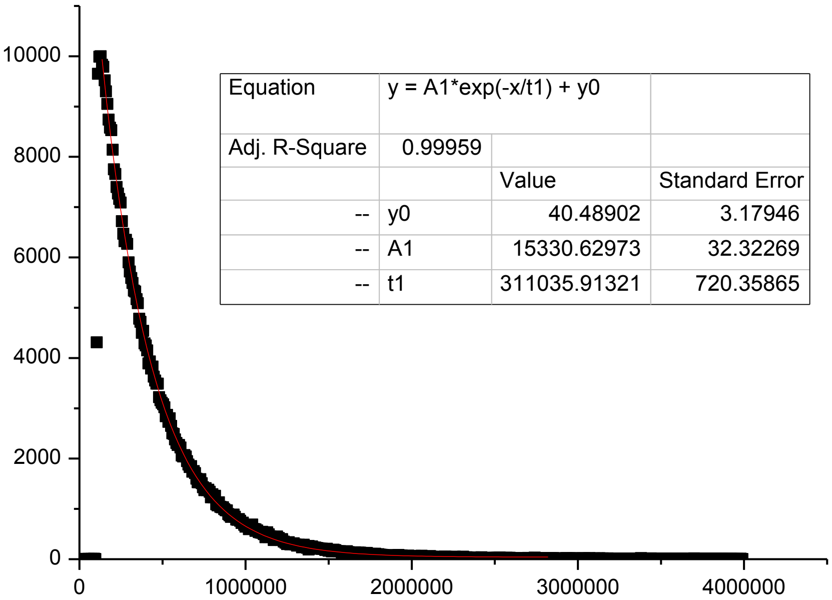

Equation	y = A1*exp(-x/t1) + y0		
Adj. R-Square	0.99959		
		Value	Standard Error
--	y0	40.48902	3.17946
--	A1	15330.62973	32.32269
--	t1	311035.91321	720.35865

Figure 4. 57 Decay curve of luminescence lifetime of EuL5 in toluene

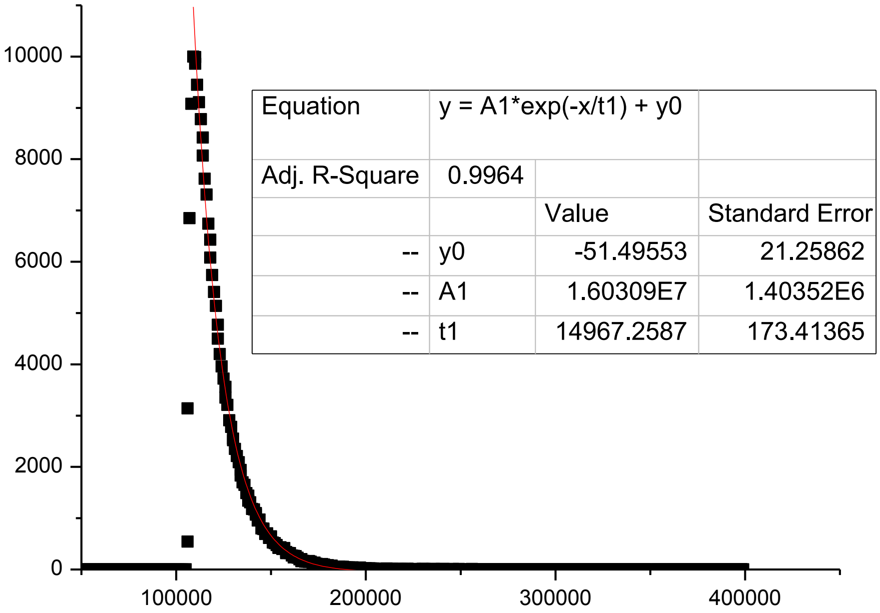

Equation	y = A1*exp(-x/t1) + y0		
Adj. R-Square	0.9964		
		Value	Standard Error
--	y0	-51.49553	21.25862
--	A1	1.60309E7	1.40352E6
--	t1	14967.2587	173.41365

Figure 4. 58 Decay curve of luminescence lifetime of SmL5 in methanol

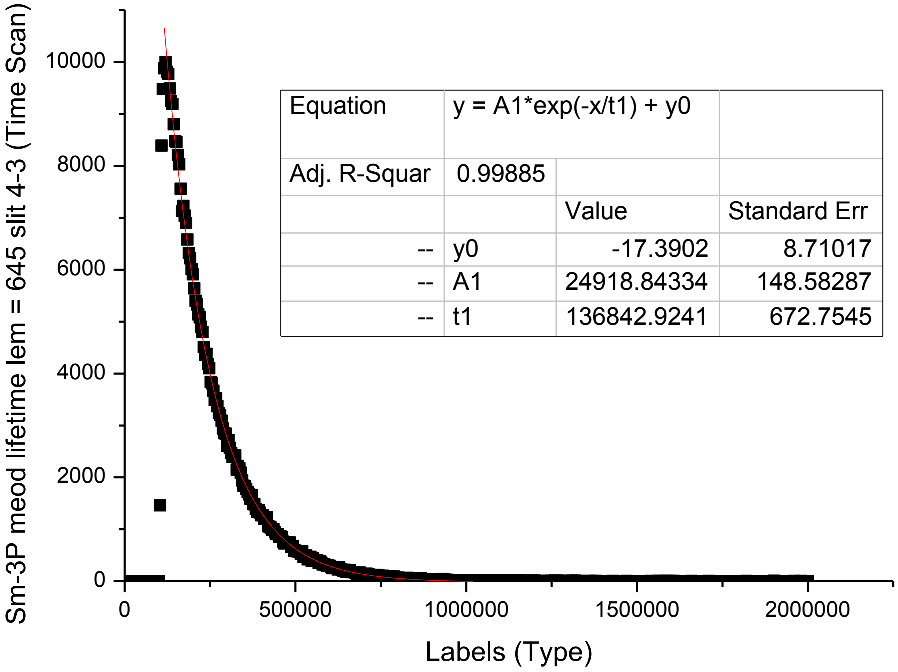

Equation	y = A1*exp(-x/t1) + y0		
Adj. R-Squar	0.99885		
		Value	Standard Err
--	y0	-17.3902	8.71017
--	A1	24918.84334	148.58287
--	t1	136842.9241	672.7545

Figure 4. 59 Decay curve of luminescence lifetime of SmL5 in methanol-d_4

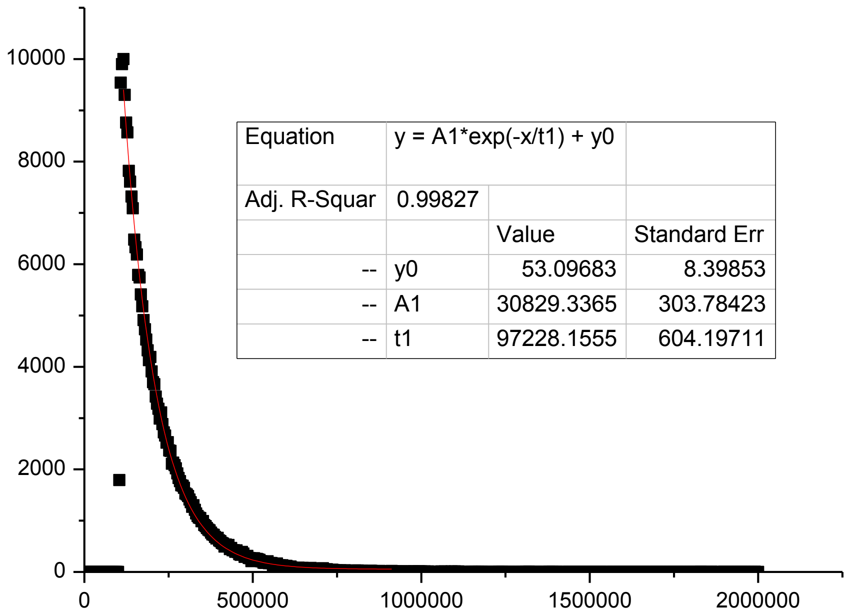

Equation	y = A1*exp(-x/t1) + y0		
Adj. R-Squar	0.99827		
		Value	Standard Err
--	y0	53.09683	8.39853
--	A1	30829.3365	303.78423
--	t1	97228.1555	604.19711

Figure 4. 60 Decay curve of luminescence lifetime of SmL5 in toluene

5. Synthesis of Multidentate Water-Soluble Pockets with Intraligand Charge Transfer Character for Sensitization of Lanthanide(III) Luminescence

5.1. Introduction and Design Rationale

Sensitization of Eu(III), Sm(III) and Yb(III) luminescence with good quantum yields was demonstrated in the previous chapters by a series of detailed photophysical measurements in a wide range of solvents. Nevertheless, to improve the scope of potential applications of these complexes beyond non-polar organic solvents and gel- or solid-based materials, the water-solubility must be improved. Neither the ligand, Ln(tta)$_3$ nor the complex are soluble in water; implying significant modifications have to be made in order to alter its solvation properties.

Moreover, as the complexes are vulnerable towards solvent coordination, a concurrent dilemma surfaces in protecting the Ln(III) center from the highly-quenching water molecules while improving the overall water-solubility. The increased stability would allow the complexes to retain the highly efficient luminescence *via* ILCT sensitization and be used in biological applications such as optical imaging, especially with Sm(III) and Yb(III) that are capable of emitting in the NIR region where skin tissues are more transparent.[136]

The incorporation of anionic hard donors have proved to be an effective strategy in providing strong chelation and water solubility. MRI contrast agents in clinical use are cyclen-based Gd(III) complexes and many cyclen-based Ln(III) complexes are developed as optical imaging agents, all down to the presence of carboxylic acid arms on the macrocycle. The direct incorporation of carboxylic acid substituents onto chromophoric ligands are also common. Some ligand designs could be found in Chapter 1 and detailed reviews are recommended.[43,44,137,138]

Figure 5.1 shows two examples (**1**, **2**) of chelates with ILCT character by Maury's group[87,139] for sensitization of Ln(III) luminescence. The carboxylic acid groups on the dipicolinic acid and DTPA derivatives are good chelators and increase the overall polarity of the ligand, enhancing its and the complexes' water-solubility. The polyethylene glycol (PEG) pendant were used to 'ensure' solubility in water. **3** is one of the examples in a library of ligands researched by Charbonnière and his co-workers[140] with ILCT sensitization of water-soluble Ln(III) complexes.

The new design of the water-soluble multidentate pockets takes reference to the design of ligand **3** in which the carboxylic groups are extended from the pyrazoles. Further modifications will be introduced by replacing the carboxylic acid arms with phosphonic acids to investigate the effects on photophysical properties of different coordination strength, as energy transfer is distance-dependent and is directly affected by ligand-lanthanide interaction.

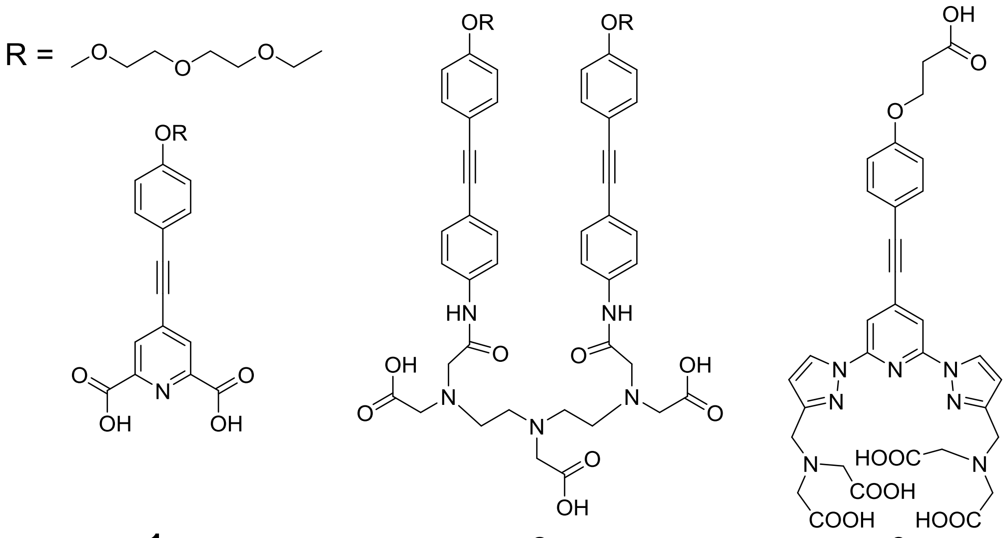

1 2 3

Figure 5. 1 Multidentate chelates with ILCT character

5.2. Results and Discussion

Syntheses of Multidentate Pockets

The general synthetic strategy is to introduce a good leaving group extended from the pyrazole for undergoing nucleophilic substitution with an iminodiacetic acid ester. Direct bromination was tried with **WSL007** with the radical-mediated *N*-bromosuccinimide (NBS) reaction (Scheme 5.1). The use of azo-*bis*-isobutyronitrile (AIBN) or benzoyl peroxide as radical initiator gave the same results in which the starting material was consumed by the desired product **WSL026** was not obtained. ^{1}H NMR spectroscopy revealed that the methyl protons of the 3-methylpyrazole was still present but one of the protons in the aromatic region – consisting of protons from both the pyrazolyl and phenyl moieties – was missing. Literature research[141] revealed that **WSL027** was formed instead, as the π-electron and total electron (π + σ) densities are highest at the 4-position, implying it’s the most favorable position for electrophilic attack by NBS. This synthetic route, therefore, should be abandoned.

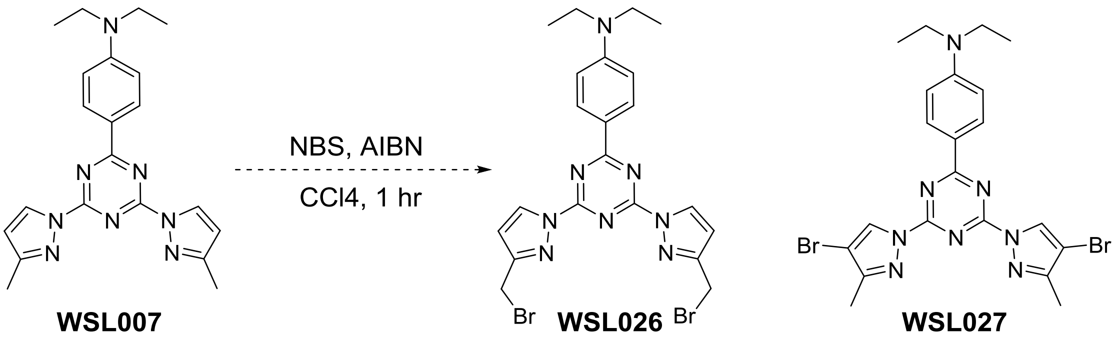

Scheme 5. 1 Synthetic scheme of WSL026 using radical-mediate NBS substitution

An alternative synthetic route was devised with the main idea of producing a hydroxyl group on the peripheral for further bromination (Scheme 5.2). 3-methylpyrazole was first oxidized to become 1*H*-pyrazole-3-carboxylic acid, followed by esterification with ethanol to produce the corresponding ethyl ester **WSL029**. The ester will be reserved for reduction to give the desired hydroxyl group after incorporation to the triazine-core with or without the ILCT moiety to prevent the hydroxyl group being deprotonated and result in intermolecular nucleophilic attacks. Sodium hydride was used as a base to abstract the pyrazolyl proton to yield the nucleophile for subsequent attack onto the chlorine atom of triazine at room temperature. No major difficulties were encountered in the syntheses of **WSL030-31**.

Reduction of the ester would be able to give a hydroxylmethyl group at the peripheral for further modifications into a good leaving group. The reduction was carried out with commonly used lithium aluminum hydride in tetrahydrofuran at 0 °C and, without purifying the crude,[142] bromination by phosphorous pentabromide followed.

However, there were various spots of similar polarity (but markedly different from the starting material) in the reaction crude and, when **WSL030** was used, the major spots were not yellow, as the ILCT moiety should impart yellow color to the compound.

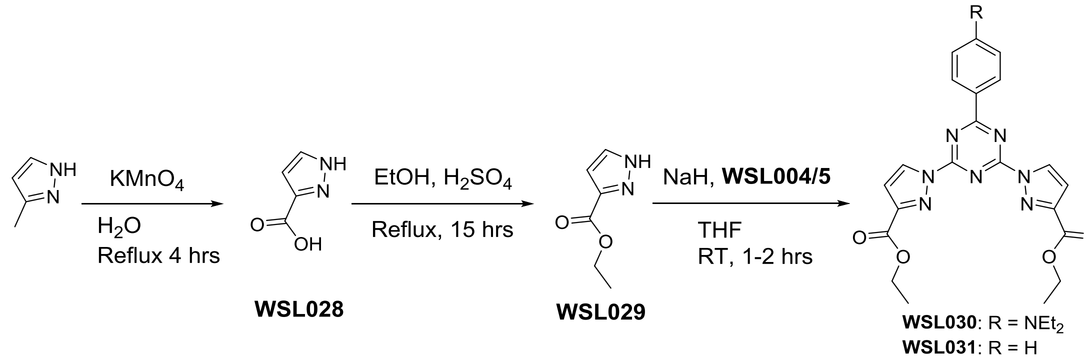

Scheme 5. 2 Synthesis of WSL030-31 *via* oxidation of 3-methylpyrazole

While phosphorous pentabromide itself is highly reactive, it is believed that the compound should be stable in its presence. The obstacle is suspected to be the reduction step. Lithium aluminum hydride is a strongly basic reagent and may be destructive towards the substrate. The C-N bond between the triazine and the pyrazole moieties is rather weak and the strongly basic hydride ion may have cleaved the bond and caused the compound to decompose even at 0 °C. The ^{1}H NMR spectrum of the crude no longer had any ethyl protons from the ester, but it also gave a messy TLC chromatogram, which corroborated with the suspicion of producing various side-products.

It has become clear that the reduction step should precede the incorporation of the pyrazolyl part into the triazine skeleton, hence it also meant the functionalization of the pyrazole, including the incorporation of the carboxylic acid arms should be performed beforehand. A new synthetic scheme was devised and presented in Scheme 5.4.

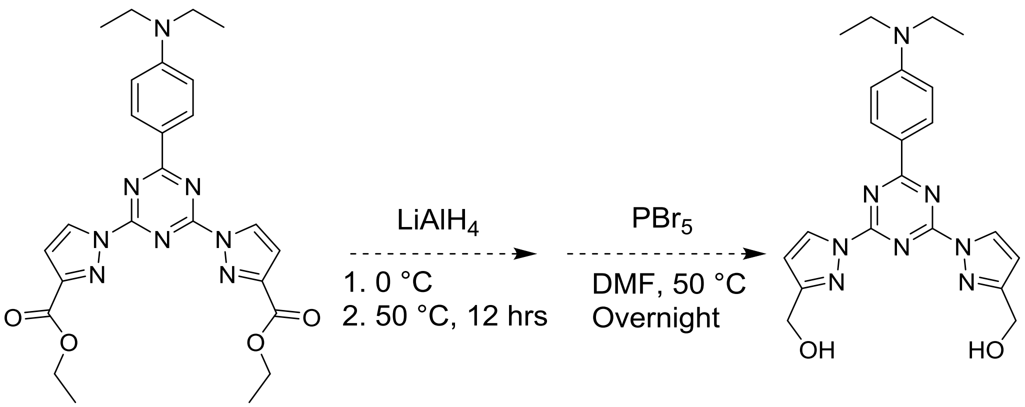

WSL030

WSL032

Scheme 5. 3 Failed synthesis of WSL032

3-Methylpyrazole was oxidized by potassium permanganate in refluxing water. The reaction yield is primarily dependent on the slow addition of aqueous potassium permanganate into 3-methylpyrazole (optimized rate of approx. 1 mL / min). As the product was recrystallized after tuning the pH to an acidic environment, concentrated hydrochloric acid should be used to minimize the amount of water introduced in order to minimize interference to the recrystallization process. The carboxylic acid was either directly reduced to give **WSL033** or *via* **WSL029** to give a higher yield. The reduction could be carried out by using either lithium aluminum hydride or borane dimethyl sulfide complex. The former requires a delicate Fieser workup treatment due to the formation of aluminate but is relatively less hazardous, and odorless compared to the latter. If LAH was used, the oily product was obtained by washing the treated crude multiple times with tetrahydrofuran and evaporating the solvent whereas if borane was used, **WSL033** was recovered in the form of its HCl salt by solvent-solvent extraction of water and dichloromethane in which the aqueous part was evaporated followed by recrystallization.

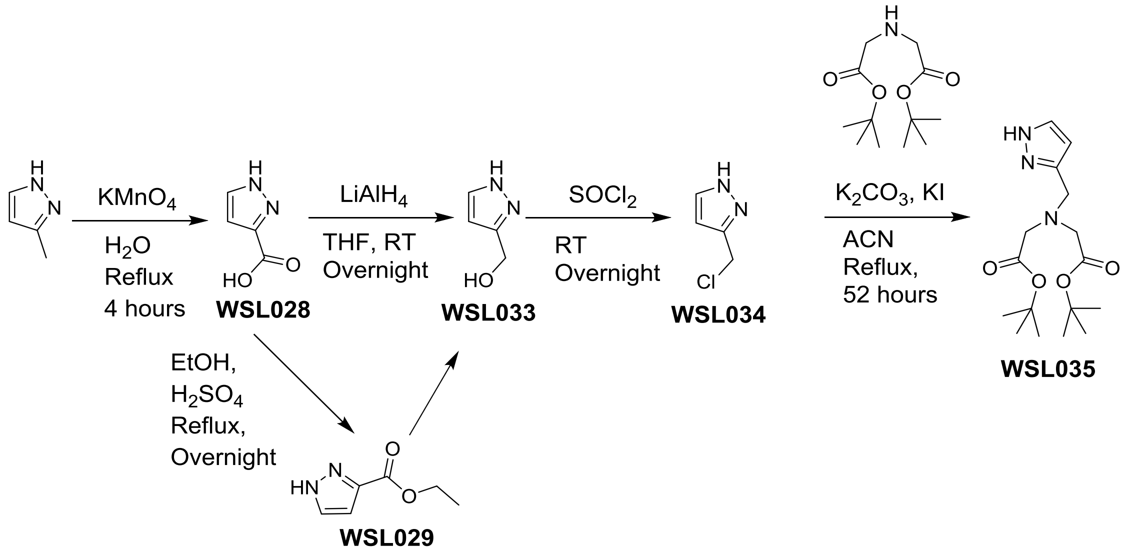

Scheme 5. 4 Multiple syntheses of WSL035 *via* WSL028

WSL033 is extremely hygroscopic and it was either stored in a dry cabinet or used immediately in the chlorination experiment – chlorination was chosen over bromination as literature procedures were available. **WSL034** was synthesized by reacting with thionyl chloride under a dry and inert atmosphere overnight (> 15 hours) in very good yields. The product may appear to be slightly beige due to sulfur contamination but the ^{1}H spectrum was not affected. Purification is not necessary as sulfur poses insignificant interference towards the next coupling reaction.

Commercially available di-tert-butyl-iminodiacetate was used to react with **WSL034** in a nucleophilic substitution reaction. The iminodiacetate protected with tert-butyl groups was chosen over the ethyl-protected one as it is believed that the triazine-pyrazole C-N bond and the molecule as a whole is more tolerable towards strong acids than strong bases. Deprotection of the ethyl group requires strong bases while tert-butyl groups can be deprotected by trifluoroacetic acid. The reaction was performed in acetonitrile with potassium carbonate as base – similar to various amine alkylation reactions. After refluxing for 52 hours, though, the yield of the desired product (**WSL035**) was low and mass spectrum results showed that over-alkylation occurred.

Over-alkylation may occur if the product formed (**WSL035**) is more reactive than the starting material. While it is not possible to alter the reactivity of the product, the reactivity of the starting material (**WSL033**) could be increased by adopting the Finkelstein reaction – a halogen substitution reaction – prior to alkylation. The addition of catalytic amount of sodium iodide would lead to the replacement of the chlorine on **WSL034** by an S_N2 reaction with an iodine group, which is a very good leaving group. The reactivity of **WSL034-I** is then increased and will compete more favorable with over-alkylation. The extremely low solubility[143] of sodium chloride (0.003 g/1 kg solvent) in acetonitrile compared to sodium iodide (24.9 g/1 kg solvent) makes it easy to be removed by filtration after the reaction. The increase in reactivity was evidenced by a much shorter reaction time (overnight), a substantially higher yield and much less over-alkylation.

The functionalized pyrazole **WSL035** was then incorporated into the triazine core using similar experimental conditions for **WSL029**. **WSL035** was deprotonated with sodium hydride in acetonitrile due to its relatively poor solubility in tetrahydrofuran. After reacting for overnight, the triazine core was consumed but the product had very similar polarity with **WSL035**, rendering purification rather difficult and thus a low yield. Nevertheless, the desired products **WSL035-7**, protected esters, were obtained. The tert-butyl groups were then deprotected by excess trifluoroacetic acid in dichloromethane quantitatively. The crudes of **WSL038-9**, with the presence of the free carboxylic acid arms, were soluble in water and methanol and became insoluble in dichloromethane or chloroform. Purification by normal-phase column chromatography could not be performed and the products were finally purified by reversed-phase HPLC. The purification was not ideal, though, as only ~ 85 % of purity of the products were obtained.

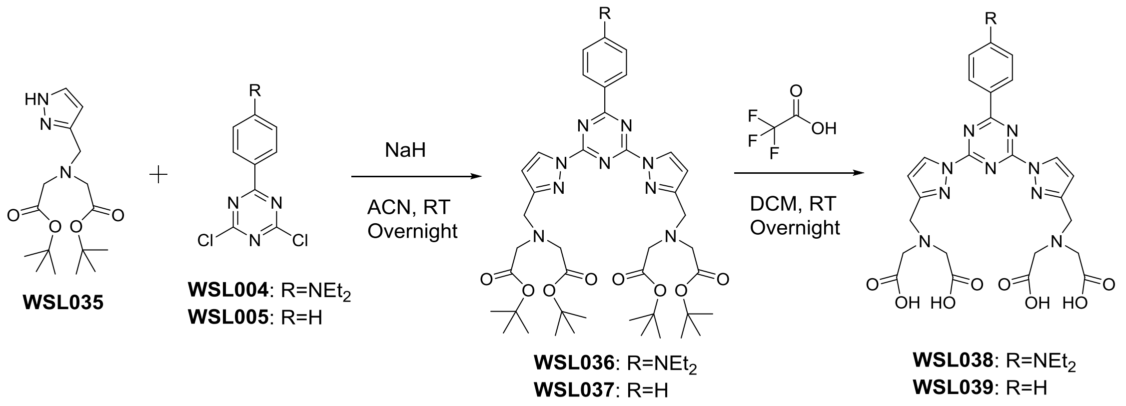

Scheme 5. 5 Syntheses of WSL038 and WSL039

The ligands were tried to complex with Ln(III) in methanol using pyridine as base to tune the pH ≈ 6 and heated at 60 °C. However, no observations pointed to complexation were recorded: unable to observe the mother peak in mass spectrometry, the UV-vis spectrum before and after complexation were the same, and there were no Eu(III) luminescence under a hand-held UV lamp (365 nm excitation) or excited by a spectrophotometer. The complexation conditions were modified for several times, including using a mixed solvent system with methanol and water, tuning the pH to 7, leaving out the base and altering the temperature. Eventually, the 1:1 Eu(III) complex, **EuWSL039**, was successfully obtained in refluxing methanolic solution using trimethylamine as base. Complex formation was verified by mass spectrometry and luminescence under a hand-held UV lamp. Due to the minute amounts of ligands available and various trials in complexation conditions, only **WSL039** was sufficient for lanthanide(III) complexation in the end.

Syntheses of Alternative Side-Arms

As mentioned above, this project would also like to look into the effect of having chelates of different donor strength. A DO3A-based Gd(III) complex with a phosphonic acid substituted at the fourth N atom is known to have higher relaxivity than the Gd-DOTA, due to the greater steric demand[144,145] it poses compared to carboxylic acids. It has also been demonstrated that phosphonate-containing Ln(III) complexes have better protection of the first coordination[145-149] sphere but increases the number of water molecules in the second coordination sphere.

For luminescence studies, Parker's group[150-152] have designed several phosphinate-containing ligand systems for sensitizing Ln(III) luminescence and found that the steric bulkiness of phosphonates minimizes solvent quenching processes. Phosphinate ($H_2PO(OH)$) is a sister compound of phosphonate ($HPO(OH)_2$). Both have a P=O bond but the former only has one P-O bond whereas the latter has two. When deprotonated, phosphonates would have three oxygen atoms available for coordination – one more than phosphinates – hence phosphonates are chosen as a candidate for comparison with carboxylate chelates.

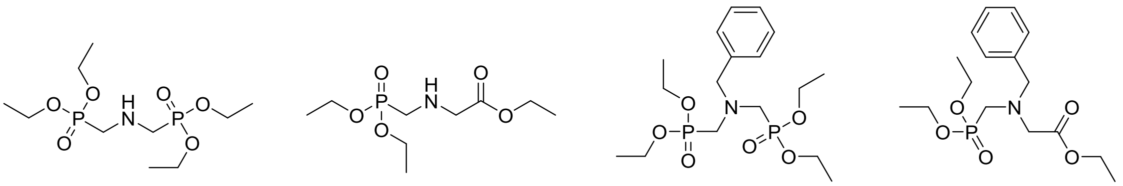

WSL040 **WSL041** **WSL042** **WSL043**

Figure 5. 2 Starting materials for alternative side-arms

WSL040 and **WSL041** are alternatives to di-tert-butyl-iminodiacetate to coordination onto the pyrazole. **WSL042** and **WSL043** are the respective benzyl-protected precursors in which the syntheses will be discussed.

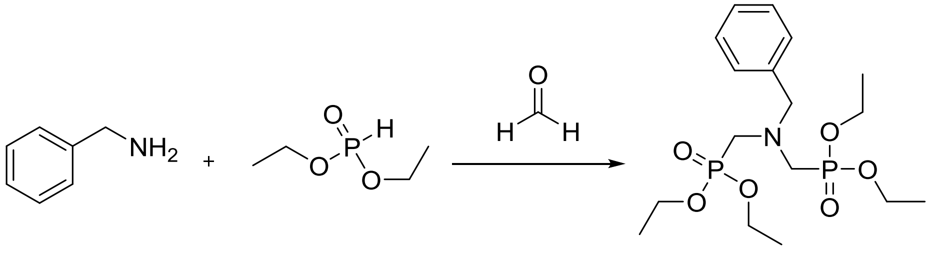

WSL042

Scheme 5. 6 Synthesis of WSL042

Commercially available benzylamine, diethyl phosphite and formaldehyde were reacted in a double-Kabachnik-Fields[153-155] reaction to produce an α-aminophosphonic acid. It was reviewed[156] that the reaction involves the formation of an imine (**3**) from the condensation of carbonyl compound (**1**) and the primary amine. The dialkyl phosphite is then added to the imine unit to yield the α-aminophosphonate product (**4**). It was also suggested that the addition of the dialkyl phosphite to the carbonyl compound (**1**) yields an α-hydroxyphosphonate (**5**), and subsequent substitution by the amine group would give the product. Kinetic studies revealed that the nature of the reactants determines which mechanism is more favorable. More specifically, as the dialkyl phosphite is a soft nucleophile whereas the amine is hard,[157] the imine pathway (**1→2**) is more preferable if the carbonyl compound is soft and *vice versa*.

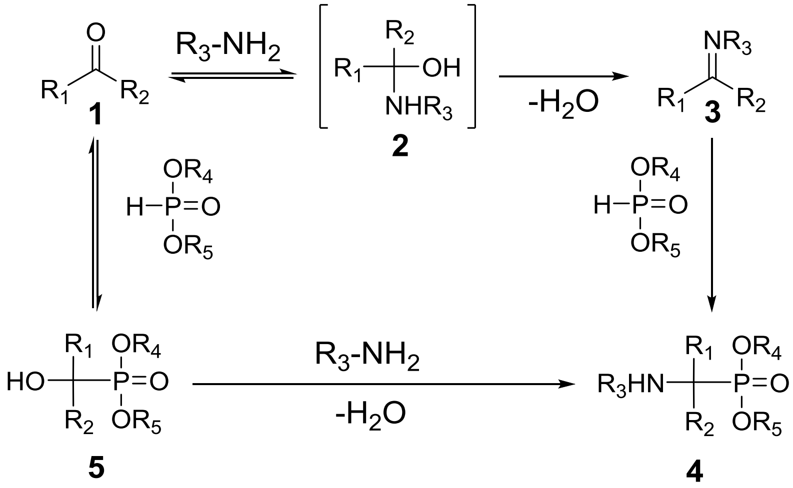

Scheme 5. 7 Possible mechanistic pathways of the Kabachnik-Fields Reaction

The reaction was carried out in equimolar quantities without additional solvent aside from the water in aqueous formaldehyde solution. Due to the presence of water, Lewis acid catalysts are not used. The yield is quite decent and purification is not necessary after evaporating excess formaldehyde and water.

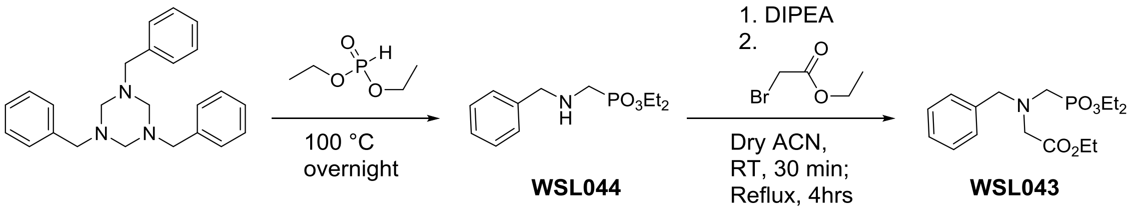

Scheme 5. 8 Synthesis of WSL043

WSL044 was synthesized by the condensation of 1,3,5-tribenzylhexahydro-1,3,5-triazine with three equivalents of diethyl phosphite at 100 °C. This reaction is different than the above Kabachnik-Fields reaction as no carbonyl compounds are involved and a tertiary amine is used. **WSL044** was synthesized in good yields and used without purification to yield **WSL043** by alkylation at the nitrogen atom with ethyl bromoacetate with diisopropylethylamine as base. Similar to general alkylation reactions, the rate of addition of ethyl bromoacetate should be carefully controlled to prevent over-alkylation.

Unfortunately, the deprotection (debenzylation) reaction for both **WSL042** and **WSL043** were not as straightforward as literature procedures, which utilized the decomposition of aqueous ammonium formate to generate hydrogen *in situ* with palladium on charcoal in refluxing ethanol. The ^{1}H NMR spectrum indicated the benzyl protecting group remained intact, despite the evolution of hydrogen being visible to the naked eye during the process.

Changing the palladium source to Pearlman's Catalyst (palladium hydroxide on charcoal) was unsuccessful. Using a hydrogen balloon in a closed system as the hydrogen source and lowering the temperature did not deprotect it at all; neither did the use of methanol instead of ethanol. Hence, it is believed that both hydrogen sources and both palladium catalysts should not be the deciding factor.

Scheme 5.9 shows the mechanism of the debenzylation reaction. The palladium(0) catalyst is involved in the oxidative addition of the benzyl group. After a dihydrogen molecule is adsorbed onto the palladium surface, the deprotected amine leaves with one hydrogen atom after rearrangement and 1 equivalent of toluene is generated by reductive elimination to regenerate the Pd(0) catalyst. The prime factor for the deprotection to proceed is to have bring the tertiary amine and hydrogen together at the palladium catalyst. The coordination ability of the tertiary amines **WSL042-3** and the generation of hydrogen is in no doubt; therefore, if the amines could not be deprotected, the deciding factor lies in whether the unprotected amine and/or hydrogen would be able to be on the palladium surface simultaneously.

The quality of the palladium catalysts used was confirmed by separate experiments and the debenzylation reaction was performed again in the presence of some acetic acid to ensure the deprotected amines would leave the palladium surface by protonating them, in case the alcoholic solvent was not sufficient.

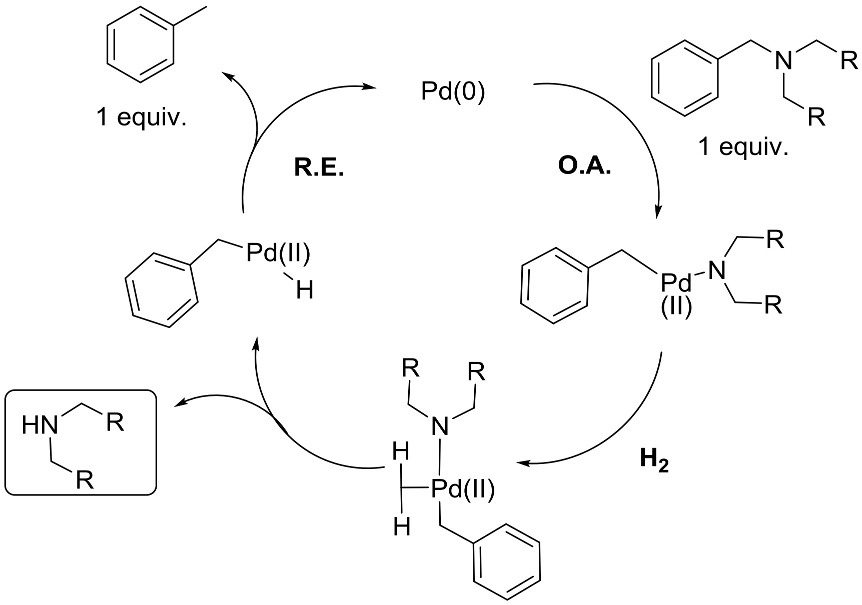

Scheme 5. 9 Mechanism of debenzylation with hydrogen and palladium catalyst

The deprotected product was finally obtained after refluxing for 48 hours in ethanol with palladium on charcoal and a hydrogen balloon, plus 1.5 equivalents of acetic acid. Excess acetic acid was used to ensure all protected amines were protonated and the surface of the palladium catalyst is free after every catalytic cycle. Nevertheless, further research in older literature reports[158-160] indicated that purification is required and crucial for the debenzylation reaction to proceed, at least for symmetric phosphonates such as **WSL042**. The amine should be purified[160] in the form of its HCl-salt but dissolving the compound in diethyl ether before precipitation by slow addition of 0.9 equivalent of HCl in diethyl ether. The debenzylation of the HCl-salt would proceed readily and the deprotected ammonium salt should be neutralized with sodium methoxide in methanol to give the free amine. Alternative neutralization means such as ammonia in chloroform would result in very fine precipitate of ammonium chloride that is hard to filter away and neutralization with aqueous bases would require exhaustive solvent-solvent extraction to recover the majority of the free amine due to its amphiphilic nature.

5.3. Conclusion and Future Work

Multidentate pockets containing ILCT character were designed and one of the compounds is synthesized. The syntheses were more problematic than expected, specifically at the C-N connection between the *s*-triazine and pyrazole moieties – due to the peculiar stability of *s*-triazine – but were resolved or circumvented by re-designing the synthetic routes. The general synthesis of the pockets are established: the chloro-functionalized pyrazole extension is ready to incorporation of various amino-side-arms and the deprotection of **WSL042** and **WSL043** was finally successful. By mixing the choice of side-arms and *N*,*N*-diethylanilinyl/phenyl moiety, the series of the multidentate ligands will be completed.

The general protocol for complexation has also been established in the synthesis of **EuWSL039**. The complex is water-soluble and luminescent under a hand-held UV lamp, giving confidence to achieving long wavelength sensitization of Ln(III) luminescence in aqueous medium, with the ILCT analog and therefore expanding the potential applications of these ILCT-based Ln(III) complexes.

The syntheses of multidentate pockets and subsequent complexation will continue in the near future, followed by detailed photophysical studies in order to elucidate more information on the ILCT sensitization mechanism which is still ambiguous with the triplet-mediated mechanism.

6. Conclusion and Future Direction

The previous chapters demonstrated the efficiency of using an intra-ligand charge transfer band to sensitize Eu(III), Sm(III) and Yb(III) luminescence. Such a non-triplet sensitization pathway was confirmed by low temperature experiments that ruled out the involvement of an intersystem crossing process. The photophysical properties of the complexes were studied in a range of solvents with different dipole moments including protic and aprotic solvents. It was found that in non-polar solvents, the luminescence intensities and quantum yields are much higher than those in polar solvents; and one ILCT moiety was able to sensitize Ln(III) luminescence better than three moieties of TTA – a well-known good antenna.

Luminescence lifetime and quantum yield studies revealed detrimental quenching effects by high energy oscillators in the proximity of the Ln(III) in solvent with coordinating properties. Protic solvents also formed hydrogen bonds to hinder energy transfer – most particularly the long range electron transfer mechanism believed to be behind the sensitization of Yb(III). Numerical analyses of the energy levels in Sm(III) and Yb(III) complexes demonstrated the inadequacy of the Energy Gap Law for predicting the extent of nonradiative quenching by nearby oscillators.

In addition to the advantage of using lower energy excitation, the work reported herein demonstrated the efficiency of using the ILCT state as an excited state donor for sensitizing Eu(III), Sm(III) and Yb(III) luminescence. As the detailed solvent studies have shown that solvent coordination, hydrogen bonding capability govern the effectiveness of sensitization, the fundamental studies could be progressed by designing and synthesizing a multidentate chelate to replace the current tridentate chelate so that the coordination of Ln(III) could be fulfilled with the same macrocyclic ligand that also offers stability (by macrocyclic effect) and better water solubility in order to achieve higher sensitization efficiencies and broadening the range of applications.

Furthermore, it is possible to tune the energy of such solvatochromic ILCT transition by varying the polarity of the medium of application or altering the structure by synthetic modifications for sensitizing other Ln(III) such as Tb(III). It is envisaged that this work could provide a platform with sufficient fundamental information to springboard the development of new chromophores sensitizing lanthanide luminescence *via* the non-triplet pathway.

7. Experimental

7.1. General Procedures

7.1.1. Reagents and Solvents

Chemicals for organic syntheses are purchased from Sigma-Aldrich, Acros, TCI and Meryer, and were used without further purification. AR grade solvents were purchased from LabScan, Anaqua Chemical Supply and Duksan. Anhydrous THF and DCM was dried over benzophenone ketyl and calcium hydride respectively. Anhydrous DMF was purchased from Acros and anhydrous diisopropylethylamine was purchased from Sigma-Aldrich. Deuterated solvents were purchased from Cambridge Isotope Laboratories and Sigma-Aldrich. Lanthanide(III) salts of 99.99 % purity or above were purchased from Sigma-Aldrich and Strem. $Eu(tta)_3{\cdot}xH_2O$ and anhydrous $Eu(tta)_3$ were purchased from Alfa Aesar. Air and moisture sensitive reactions were carried out with Schlenk line techniques under nitrogen atmosphere with glassware pre-dried at 140 ° overnight.

Fluorescence quartz cuvettes were purchased from Starna. Spectrophotometric grade (CHROMASOLV®) solvents, quinine sulfate and sulfuric acid concentrate were purchased from Sigma-Aldrich and used without further treatment unless specified. $Sm(tta)_3$ and $Yb(tta)_3$ were synthesized according to literature procedures;[81] samarium(III) chloride hexahydrate, ytterbium(III) chloride hexahydrate and 2-thenoyltrifluoroacetone were purchased from Sigma-Aldrich.

7.1.2. Chromatography

Thin-layer chromatography was carried out with silica gel F254 plates (Merck 100390) and visualized with UV irradiation (254 and 365 nm) or stained with iodine or potassium permanganate. Column chromatography was carried out with fine or coarse Davisil® silica (Grace LC60A 40 – 63 Å, 70 – 200 Å)

7.1.3. NMR Spectroscopy

^{1}H NMR and ^{13}C NMR spectra were acquired on a Bruker Advance III 400 with automated software at a frequency of 400.13 MHz at room temperature and chemical shifts were generally referenced to resonance of chloroform-d_1 at δ 7.26 and δ 77.16 ppm respectively.

7.1.4. ESI-Mass Spectrometry

Electrospray mass spectra were recorded on a Finnigan MAT LCQ with methanol as carrier solvent. HRMS were obtained from departmental staff using an Agilent 6540 UHD Accurate-Mass Q-TOF LC/MS.

7.1.5. Cyclic Voltammetry

Electrochemical study of the complexes was performed on a CHI 1030 A instrument and the electrochemical cell was of conventional design. A glassy carbon disk (3 mm diameter) was used as working electrode, a Pt wire as counter electrode and a non-aqueous Ag/AgNO3 as reference electrode. All the electrochemical experiments were performed using 0.1 M tetrabutylammonium hexafluorophosphate (TBHP) in tetrahydrofuran and the solution was purged with argon. Ferrocene (Fc) was used as the internal standard, and all potentials are referenced to the ferrocene/ferrocenium (Fc/Fc+) couple. All scans were done at 100 mVs^{-1}.

7.1.6. Optical Spectroscopy

Unless stated otherwise, photophysical measurements were average of triplicates.

UV-vis absorption spectra were recorded with an HP UV-8453 spectrophotometer. Room temperature photoluminescence measurements data obtained with 1) Edinburgh Instruments FLSP920 spectrophotometer equipped with a Xe900 continuous xenon lamp (450 W), xenon flashlamp (60 W) and a Hamamatsu R928P cooled at -20 °C (for visible emission) and 2) PTI QuantaMaster™ 50 equipped with a 75 W xenon arc lamp, double emission monochromator using 400 nm blazed 1200 lines/mm or 1200 nm blazed 600 lines/mm gratings, a Hamamatsu R928 PMT (for visible emission) and a Hamamatsu R5108 PMT (for visible and/or NIR emission), both thermoelectrically cooled. Visible emission spectra were corrected for detector responses (FLSP920 and QM50). NIR emissions of samarium(III) complexes (acquisition range up to 1050 nm) were corrected for detector responses but not for Yb(III) emissions (acquisition range up to 1200 nm) due to weak signals.

Steady state room temperature emission and excitation spectra were recorded with freshly prepared solutions of 0.1 and 0.3 absorbances at 350 nm for visible and NIR detection respectively. Measurements were prepared in the unit of absorbance instead of concentration as the relative absorbances at 350 nm are different for the complexes in different solvents due to the ILCT character. The concentrations at 0.1 and 0.3 absorbances could be estimated to be *ca.* 1.4 to 1.8 μM and 4.3 to 5.4 μM respectively.

The same sample solution was used for both acquisitions. Emission and excitation slits were kept constant in acquisitions used for comparison amongst solvents and excitation wavelength. Longpass filters were used to prevent the second order of the excitation light from interfering the emission and excitation spectra.

7.1.7. Lifetime Measurements

Room temperature luminescence lifetimes of visible emissions were acquired with FLSP290 (stop condition 10000 counts) and the decay curve was fitted with Origin 8:

Monoexponential fit: $y = y_0 + Ae^{-x/t}$

Bi-exponential fit: $y = y_0 + A_1e^{-x/t} + A_2e^{-x/t}$

7.1.8. Quantum Yield Measurements

Relative quantum yields were determined relative[99] to quinine sulfate in 0.1 M sulfuric acid (λ_{ex} = 350 nm, Φ = 0.577) for visible emission and Yb(tta)$_3$ in toluene (λ_{ex} = 340 nm, Φ = 0.35 %) for NIR emissions. These standards were chosen as the excitation and emission wavelengths match well with our samples.

Absolute quantum yields were measured using an integrating sphere from Edinburgh Instruments and the quantum yield values were calculated using the F900 software.

7.1.9. Cryogenic Measurements

Low temperature (77 K) measurements were measured on FLSP920 using an EPR dewar from Edinburgh Instruments. Samples were dissolved in 2-methyltetrahydrofuran (Sigma-Aldrich) and transferred to an EPR Quartz sample tube and cooled with liquid nitrogen. Spectra were recorded at 30-minute intervals to ensure the sample is complete cooled – comparing emission intensities and band profiles.

7.2. Syntheses

2-chloro-4,6-bis(3,5-dimethyl-1H-pyrazol-1-yl)-1,3,5-triazine (**WSL001**)
2-chloro-4,6-bis(3-methyl-1H-pyrazol-1-yl)-1,3,5-triazine (**WSL002**)
2-chloro-4,6-di(1H-pyrazol-1-yl)-1,3,5-triazine (**WSL003**)

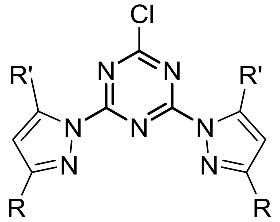

WSL001: R'=R=CH_3
WSL002: R'=H, R=CH_3
WSL003: R'=R=H

a. 0.96 g of 3,5-dimethylpyrazole (10 mmol) was dissolved in 150 mL dry THF before the addition of 0.32 g of potassium metal (8 mmol). The resulting mixture was stirred under reflux until the potassium metal has completely disappeared. 0.736 g of cyanuric chloride (4 mmol) was separately dissolved in 150 mL dry THF and cooled with an ice bath. The naturally cooled deprotonated pyrazoles were dropped into the cyanuric chloride solution in an ice bath. Upon complete addition, the reaction mixture was refluxed for 4 hours and cooled to room temperature afterwards. The precipitate was filtered and the solvent was evaporated. The crude was treated with a DCM/H_2O workup and the organic layer was extracted against brine, dried over anhydrous $MgSO_4$ and concentrated *in vacuo*. The crude was purified by column chromatography with DCM:MeOH/100:2 to give white solids. Yield: 55 – 65 %. ^{1}H NMR ($CDCl_3$): 6.02 (s, 1H), 2.66 (s, 3H), 2.24 ppm (s, 3H). ^{13}C NMR ($CDCl_3$): 172.5, 164.1, 154.9, 145.5, 113.2, 16.2, 14.5 ppm. MS (ESI$^+$): $[M+Na]^+$ 326 m/z.

The use of 3-methylpyrazole and pyrazole would give **WSL002** and **WSL003**.

WSL002: ^{1}H NMR ($CDCl_3$): 8.55 (d, 2H), 6.39 (d, 2H). 2.43 ppm (s, 6H). ppm. MS (ESI$^+$): [M-H]$^+$ 298 m/z.

WSL003: ^{1}H NMR ($CDCl_3$): 8.83 (m, 2H), 7.97 (s, 2H), 6.59 ppm (s, 2H). MS (ESI$^+$): [M-H]$^+$ 269 m/z.

b. 0.54 g of cyanuric chloride (2.9 mmol) and 0.98 mL of DIPEA (5.8 mmol) was dissolved in 20 mL of toluene. A 20 mL toluene solution of 0.4 g of pyrazole (5.8 mmol) was then dropped into the solution at room temperature. The mixture was stirred at room temperature for 24 hours and the solvent was evaporated. The solids were then shaken vigorously with 25 mL of water for 30 minutes before collected by filtration and further washed with 20 mL of water and finally dried under vacuum. Yield: 50 – 70 %.

4-(4,6-dichloro-1,3,5-triazin-2-yl)-N,N-diethylaniline (**WSL004**)

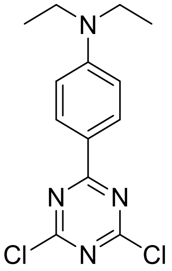

a. 0.94 g of 4-bromo-*N*,*N*-dimethylaniline (4 mmol) was added into 30 mL of dry THF under -78 °C and 4 mL of *n*-butyllithium (6.4 mmol, 1.6 M in hexane) was dropped into the solution and stirred for 1 hour.[161] 1 g of cyanuric chloride (5.4 mmol) was dissolved into 10 mL of dry THF under -78 °C and the lithiated species was dropped very slowly into the solution under -78 °C. Upon complete addition, the reaction mixture was naturally warmed to room temperature then stirred overnight before quenching with milli-Q water followed by a DCM/H_2O workup. The organic layer was then dried over anhydrous $MgSO_4$ and concentrated *in vacuo*. The crude was purified with column chromatography with DCM:Hex / 1:3 to elute a bright yellow solid which was further recrystallized in petroleum ether to give the product. The product could also be obtained directly from recrystallization of the crude in acetone. Yield: 67 %. ^1H NMR ($CDCl_3$): 8.32 (d, 2H), 6.82 (d, 2H), 3.49 (q, 4H), 1.25 ppm (t, 6H). ^{13}C NMR: 173.74, 170.87, 152.74, 132.54, 118.60, 111.02, 44.80, 12.57 ppm. MS (ESI^+): $[M-H]^+$ 296 m/z.

b. 0.134 g of magnesium turnings (5.5 mmol) and catalytic amount of iodine was added into 5 mL of dry THF and stirred until the solution became cloudy. Then, a 15 mL of dry THF solution with 1.14 g of 4-bromo-*N*,*N*-dimethylaniline (5 mmol) dissolved was added slowly at room temperature. The rate of addition should be adjusted so that the solution does not become too hot. Upon complete addition, the reaction mixture was refluxed for 3 hours to obtain the Grignard reagent. The cooled Grignard reagent was then added slowly into a 30 mL dry THF solution with 1 g of cyanuric chloride (5.4 mmol) dissolved in an ice bath. The reaction mixture was stirred for an additional 4 hours at room temperature. The reaction was quenched with saturated ammonium chloride solution and the solution was filtered. The THF was evaporated and the crude was subjected to a Et_2O/H_2O workup. The organic layer was extracted against brine, dried over anhydrous

$MgSO_4$ and concentrated *in vacuo*. The product was obtained after purification by column chromatography. Yield: 57 %.

2,4-dichloro-6-phenyl-1,3,5-triazine (**WSL005**)

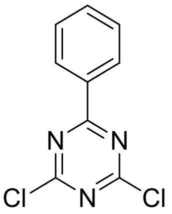

The synthesis is the same as **WSL005**, using phenylmagnesium bromide. Yield: 65 %. ^{1}H NMR ($CDCl_3$): 8.49 (d, 2H), 7.66 (m, 1H), 7.53 ppm (m, 2H). ^{13}C NMR MS ($CDCl_3$): 175.44, 169.24, 133.61, 130.87, 127.53, 124.48 ppm. MS (ESI$^+$): $[M+Na]^+$ 246 m/z.

4-(4,6-bis(3,5-dimethyl-1H-pyrazol-1-yl)-1,3,5-triazin-2-yl)-N,N-diethylaniline (**WSL006**)

4-(4,6-bis(3-methyl-1H-pyrazol-1-yl)-1,3,5-triazin-2-yl)-N,N-diethylaniline (**WSL007**)

4-(4,6-di(1H-pyrazol-1-yl)-1,3,5-triazin-2-yl)-N,N-diethylaniline (**WSL008**)

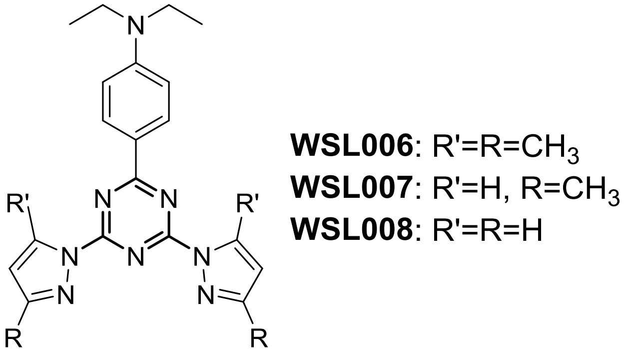

a. 0.288 g of 3,5-dimethylpyrazole (1.5 mmol) was dissolved into 10 mL of dry THF and 108 mg of potassium metal (1.4 mmol) was added and the reaction mixture was refluxed until the potassium disappeared. The deprotonated species was transferred to 300 mg of **WSL004** dissolved into a 10 mL of dry THF solution at room temperature. The resulting yellow suspension was refluxed overnight and then subjected to a EA/H_2O workup. The organic layer was extracted against brine, dried over anhydrous $MgSO_4$ and concentrated *in vacuo*. The yellow crude was purified with column chromatography with DCM:EA/100:1 to elute a yellow product. Yield: 48 %. ^1H NMR ($CDCl_3$): 8.29 (d, 2H), 6.63 (d, 2H), 5.99 (s, 2H), 3.375 (q, 4H), 2.76 (s, 6H), 2.28 (s, 6H), 1.15 ppm (t, 6H). ^{13}C NMR ($CDCl_3$): 173.24, 163.90, 152.33, 151.55, 143.94, 131.44, 121.13, 111.31, 110.66, 44.57, 16.06, 13.96, 12.55 ppm. HRMS (ESI^+): $[M+H]^+$ 417.2 m/z.

WSL007 was synthesized with 3-methylpyrazole. Yield: 45 %. **WSL007**: ^1H NMR ($CDCl_3$): 8.68 (m, 2H), 8.5 (d, 2H), 6.73 (d, 2H), 6.35 (d, 2H), 3.49 (q, 4H), 2.45 (s, 6H), 1.15 ppm (t, 6H). ^{13}C NMR ($CDCl_3$): 173.75, 162.15, 154.53, 151.72, 131.72, 130.69, 120.41, 110.43, 109.78, 53.6, 44.48, 14.20, 12.47 ppm. HRMS (ESI^+): $[M+H]^+$ 389.2 m/z.

WSL008 was synthesized with pyrazole. Yield: 50 %. **WSL008**: ^1H NMR ($CDCl_3$): 8.79 (m, 2H), 8.53 (d, 2H), 7.92 (s, 2H), 6.71 (d, 2H), 6.54 (m, 2H), 3.48 (q, 4H), 1.24 ppm (t, 6H). ^{13}C NMR ($CDCl_3$): 174.26, 162.67, 152.09, 144.92, 131.99, 130.16, 120.36, 110.66, 109.3, 44.65, 12.59 ppm. HRMS (ESI^+): $[M+H]^+$ 383.2 m/z.

b. 0.46 g of **WSL001** (1.5 mmol) was dissolved in 80 mL of degassed 1,4-dioxane at room temperature.[67] Upon complete dissolution, 1.5 equivalent of 4-(diethylamino)phenylboronic acid, 3 equivalent of sodium carbonate, 20 mL of water and 10 mol% of [1,1’-bis(diphenylphosphino)ferrocene]palladium(II) dichloride was added sequentially. The reaction mixture was stirred at 90 °C under nitrogen for 5 hours. The crude solvent was evaporated and subjected to a DCM/H_2O workup. The product was then purified by column chromatography. Yield: 45 %.

2-phenyl-4,6-di(1H-pyrazol-1-yl)-1,3,5-triazine (**WSL009**)
2,4-bis(3-methyl-1H-pyrazol-1-yl)-6-phenyl-1,3,5-triazine (**WSL010**)
2,4-bis(3,5-dimethyl-1H-pyrazol-1-yl)-6-phenyl-1,3,5-triazine (**WSL011**)

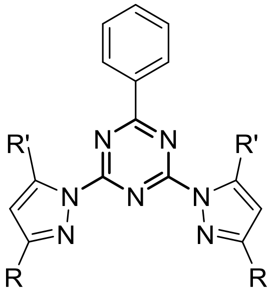

WSL009: R'=R=CH_3
WSL010: R'=H, R=CH_3
WSL011: R'=R=H

The syntheses of **WSL009-011** are the same for **WSL006-008** using **WSL005** (route a, yield: 55 %) or with **WSL001-003** and phenylboronic acid (route b, yield: 60 %).

WSL009: ^{1}H NMR ($CDCl_3$): 8.53 (d, 2H), 7.63 (m, 1H), 7.57 (m, 2H), 6.13 (s, 2H), 2.89 s, 6H), 2.37 (s, 6H). MS (ESI$^+$): [M+Na]$^+$ 367 m/z.

WSL010: ^{1}H NMR ($CDCl_3$): 8.57 (m, 2H), 8.53 (d, 2H), 7.5 (m, 1H), 7.42 (m, 2H), 6.37 (s, 2H), 2.35 (s, 6H). MS (ESI$^+$): [M+Na]$^+$ 339 m/z.

WSL011: ^{1}H NMR ($CDCl_3$): 8.84 (m, 2H), 8.69 (d, 2H), 7.97 (s, 2H), 7.67 (m, 1H), 7.57 (m, 2H), 6.6 (s, 2H). MS (ESI$^+$): [M+Na]$^+$ 312 m/z.

2,4-dichloro-6-(thiophen-2-yl)-1,3,5-triazine (**WSL012**)[67,68]
2,4-dichloro-6-(5-methylthiophen-2-yl)-1,3,5-triazine (**WSL013**)

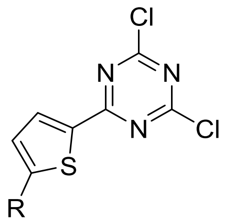

WSL012: R=H
WSL013: R=CH_3

0.34 g of magnesium turnings (14 mmol) and catalytic amount of iodine was added into 15 mL of dry THF and stirred until the solution became cloudy. A 15 mL of dry THF solution with 1.6 mL of 2-bromothiophene (13 mmol) dissolved was added slowly at room temperature and reaction mixture was refluxed for 3 hours to obtain the Grignard reagent. The cooled Grignard reagent was then added slowly into a 20 mL dry THF solution with 2 g of cyanuric chloride (10.8 mmol) dissolved in an ice bath. The reaction mixture was stirred for an additional 4 hours at room temperature. The reaction was quenched with saturated ammonium chloride solution and the solution was filtered. The THF was evaporated and the crude was subjected to a DCM/H_2O workup. The crude was purified by column chromatography with PE:DCM / 6:1. Yield: 35 %. ^1H NMR ($CDCl_3$): 8.23 (m, 1H), 7.64 (m, 1H), 7.2 ppm (m, 1H).

WSL013 was synthesized with 2-bromo-5-methylthiophene. Yield: 35 %. ^1H NMR ($CDCl_3$): 8.04 (m, 1H), 6.87 (m, 1H), 2.58 ppm (s, 3H).

2-chloro-4,6-di(thiophen-2-yl)-1,3,5-triazine (**WSL014**)
2-chloro-4,6-bis(5-methylthiophen-2-yl)-1,3,5-triazine (**WSL015**)

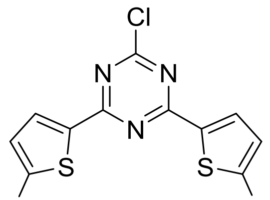

WSL014: R=H
WSL015: R=CH_3

WSL014 was synthesized similarly to **WSL012**, with the following modifications: 0.61 g of magnesium turnings and 3.89 g of 2-bromothiophene were used. Upon complete addition of the Grignard reagent, the reaction mixture was stirred at 35 °C overnight. Yield: 55 %. ^{1}H NMR ($CDCl_3$): 8.26 (m, 2H), 7.69 (m, 2H), 7.26 ppm (s, 6H). ^{13}C NMR 171.3, 169.0, 139.6, 134.0, 133.3, 123.8 ppm. MS (ESI$^+$): $[M+H]^+$ 281 m/z.

WSL015 was synthesized with 2-bromo-5-methylthiophene. Yield: 55 %. ^{1}H NMR ($CDCl_3$): 8.03 (d, 2H), 6.87 (m, 2H), 2.57 ppm (s, 6H). MS (ESI$^+$): $[M+H]^+$ 309 m/z.

2-chloro-4-(1H-pyrazol-1-yl)-6-(thiophen-2-yl)-1,3,5-triazine (**WSL016**)
2-chloro-4-(3-methyl-1H-pyrazol-1-yl)-6-(5-methylthiophen-2-yl)-1,3,5-triazine (**WSL017**)

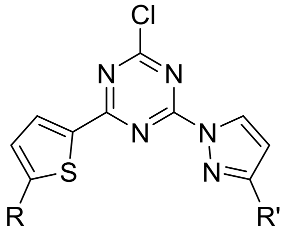

WSL016: R=R'=H
WSL017: R=R'=CH_3

1.2 equivalent of potassium metal was added into 1.5 equivalent of pyrazole dissolved in dry THF. The reaction mixture was refluxed until potassium disappeared. The reaction mixture was then cooled to room temperature and added to a dry THF solution containing **WSL012** in ice bath. Upon complete addition, the reaction mixture was refluxed for 4 hours and cooled to temperature prior to filtration. The crude THF solution was evaporated and the crude solids were subjected to a DCM/H_2O workup. The product was obtained as a light beige solid after purification by column chromatography with DCM:MeOH/100:1. Yield: 40 %. ^{1}H NMR ($CDCl_3$): 8.84 (m, 1H), 8.31 (m, 1H), 7.98 (s, 1H), 7.79 (m, 1H), 7.49 (m, 1H), 6.61 ppm (s, 1H). MS (ESI$^+$): $[M+Na]^+$ 285 m/z.

WSL017 was synthesized with 2-bromo-5-methylthiophene. Yield: 40 %. ^{1}H NMR ($CDCl_3$): 8.62 (d, 1H), 8.08 (d, 1H), 6.83 (m, 1H), 6.42 (d, 1H), 2.59 (s, 3H), 2.41 ppm (s, 3H). ^{13}C NMR ppm. MS (ESI$^+$): $[M+Na]^+$ 314 m/z.

4-(4,6-di(thiophen-2-yl)-1,3,5-triazin-2-yl)-N,N-diethylaniline (**WSL018**)
4-(4,6-bis(5-methylthiophen-2-yl)-1,3,5-triazin-2-yl)-N,N-diethylaniline (**WSL019**)

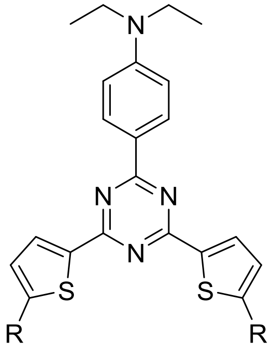

WSL018: R=H
WSL019: R=CH_3

0.46 g of **WSL014** (1.5 mmol) was dissolved in 80 mL of degassed 1,4-dioxane at room temperature. Upon complete dissolution, 1.5 equivalent of 4-(diethylamino)phenylboronic acid, 3 equivalent of sodium carbonate, 20 mL of water and 10 mol% of [1,1’-bis(diphenylphosphino)ferrocene]palladium(II) dichloride was added sequentially. The reaction mixture was stirred at 90 °C under nitrogen for 5 hours. The crude solvent was evaporated and subjected to a DCM/H_2O workup. The product was then purified by column chromatography with PE:DCM/5:1. Yield: 50 %. ^{1}H NMR ($CDCl_3$): 8.54 (d, 2H), 8.29 (m 2H), 7.6 (m, 2H), 7.22 (m, 2H), 6.77 (d, 2H), 3.49 (q, 4H), 1.25 (t, 6H). MS (ESI$^+$): $[M+H]^+$ 393 m/z.

WSL019 was synthesized similarly with **WSL015**. Yield: 56 %. ^{1}H NMR ($CDCl_3$): 8.58 (d, 2H), 8.05 (d, 2H), 6.91 (m, 2H), 6.7 (d, 2H), 3.48 (q, 2H), 2.55 (s, 6H), 1.24 ppm (t, 6H). MS (ESI$^+$): $[M-H]^+$ 421.5 m/z.

2-phenyl-4,6-di(thiophen-2-yl)-1,3,5-triazine (**WSL020**)
2,4-bis(5-methylthiophen-2-yl)-6-phenyl-1,3,5-triazine (**WSL021**)

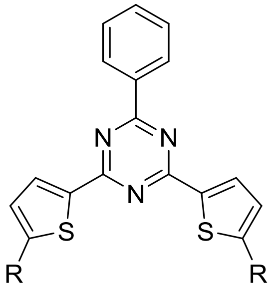

WSL020: R=H
WSL021: R=CH_3

WSL020 was synthesized similarly to **WSL018** with phenylboronic acid. Yield: 67 %. ^{1}H NMR ($CDCl_3$): 8.67 (m, 2H), 8.32 (m, 2H), 7.63 (m, 5H), 7.23 ppm (m, 2H). MS (ESI$^+$): $[M+H]^+$ 322 m/z.

WSL021 was synthesized similarly to **WSL019** with phenylboronic acid. Yield: 66 %. ^{1}H NMR ($CDCl_3$): 8.64 (d, 2H), 8.12 (d, 2H), 7.6 (m, 3H), 6.89 (m, 1H), 2.59 ppm (s, 3H). MS (ESI$^+$): $[M+H]^+$ 351 m/z.

4-(4-(1H-pyrazol-1-yl)-6-(thiophen-2-yl)-1,3,5-triazin-2-yl)-N,N-diethylaniline (**WSL022**)

N,N-diethyl-4-(4-(3-methyl-1H-pyrazol-1-yl)-6-(5-methylthiophen-2-yl)-1,3,5-triazin-2-yl)aniline (**WSL023**)

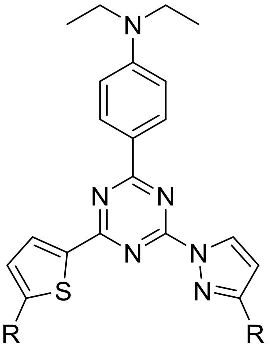

WSL022: R=H
WSL023: R=CH_3

\

WSL022 was synthesized similarly to **WSL018** with **WSL016** and purified by column chromatography with DCM:MeOH/100:3. Yield: 50 %. ^{1}H NMR ($CDCl_3$): 8.62 (d, 1H), 8.08 (d, 1H), 6.83 (m, 1H), 6.42 (d, 1H). MS (ESI$^+$): $[M+Na]^+$ 285 m/z.

WSL023 was synthesized similarly to **WSL018** with **WSL017** and purified by column chromatography with DCM:MeOH/100:3. Yield: 52 %. ^{1}H NMR ($CDCl_3$): 8.79 (m, 1H), 8.53 (d, 2H), 8.33 (m, 1H), 7.92 (m, 1H), 7.62 (d, 1H), 7.21 (m, 1H), 6.74 (d, 2H), 6.54 (m, 2H), 3.48 (q, 4H), 1.24 ppm (t, 6H). MS (ESI$^+$): $[M+Na-H]^+$ 426 m/z.

2-phenyl-4-(1H-pyrazol-1-yl)-6-(thiophen-2-yl)-1,3,5-triazine (**WSL024**)

2-(3-methyl-1H-pyrazol-1-yl)-4-(5-methylthiophen-2-yl)-6-phenyl-1,3,5-triazine (**WSL025**)

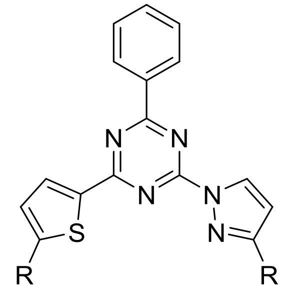

WSL024: R=H
WSL025: R=CH_3

WSL024 was synthesized similarly to **WSL018** with **WSL016** and phenylboronic acid and purified by column chromatography with DCM:MeOH/100:2. Yield: 60 %. ^{1}H NMR ($CDCl_3$): 8.84 (m, 1H), 8.67 (m, 2H), 8.31 (m, 1H), 7.98 (s, 1H), 7.79 (m, 1H), 7.62 (m, 3H), 7.49 (m, 1H), 6.61 ppm (s, 1H). MS (ESI$^+$): [M-H]$^+$ 327 m/z.

WSL025 was synthesized similarly to **WSL018** with **WSL017** and phenylboronic acid and purified by column chromatography with DCM:MeOH/100:2. Yield: 60 %. ^{1}H NMR ($CDCl_3$): 8.8 (m, 1H), 8.68 (m, 2H), 8.38 (m, 1H), 7.96 (s, 1H), 7.67 (m, 1H), 7.62 (m, 1H), 7.56 (m, 2H), 7.24 (t, 1H), 6.58 ppm (s, 1H). MS (ESI$^+$): [M+Na]$^+$: 355 m/z.

Tris(4,4,4-trifluoro-1-(2-thienyl)-1,3-butanediono)samarium(III) (**Sm(tta)$_3$**)[81]
Tris(4,4,4-trifluoro-1-(2-thienyl)-1,3-butanediono)ytterbium(III) (**Yb(tta)$_3$**)

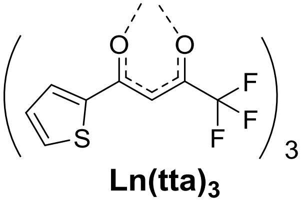

Ln(tta)$_3$

2 g of thenoyltrifluoroacetone (9 mmol) was dissolved in 30 mL of absolute ethanol and 9 mL of 1 M of ammonium hydroxide was added. The mixture was allowed to stir until clear and 3 mmol of lanthanide(III) chloride in 36 mL of water was added. Stirring was stopped upon complete addition and the mixture was allowed to stand and solidify for several hours. The solution was removed and the solid was washed with water and subsequently dried in a vacuum desiccator overnight. The solids were dissolved in 4.5 mL of acetone and precipitated with 36 mL of deionized water. The solution was removed and the thick oil was allowed to solidify. The solid was then dried under high vacuum at room temperature and recrystallized in petroleum ether to remove excess TTA. Yield: 24 %. $[Yb(tta)_2]^+$ 860, $[Sm(tta)_2]^+$ 593.9; $[Sm(tta)_3+H]^+$ 815.9 m/z.

Complexation of $Ln(tta)_3$ with tridentate ligands

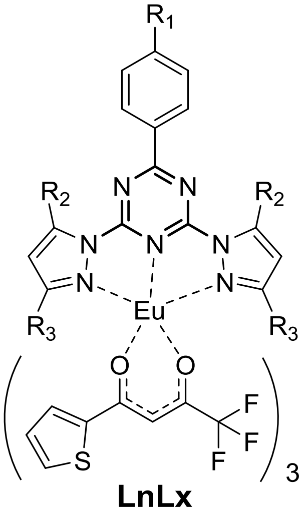

LnLx

$Ln(tta)_3$ and the ligand was mixed in a 1:1 ratio in a solution of methanol and stirred at 50 °C overnight. The solvent was subsequently evaporated and the residue was re-dissolved in minimum amount of diethyl ether and precipitated by *n*-hexanes. The bright yellow complex was obtained by repeated precipitation. Yield: 80%. ESI-MS: [**SmL1**-tta]$^+$ 1010, [**SmL2**-tta]$^+$ 978, [**SmL3**-tta]$^+$ 954, [**EuL1**-tta]$^+$ 1011, [**EuL2**-tta]$^+$ 979, [**EuL3**-tta]$^+$ 955, [**YbL1**-tta]$^+$ 1032, [**YbL2**-tta]$^+$ 1000, [**YbL3**-tta]$^+$ 976 m/z.

4-(4,6-bis(3-(bromomethyl)-1H-pyrazol-1-yl)-1,3,5-triazin-2-yl)-N,N-diethylaniline (**WSL026**)

4-(4,6-bis(4-bromo-3-methyl-1H-pyrazol-1-yl)-1,3,5-triazin-2-yl)-N,N-diethylaniline (**WSL027**)

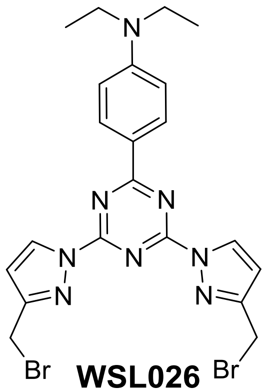

WSL026

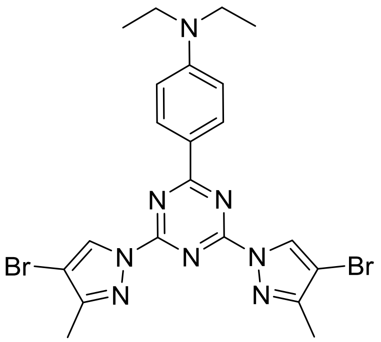

WSL027

0.1 g of **WSL007** (0.257 mmol) and 0.1 g of N-bromosuccinimide[67] (0.565 mmol) were dissolved in CCl_4. The mixture was refluxed for 10 mins and 5 mol% of AIBN (or benzoyl peroxide) was added. The reaction mixture was refluxed for another hour (monitored by TLC) and naturally cooled to room temperature. The precipitated succinimide was filtered and the solvent was evaporated to afford crude solids. ^{1}H NMR spectroscopy revealed the major product was in fact **WSL027**. Yield: undetermined.

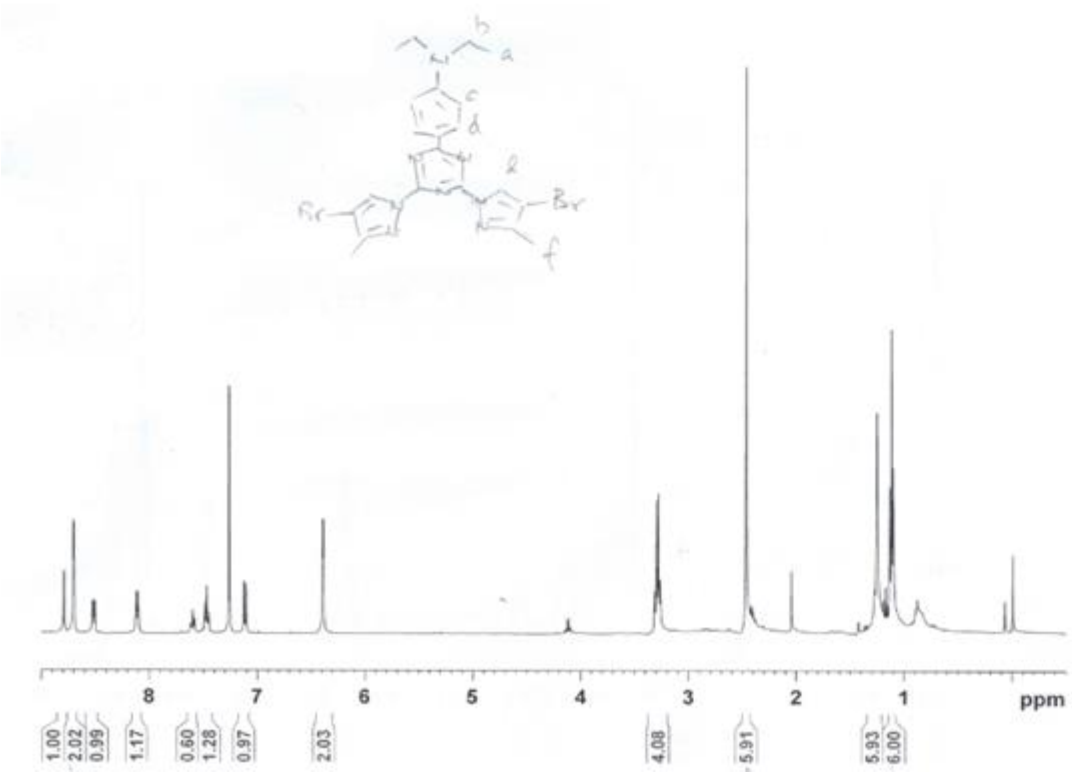

1H-pyrazole-3-carboxylic acid (**WSL028**)

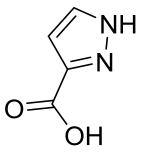

4.9 mL of 3-methylpyrazole (58.5 mmol) was dissolved into 225 mL of deionized water at room temperature. 20.45 equivalent of potassium permanganate (129 mmol) was added slowly at room temperature. The reaction mixture was then refluxed for 4 hours upon complete addition. It was then cooled to room temperature, filtered and evaporated to a small volume. The water solution was tuned to acidic pH (~ 2) by concentrated hydrochloric acid and allowed to recrystallize at 0 °C for 4 hours to obtain white solids. Yield: 62 %. %). ^{1}H NMR (400 MHz, D_2O): 6.86 (d, 1H), 7.74 ppm (d, 1H); ^{13}C NMR

(100MHz, D_2O): 165.3, 142.0, 132.3, 108.2 ppm. MS (ESI$^+$) 112.9 $[M+H]^+$ 112.9, $(M+K)^+$ 150.9 m/z.

ethyl 1H-pyrazole-3-carboxylate (**WSL029**)

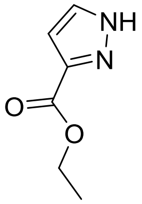

1 g of **WSL028** (9.1 mmol) was dissolved and 1.5 mL of concentrated H_2SO_4 was added in 20 mL of absolute ethanol under nitrogen and the reaction mixture was refluxed for 5 hours. The solvent was then evaporated and 50 mL of deionized water was added to dissolve the crude, followed by neutralization of the acid with $NaHCO_3$. EA was added to extract the solids and the organic part was evaporated to a little volume. Several drops of PE was added to initiate recrystallization to yield the white solid products. Yield: 80 %. ^{1}H NMR ($CDCl_3$): 7.71 (m, 1H), 6.87 (m, 1H), 4.44 (q, 2H), 1.13 ppm (t, 3H).

diethyl 1,1'-(6-phenyl-1,3,5-triazine-2,4-diyl)bis(1H-pyrazole-3-carboxylate) (**WSL030**)

diethyl 1,1'-(6-(4-(diethylamino)phenyl)-1,3,5-triazine-2,4-diyl)bis(1H-pyrazole-3-carboxylate) (**WSL031**)

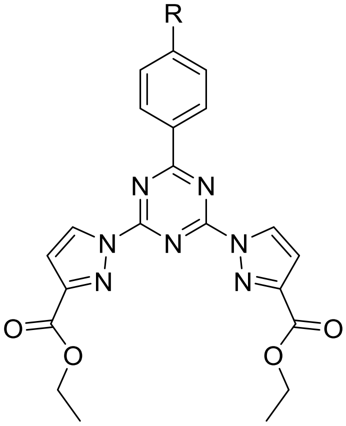

WSL030: R = NEt_2
WSL031: R = H

1.747 g of **WSL004** (5.88 mmol) and 1.65 g of **WSL029** (11.76 mmol) were dissolved in 40 mL of anhydrous DMF. 0.517 g of NaH (60 % in mineral oil, 12.9 mmol) was added slowly into the reaction mixture at 0 °C. Upon complete addition, the reaction mixture was stirred at room temperature overnight. The solvent was evaporated and the crude was subjected to a DCM/H_2O workup. The product was obtained as a yellow solid after purification by column chromatography with DCM:EA. Yield: 90 %. ^{1}H NMR ($CDCl_3$): 8.86 (m, 2H), 8.56 (d, 2H), 7.06 (m, 2H), 6.74 (d, 2H), 4.5 (q, 4H), 3.51 (q, 4H), 1.49 (t, 6H), 1.27 ppm (t, 6H). MS (ESI^+): $[M+Na]^+$ 526.5 m/z.

WSL031 was synthesized similarly using **WSL005**. Yield: 92 %. ^{1}H NMR ($CDCl_3$): 8.88 (m, 2H), 8.7 (d, 2H), 7.67 (m, 1H), 7.56 (m, 2H), 7.07 (m, 2H), 4.49 (q, 4H), 1.47 ppm (t, 6H). MS (ESI^+): $[M+Na]^+$ 455 m/z.

(1H-pyrazol-3-yl)methanol (**WSL033**)

3-(chloromethyl)-1H-pyrazole hydrochloride (**WSL034**)

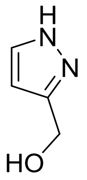

WSL033

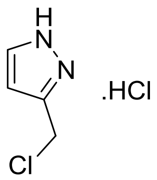

WSL034

3.12 g of **WSL028** (27.8 mmol) was dissolved in 50 mL of dry THF under nitrogen. 2.11 g of $LiAlH_4$ (55.7 mmol) was added slowly at °C and the reaction mixture was stirred overnight at room temperature. The reaction was worked up according to the Fieser procedure: 2.11 mL of deionize water was added slowly at 0 °C, followed by 2.11 mL of 15 % aqueous sodium hydroxide solution and 6.33 mL of deionize water. The reaction mixture was then stirred at room temperature for 1 hour and the solids were filtered, rinsed with THF for multiple times and the combined THF solution was evaporated to give the product as a colorless oil. Yield: 48 %. **WSL033** was used without further purification by reacting it with 5 mL of thionyl chloride at room temperature overnight. 10 mL of deionized water was added slowly to quench the excess thionyl chloride (Caution: irritating gas evolution). The reaction mixture was allowed to stir for an additional hour to ensure complete consumption of thionyl chloride and the solvent was evaporated to give a light beige solid as the product. Yield: 60 %. ^{1}H NMR (CD_3OD): 4.93 (s, 2H), 6.90 (d, 1H), 8.31 ppm (d, 1H). ^{13}C NMR (CD_3OD): 145.3, 134.7, 107.6, 33.7 ppm. MS (ESI$^+$): $[M–Cl]^+$, 117.15, $[M–Cl–HCl]^+$ 81.10 m/z.

di-tert-butyl 2,2'-(((1H-pyrazol-3-yl)methyl)azanediyl)diacetate (**WSL035**)

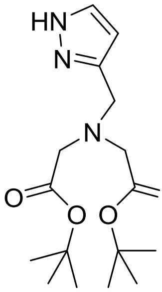

1.06 g of di-tert-butyl iminodiacetate (4.31 mmol) was dissolved in 30 mL dry ACN under nitrogen. 0.6 g of **WSL034** (3.92 mmol), 010 mol% of sodium iodide and 2.17 of K_2CO_3 (15.7 mmol) was added to the solution at room temperature and the resulting mixture was refluxed overnight. The crude was filtered and the solution was evaporated to give a brown crude oil, which gave the product as a light yellow oil after purification by column chromatography with solvent gradient from DCM:MeOH/100:0 to 100:3. Yield: 72 %. ^{1}H NMR ($CDCl_3$): 1.39 (s, 18H), 3.39 (s, 4H), 3.96 (s, 2H), 6.15 (d, 1H), 7.48 ppm (d, 1H). ^{13}C NMR ($CDCl_3$): 170.6, 104.7, 81.3, 55.1, 49.6, 28.1 ppm. MS (ESI$^+$): $[M+H]^+$ 326.1, $[M+Na]^+$ 348.1 m/z.

tetra-tert-butyl 2,2',2'',2'''-((((6-(4-(diethylamino)phenyl)-1,3,5-triazine-2,4-diyl)bis(1H-pyrazole-1,3-diyl))bis(methylene))bis(azanetriyl))tetraacetate (**WSL036**)

tetra-tert-butyl 2,2',2'',2'''-((((6-phenyl-1,3,5-triazine-2,4-diyl)bis(1H-pyrazole-1,3-diyl))bis(methylene))bis(azanetriyl))tetraacetate (**WSL037**)

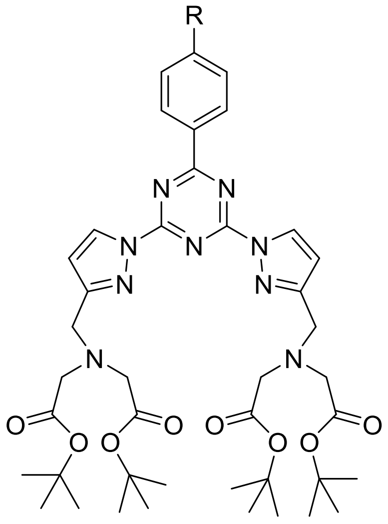

WSL036: R=NEt$_2$
WSL037: R=H

0.5 g of **WSL035** (1.54 mmol) was dissolved in 30 mL of dry ACN under nitrogen. 0.063 g of NaH (60 % in mineral oil, 1.57 mmol) was added under nitrogen. The mixture was allowed to react until gas evolution ceased (approx. 30 minutes) and 0.223 g of **WSL004** (0.749 mmol) was added at room temperature and the reaction mixture was stirred at overnight. The solvent was evaporated and the product was purified by column chromatography with a solvent gradient of DCM:MeOH/100:0 to 100:3 as a colorless liquid. Yield: 15 %. ^{1}H NMR (CDCl$_3$): 1.15 (t, 6H), 1.39 (s, 36H), 3.39 (q, 4H), 3.42 (s, 8H), 4.02 (s, 4H), 6.63 (s, 2H), 6.65 (d, 2H), 8.42 (d, 2H), 8.66 ppm (s, 2H). ^{13}C NMR (CD$_3$OD): 170.4, 157.1, 131.9, 131.0, 110.6, 109.7, 81.0, 55.5, 51.9, 44.6, 28.9, 28.1, 12.6 ppm. MS (ESI$^+$): [M+Na]$^+$ 898.4, [M+K]$^+$ 914.4 m/z.

WSL037 was synthesized similarly with **WSL005**. Yield: 29 %. ^{1}H NMR ($CDCl_3$): 1.37 (s, 36H), 3.40 (s, 8H), 4.00 (s, 4H), 6.67 (d, 2H), 7.41 (t, 2H), 7.50 (t, 1H), 8.52 (d, 2H), 8.66 ppm (d, 2H). ^{13}C NMR (CD_3OD): 174.6, 170.3, 162.7, 157.6, 134.2, 133.6, 131.2, 129.4, 128.6, 110.4, 81.0, 55.4, 51.6, 28.1 ppm. MS (ESI$^+$): $[M–C_4H_8+H]^+$ 748.7, $[M+Na]^+$ 826.5 m/z.

2,2',2'',2'''-((((6-(4-(diethylamino)phenyl)-1,3,5-triazine-2,4-diyl)bis(1H-pyrazole-1,3-diyl))bis(methylene))bis(azanetriyl))tetraacetic acid (**WSL038**)

2,2',2'',2'''-((((6-phenyl-1,3,5-triazine-2,4-diyl)bis(1H-pyrazole-1,3-diyl))bis(methylene))bis(azanetriyl))tetraacetic acid (**WSL039**)

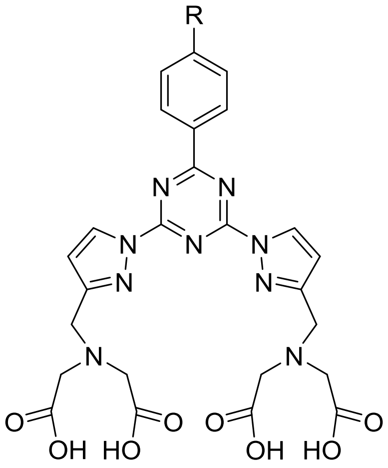

WSL038: R=NEt_2
WSL039: R=H

WSL036 (0.35 mmol) was dissolved in 5 mL of dichloromethane and stirred at room temperature. 5 mL of trifluoroacetic acid was added to the solution at room temperature and stirred overnight. The reaction mixture was then evaporated under reduced pressure to give the unprotected product **WSL037** in quantitative yield. ^{1}H NMR (D_2O): 4.28 (s, 8H), 4.71 (s, 4H), 6.89 (s, 2H), 7.58 (t, 2H), 7.69 (t, 1H), 8.68 (d, 2H), 9.04 ppm (s, 2H).

^{13}C NMR (D_2O): 51.3, 54.5, 110.3, 128.5, 129.4, 132.1, 133.6, 134.3, 155.4, 162.6, 172.3, 175.1 ppm. HRMS (ESI$^+$): [M+Na]$^+$ 602.1724 *m/z*

WSL039 was synthesized similarly with **WSL037**. ^{1}H NMR (D_2O): 1.22 (s, 6H), 3.62 (s, 4H), 4.37 (s, 8H), 4.79 (s, 4H), 6.88 (s, 2H), 7.25 (s, 2H), 8.63 (s, 2H), 8.98 ppm (s, 2H). ^{13}C NMR (D_2O): 10.8, 48.5, 51.8, 53.8, 111.5, 115.0, 131.7, 132.5, 147.5, 162.4, 167.3, 174.0 ppm. HRMS (ESI$^+$): [M+H]$^+$: 651.2627 *m/z*.

Eu(III) Complex with **WSL039** (**[EuWSL039]**$^-$)

WSL039 (20 mg) was dissolved in 10 mL of methanol. 4 equivalents of trimethylamine was added and the mixture was stirred for 10 minutes at room temperature before the addition of 1 equivalent of $EuCl_3 \cdot 6H_2O$. The reaction mixture was then refluxed for 3 hours. The solvent was removed under reduced pressure and dried under vacuum. Yield: 80 %. MS (ESI$^+$): 728.3 *m/z*.

Tetraethyl *N*,*N*'-(benzylamine)di(methyl phosphonate) (**WSL042**)[156]

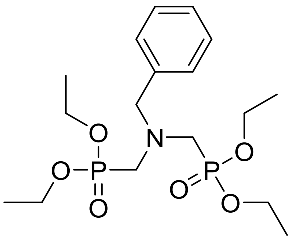

WSL042

1 mL of benzylamine (9.33 mmol) and 2.4 mL of diethyl phosphate (18.7 mmol) were mixed without solvent and cooled to 0 °C. 2.1 mL of formaldehyde (37 % aqueous solution, 28 mmol) was added over 15 mins slowly so the temperature of the mixture does not exceed 10 °C. The resulting emulsion was then stirred at room temperature for 30 minutes and at 100 °C for 1 hour. Excess water and formaldehyde were evaporated and the colorless oily product was obtained without purification. Yield: 80 %. ^{1}H NMR ($CDCl_3$): 7.21 (m, 5H), 3.96 (m, 8H), 3.92 (s, 2H), 3.0 (d, 4H), 1.15 ppm (t, 12 H). MS (ESI^+): $[M+H]^+$ 344 m/z.

Tetraethyl iminodi(methyl phosphonate) (**WSL040**)

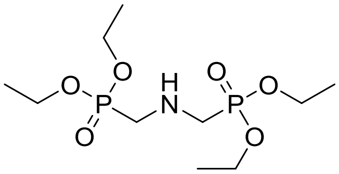

WSL040

3.2 g of **WSL042** (7.86 mmol) was dissolved in 20 mL ethanol. 0.5 of 10 % Pd/C was added at 0 °C and a hydrogen balloon was connected. 0.674 mL of acetic acid (11.8 mmol) was added and the reaction mixture was refluxed for 48 hours, refilling the balloon if necessary. The mixture was filtered and the solvent was evaporated. The crude oil was dissolved in DCM and extracted against saturated $NaHCO_3$. The organic layer was dried and evaporated to obtain the colorless product. Yield: 95 %. ^{1}H NMR ($CDCl_3$): 4.18 (m, 8H), 3.16 (d, 4H), 1.36 ppm (t, 12H). MS (ESI^+): $[M+H]^+$ 318 m/z.

N-benzyl-*N*'-(diethoxyphosphorylmethyl)glycine ethyl ester (**WSL043**)

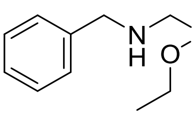

WSL044

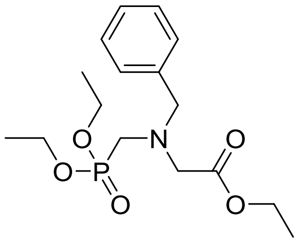

WSL043

1 g of 1,3,5-tribenzyl hexahydro-1,3,5-triazine (2.82 mmol) and 1.08 mL of diethyl phosphonate were heated at 100 °C overnight. The reaction mixture was then dried under high vacuum to give **WSL044** and used without purification. **WSL044** was dissolved in 10 mL of dry ACN. 2.96 mL of diisopropylethylamine (17 mmol) was added and 1.88 mL of ethyl bromoacetate (17 mmol) was dropped into the resulting mixture at room temperature. The reaction mixture was stirred at room temperature for 30 minutes and then refluxed for 4 hours. The solvent was then evaporated and the crude oil was diluted with 10 mL of DCM, washed with 10 mL of 10 % of aqueous $NaCHO_3$ twice. The DCM portion was then concentrated and purified by column chromatography DCM:EA to give a yellow oil. Yield: 45 %. ^{1}H NMR ($CDCl_3$): 7.41 (m, 5H), 4.13 (m, 6H), 3.95 (s, 2H), 3.90 (s, 2H), 3.16 (d, 2H), 1.32 ppm (m, 9H). MS (ESI$^+$): $[M+H]^+$ 344 m/z.

Ethyl 2-[*N*-(diethoxyphosphoryl)methylamino] acetate (**WSL041**)

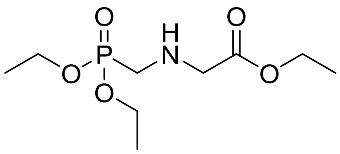

WSL041

WSL041 was deprotected from **WSL043** similarly as **WSL040**. ^{1}H NMR ($CDCl_3$): 4.19 (m, 6H), 3.47 (s, 2H), 3.01 (d, 2H), 1.35 ppm (m 9H). ^{13}C NMR ppm. MS (ESI$^+$): $[M+H]^+$ 254 m/z.

8. References

1. Cotton, S. In *Lanthanide and Actinide Chemistry*, Wiley, **2006**
2. Bünzli, J.-C. G.; Eliseeva, S. V. Lanthanide Luminescence: Photophysical, Analytical and Biological Aspects. In *Springer Series on Fluorescence*; Hänninen, P., Härmä, H., Eds.; Springer Verlag: Berlin, Heidelberg, **2011**; Vol. 7, pp 1– 46.
3. Richardson, F. S. *Chem. Rev.* **1982**, *82*, 541-552.
4. Prandtl, W.; Scheiner, K. *Zeit. Anorg. Allgem. Chem.* **1934**, *220*, 107-112.
5. Tanner, P. A.; Duan, C.-K. *Coord. Chem. Rev.* **2010**, *254*, 3026-3029.
6. Tanner, P. A. *Chem. Soc. Rev.* **2013**, *42*, 5090-5101.
7. Judd, B. R. *Phys. Rev.* **1962**, *127*, 750-761.
8. Ofelt, G. S. *J. Chem. Phys.* **1962**, *37*, 511-520.
9. Jørgensen, C. K.; Judd, B. R. *Mol. Phys.* **1964**, *8*, 281-290.
10. Binnemans, K. *Coord. Chem. Rev.* **2015**, *295*, 1-45.
11. Rudzinski C. M.; Engebretson D. S.; Hartmann W. K.; Nocera D. G. *J. Phys. Chem. A* **1998**, *102*, 7442–7446.
12. Latva M.; Takalo H.; Mukkala V.-M.; Matachescu C.; Rodriguez-Ubis J. C.; Kankare J. *J. Lumin.* **1997**, *75*, 149–169.
13. Kleinerman, M. *J. Chem. Phys.* **1969**, *51*, 2370-2381.
14. Lamture, J. B.; Zhou, Z. H.; Kumar, A. S.; Wensel, T. G. *Inorg. Chem.*, **1995**, *34*, 864-869.
15. Nah M.-K.; Cho H.-G.; Kwon H.-J.; Kim Y.-J.; Park C.; Kim H. K.; Kang J.-G. *J. Phys. Chem. A* **2006**, *110*, 10371–10374.

16. Thorne J. R. G.; Rey J. M.; Denning R. G.; Watkins S. E.; Etchells M.; Green M.; Christou V. *J. Phys. Chem. A* **2002**, *106*, 4014–4021.
17. Ha-Thi, M.-H.; Delaire J. A.; Michelet V.; Leray I. *J. Phys. Chem. A* **2010**, *114*, 3264–3269.
18. Förster, Th. *Zwischenmolekulare Energiewanderung und Fluoreszenz. Ann. Phys.* **1948**, *437*, 55-75.
19. Förster, Th. *Discuss. Faraday Soc.* **1959**, *27*, 1-6.
20. Englman, R.; Jortner, *J. Mol. Phys.* **1970**, *18*, 145– 164.
21. Schuurmans, M. F. H.; van Dijk, J. M. F. *Physica B+C* **1984**, 131-155.
22. Beeby, A.; Clarkson, I. M.; Dickins, R. S.; Faulkner, S.; Parker, D.; Royle, L.; de Sousa, A. S.; Gareth Williams, J. A.; Woods, M. *J. Chem. Soc., Perkin Trans. 2* **1999**, 493-502.
23. Supkowski, R. M.; Horrocks Jr., W. D. *Inorg. Chim. Acta* **2002**, *340*, 44-48.
24. Kimura, T.; Kato, Y. *J. Alloys Compounds* **1995**, *225*, 284-284.
25. Hakala, H.; Liitti, P.; Peuralahti, J.; Karvinen, J.; Mukkala, V.-M.; Hovinen, J. *J. Lumin.* **2005**, *113*, 17-26.
26. Faulkner, S.; Beeby, A.; Carrie, M. C.; Dadabhoy, A.; Kenwright, A. M.; Sammes, P. G. *Inorg. Chem. Commun.* **2001**, *4*, 187-190.
27. Holz, R. C.; Chang, C. A.; Horrocks, W. D. *Inorg. Chem.* **1991**, *30*, 3270-3275.
28. Bassett, A. P.; Magennis, S. W.; Glover, P. B.; Lewis, D. J.; Spencer, N.; Parsons, S.; Williams, R. M.; De Cola, L.; Pikramenou, Z. *J. Am. Chem. Soc.* **2004**, *126*, 9413-9424.

29. Görller-Walrand, C.; Binnemans, K. In *Handbook on the Physics and Chemistry of Rare Earths*, (ed. K. A. Gschneidner, Jr and L. Eyring), Elsevier Science B.V., Amsterdam, **1998**, chp. 167, vol. 25.
30. Reid MF (2005) In Spectroscopic properties of rare earth in optical materials (ed. Liu G, Jacquier B), Tsuinghua University Press and Springer-Verlag: Beijing, Heidelberg, pp 95–129.
31. Werts, M. H. V.; Jukes, R. T. F.; Verhoeven, J. W. *Phys. Chem. Chem. Phys.* **2002**, *4*, 1542-1548.
32. Rilliams, A. T. R.; Winfield, S. A.; Miller, J. N. *Analyst* **1983**, *108*, 1067-1071.
33. Zucchi, G.; Scopelliti, R.; Bünzli, J.-C. G. *Dalton Trans*. **2001**, 1975−1985.
34. Nakamaru, K. *Bull. Chem. Soc. Jpn.* **1982**, *55*, 2697-2705.
35. Van Houten, J.; Watts, R. J. *J. Am. Chem. Soc.* **1976**, *98*, 4853-4858.
36. Chauvin, A.-S.; Gumy, F.; Imbert, D.; Bünzli, J.-C. G. *Spectroscopy Lett*. **2007**, *40*, 193.
37. Chauvin, A.-S.; Gumy, F.; Imbert, D.; Bünzli, J.-C. G. *Spectroscopy Lett*. **2004**, *37*, 517−532.
38. Meshkova, S. B.; Topilova, Z. M.; Bolshoy, D. V.; Beltyukova, S. V.; Tsvirko, M. P.; Venchikov, V. Y. *Acta Phys. Pol. A* **1999**, *95*, 983−990.
39. De Mello, J. C.; Wittmann, F. H.; Friend, R. H. *Advanced Materials* **1997**, *9*, 230−232.
40. Porrès, L.; Holland, A.; Pålsson, L.-O.; Monkman, A. P.; Kemp, C.; Beeby, A. *J. Fluoresc.* **2006**, *16*, 267−273.
41. de Mello, J. C.; Wittmann, H. F.; Friend, R. H. *Adv. Mater.* **1997**, *9*, 230-232.

42. Bünzli, J.-C. G. (2014) Luminescence Bioimaging with Lanthanide Complexes, in Luminescence of Lanthanide Ions in Coordination Compounds and Nanomaterials (ed A. de Bettencourt-Dias), John Wiley & Sons Ltd, Chichester, United Kingdom, pp 132.
43. Bünzli, J.-C. G. *Chem. Rev.* **2010**, *110*, 2729-2755.
44. Moore, E. G.; Samuel, A. P. S.; Raymond, K. N. *Acc. Chem. Res.* **2009**, *42*, 542-552.
45. Eliseeva, S. V.; Bünzli, J.-C. G. *Chem. Soc. Rev.* **2010**, *39*, 189-227.
46. Parker, D. *Coord. Chem. Rev.* **2000**, *1*, 109-130.
47. Montgomery, C. P.; Murray, B. S.; New, E. J.; Pal, R.; Parker, D. *Acc. Chem. Res.* **2009**, *42,* 925-937.
48. Que, E. L.; Chang, C. J. *Chem. Soc. Rev.* **2010**, *39*, 51-60.
49. Ekanger, L. A.; Polin, L. A.; Shen, Y.; Haccke, E. M.; Martin, P. D.; Allen, M. J. *Angew. Chem. Int. Ed.* **2015**, *48*, 14398-14401.
50. Kanger, L. A.; Ali, M. M.; Allen, M. J. *Chem. Commun.* **2014**, *50*, 14835-14838.
51. Garcia, J.; Neelavalli, J.; Haacke, E. M.; Allen, M. J. *Chem. Commun.* **2011**, *47*, 12858-12860.
52. Caravan, P.; Tóth, E.; Rockenbauer, A.; Merbach, A. E. *J. Am. Chem. Soc.* **1999**, *121*, 10403-10409.
53. Burai, L.; Tóth, E.; Moreau, G.; Sour, A.; Scopelliti, R.; Merbach, A. D. *Chem. Eur. J.* **2003**, *9*, 1394-1404.
54. Bottrill, M.; Kwok, L.; Long, N. J. *Chem. Soc. Rev.* **2006**, *35*, 557-571.
55. Yang, X.; Zhou, G.; Wong, W.-Y. *Chem. Soc. Rev.* **2015**, *44*, 8484-8575.
56. Kido, J.; Nagai, K.; Ohashi, Y. *Chem. Lett.*, **1990**, 657.

57. Xin, X.; Li, F. Y.; Shi, M.; Bian, Z. Q.; Huang, C. H. *J. Am. Chem. Soc.* **2003**, *125*, 7166-7167.

58. Xu, H.; Yin, K.; Huang, W. *Chem. Eur. J.* **2007**, *13*, 10281-10293.

59. Xu, H.; Yin, K.; Huang, W. *ChemPhysChem* **2008**, *9*, 1752-1760.

60. Yu, J.; Zhang, H.; Zhou, L.; Deng, R.; Peng, Z.; Li, Z.; Fu, L.; Guo, Z. *J. Lumin.* **2007**, *122-123*, 678-682.

61. Li, Z.-F.; Zhou, L.; Yu, J.-B.; Zhang, H.-J.; Deng, R-P.; Peng, Z.-P.; Guo, Z.-Y. *J. Phys. Chem. C.* **2007**, *111*, 2295-2300.

62. Giacomelli, G.; Porcheddu, A.; De Luca, L. *Curr. Org. Chem.* **2004**, *8*, 1497-1519.

63. Banks, C. K.; Gruhzit, O. M.; Tillitson, E. W.; Controulis, J. *J. Am. Chem. Soc.* **1944**, *66*, 1771-1775.

64. Friedheim, E. A. H. *J. Am. Chem. Soc.* **1944**, *66*, 1775-1778.

65. Steffensen, M. B.; Hollink, E.; Kuschel, F.; Bauer, M.; Simanek, E. E. *J. Polym. Sci. A: Polyum. Chem.* **2006**, *44*, 3411-3433.

66. Di Nicola, C.; Garau, F.; Marchetti, F.; Monari, M.; Pandolfo, L.; Pettinari, C.; Venzo, A. *Dalton Trans.* **2011**, *40*, 4941-4953.

67. Liu, J.; Wang, K.; Zhang, X.; Li, C.; You, X. *Tetrahedron* **2013**, *69*, 190-200.

68. An, Z.-F.; chen, F.-F.; Yin, J.; Xie, G.-H.; Shi, H.-F.; Tsuboi, T.; Huang, W. *Chem. Eur. J.* **2011**, *17*, 10871-10878.

69. Khoo, V. S.; Dearnaley, D. P.; Finnigan, D. J.; Padhani, A.; Tanner, S. F.; Leach, M. O. *Radiother Oncol.* **1997**, *42*, 1-15.

70. Ersoy, H.; Rybicki, F. J. *J. Magn. Reson. Imaging* **2007**, *26*, 1190-1197.

71. Binnemans, K. *Chem. Rev.* **2009**, *109*, 4283-4374.

72. Binnemans, K. Rare-Earth Beta-Diketonates. In *Handbook on the Physics and Chemistry of Rare Earths* (ed. Gschneidner, K. A., Jr, Bünzli, J.-C. G., and Pecharsky, V. K.), Elsevier: Amsterdam, 2005; Volume 35, Chapter 225.
73. Bünzli, J.-C. G.; Moret, E.; Foiret, V.; Schenk, K. J.; Wang, M.; Jin, L. *J. Alloys. Compd.* **1994**, *207-208*, 107-111.
74. Wu, S. L.; Yang, Y. S. *J. Alloys Compd.* **1992**, *180*, 403-408.
75. Wu, S. L.; Wu, Y. L.; Yang, Y. S. *J. Alloys Compd.* **1992**, *180*, 399-402.
76. Yang, Y. S.; Gong, M. L.; Li, Y. Y.; Lei, H. Y.; Wu. S. L. *J. Alloys. Compd.* **1994**, *207-208*, 112-114.
77. Filipescu, N.; Sager, W. F.; Serafin, F. A. *J. Phys. Chem.* **1964**, *68*, 3324-3346.
78. Sager, W.F., Filipescu, N., Serafin, F.A. *J. Phys. Chem.* **1965**, *69*, 1092-1100.
79. Melby, L. R.; Rose, N. J.; Abramson, E.; Caris, J. C. *J. Am. Chem. Soc.* **1964**, *86*, 5117-5125.
80. Bauer, H.; Blanc, J.; Ross, D. L. *J. Am. Chem. Soc.* **1964**, *86*, 5125-5131.
81. Charles, R. G.; Ohlmann, R. C. *J. Inorg. Nucl. Chem.* **1965**, *27*, 255-259.
82. Karvinen, J.; Elomaa, A.; Mäkinen, M.-L.; Hakala, H.; Mukkala, V.-M.; Peuralahti, J.; Hurskainen, P.; Hovinen, Hemmilä, I. *Anal. Biochem.* **2004**, *325*, 317-325.
83. Hovinen, J.; Guy, P. M. *Bioconjugate Chem.* **2009**, *20*, 404-421.
84. Piszczek, G.; Maliwal, B. P.; Gryczynski, I.; Dattelbaum, J.; Lakowicz, J. R. *J. Fluoresc.* **2001**, *11*, 101-107.
85. Sénéchal, K.; Toupet, L.; Ledoux, I.; Zyss, J.; Le Bozec, H.; Maury, O. *Chem. Commun.* **2004**, 2180-2181.
86. Liu, G. K.; Jensen, M. P.; Almond, P. M. *J. Phys. Chem. A.* **2006**, *110*, 2081-2088.

87. D'Aléo, A.; Picot, A.; Beeby, A.' Gareth Williams, J. A.; Le guennic, B.; Andraud, C.; Maury, O. *Inorg. Chem.* **2008**, *47*, 10258-10268.

88. Andraud, C.; Maury, O. *Eur. J. Inorg. Chem.* **2009**, *29-30*, 4357-4371.

89. D'Aléo, A.; Pointillart, F.; Ouahab, L.; Andraud, C.; Maury, O. *Coord. Chem. Rev.* **2012**, *256*, 1604-1620.

90. Förster, Th. *Z. Elektrochem. Angew. Phys. Chem.* **1939**, *45*, 571

91. Grabowski, Z. R.; Rotkiewicz, K. *Chem. Rev.* **2003**, *103*, 3899-4032.

92. Yang, C.; Fu, L.-M.; Wang, Y.; Zhang, J. P.; Wong, W.-T.; Ai, X.-C.; Qiao, Y.-F.; Zou, B.-S.; Gui, L.-L. *Angew. Chem., Int. Ed.* **2004**, *43*, 5010– 5013.

93. Fu, L.-M.; Ai, X.-C.; Li, M.-Y.; Wen, X.-F.; Hao, R.; Wu, Y.-S.; Wang, Y.; Zhang, J.-P. *J. Phys. Chem.* **2010**, *114*, 4494-4500.

94. Reichardt, C.; Welton, T. Solvent Effects on the Absorption Spectra of Organic Compounds. In *Solvents and Solvent Effects in Organic Chemistry, Fourth Edition*, Wiley-VCH Verlag GmbH & Co. KGaA

95. Reichardt, C. *Chem. Rev.* **1994**, *94*, 2319-2358.

96. Dutra, J. D. L.; Bispo, T. D.; Freire, R. O. *J. Comput. Chem.* **2014**, *35*, 772-775.

97. http://lumpac.pro.br/

98. Foster, D. R.; Richardson, F. S.; Vallarino, L. M.; Shillady, D. *Inorg. Chem.* **1983**, *22*, 4002-4009.

99. A Guide to Recording Fluorescence Quantum Yields; HORIBA Jobin Yvon Inc.: Middlesex, United Kingdom; http://www.jobinyvon.com/usadivisions/fluorescence/applications/quantumyieldstrad.pdf

100. Fletcher, A. N. *Photochem. Photobiol.* **1969**, *9*, 439-444.

101. Wang, F.; Liu, X. *Chem. Soc. Rev.* **2009**, *38*, 976-989.

102. Liu, Y.; Tu, D.; Zhu, H.; Chan, X. *Chem. Soc. Rev.* **2013**, *42*, 6924-6958.

103. Comby, S.; Bünzli, J.-C. G. Lanthanide Near-Infrared Luminescence in Molecular Probes and Device. In *Handbook on the Physics and Chemistry of Rare Earths, Vol. 37*; Gschneidner, K. A., Jr.; Bünzli, J.-C. G.; Pecharsky, V. K., eds.; Elsevier: Amsterdam, **2007**; pp 217– 470.

104. Comby, S.; Bünzli, J.-C. G. Lanthanide Near-Infrared Luminescence in Molecular Probes and Device. In *Handbook on the Physics and Chemistry of Rare Earths, Vol. 37*; Gschneidner, K. A., Jr.; Bünzli, J.-C. G.; Pecharsky, V. K., eds.; Elsevier: Amsterdam, **2007**; pp 217– 470.

105. van der Ende, B. M.; Aarts, L.; Meijerink, A. *Phys. Chem. Chem. Phys.* **2009**, *11*, 11081-11095.

106. Strümpel, C.; McCann, M.; Beaucarne, G.; Arkhipov, V.; Slaoui, A.; Švrček, V.; del Cañizo, C.; Tobias, I. *Sol. Energ. Mat. Sol.* **2007**, *91*, 238-249.

107. Shalav, A.; Richards, B. S.; Green, M. A. *Sol. Energ. Mat. Sol.* **2007**, *91*, 829-842.

108. Carnall, W. T.; Fields, P. R.; Rajnak, K. *J. Chem. Phys.* **1968**, *49*, 4424-4442.

109. Bünzli, J.-C. G.; Eliseeva, S. V. *J. Rare Earth* **2010**, *28*, 824-842.

110. Beeby, A.; Faulkner, S.; Parker, D.; Gareth Williams, J. A. *J. Chem. Soc., Perkin Trans. 2*, **2001**, 1268-1273.

111. Placidi, M. P.; Natrajan, L. S.; Sykes, D.; Kenwright, A. M.; Faulkner, S. *Helv. Chim. Acta.* **2009**, *11*, 2427-2438.

112. Perry, W. S.; Pope, S. J. A.; Allain, C.; Coe, B. J.; Kenwright, A. M.; Faulkner, S. *Dalton Trans.* **2010**, *39*, 10974-10983.

113. Watkis, A.; Hueting, R.; Sørensen, T. J.; Tropiano, M.; Faulkner, S. *Chem. Commun.* **2015**, *51*, 15633-15636.

114. Gaiduk, M. I.; Grigoryants, V. V.; Mironov, A. F.; Rumyantseva, V. D.; Chissov, V. I.; Sukhin, G. M. *J. Photochem. Photobiol. B.* **1990**, *7*, 15−20.

115. Wong, W.K.; Zhu, X.; Wong, W.-Y. *Coord. Chem. Rev.* **2007**, *251*, 2386-2399.

116. Zhang, T.; Zhu, X.; Cheng, C. C. W.; Kwok, W.-M.; Tam, H.-L.; Hao, J.; Kwong, D. W. J.; Wong, W.-K.; Wong. K.-L. *J. Am. Chem. Soc.* **2011**, *133*, 20120-20122.

117. Horrocks, Jr., W. D.; Bolender, J. P.; Smith, W. D.; Supkowski, R. M. *J. Am. Chem. Soc.* **1997**, *119*, 5972-5973.

118. Faulkner, S.; Burton-Pye, B. P.; Khan, T.; Martin, L. R.; Wray, S. D.; Skabara, P. J. *Chem. Commun.* **2002**, 1668-1669.

119. Ziessel, R. F.; Ulrich, G.; Charbonnière, L.; Imbert, D.; Scopelliti, R.; Bünzli, J.-C. G. *Chem. Eur. J.* **2006**, *12*, 5060-5067.

120. Shavaleev, N. M.; Scopelliti, R.; Gumy, F.; Bünzli, J.-C. G. *Inorg. Chem.* **2009**, *48*, 2908-2918.

121. Lazarides, T.; Alamiry, M. A. H.; Adams, H.; Pope, S. J. A.; Faulkner, S.; Weinstein, J. A.; Ward, M. D. *Dalton Trans.* **2007**, 1484-1491.

122. Robinson, G. W.; Frosch, R. P. *J. Chem. Phys.* **1963**, *38*, 1187-1203.

123. Lakowicz, J. R. *Principles of Fluorescence Spectroscopy;* Springer: New York, **2006**; pp 687.

124. Tsvirko M.P.; Meshkova S. B.; Venchikov V. Y.; Topilova Z. M.; Bol'shoi D. V. *Opt. Spectrosc. (Engl. Transl.)*, **2001**, *90*, 669-673.

125. Doffek, C.; Wahsner, J.; Kreidt, E.; Seitz, M. *Inorg. Chem.* **2014**, *53*, 3263-3265.

126. Crosby, G. A.; Kasha, M. *Spectrochim. Acta* **1958**, *10*, 377−382.

127. Perkins, W. G.; Crosby, G. A. *J. Chem. Phys.* **1965**, *42*, 407−414.

128. Beeby, A.; Faulkner, S.; Williams, J. A. G. *Dalton Trans.* **2002**, 1918– 1922.

129. Lazarides, T.; Sykes, D.; Faulkner, S.; Barbieri, A.; Ward, M. D. *Chem. Eur. J.* **2008**, *14*, 9389-9399.

130. Hebbink, G. A.; Grave, L.; Woldering, L. A.; Reinhoudt, D. N.; van Veggel, F. C. J. M. *J. Phys. Chem. A* **2003**, *107*¸2483-2491.

131. Rehm, D.; Weller, A. *Isr. J. Chem.* **1970**, *8*, 259-271.

132. Weller, A. *Pure Appl. Chem.* **1968**, *16*, 115-123.

133. Faulkner, S.; Burton-Pye, B. P.; Khan, T.; Martin, L. R.; Wray, S. D.; Skabara, P. J. *Chem. Commun.* **2002**, 1668-1669.

134. Beeby, A.; Faulkner, S.; Gareth Williams, J. G. *J. Chem. Soc., Dalton Trans.* **2002**, 1918-1922.

135. Klink, S. I.; Grave, L.; Reinhoudt, D. N.; van Veggel, F. C. J. M.; Werts, M. H. V.; Geurts, F. A. J.; Hofstraat, J. W. *J. Phys. Chem. A* **2000**, *104*, 5457-5468.

136. Smith, A. M.; Mancini, M. C.; Nie, S. *Nat. Nanotechnol.* **2009**, *4*, 710-711.

137. Bünzli, J.-C. G. (2014) Luminescence Bioimaging with Lanthanide Complexes, in *Luminescence of Lanthanide Ions in Coordination Compounds and Nanomaterials* (ed A. de Bettencourt-Dias), John Wiley & Sons Ltd, Chichester, United Kingdom, ch 4.

138. Mathis, G.; Bazin, H. Stable Luminescent Chelates and Macrocyclic Compounds. In *Lanthanide Luminescence*; Hänninen, P.; Härmä, H., Eds.; Springer: Berlin, Heidelberg, 2011; Vol. 7, pp 47– 88.

139. Picot, A.; Malvolti, F.; Le Guennic, B.; Baldeck, P. L.; Gareth Williams, J. A.; Andraud, C.; Maury, O. *Inorg. Chem.* **2007**, *46*, 2659-2665.

140. Starck, M.; Kadjane, P.; Bois, E.; Darbouret, B.; Incamps, A.; Ziessel, R. Charbonnière, L. J. *Chem. Eur. J.* **2011**, *17*, 9164-9179.

141. Katritzky, A. R.; Ramsden, C. A.; Joule, J. A.; Zhdankin, V. V. Structure of Five-membered Rings with Two or More Heteroatoms, in *Handbook of Heterocyclic Chemistry*, Elsevier, 2010. Ch 2.4.

142. Kadjane, P.; Starck, M.; Camerel, F.; Hill, D.; Hildebrandt, N.; Ziessel, R.; Charbonnière, L. J. *Inorg. Chem.* **2009**, *48*, 4601-4603.

143. Burgess, J. *Metal Ions in Solution*, Ellis Horwood, Chichester, **1978**.

144. Jacques, V.; Desreux, J. F. *Top. Curr. Chem.* **2001**, *221*, 123-164.

145. Aime, S.; Botta, M.; Fasano, M.; Terreno, E. *Chem. Soc. Rev.* **1998**, *27*, 19-29.

146. Aime, S.; Botta, M.; Frullano, L.; Crich, S. G.; Giovenzana, G.; Pagliarin, R.; Palmisano, G.; Sirtori, F. R.; Sisti, M. *J. Med. Chem.* **2000**, *43*, 4017-4024.

147. Aime, S.; Botta, M.; Crich, S. G.; Giovenzana, G.; Pagliarin, R.; Palmisano, G.; Sisti, M. *Chem. Eur. J.* **2000**, *6*, 2609-2617.

148. Aime, S., Gianolio, E., Corpillo, D., Cavallotti, C., Palmisano, G., Sisti, M., Giovenzana, Giovanni B. and Pagliarin, R. *Helv. Chim. Acta* **2003**, *86*, 615-632.

149. Baranyai, Z.; Gianolio, E.; Ramalingam, K.; Swenson, R.; Ranganathan, R.; Brücher, E>; Aime, S. *Contrast Media Mol Imaging*, **2007**, *2*, 94-102.

150. Walton, J. W.; Di Bari, L.; Parker, D.; Pescitelli, G.; Puschmann, H.; Yufit, D. S. *Chem. Commun.* **2011**, *47*, 12289-12291.

151. Walton, J. W.; Bourdolle, A.; Butler, S. J.; Soulie, M.; Delbianco, M.; McMahon, B. K.; Pal, R.; Puschmann, H.; Zwier, J. M.; Lamarque, L.; Maury, O.; Andraud, C.; Parker, D. *Chem. Commun.* **2013**, *49*, 1600-1602.

152. Butler, S. J.; McMahon, B. K.; Pal, R.; Parker, D.; Walton, J. W. *Chem. Eur. J.* **2013**, *19*, 9511-9517.

153. Kabachnik, M. I.; Medved, T. Y. *Dokl. Akad. Nauk SSSR* **1952**, *83*, 689-692.

154. Fields, E. K. *J. Am. Chem. Soc.* **1952**, *74*, 1528–1531.

155. Song, X.-P.; Bouillon, C.; Lescrinier, E.; Herdewijn, P. *ChemBioChem*, **2011**, *12*, 1868-1880.

156. Cherkasov, R. A.; Galkin, V. I. *Russ. Chem. Rev.* **1998**, *67*, 857-882.

157. Gancarz, R. *Tetrahedron* **1995**, *51*, 10627–10632.

158. Ratcliffe, R. W.; Christensen, B. G. *Tetrahedron Lett.* **1973**, *14*, 4645-4648.

159. Lewis, R. T.; Motherwell, W. B. *Tetrahedron* **1992**, *48*, 1465-1484.

160. Oberhauser, T.; Meduna, V. *Tetrahedron* **1996**, *52*, 7691-7702.

161. Zhang, C.; Zou, C.-L.; Yan, Y.; Hao, R.; Sun, F.-W.; Han, Z.-F.; Zhao, Y. S.; Yao, J. *J. Am. Chem. Soc.* **2011**, *133*, 7276-7279.